

Role of melanoma-derived ADAM-9 for invasion and
metastasis of melanoma

Inaugural-Dissertation

Zur

Erlangung des Doktorgrades
der Mathematisch-Naturwissenschaftlichen Fakultät
der Universität zu Köln

vorgelegt von

Alexander Schönefuß
aus Mülheim an der Ruhr

Hundt Druck GmbH, Köln

2012

Berichterstatter (Gutachter):

PD Dr. Roswitha Nischt
Prof. Dr. Matthias Hammerschmidt

Tag der mündlichen Prüfung:

18.06.2012

Table of Contents

Summary	1
Zusammenfassung	3
1. Introduction	5
1.1 Human melanoma	5
1.1.1 Melanoma origin	5
1.1.2 Etiology of melanoma	6
1.1.3 Melanoma development, growth and metastasis	7
1.2 Mouse models to study melanoma	10
1.3 ADAM proteases	11
1.3.1 Structure	11
1.3.2 Regulation	12
1.3.3 ADAM function in physiology and pathology	13
1.4 Current knowledge on ADAM-9 function in physiology and pathology	14
1.5 Aims of the thesis	16
2. Materials and Methods	17
2.1 Material	17
2.1.1 Chemicals	17
2.1.2 Recombinant and purified proteins	17
2.1.3 Cell culture material	17
2.1.4 Consumable materials	18
2.1.5 Buffers and solutions	18
2.1.6 Devices	18
2.1.7 Software	19
2.2 Methods	20
2.2.1 Cell culture	20
2.2.1.1 Melanoma cell lines	20
2.2.1.2 Endothelial cell lines	21
2.2.1.3 Isolation and culture of primary human dermal fibroblasts	21
2.2.1.4 Stimulation of BLM melanoma cells and fibroblasts	21
2.2.1.5 Generation of IL-1 α or ADAM-9 silenced stable melanoma cell clones	22
2.2.1.6 Cell area and volume determination	23
2.2.1.7 Proliferation Assay	23
2.2.1.8 Soft agar colony formation assay	23
2.2.1.9 Dead de-epidermized skin assay	24

2.2.1.10 Cell migration assay	25
2.2.1.11 Adhesion assay	25
2.2.1.12 Cell-cell adhesion assay	26
2.2.1.13 Fluorescence activated cell sorting (FACS)	26
2.2.2 Protein analysis	27
2.2.2.1 Preparation of cell lysates	27
2.2.2.2 SDS-PAGE and immunoblotting	28
2.2.2.3 Immunohistochemistry	28
2.2.2.4 Immunocytochemistry	30
2.2.2.5 Histological analysis	31
2.2.2.6 Processing of basement proteins by ADAM-9	31
2.2.2.7 Cytokine antibody array	32
2.2.3 Analysis of nucleic acids	32
2.2.3.1 RNA isolation	32
2.2.3.2 Reverse transcription and polymerase chain chain reaction (RT-PCR)	32
2.2.3.3 Quantitative real time PCR	34
2.2.3.4 Analysis of genomic DNA	35
2.2.4 <i>In vivo</i> experiments	35
2.2.4.1 Animal housing	35
2.2.4.2 Generation of Adam-9 ^{-/-} //Hgf/Cdk4 ^{R24C/R24C} animals	35
2.2.4.3 Induction and analysis of melanoma formation	36
2.2.4.4 Tail vein injection of B16-F1 melanoma cells	37
2.2.5 Statistical analysis	37
3. Results	38
3.1 Analysis of ADAM expression in melanoma cells	38
3.1.1 ADAM expression in human melanoma cell lines	38
3.1.2 ADAM-9 transcript and protein expression	38
3.2 <i>In vitro</i> analysis of ADAM-9 function in melanoma cells	39
3.2.1 Stable down-regulation of ADAM-9	39
3.2.1.1 Regulation of cell size by ADAM-9	41
3.2.1.2 Analysis of proliferation	44
3.2.1.3 <i>In vitro</i> cell invasion	45
3.2.1.4 Adhesion to basement membrane proteins	47
3.2.1.5 Analysis of integrin expression	48
3.2.1.6 Analysis of cell migration	50
3.2.2 Processing of basement membrane proteins by ADAM-9	51

3.3 Regulation of ADAM-9 expression	54
3.3.1 Analysis of ADAM-9 regulation by IL-1 α	54
3.3.1.1 Regulation of ADAM-9 by exogenous IL-1 α	54
3.3.1.2 Analysis of melanoma cell derived IL-1 α on ADAM-9 expression in high invasive melanoma cells	56
3.3.1.3 Invasion through the basement membrane upon IL-1 α down-regulation	58
3.3.2 Modulation of ADAM-9 expression by indirubins	60
3.4 <i>In vivo</i> analysis of ADAM-9 function in a mouse model for spontaneous melanoma development	61
3.4.1 Generation of Adam-9 ^{-/-} /Hgf/Cdk4 ^{R24C/R24C} animals	62
3.4.1.1 Analysis of skin architecture and differentiation	63
3.4.2 ADAM-9 expression in melanomas developed in control mice	66
3.4.3 Analysis of DMBA-induced tumor growth and development	67
3.4.3.1 Histology of DMBA-induced tumors	69
3.4.3.2 Analysis of vascularization and proliferation of DMBA-induced tumors	70
3.4.3.3 Inflammatory infiltration of DMBA-induced tumors	71
3.4.4 Metastatic spread in control and Adam-9 ^{mutated/ko} animals	72
3.4.5 Characterization of mechanisms responsible for reduced lung metastases formation in Adam-9 ^{mutated/ko} animals	76
3.4.5.1 Melanoma cell chemoattraction	76
3.4.5.2 Basement membranes in DMBA-induced tumors	78
3.4.5.3 Intra- and extravasation of melanoma cells	80
3.5 Role of ADAM-15 in growth and invasion of melanoma	83
4. Discussion	85
4.1 Expression of ADAMs in melanoma cells	85
4.2 Role of ADAM-9 for melanoma growth and invasion <i>in vitro</i>	86
4.2.1 Involvement of ADAM-9 in melanoma cell proliferation	86
4.2.2 Regulation of cell size by ADAM-9	88
4.2.3 Basement membrane penetration mediated by ADAM-9	89
4.3 Regulation of ADAM-9 expression in melanoma cells by IL-1 α	92
4.4 Role of ADAM-9 for melanoma growth and invasion <i>in vivo</i>	93
4.4.1 Role of ADAM-9 for melanoma development and growth	93
4.4.2 Role of ADAM-9 for metastases formation	95
4.5 Outlook	98
5. References	99
6. Abbreviations	107

Acknowledgement	111
Publication ADAM-15	112
Erklärung	118
Curriculum vitae	119

Summary

The protein ADAM-9 (A disintegrin and metalloprotease-9) belongs to the family of the ADAM proteases, which are type I transmembrane proteins and are unique among transmembrane proteins as they exhibit protease as well as adhesive functions. The ADAM proteases are involved in ectodomain shedding of membrane-bound molecules as well as in cell-cell and cell-matrix interactions.

In human melanoma ADAM-9 is located at the tumor-stroma border in the stromal cells, but also in the melanoma cells. The aim of this work was to find out the function of ADAM-9, produced by the melanoma cells, for the development and invasion of melanoma.

In vitro experiments, in which high invasive melanoma cells with stable down-regulation of ADAM-9 mediated via shRNA were used, showed that silencing of ADAM-9 slightly increased melanoma cell proliferation and remarkably reduced basement membrane penetration in an *in vivo* like invasion system. The reduced invasion through the basement membrane might be due to decreased adhesion to the basement membrane, as the ADAM-9 down-regulated cells exhibited significantly reduced adhesion towards type IV collagen and matrigel. Additionally it was found that the laminin β 3-chain, which is a component of the basement membrane protein laminin 332, was cleaved by ADAM-9 in the N-terminal region. This work further confirmed that extracellular IL-1 α down-regulates ADAM-9 expression in melanoma cells, which is mediated via a JNK dependent pathway and showed that in melanoma cells intracellularly active IL-1 α controls constitutive expression levels of ADAM-9 via the involvement of ERK. Despite the activity of IL-1 α as regulator of ADAM-9 expression, also indirubins, which are anti-cancer drugs, were identified as molecules down-regulating ADAM-9 expression in high invasive melanoma cells, but not in fibroblasts.

To analyze if ADAM-9 also influences melanoma development and invasion *in vivo*, HGF/CDK^{R24C/R24C} animals, which spontaneously develop melanomas as well as upon DMBA treatment, were crossbred with ADAM-9^{-/-} mice. This strategy enabled to investigate melanoma development and progression in the absence of ADAM-9 in stromal as well as in the tumor cells. The created Adam-9^{mutated/ko} (Adam-9^{-/-}//Hgf/Cdk4^{R24C/R24C}) animals developed more tumors compared to control (Adam-9^{+/+}//Hgf/Cdk4^{R24C/R24C}) mice at week four after DMBA treatment, whereas from week six onwards the Adam-9^{mutated/ko} animals exhibited a reduced tumor number. This finding is most likely attributed to a differential proliferation of the tumor cells at both analyzed time-points.

Interestingly lung metastases formation was significantly reduced in the Adam-9^{mutated/ko} mice. This might be attributed to an impaired extravasation generated by a decreased adhesion of

ADAM-9 deficient melanoma cells to endothelial cells, because it could be shown that ADAM-9 down-regulated melanoma cells exhibited a significantly reduced adhesion towards endothelial cells. Additionally the intravasation might also be reduced indicated by immunohistochemical stainings for laminin β 3-chain. This staining was confined to the basement membrane zone and appeared continuous in the tumors obtained from the Adam-9^{mutated/ko} animals, whereas in the control animals the basement membrane appeared destructed and discontinuous. This indicates that in the absence of ADAM-9 break down of the basement membrane by the melanoma cells might be reduced resulting in decreased intravasation.

To summarize the *in vitro* and *in vivo* data, melanoma-derived ADAM-9 is involved in basement penetration and melanoma metastases formation in the lungs. The obtained data suggest that ADAM-9 can contribute to lung metastases formation by facilitating basement membrane penetration and mediating adhesion of melanoma cells to endothelial cells.

Zusammenfassung

Das Protein ADAM-9 (A disintegrin and metalloprotease-9) ist ein Mitglied der Familie der ADAM Proteasen, welche zur Klasse der Typ I Transmembranproteine gehören und als einzige Transmembranproteine eine Funktion als Protease sowie als Adhäsionsmolekül ausüben. ADAM Proteasen sind beteiligt an der Prozessierung von membrangebundenen Proteinen (ectodomain shedding) sowie an Zell-Zell und Zell-Matrix Interaktionen.

In histologischen Färbungen von humanen Melanomen ist ADAM-9 an der Stroma-Tumor Grenze, sowohl in stromalen Zellen als auch in Melanomzellen, nachgewiesen worden. Das Ziel dieser Arbeit war es die Beteiligung von ADAM-9, das in Melanomzellen produziert wird, an der Melanomentstehung und -invasion herauszufinden.

In *in vitro* Experimenten mit hoch invasiven Melanomzellen, in welchen die ADAM-9 Expression mittels shRNA stabil herunterreguliert wurde, zeigte sich dass die Herunterregulation von ADAM-9 die Proliferation von Melanomzellen leicht erhöht und die Invasion der Zellen durch die Basalmembran stark verringert. Ein Grund für die reduzierte Basalmembraninvasion könnte eine verringerte Adhäsion der ADAM-9 herunterregulierten Melanomzellen auf der Basalmembran sein, da diese Zellen eine signifikant reduzierte Adhäsion gegenüber Typ IV Kollagen sowie Matrigel aufwiesen. Außerdem wurde gezeigt, dass die Laminin β 3-Kette, welche ein Bestandteil des Basalmembranproteins Laminin 332 ist, von ADAM-9 in ihrem N-terminal Ende proteolytisch geschnitten werden kann.

Des Weiteren konnte durch diese Arbeit bestätigt werden, dass extrazelluläres IL-1 α die Expression von ADAM-9 in Melanomzellen, unter der Beteiligung von JNK, herunterregulieren kann und dass in Melanomzellen interzellulär aktives IL-1 α die konstitutive Expression von ADAM-9 durch einen ERK abhängigen Signalweg kontrolliert. Außer der Aktivität von IL-1 α als Regulator der ADAM-9 Expression, konnten zudem Indirubine, welche in der Krebstherapie eingesetzt werden, als Moleküle identifiziert werden, welche die ADAM-9 Expression in hoch invasiven Melanomzellen, aber nicht in Fibroblasten reduzieren.

Um die Beteiligung von ADAM-9 an der Melanomentstehung und -invasion in der *in vivo* Situation zu analysieren, wurden HGF/CDK^{R24C/R24C} Mäuse, welche sowohl spontan als auch nach DMBA Behandlung Melanome entwickeln, mit ADAM-9^{-/-} Mäusen gekreuzt. Diese Strategie ermöglichte es die Melanomentstehung und -progression in einer Situation, in der sowohl die Stroma-, als auch die Tumorzellen kein ADAM-9 exprimieren, zu untersuchen. Die generierten Adam-9^{-/-}//Hgf/Cdk4^{R24C/R24C} Tiere wiesen vier Wochen nach der DMBA Behandlung zunächst mehr Tumore im Vergleich zu Adam-9^{+/+}//Hgf/Cdk4^{R24C/R24C}

Kontrolltieren auf ab Woche sechs hingegen entwickelten die Adam-9^{-/-}//Hgf/Cdk4^{R24C/R24C} Tiere weniger Tumore. Dieses Ergebnis könnte auf eine unterschiedliche Proliferation der Tumorzellen zu beiden untersuchten Zeitpunkten zurückzuführen sein.

Interessanterweise entwickelten die Adam-9^{-/-}//Hgf/Cdk4^{R24C/R24C} Mäuse signifikant weniger Lungenmetastasen als die Adam-9^{+/+}//Hgf/Cdk4^{R24C/R24C} Tiere. Dieser Effekt könnte auf eine gestörte Extravasation zurückzuführen sein, da gezeigt werden konnte, dass die Adhäsion von Melanomzellen, in denen ADAM-9 herunterreguliert wurde, gegenüber Endothelzellen signifikant reduziert ist. Zusätzlich könnte auch die Intravasation reduziert sein, da in immunhistochemischen Färbungen der Tumore gegen die Laminin β 3-Kette, die Färbung in den Adam-9^{-/-}//Hgf/Cdk4^{R24C/R24C} Tieren eine intakte und kontinuierliche Basalmembran zeigte. In den Adam-9^{+/+}//Hgf/Cdk4^{R24C/R24C} Tieren hingegen war die Basalmembran degradiert und diskontinuierlich. Dieses Ergebnis weist darauf hin, dass in ADAM-9 defizienten Tieren die Degradierung der Basalmembran durch die Melanomzellen vermindert sein könnte, was zu einer reduzierten Intravasation führt.

Zusammenfassend haben die *in vitro* und *in vivo* Daten gezeigt, dass von Melanomzellen produziertes ADAM-9 an der Basalmembraninvasion und der Entstehung von Lungenmetastasen beteiligt ist. Die erhaltenen Ergebnisse lassen vermuten, dass ADAM-9 in der Überwindung der Basalmembran durch Melanomzellen eine Rolle spielt und in der Lage ist Adhäsion zwischen Melanom- und Endothelzellen zu vermitteln.

1. Introduction

1.1 Human melanoma

1.1.1 Melanoma origin

Melanoma is a highly malignant tumor arising from the malignant transformation of melanocytes (de Vries *et al.*, 2003). Melanocytes are derived from highly migratory embryonic cells called neural crest cells (Uong and Zon, 2010). These cells differentiate into melanocyte precursor cells, the melanoblasts, and subsequently, under the influence of melanocyte-stimulating hormone, are converted into pigment producing melanocytes (Herlyn *et al.*, 2000). In healthy human epidermis melanocytes are scattered among keratinocytes at the epidermal-dermal border, forming structural and functional contacts with keratinocytes, which control melanocyte proliferation, differentiation and expression of surface molecules (Mc Gary *et al.*, 2002). The localization of melanocytes in the skin differs between human and mice, being present in hair follicles and the basal layer of the interfollicular epidermis in humans and in the hair follicles and dermis, but not in the epidermis in the mouse (Herlyn *et al.*, 2000). In Figure 1 the development of melanoma is illustrated.

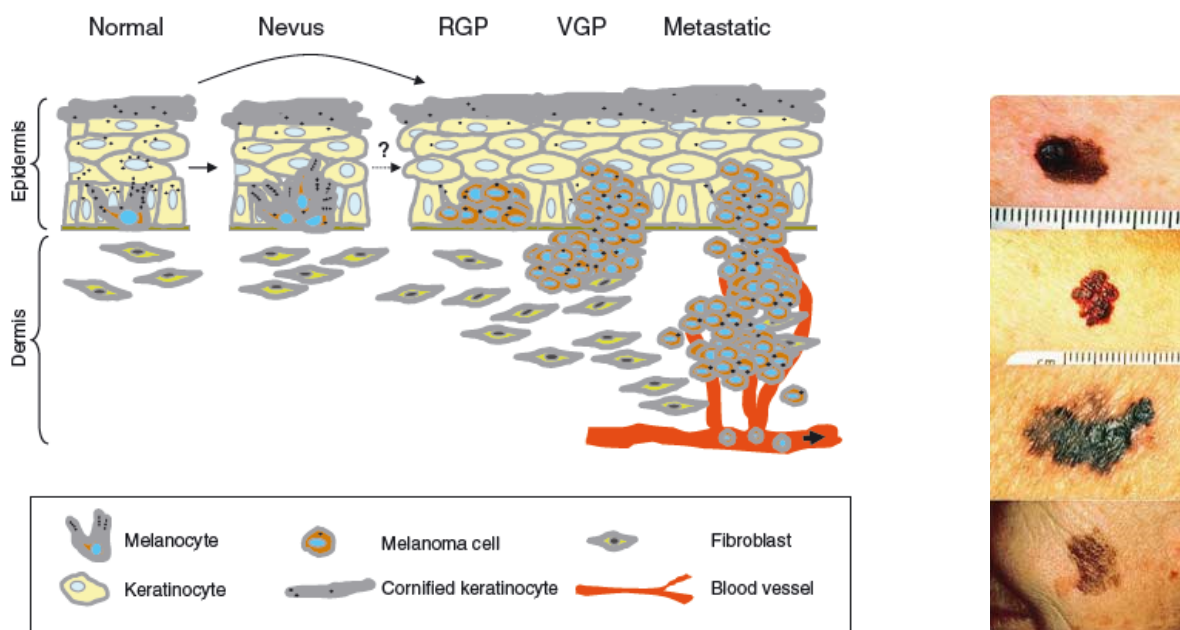


Figure 1: Development of melanoma. Melanoma evolves from normal melanocytes located in the basal layer of the epidermis. The melanocytes can either develop directly into melanoma cells or first transform into nevi cells, which can also give rise to melanoma cells. In the radial growth phase (RGP) melanoma first grows in horizontal direction without substantial penetration of the underlying dermis. With entering the vertical growth phase (VGP) the transformed cells invade into the dermis and finally enter the circulation where they are transported to distant organs with the potential to form metastases (Gaggioli and Sahai, 2007). The right panel shows some examples of the macroscopic appearance of melanoma with typical morphologic characteristics like unequal borders, brown-black color, asymmetry and elevation.

In human skin, increased proliferation of melanocytes in the epidermis marks their benign transformation into melanocytic nevi. These nevi can show some cellular aberrations, but are not invasive. Although some melanomas can develop from pre-existing nevi, most

melanomas evolve *de novo* from melanocytes without the presence of a premelanocytic nevus lesion (Haass and Herlyn, 2005). Initially melanoma grows in horizontal direction within in epidermis without crossing the basement membrane (BM), this phase is called the radial growth phase. In later stages the tumor cells degrade the BM and enter the dermis, which is defined as vertical growth phase. Invasion through the dermis is followed by invasion into the circulation via the bloodstream or the lymphatic vessels and leads to metastatic spread to distant organs (Gaggioli and Sahai, 2007).

1.1.2 Etiology of melanoma

Risk factors for melanoma comprise light skin phenotype, high number of nevi, chronic sun exposure, particularly in childhood and a familial history of melanoma (Tucker *et al.*, 2003; Benjamin *et al.*, 2007). The influence of exposure to UV irradiation as a cause for melanoma is discussed controversially, because melanomas lack typical UV signature mutations, as induction of thymidin dimers in DNA by UV-B radiation (Fu *et al.*, 2003; Holmes *et al.*, 2007). Moreover melanoma can also arise in completely sun-protected areas. On the other hand UV treatment in animal models suggests a connection between melanoma and UV exposure. Thus for example irradiation of hepatocyte growth factor/scatter factor (HGF/SF) transgenic mice with UVB, but not UVA light, induces melanoma formation (De Fabo *et al.*, 2004).

The recent advances in sequencing technology allowed performing genome-wide screening studies using melanoma cell lines and tissues, identifying several chromosomal aberrations, like alterations in gene copy number or loss of heterozygosity, in melanoma. These studies discovered several hot spots, which are frequently mutated in melanoma including the *CDKN2A* locus, *BRAF*, *NRAS* or *MITF*, suggesting that the onset of melanoma is caused by the sequential accumulation of inherited and/or acquired mutations (Curtin *et al.*, 2005; Stark and Hayward, 2007).

As already mentioned several genes are frequently mutated in melanoma, including the *CDKN2A* locus encoding the two tumor suppressor genes *p16^{Ink4a}* and *p14^{ARF}*. Germline mutations in this locus were observed in 25-50% of familial and somatic mutations in about 40% of sporadic melanomas (Tsai and Tsao, 2004; Hocker *et al.*, 2007). The protein *p16^{Ink4a}* inhibits CDK4, which no longer phosphorylates the retinoblastoma protein thereby blocking transition from G₁- to S-phase of the cell cycle. On the contrary, abrogation of the inhibitory activity of *p16^{Ink4a}* results in constantly active CDK4 and increased cell survival and proliferation (Hocker *et al.*, 2007). Activating mutations in CDK4 have also been described in familial melanoma and lead to enhanced cell proliferation and survival (Zuo *et al.*, 1996). The other protein encoded by the *CDKN2A* locus, *p14^{ARF}* functions as tumor suppressor by inhibiting the action of MDM2 thereby promoting the activity of p53. Mutations in *p14^{ARF}* lead to increased levels of MDM2, subsequent inhibition of p53 and loss of cell cycle control (Lowe and Sheer, 2003). Mutations in melanoma are also often found in the RAS pathway,

particular in *NRAS* as well as in downstream targets of *NRAS* in the MAPK pathway, like *BRAF*. Thus in up to 90% of melanomas activating mutations in one of the two key MAPK genes, *BRAF* or *NRAS* are present (Hocker *et al.*, 2007). Genome-based oncogene scanning studies showed that the most common mutation in *BRAF* is an amino acid substitution in exon 15 in codon 600 from valine to glutamic acid (*BRAF*^{V600E}) (Davies *et al.*, 2002). Interestingly, selective inhibition of this mutated *BRAF* in clinical trials led to complete or partial tumor regression in the majority of the patients (Flaherty *et al.*, 2010), however follow up studies showed that one third of the patients developed squamous cell carcinomas (Sosman *et al.*, 2012). In 50-60% of melanomas mutations are found in molecules of the PI3K/AKT pathway, e.g. in *PTEN* and *AKT* (Chudnovsky *et al.*, 2004; Hocker *et al.*, 2007), resulting in increased cell survival and proliferation (Wu *et al.*, 2003). Mainly these two networks, the MAPK and the PI3K/AKT pathway, regulate melanoma proliferation, survival and invasion. Mutations in one of the most prominent tumor suppressor genes *TP53* encoding for the p53 protein were only found in 10% of melanomas, suggesting that this pathway is not one of the major networks responsible for melanoma development (Chudnovsky *et al.*, 2004; Tsai and Tsao, 2004; Hocker *et al.*, 2007).

1.1.3 Melanoma development, growth and metastasis

Under physiological conditions melanocyte growth and behaviour is controlled by growth factors released from keratinocytes as well as by direct cell-cell interactions or interactions with the underlying matrix (Haass *et al.*, 2005). It has been shown for example *in vitro* that the intercellular adhesion molecule E-cadherin is the main mediator of human melanocyte adhesion to keratinocytes (Tang *et al.*, 1994) and loss of expression of E-cadherin, leads to melanoma cell escape from keratinocyte-mediated control during melanoma progression (Kuphal and Bosserhoff, 2011). Moreover, while expression of E-cadherin is lost, melanoma cells acquire expression of other receptors, e.g. N-cadherin, which mediate homotypic interaction of melanoma cells and heterotypic interaction of melanoma cells with other N-cadherin expressing cells in the stroma, like fibroblasts and endothelial cells (McGary *et al.*, 2002; Alonso *et al.*, 2007). Another up-regulated receptor found in melanoma cells is the melanoma cell adhesion molecule (MCAM), which mediates cell interactions with the extracellular matrix or other adhesion molecules on endothelial cells (e.g. platelet endothelial cell adhesion molecule-1 (PECAM-1) (McGary *et al.*, 2002).

Other cellular receptors, which are altered during the transformation of a melanocyte into a melanoma cell, are integrin receptors, which are known to mediate prominently cell-matrix interactions. Melanocytes were shown to express $\alpha 3\beta 1$, $\alpha 6\beta 1$ and $\alpha v\beta 1$ integrins, but in melanoma cells increased expression of the fibronectin binding integrins $\alpha v\beta 3$ and $\alpha 5\beta 1$ was detected (Haass *et al.*, 2005). Likely, these receptor are necessary for cells to better adhere

and migrate through the underlying tissue or they can bind proteolytic enzymes, e.g. MMP-2, localizing them to the cell surface as shown for the $\alpha\beta 3$ integrin (Brooks *et al.*, 1996).

As soon as the tumor cells have lost contact to their surrounding cells, they interact with and degrade the BM in order to invade the underlying tissue. It was shown that membrane-type matrix metalloproteases (MT-MMPs) expressed by cancer cells are mainly responsible for the breakdown of the BM in an *ex vivo* invasion system. This was true for all three members of this family, MMP-14, MMP-15 and MMP-16 (Hotary *et al.*, 2006). However, *in vitro*, other MMPs, like MMP-2 or MMP-9, are also able to degrade type IV collagen, one of the main components of the BM, but these molecules were not able to promote cell penetration of the BM in an *ex vivo* like invasion system in which different cancer cells including melanoma were used (Hotary *et al.*, 2006).

These proteolytic enzymes may also play a role in the invasion through the dermal tissue, not only by mediating cellular migration, but also necessary to modify the extracellular matrix and release factors to create more favourable environment for melanoma progression (Zigrino *et al.*, 2005). Expression of a number of MMPs, including MMP-1, -2, -9, -13 and MMP-14 has been detected in melanoma (Hofmann *et al.*, 2000). High expression of MMP-1 and MMP-3 correlated with shorter patient survival in agreement with the known function of MMP-1 to degrade type I and type IV collagens (Durko *et al.*, 1997; Nikkola *et al.*, 2002). Similarly MMP-9 seems to be involved in metastases formation (Itoh *et al.*, 1999). *In vitro* studies with melanoma cells have further shown that expression of MMP-2 and MMP-14 in melanoma cells modulates melanoma cell adhesion, spreading and migration in the extracellular matrix (Nakahara *et al.*, 1997; Iida *et al.*, 2004). Stromal expression of MMP-13 seems instead to be required for the induction of peritumoral angiogenesis in melanoma (Zigrino *et al.*, 2009). Other enzymes have also been implicated in mediating melanoma invasion, one example of these are cathepsins, lysosomal proteases. Inhibition of cathepsin K reduced invasion of melanoma cells through matrigel (Quintanilla-Dieck *et al.*, 2008). The activity of cathepsins B and L were detected in high invasive melanoma cells *in vitro* (Klose *et al.*, 2006a) and contact of high invasive melanoma cell lines with type I collagen induced the release of cathepsin B in the extracellular environment (Klose *et al.*, 2006b). More recently, also ADAM proteases have been implicated in melanoma progression. Stromal expression of ADAM-15 contributes to melanoma metastases formation (Schönefuß *et al.*, 2012), whereas stromal expression of ADAM-8 decreased melanoma growth (Guaiquil *et al.*, 2010). Interestingly, also expression of ADAM-9 by the host is required to counteract murine melanoma growth *in vivo* (Abety *et al.*, 2012).

During the invasive process, tumor cells not only degrade the extracellular matrix, but also influence the surrounding cells. Via the secretion of growth factors and cytokines or cell-cell interactions, tumor cells can alter the activities of fibroblasts and inflammatory cells with

respect to migration, proliferation and release of additional growth factors and proteases (Zigrino *et al.*, 2005). Tumor cells that left the primary tumor, once migrated into the dermal compartment can form metastases using three principal routes: The cells can either disseminate via the lymphatic vessels (lymphogenous), the blood vessels (haematogenous) or via migration along visceral cavities (cavitary). The most common routes are the lymphogenous, mainly found in carcinomas, and the hematogenous, predominately occurring in sarcomas (Bacac and Stamenkovic, 2008). In Figure 2 the principal steps of melanoma invasion and metastases formation are summarized.

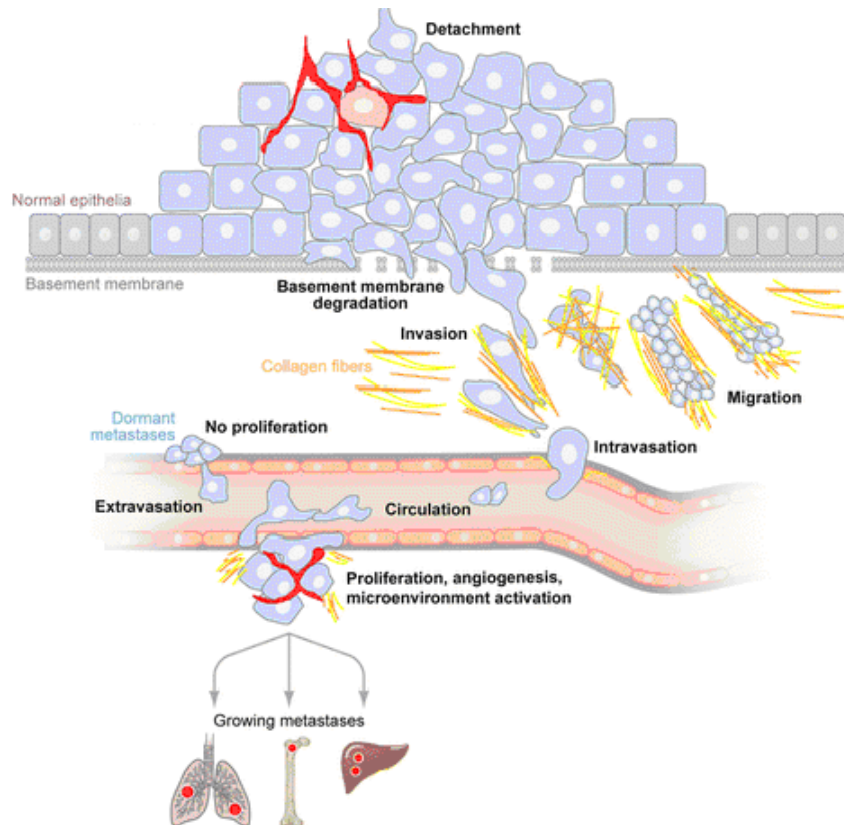


Figure 2: Principal steps of melanoma invasion and metastases formation. Upon transformation from normal cells into an invasive cancer, cells first loose adherens junctions and detach from the surrounding cells. Subsequently they degrade the basement membrane and invade into the underlying tissue, penetrate the circulation and are transported to distant organs. Upon attachment to the vessel wall, cells extravasate and adapt to the new microenvironment, where they proliferate and form a metastasis. Some cancer cells have also the ability to be dormant in the invaded tissue for a long period of time before they begin to proliferate (modified according to: Bacac and Stamenkovic, 2008).

In melanoma the most frequently metastasized organs are the skin, lymph nodes, subcutaneous tissues, lung, liver, central nervous system and the bone (Leiter *et al.*, 2004). Attraction of tumor cells to these organs is thought to occur by the interaction of chemokines with their receptors located on tumor cells. It was for example shown that melanoma cells express the chemokine receptors CXCR4, CCR7 and CCR10 (Leiter *et al.*, 2004) and the release of the respective ligands CXCL12, CCL21 and CCL27 in the lung, lymphatic system or the skin, respectively contributes to the spreading of metastatic tumor cells to these

specific organs (Kakinuma and Hwang, 2006). After the cells have been transported to the target organs, the circulating tumor cells are retained in the target organs mechanically due to size restrictions in small capillaries and/or interact with endothelial cells and transmigrate into the tissue (Chambers *et al.*, 2002; McGary *et al.*, 2002).

1.2 Mouse models to study melanoma

Since the past 50 years different *in vivo* models for the investigation of the complex biological processes involved in melanoma have been established. One of the earliest models relied on the grafting of murine B16 melanoma cells into mice (Fidler and Nicolson, 1976). While this may represent a syngeneic system when using C57BL6 mice, xenogeneic models are also available and in these cells from a different species are injected (human cells into a mouse), requiring the use of immunodeficient mice to prevent cell rejection by the immune system (Becker *et al.*, 2010). Since syngeneic models are often used to study melanoma immunology, xenogeneic models are employed to determine the behaviour of melanoma cells with respect to their invasiveness, metastatic potential or the role of melanoma stem cells. In contrast to transplantation models, genetically modified animals are largely used to analyze melanomagenesis (Becker *et al.*, 2010). Currently several genetic models are available, in which mutations lead to spontaneous melanoma development after a period of latency and/or after physical or chemical treatment of the animals with UV light or carcinogens, e.g. 7,12-dimethylbenzanthracene (DMBA) (Larue and Beermann, 2007). One of these models is the hepatocyte growth factor overexpressing / cyclin dependent kinase 4 knock-in mutant (HGF/CDK4) mouse model. The HGF/CDK4 mice carry a mutation in the *CDK4* gene (*Cdk4*^{R24C}), which was knocked into the germline. This mutation creates an altered binding pocket for p16^{Ink4a}, the most important inhibitor for CDK4, and renders the CDK4 protein insensitive to inhibition by p16^{Ink4a} resulting in a constitutively active CDK4 and impaired control of the G₁ phase of the cell cycle (Tormo *et al.*, 2006). The *Cdk4*^{R24C} mutation, which functions as a dominant negative oncogene was also observed in some cases of sporadic and hereditary melanomas in humans (Zuo *et al.*, 1996). It was shown that melanoma cells, but not normal melanocytes, express HGF and c-met, leading to constitutive autocrine activation of the MAPK and PI3K pathway (Li *et al.*, 2001). In human melanoma specimen c-met expression correlated with melanoma growth and metastatic spread (Cruz *et al.*, 2003) and the HGF was shown to stimulate the proliferation of melanocytes (Hirobe *et al.*, 2004). In the HGF/CDK4 mouse model, different from wild-type mice, but similar to the human situation, melanocytes are not only located in the hair follicles and the dermis, but also in the basal layer of the epidermis and the dermo-epidermal junction. These mice develop melanomas spontaneously after about eight-to-ten month after birth and tumor formation can also be promoted by treatment with DMBA. The spontaneous as well as induced tumors recapitulate the histopathology of human melanoma and metastasize to the

lymph nodes and lungs (Tormo *et al.*, 2006; Landsberg *et al.*, 2010). Moreover melanoma formation can also be induced in these animals by neonatal UVB treatment, which closely mimics the human situation (Gaffal *et al.*, 2011).

For the sake of completeness it should be mentioned that several other transgenic models exist, which develop melanomas after carcinogen treatment as well as spontaneously. These mice carry different mutated genes under the control of melanocyte specific promoters. For example one widely used model is the transgenic overexpression of mutated *NRAS* or *HRAS* genes under the control of a melanocyte specific tyrosinase promoter (Walker and Hayward; 2002; Larue and Beermann, 2007).

1.3 ADAM proteases

1.3.1 Structure

The protein family of the ADAMs are multidomain type I transmembrane glycoproteins, which belong to the adamalysin family of proteins a subgroup of the metzincin zinc metalloproteases (Wolfsberg *et al.*, 1995). To date 40 ADAMs have been identified in various species from human (23 ADAMs) and mice (33) to *Xenopus laevis* (6) and *Drosophila melanogaster* (2) (Blobel, 2005).

ADAMs exhibit a conserved domain structure containing a pro- and a metalloprotease domain, a disintegrin-like and a cysteine-rich domain. Additionally most ADAMs also contain an EGF-like domain and a short cytoplasmic tail (Edwards *et al.*, 2008). Only 13 of the known 23 human ADAMs are suggested to be proteolytically active (Edwards *et al.*, 2008) as they contain an HExxHxxGxxH...M motif with three histidine residues binding the zinc ion in the metalloprotease domain and an invariant methionin turn in the active site (Murphy, 2008). The inactive state of the ADAMs is maintained by the interaction of a cysteine residue located in the prodomain with the zinc ion in the catalytic site of the metalloprotease domain (Edwards *et al.*, 2008). Enzyme activation is achieved by removal of the prodomain mediated via proprotein-convertases such as furin or by autocatalytic processing, by which the prodomain is cleaved off in the Golgi network (Blobel, 2005). This process is called the "cysteine switch mechanism". Furthermore, the released prodomain functions as a chaperone mediating correct protein folding (Edwards *et al.*, 2008). Once activated the metalloprotease domain exhibits proteolytic activity towards extracellular matrix proteins (Mochizuki and Okada, 2007) and acts as sheddase for many cell surface bound molecules activating and liberating them from the cell membrane. This leads to the induction of signals in auto- and paracrine manner (Blobel, 2005; Mochizuki and Okada, 2007). The disintegrin and the cysteine-rich domains can mediate cell-cell and cell-matrix interactions, via binding to integrins or heparansulfate proteoglycans, e.g syndecans (Edwards *et al.*, 2008). The cytoplasmic domain of the individual ADAMs is highly variable, but the majority contains signalling motifs, such as phosphorylation sites for serine-threonine or tyrosine kinases and

proline rich regions, which bind Src-homology-3 (SH-3) domain containing proteins important for signal transduction (Edwards *et al.*, 2008). In Figure 3 the structure of the ADAMs in inactive and active state is illustrated.

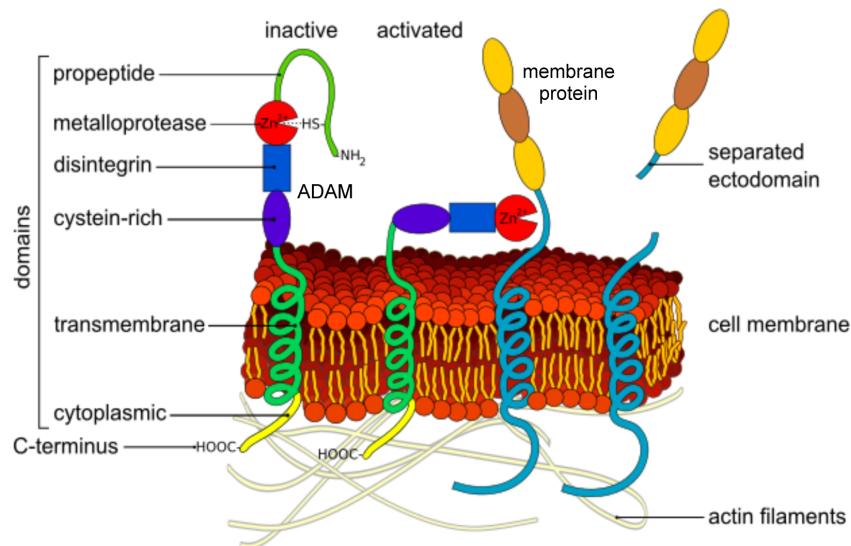


Figure 3: Structure of ADAMs and ectodomain shedding. The general structure of the ADAM proteases with the C-terminal cytoplasmic tail, the transmembrane domain, the cysteine-rich, the disintegrin, the metalloprotease and the prodomain is shown. The metalloprotease domain contains a zinc ion in the catalytic site, which binds to a cysteine residue located in the prodomain keeping the protein in a latent state. In the trans-Golgi network the prodomain is removed leading to the activation of the protein (modified according to: http://en.wikipedia.org/wiki/File:Ectodomain_shedding_en.svg).

1.3.2 Regulation

The ADAM proteases can be regulated on transcriptional as well as on posttranscriptional level. The interaction of the cytoplasmic tail with intracellular proteins might be important for the localization and activation of the ADAMs (Edwards *et al.*, 2008). Thus for example phosphorylation of the cytoplasmic tail of ADAM-17 by extracellular signal related kinase (ERK) induces translation of ADAM-17 to the cell surface (Soond *et al.*, 2005). Other posttranscriptional control points for ADAM activity include regulation on the level of the zymogen activation and by interaction with tissue inhibitors of metalloproteinases (TIMPs) (Mochizuki and Okada, 2007). In contrast to the MMPs, ADAMs are only selectively inhibited by TIMPs, thus for example ADAM-17 is exclusively inhibited by TIMP-3 and ADAM-10 can be inhibited by TIMP-1 and -3, but not TIMP-2 and -4 (Amour *et al.*, 1998; Amour *et al.*, 2000). Other ADAMs, like ADAM-8 and -9, are not sensitive to inhibition by TIMPs (Amour *et al.*, 2002). Apart from the posttranscriptional regulation, ADAMs can also be regulated on gene expression level. It was shown that the estrogen receptor can bind to the ADAM-9 promoter region, thereby acting as a transcription factor (Cong and Jia, 2009). ADAM-17 expression was induced by the transcription factor Sp1 in glioma cells (Szalad *et al.*, 2009) and TGF- β can induce ADAM-12 expression by degradation of the transcriptional repressor SnoN (Solomon *et al.*, 2010).

1.3.3 ADAM function in physiology and pathology

Due to their multidomain structure, physiologically ADAMs are involved in various cellular processes such as cell proliferation, adhesion, migration and signalling (Rocks *et al.*, 2008). The first ADAMs, which have been described were ADAMs 1 and 2 and were identified in the testis as molecules mediating the fusion of sperm and egg (Wolfsberg *et al.*, 1995). Beside their function in fertilization, ADAMs contribute to proliferation, angio-, neuro and myogenesis, by their ability to mediate cellular interactions leading for instance to cell fusion or by shedding of surface molecules, which can induce para- and autocrine signalling (Edwards *et al.*, 2008). ADAM-17 was described as the major sheddase for pro tumor necrosis factor- α (TNF- α) (Black *et al.*, 1997), inducing paracrine TNF- α signalling, which for instance is crucial for adult myogenesis (Liu *et al.*, 2010). ADAM-9 and ADAM-17 can shed heparin binding-hepatocyte growth factor (HB-EGF), which can induce proliferation and was for example shown to be important for heart development (Jackson *et al.*, 2003). The mechanism, by which ADAM mediated activation of the EGF receptor is achieved, is called “triple membrane-passing signalling” (Blobel, 2005). This includes the activation of a membrane bound ADAM by ligand binding to a G-protein-coupled-receptor (GPCR), inducing intracellular signalling molecules, which phosphorylate the cytoplasmic domain of ADAMs, leading to their activation and subsequent shedding of ligands for the EGFR (Blobel, 2005). Another process, in which ADAM mediated shedding of surface molecules, plays an important role is called “regulated intramembrane proteolysis” (RIP). This process is defined as a sequential proteolytic cascade, which includes an initial shedding of the ectodomain of a transmembrane protein by an ADAM and a second cleavage in the membrane itself by another enzyme, generating an intracellular fragment, which can induce other intracellular events (Edwards *et al.*, 2008; Murphy, 2008). The classical examples for RIP are the processing of amyloid-precursor-protein (APP) and Notch signalling (Edwards *et al.*, 2008). It was shown that ADAM-10 and -17 cleave the extracellular domain of Notch, when it is bound to ligands like Delta or Jagged, followed by subsequent intramembrane processing of Notch by γ -secretase activity. This process is particularly important in neurogenesis (Bray, 2006). Similarly APP is processed by α -secretase activity of ADAM-9, -10 and -17, followed by sequential cleavages by β - and γ -secretases (Edwards *et al.*, 2008). Also the adhesive functions of the ADAMs contribute to biological processes, like the involvement of ADAM-8 in neuron-glia interactions or the binding of ADAM-12 to integrins, which leads to cell differentiation during muscle development (Schlomann *et al.*, 2000; Lafuste *et al.*, 2005). In various studies it has been shown that members of the ADAM family of proteases play a role in cancer. ADAMs can promote tumor cell adhesion and migration, shown for example for ADAM-12 (Iba *et al.*, 1999). In addition, ADAMs exhibit enzymatic activity towards extracellular matrix proteins as shown for the cleavage of type IV collagen by ADAM-10 and

ADAM-15, whereas ADAM-12 can degrade in addition also fibronectin (Mochizuki and Okada, 2007). Even though the relevance of these activities for the *in vivo* situation has not been clarified, one can envision that all these activities may contribute to migration through tissues. Furthermore, ADAMs can shed as well as bind to cell adhesion molecules, which mediate tumor cell interactions with the vasculature, like selectins and VCAM-1 (Murphy, 2008). ADAM proteases are also involved in the inflammatory reaction, which accompanies cancer progression. Hence ADAM-9 and -17 are able to shed ligands of the activating natural killer cell receptor, NKG2D, like major histocompatibility complex chain 1 related proteins, MICA and MICB, from the tumor cell surface, leading to escape from NKG2D-mediated tumor immunosurveillance (Waldhauer *et al.*, 2008; Kogha *et al.*, 2009).

1.4 Current knowledge on ADAM-9 function in physiology and pathology

ADAM-9 was first identified in 1996 in breast carcinoma (Weskamp *et al.*, 1996). The protein is produced as a 110kDa glycosylated proprotein, which is activated in the Golgi apparatus by furin activity to the 85kDa mature form that is found on the cell surface after prodomain removal (Roghani *et al.*, 1999). As some other members of the ADAM family, in addition to its membrane bound form, ADAM-9 exists also as soluble form derived either from a deletion in the EGF-like domain creating an early stop codon or from alternative splicing (Hotoda *et al.*, 2002; Mazzocca *et al.*, 2005). The protein is ubiquitously expressed, however ADAM-9 deficient mice show no obvious phenotype and develop normally (Weskamp *et al.*, 2002). In adult animals at 20 month after birth, retinal degeneration appeared (Parry *et al.*, 2009). *In vitro* proteolytic activity of ADAM-9 was shown towards various proteins like EGF (epidermal growth factor), FGFR2iiib (fibroblast growth factor receptor2 iiib), a murine variant of the human FGFR2, type XVII collagen or EphB4 (ephrin type-B receptor 4) (Peduto, 2009). The shedding of FGFR2iiib for example has been shown to be relevant for the regulation of growth factor signalling during pathological events such as prostate cancer development (Peduto *et al.*, 2005). *In vivo*, shedding of type XVII collagen by ADAM-9 modulated keratinocyte migration during skin repair (Mauch *et al.*, 2010). ADAM-9 is also able to degrade extracellular matrix proteins such as fibronectin, gelatin and laminin 111 *in vitro* (Schlöndorff and Blobel, 1999; Schwettmann *et al.*, 2001). Due to the presence of the disintegrin domain ADAM-9 provides also adhesive functions. The adhesive activity of ADAM-9 to integrin receptors has been shown by several *in vitro* studies, showing a cell-type specificity. Thus for example binding to $\alpha 2\beta 1$ integrins was observed in activated stellate cells, but to the $\alpha 3\beta 1$ integrin in keratinocytes and fibroblasts (Mazzocca *et al.*, 2005; Zigrino *et al.*, 2007; Zigrino *et al.*, 2011). Furthermore *in vitro* studies showed that membrane bound ADAM-9 suppresses, whereas the soluble form promoted breast cancer cell migration (Fry *et al.*, 2010).

In vitro studies revealed that among several environmental factors, IL-1 α and fibrillar type I collagen regulate the expression of ADAM-9 in melanoma cells (Zigrino *et al.*, 2005). Additional studies have also identified reactive oxygen species as regulators of ADAM-9 expression in prostate cancer cells (Sung *et al.*, 2006) and in myeloma cells (Fischer *et al.*, 2004). Recently several studies showed that ADAM-9 expression in hepatocellular carcinoma and pancreatic cancer cells is also regulated by microRNAs (Zhou *et al.*, 2011; Kim *et al.*, 2011; Hamada *et al.*, 2011).

Several authors detected increased expression of ADAM-9 in different cancers including breast, intestinal, renal and prostate cancer (Lendeckel *et al.*, 2005; Sung *et al.*, 2006; Fritzsche *et al.*, 2008) suggesting a role for ADAM-9 in cancerous processes. In prostate cancer ADAM-9 expression was associated with shorter relapse-free survival of patients (Fritzsche *et al.*, 2008) and in agreement with these results in animals lacking expression of ADAM-9, development of aggressive prostate tumors was reduced (Peduto *et al.*, 2005). Various melanoma cell lines also express ADAM-9 and *in vivo* it is expressed in primary human melanomas in both, the peripheral parts of the tumor and in stroma cells adjacent to the tumor border, whereas little if any expression was detected in metastases (Zigrino *et al.*, 2005). *In vivo*, the role of ADAM-9 in melanoma development is controversial being described as both a tumor suppressor and promoter in mouse studies (Guaiquil *et al.*, 2009; Abety *et al.*, 2012). Microarray analysis of human melanoma revealed an association of ADAM-9 expression with melanoma progression (Alonso *et al.*, 2007). Thus the functional role of ADAM-9 in melanoma is presently unclear.

1.5 Aims of the thesis

ADAM-9 is expressed in human melanoma cell lines and in tumor cells located at the tumor-stroma border (Zigrino *et al.*, 2005). Stromal expression of ADAM-9 influences melanoma growth *in vivo* (Abety *et al.*, 2012), however the function of ADAM-9 expression in the melanoma cells remains unclear. The overall aim of this thesis is to elucidate the role of ADAM-9 produced by melanoma cells for tumor growth, invasion and metastases formation. To first study the function of ADAM-9 expression in melanoma cells for these processes *in vitro*, ADAM-9 expression in melanoma cells will be stably down-regulated using shRNA. This strategy allows to perform long-term experiments *in vitro* and to investigate proliferation and invasiveness of melanoma cells in an *in vivo* like system. According to the known function of ADAM-9 as an adhesive and proteolytic molecule, besides key processes for melanoma progression, like proliferation and invasion, further investigations are aimed to address melanoma cell adhesion, migration and matrix proteolysis, cellular processes also contributing to melanoma progression.

To answer the question what is the function of melanoma-cell derived ADAM-9 for melanomagenesis and progression *in vivo*, ADAM-9^{-/-} mice are planned to crossbred with HGF/CDK4 double mutant transgenic mice, which develop spontaneous melanomas and closely resemble human tumors (Tormo *et al.*, 2006). These animals can be treated with DMBA to induce tumor growth and to monitor melanoma development and metastases formation in the absence of ADAM-9. These analyses will clarify if ADAM-9 participates in any of these processes and further investigations will help to unveil underlying cellular and molecular mechanisms by which ADAM-9 contributes to melanoma formation and progression. On the one hand it is important to understand the function of melanoma-derived ADAM-9 in all processes involved in melanoma formation, but it is equally important to understand how this protein is regulated in these processes. The cytokine IL-1 α , which is expressed in high amounts intracellularly and as well as secreted protein by melanoma cells (Löffek *et al.*, 2005; Apte *et al.*, 2006), was indicated as one key regulatory factor of ADAM-9 expression in melanoma cell lines (Zigrino *et al.*, 2005). Thus we hypothesized that there exists a threshold of this cytokine above which ADAM-9 is down-regulated and vice versa in these cells. To prove this hypothesis and to understand the molecular events leading to the regulation of the expression and activity of ADAM-9 in melanoma cells the intracellular pathways mediating regulation of ADAM-9 by either exogenous as well as intracellular IL- α will also be analyzed. For this purpose the effect of exogenously added IL-1 α will be investigated using a pharmacological approach by inhibiting downstream mediators of the IL-1 α signalling pathway (JNK, NF κ B). To investigate the intracellular pools, high invasive melanoma cells, in which IL-1 α expression was stably down-regulated, will be used.

2. Material and Methods

2.1 Material

2.1.1 Chemicals

All chemicals were purchased in analytical grade from Roth (Karlsruhe, Germany), Sigma Aldrich (München, Germany), Merck (Darmstadt, Germany), GIBCO (Karlsruhe, Germany) and Perbio (Lausanne, Switzerland).

Tissue-Tek[®] (Polyvinyl alcohol < 11%, carbowax < 5%, nonreactive ingredients 85%) was purchased from Sakura, Zoeterwoude, Netherlands. RNA inhibitors, Oligod(T)₁₆ primers primers and MuLV reverse transcriptase were used from Applied Biosciences (Foster City, CA, USA); dNTPs were purchased from Roche (Mannheim, Germany).

Molecular weight markers for proteins, PageRuler[™]PlusPrestained Protein ladder and PageRuler[™]Unstained Protein ladder were from Fermentas (St. Leon-Roth, Germany). DNA marker, 100bp DNA ladder were from NEB (Frankfurt/Main, Germany). The indirubin derivates SL-22, SL-85 and KD-65 were synthesized in the Department for Organic Chemistry at the University of Rostock and were a kind gift of Prof. Manfred Kunz.

2.1.2 Recombinant and purified proteins

Human recombinant or purified proteins used are summarized in Table 1.

Table 1: Human recombinant and purified proteins.

Human protein	Source	Application
rec. ADAM-9	R&D Systems	enzymatic assay
rec. collagen I	BD Biosciences	enzymatic assay
rec. collagen IV	BD Biosciences	adhesion, enzymatic assay, migration
rec. fibronectin	R&D Systems	migration, enzymatic assay
laminin 332, isolated from foreskin kerationocytes	Immundiagnostik	adhesion, enzymatic assay, migration
rec. laminin β3-chain	Prof. M. Koch, Institute for Experimental Dental Medicine and Oral Muscoskeletal Biology, Cologne	enzymatic assay
rec. laminin 511	BioLamina	enzymatic assay
matrigel	BD Biosciences	adhesion, migration

2.1.3 Cell culture material

Plastic ware for cell culture was purchased from Greiner (Nürtingen, Germany), TPP (Trasadingen, Switzerland) and BD Biosciences (Heidelberg, Germany). Cell culture medium was purchased from PAA (RPMI, Cölbe, Germany) and GIBCO (DMEM, Karlsruhe, Germany). Antibiotics (Penicillin/Streptomycin) and L-Glutamine were from Biochrom (Berlin, Germany), FCS and non-essential amino acids from PAA (Cölbe, Germany).

2.1.4 Consumable materials

CL-XPosure™ X-Ray exposure films	Thermo Fischer Scientific
Cryomolds (standard, intermediate)	Sakura
Embedding cassettes	KABE Labortechnik
Eppendorf tubes (1.5 ml, 2 ml)	Eppendorf
PCR tubes (0.5 ml)	peQlabBiotechnologie
Microscopic slides	Menzel
Microscopic coverslips, ø 12 mm	Assistent®
Nitrocellulose membrane	AmershamBioscience
Syringes and needles	BD Biosciences
Whatman paper	VWR

2.1.5 Buffers and solutions

Anode Buffer I	Tris 0.3M, 20% methanol
Anode Buffer II	Tris 25mM, 20% methanol
Cathode Buffer	6-Aminohexan acid 40mM, 20% methanol
DEPC-treated H ₂ O	H ₂ O, 0.1% DEPC
DNA extraction buffer	50mM Tris base, pH 8.0, 100mM EDTA, 100mM NaCl, 1%SDS
FACS buffer	PBS, 1% BSA, 2mM EDTA
Laemmli reducing loading bromphenolblue buffer	60mM Tris-HCl pH 6.8, 2% SDS, 0.1% 25% glycerol, 14.4mM 2-mercaptoethanol
PBS	137mM NaCl, 2.7mM KCl, 8.4mM Na ₂ HPO ₄ , 1.4mM KH ₂ HPO ₄ , pH 7.4
PBST	0.5% Tween/PBS
Ponceau Red solution	0.1% Ponceau S (w/v) in 5% acetic acid (v/v)
Running Buffer (PAGE)	250mM Tris base, 0.2M glycine, 1%SDS, pH 8.3
RIPA Buffer	150mM NaCl, 0.5% sodium deoxycholate, 2% SDS, 1%NP40, 50mM Tris pH 7.4
Substrate buffer	25mM Tris, 2.5µM ZnCl ₂ , 0.005% Brij-35, pH 9.0
TBE	90mM Tris, 20mM Na ₂ EDTA, 90mM boric acid pH 8.0

2.1.6 Devices

Agarose gel electrophoresis	Easy-Cast Electrophoresis System Model 2B, Owl Scientific Model 40-0911, peQlabBiotechnologie
Cell counter	CASY® device model TT
Cell incubators	HERAcell 150i CO ₂ -incubator, Thermo Fisher Scientific

Centrifuges	Eppendorf Centrifuge 5415 R, Eppendorf Centrifuge 5415 C, HeraeusSepatechMegafuge 1.0
Cool plate	Thermo Shandon
Cryostat	Microm HM 650
ELISA MicroPlate Reader	1420 Multilabel Counter, VICTOR ³ _{TM} , Perkin Elmer
Flow cytometer	FACSCalibur flow cytometer, BD Biosciences
Microscopes	Leica DM 4000 B, Nikon Eclipse TS100, Nikon Eclipse E800, Olympus IX81
Microtome	Thermo Shandon Finesse microtome
pH-meter	WTW inolab pH level 1
Photometer	Eppendorf Bio Photometer, Eppendorf
Real-time PCR	7300 Real-time PCR System, Step One Plus Real-time PCR System, Applied Biosystem
Shaker	KS 250 basic, KIKA Labortechnik
Sterile hoods	Lamin Air 2448, Heraeus Instruments Safa 2020, Thermo Fischer Scientific
Thermocycler	T3 Thermocycler, Biometra
Thermomixer	EppendorfThermomixer 5437, TS 100 Thermoshaker
Water bath	GFL, Julabu SW-20C
Western Blot equipment	Mighty Small II SE 250, Hoefer Scientific Instruments
X-Ray film development	Curix 60 developing machine, AGFA

2.1.7 Software

Adobe Photoshop 7.0
 BD CellQuest Pro, BD Biosciences
 CellR[®] Imaging Software, Olympus
 Diskus 4.50, Hilgers
 Graph Pad Prism 4.03
 Image J 1.41(<http://rsb.info.nih.gov/ij>)
 NIS-Elements AR 2.30, NIS-Elements
 Step One TM Software v2.1, Applied Biosystems

2.2 Methods

2.2.1 Cell culture

2.2.1.1 Melanoma cell lines

The human melanoma cell lines Skmel23, Skmel28, WM164/4, IF6, BLM, MeWo, VMM5, WM75/6, A375, Ma-Mel-86a and Ma-Mel-119 were used. In Table 2 the invasive capacities of the different cell lines including references are shown. All cell lines were cultured in RPMI 1640 medium containing 10% FCS, 1% non-essential amino acids, 2% L-Glutamine, Penicillin/Streptomycin (100U/ml) (normal growth medium). Additionally, the murine melanoma cell line B16-F1 (Fiedler and Nicolson, 1976), which was stably transfected with GFP was used (Zigrino *et al.*, 2009). These cells were cultured in DMEM medium supplemented with 10% FCS, Penicillin/Streptomycin (100 U/ml) and 800µg/ml G-418 (PAA, Cölbe, Germany). All cells were cultured at 37°C and 5% CO₂ in humidified atmosphere. Cells were passaged at a ratio of 1:5 twice per week. Confluent cells were detached by incubation in Trypsin/EDTA (1% Trypsin/ 2.5% EDTA) and seeded in normal growth medium.

Table 2: Information about the used human melanoma cell lines.

Cell line	Invasive capacity <i>in vivo</i>	Origin	References
A375	high	Primary melanoma	Giard, <i>et al.</i> , 1973 Kozlowski <i>et al.</i> , 1984 Luca <i>et al.</i> , 1995
BLM	high	Lung metastasis	Lockshin <i>et al.</i> , 1985 Van Muijen <i>et al.</i> , 1991
IF6	low	Lymph node metastasis	Van Muijen <i>et al.</i> , 1991
Ma-Mel-86a	not tested	Lymph node metastasis	Ugurel <i>et al.</i> , 2007 Schwinn <i>et al.</i> , 2003
Ma-Mel-119	not tested	Skin metastasis	Ugurel <i>et al.</i> , 2007
MeWo	high	Lymph node metastasis	Carey <i>et al.</i> , 1976 Ishikawa <i>et al.</i> , 1988a Ishikawa <i>et al.</i> , 1988b Welch <i>et al.</i> , 1991
Skmel23	low	Primary melanoma	Carey <i>et al.</i> , 1976
Skmel28	low	Primary melanoma	Carey <i>et al.</i> , 1976 Luca <i>et al.</i> , 1995
VMM5	high (in collagen I matrix)	Metastatic melanoma	Benbow <i>et al.</i> , 2002
WM164/4	low	Melanoma metastasis	Herlyn, D. <i>et al.</i> , 1990
WM75/6	not tested	Primary melanoma	Herlyn, M. <i>et al.</i> , 1985

2.2.1.2 Endothelial cell lines

The mouse endothelial cell line sEND-1, which was originally isolated from middle T oncogene of polyoma virus induced hemangiomas (Williams *et al.*, 1988), was cultured in DMEM medium supplemented with 10% FCS and Penicillin/Streptomycin (100U/ml) and sub-cultivated in a ratio of 1:5 two times per week by incubation in Trypsin/EDTA (1% Trypsin/ 2.5% EDTA) and reseeding in normal growth medium.

2.2.1.3 Isolation and culture of primary human dermal fibroblasts

Primary dermal human fibroblasts were isolated from human skin obtained during surgeries in the Clinic for Dermatology and Venerology, University of Cologne. All samples were taken with the patients consent and approved by the local ethic committee (Ethikantrag: 08-144). Directly after the preparation by the surgeon the skin was freed from fat tissue and cut in ~ 5 x 5mm small pieces. These pieces were adhered to the bottom of a culture flaks and incubated for 2h at 37°C and 5% CO₂ in a humidified atmosphere. Cell culture medium (DMEM medium supplemented with 10% FCS and Penicillin/Streptomycin, 100U/ml) was introduced and the skin pieces cultured for two-three weeks until cells migrated out of the tissue. The fibroblasts were further cultured in DMEM medium supplemented with 10% FCS and Penicillin/Streptomycin (100U/ml) and used for experiments in passages two-six.

2.2.1.4 Stimulation of BLM melanoma cells and fibroblasts

For stimulation experiments melanoma cells were seeded in a density of 85,000 cells/cm² in RPMI 1640 medium containing 10% FCS, 1% non-essential amino acids, 2% L-Glutamine, Penicillin/Streptomycin (100U/ml). Human dermal fibroblasts (passages two-six) were seeded with a density of 60,000/cm² in DMEM medium containing 10% FCS and Penicillin/Streptomycin (100U/ml). All cells were grown as monolayer for 24h and washed twice with PBS before stimulation. The cells were stimulated with 10µM of indirubins (chapter 2.1.1) or 10U/ml recombinant human IL-1α (tebu-bio, Offenbach, Germany) in medium containing 1% FCS. As a control, cells were also treated with 0.001% DMSO, the solvent for the indirubins.

For pharmacological inhibition studies 10µM of the NFκB inhibitor SN50 (Biomol GmbH, Hamburg, Germany) and 18µM of the JNK inhibitor SP600125 (Biomol GmbH, Hamburg, Germany) were used. The melanoma cells were incubated for 24h with 10U/ml IL-1α alone or in combination with one of the inhibitors. Cells incubated with 0.0002% DMSO, the solvent for SP600125, were used as control. RNA or protein isolation was performed 24h after stimulation.

2.2.1.5 Generation of IL-1 α or ADAM-9 silenced stable melanoma cell clones

BLM or B16-F1 melanoma cells were stably transfected with shRNA plasmids targeted to IL-1 α or ADAM-9 by using Lipofectamine[®] (Invitrogen, Karlsruhe, Germany) or nucleofection using the Nucleofector[®] Technology and the Nucleofector[®] Kit V (both Lonza AG, Cologne, Germany), respectively, according to the manufactures instructions. When shRNAs targeted to IL-1 α or ADAM-9 were applied, five different shRNA plasmids provided by SA Biosciences (Frederick, USA) were used for the transfection: one control plasmid containing a scrambled artificial sequence, which does not match any human gene, and four additional plasmids each expressing a different shRNA sequence targeted to different areas of the IL-1 α or ADAM-9 transcript under the control of the U1 promoter. The targeting vector is shown in Figure 4 and the different inserted sequences of the shRNAs are listed in Table 3.

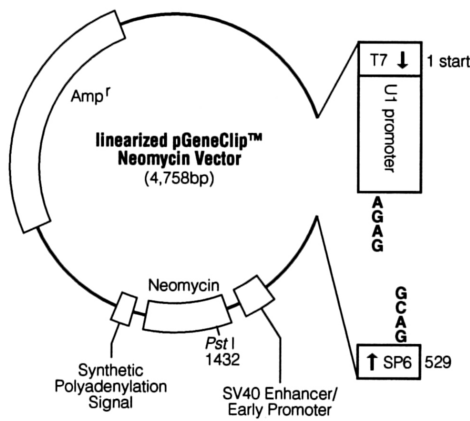


Figure 4: pGeneClip™ Neomycin vector carrying the shRNA sequences.

Table 3: Sequences of the four different shRNAs targeted to human ADAM-9 or IL-1 α and the scrambled control sequence.

ADAM-9	
Number	Sequence
1	AAAGCTTCAGTGTGAGAATGT
2	GGAGGAAACTGCCTTCTTAAT
3	AGATGATTCTCCTGGCAAAC
4	TCAACTGTGGAGAAGCTACTT
Control	GGAATCTCATTTCGATGCATAC
IL-1 α	
Number	Sequence
1	GGCTGCTGCATTACATAATCT
2	CTCCTCTTCTTCTGGGAAACT
3	TGACTCGAGGAAGAAATCAT
4	GCCCATCCAAACTTGTATT
Control	GGAATCTCATTTCGATGCATAC

For transfection of B16-F1 cells one control plasmid containing a scrambled artificial sequence, which does not match any mouse gene and a pool of five plasmids expressing different shRNA sequences targeted to ADAM-9 were used. The manufacturer (Santa Cruz, Heidelberg, Gemnay) does not provide the different shRNA sequences. The shRNAs were under the control of a H1 promoter. Two days post transfection BLM melanoma cells were selected using 600 μ g/ml G-418 (PAA, Cölbe, Germany) and B16-F1 cells using 400ng/ml puromycin (PAA, Cölbe, Germany), added to the normal growth medium (selection medium). After 14 days in culture under selection pressure, single colonies were isolated with cloning rings and further cultured in selection medium, until enough cells were available for analysis of IL-1 α or ADAM-9 expression on mRNA and protein level. The IL-1 α clones have been generated within the frame of the diploma thesis of Mrs. Birgit Seyfarth and clones used here, displayed the most efficient down-regulation of IL-1 α on mRNA and protein level.

2.2.1.6 Cell area and volume determination

For measurement of cell area, 35,000 cells/cm² were plated on 100mm plastic petri dishes and grown for 24h to about 60% confluence in selection medium. Images (200x magnification) of the cells were captured with a Nikon Eclipse TS100 microscope connected to a Nikon DS-Fi1 camera. The cell area of 50 single grown cells of each clone was measured with the ImageJ program (<http://rsb.info.nih.gov/ij>).

To quantify the cellular volume of ADAM-9 down-regulated or control cells 35,000 cells/cm² were seeded on 100mm plastic petri dishes in selection medium and cultured for three days until the cells were confluent. The cells were detached with Trypsin/EDTA (1% Trypsin/2.5% EDTA) and centrifuged at 100g for 5min at room temperature (RT). After centrifugation the cell pellet was resuspended in 10ml selection medium and 100µl of the cell suspension was diluted in 10ml isotonic NaCl solution. In this suspension cellular volume was determined using the CASY[®] device model TT (Schärfe System, Reutlingen, Germany). For each sample cell volume was determined in triplicate.

For aquaporin inhibition studies, the cells were detached (1% Trypsin/2.5% EDTA) and centrifuged at 100g for 5min at RT. Afterwards the cells were resuspended in selection medium supplemented with 0.15mM mercuric chloride (HgCl₂; Sigma Aldrich, München, Germany) and incubated at RT for 1h. Subsequently cell volume was determined as described above.

2.2.1.7 Proliferation Assay

To measure cell proliferation, 40,000 cells/cm² were seeded in 96 multiwell plates and grown for 24 and 48h. Cellular proliferation was measured using a BrdU (Bromodeoxyuridine) Proliferation Kit (Roche, Penzberg, Germany) according to the manufacturer's instructions. Briefly, cells were labeled with BrdU (10µM final concentration/well) for 2h at 37°C. After labeling, medium was removed and cells dried at RT for about 1h before being stored at 4°C until further processing.

DNA was denatured by addition of 200µl of "FixDenat" solution to each well and incubation for 30min at RT. After removing the solution, 100µl of anti-BrdU-POD antibody working solution was added for 1.5h at RT. Plates were washed three times with PBS and incubated with substrate solution for 10min. The reaction was stopped using 25µl of 1M H₂SO₄ and fluorescence was analyzed at 450 nm using Victor³_{TM} 1420 Multilabel counter. Cells in which only BrdU labelling step was omitted were used as control. For each clone BrdU labelling procedure was performed in triplicate.

2.2.1.8 Soft agar colony formation assay

For colony formation soft agar assay, 6-well culture dishes were covered with a 0.5% base agar (Noble Agar; BD Biosciences, Heidelberg, Germany) layer containing 50% selection

medium. This layer was covered by a 0.2% top agar layer containing 5000 ADAM-9 down-regulated or scramble transfected control cells and 50% selection medium. The agar layers were covered by 500 μ l medium, which was exchanged twice per week. The cells were allowed to grow for 21 days before formed colonies were fixed and stained with 0.005% crystal violet dissolved in methanol for 1h. For every clone the experiment was performed in triplicate and for each culture dish the number of formed colonies was counted in 8 randomly chosen microscopic fields (100 x magnification).

2.2.1.9 Dead de-epidermized skin assay

For dead deepidermized skin (DDS) invasion assay healthy human skin was obtained from plastic surgery. The assay was performed as previously described (Dennhöfer *et al.*, 2003), with the modification that melanoma cells were seeded in addition to the dermal side also on the basement membrane (BM) side. Briefly fat tissue was dissected and the remaining skin was repeatedly frozen and thaw at -80°C and in a 37°C water bath. This procedure led to death of all cells located in the tissue. Subsequently the epidermis was detached from the dermis by thermolysis (10min, 56°C in PBS) and stripped off mechanically retaining the BM. In the next step 1cm diameter punch biopsies were taken from the skin tissue and incubated for 10min in medium before they were placed on a stainless steel support in a 6-well culture plate with either the BM side or the fat free dermal side upside. The assembly of the skin composites and the location of melanoma cell seeding is schematically shown in Figure 5. On top of the skin composites 100,000 ADAM-9 or IL-1 α silenced or control cells were seeded in 10 μ l medium either on the BM side or the fat free dermal side. Medium was filled below the stainless steel support and comparable to the *in vivo* situation, the cells were cultured at the air/liquid interphase for 21 days. The medium was exchanged every two-three days. For further analysis, the composites were embedded in Tissue-Tek[®] or fixed for 12h in Roti[®]-Histofix 4% (Roth, Karlsruhe, Germany) at 4°C. Paraffin sections of the cultures were stained with haematoxylin and eosin (H&E) and the invasion depth of cells, which penetrated the tissue was microscopically measured under bright field illumination (Leica DM 4000 B; Leica, Wetzlar, Germany). Images were captured with a computerized imaging system (JVC, KY-F75U camera; Dikus 4.50, Hilgers, Königswinter, Germany).

The presence of the BM in the cultures was confirmed by immunohistochemical staining of BM components laminin α 3-chain and collagen IV (see 2.2.2.3).

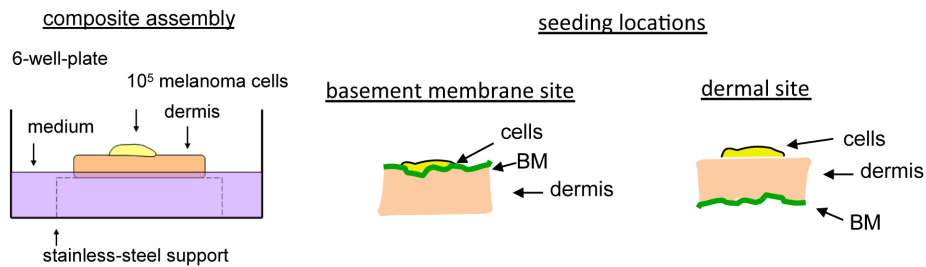


Figure 5: Assembly of DDS composite and locations for melanoma cell seeding. BM: basement membrane

2.2.1.10 Cell migration assay

Cell migration assays were performed in 24-well tissue culture plates. The culture plates were coated with the following human proteins by overnight adsorption at 4°C: 10µg/ml recombinant fibronectin or recombinant collagen IV, 5µg/ml laminin-332 and matrigel. The next day the matrix was washed twice with PBS to remove excess proteins. For the experiment mitotic activity of the cells was arrested by treatment with mitomycin-C (1.6 µg/ml; Sigma Aldrich, München, Germany) for 2h before seeding. The cells were seeded in metal cloning rings in the middle of a well and incubated for 1h at 37°C, allowing them to attach and spread. After removing the cloning rings carefully and washing the cells twice with PBS, new serum-free medium was introduced. The plates were placed under a microscope (Olympus IX81) in a chamber providing a humidified atmosphere at 37°C. Pictures of two distinct positions from each cell circle were taken every hour over a period of 24h. Areas covered by cells at different time points were measured with the ImageJ program.

2.2.1.11 Adhesion Assay

96-multiwell tissue culture plates were coated with the following human proteins by overnight adsorption at 4°C: 10µg/ml recombinant collagen IV, 10µg/ml recombinant collagen I, 5µg/ml human laminin-332, matrigel. Coating with 100% FCS or 1% heat inactivated BSA were used as positive and negative controls, respectively. After saturation of the wells with 1% heat inactivated BSA (fraction V, Sigma Aldrich, München, Germany) for 1h at 37°C, plates were washed with PBS and 40,000 ADAM-9 down-regulated or control cells were seeded in 100µl medium containing 0.5% BSA supplemented with insulin-transferrin-sodium selenite (ITS, Sigma Aldrich, München, Germany). The cells were allowed to adhere to the different proteins for 1h at 37°C. Subsequently, non adherent cells were washed away by two washes with PBS and remaining cells were fixed with 4% paraformaldehyde (PFA) for 10min at RT. After staining the cells for 15min with 0.5% crystal violet, retained stain was released using 0.1M sodium citrate and measured by color reading at 595nm with an ELISA reader (1420 Multilabel Counter VICTOR³_{TM}, Perkin Elmer, Rodgau, Germany). A blank value corresponding to uncoated wells was subtracted after the measurement.

2.2.1.12 Cell-cell adhesion assay

For cell-cell adhesion assays, B16-F1 melanoma cells, which were stably transfected with a scrambled shRNA or with shRNA targeted to ADAM-9 (chapter 2.2.1.5) were labeled by incubation of subconfluent cell layers with 10 μ M of Cell TrackerTM Green BODIPY (8-choromethyl-4-4difluoro-1,3,5,7-tetramethyl-4-bora-3a,4a-diaza-s-indacene; Invitrogen, Darmstadt, Germany) diluted in serum-free medium for 30min. The BODIPY can pass freely through the cell membrane and is intracellularly transformed into a cell-impermeable fluorescent dye-thioether by a glutathione-s-transferase mediated reaction. After labeling, the cells were washed twice with PBS, incubated for 45min in serum-free medium and subsequently detached using 0.5% EDTA.

For the assay 70,000 sEND-1 murine endothelial cells per well were seeded in 96 multiwell tissue culture plates in normal growth medium and allowed to attach and form a confluent monolayer for 6h. Subsequently the cells were washed three times with PBS and activated with 50ng/ml human recombinant TNF- α (MiltenyiBiotec, Bergisch-Gladbach, Germany) diluted in serum-free medium (Sikorski *et al.*, 1993; McAteer *et al.*, 2008). After 18h the cells were washed with PBS three times and 40,000 labeled B16-F1 cells were plated in 100 μ l serum-free medium on top of the endothelial cells. To ensure that equal cell numbers were used, the fluorescence of suspended cells was measured directly before plating the melanoma cells. After 1h incubation time at 37°C, non-attached cells were carefully removed by two washes in PBS and cells lysed with 2% SDS diluted in PBS. The extent of adhesion was measured by fluorescence reading (absorption 485nm/emission 535nm) with an ELISA reader (1420 Multilabel Counter VICTOR³_{TM}, Perkin Elmer, Rodgau, Germany). A blank value corresponding to wells containing only 2% SDS was subtracted from the measurement. Alternatively, after removing non-adherent cells, cultures were fixed with 4% PFA for 10min at RT and attached cells were visualized and images recorded using an Olympus IX81 microscope.

For analysis of adhesion molecules induced by TNF- α stimulation of sEND-1 cells, the cells were seeded and stimulated as indicated above 18h prior to processing them for RNA extraction.

2.2.1.13 Fluorescence activated cell sorting (FACS)

For FACS analysis 40,000 cells per cm² were plated in serum-free medium on plastic tissue culture plates or plates coated with 10 μ g/ml human recombinant collagen IV (BD Biosciences, Heidelberg, Germany) by overnight adsorption at 4°C. After 2h adhesion, cells were detached using 0.1% Trypsin at 37°C, collected in serum-free medium, centrifuged for 5min and resuspended in FACS buffer. For staining 100,000 cells were incubated with the first antibodies in ~100 μ l FACS buffer for 1h on ice. Subsequently the cells were washed with 1ml FACS buffer and incubated with corresponding fluorescently labelled secondary

antibodies (1:500; Invitrogen, Darmstadt, Germany) for 30min on ice. Cells were washed with 1ml FACS buffer and 7-AAD (7-Amino-Actinomycin; 1:20; eBioscience Inc., San Diego, CA, USA) was added 10min before the analysis to detect dead cells. Samples were analyzed with the flow cytometer with the appropriate laser and software. Used primary antibodies and the corresponding secondary antibodies are listed in Table 4. Each staining was performed in triplicate and included a negative control where first antibody was replaced by isotype specific antibodies.

Table 4: Primary and secondary antibodies used for FACS analysis.

Antigen	Source	Clone	Host, Type	Dilution	Secondary antibody
human integrin α 1	Chemicon	FB12	mouse, monoclonal	1:1000	Alexa Fluor 488 goat anti mouse IgG 1:500
human integrin α 2	Chemicon	P1E6	mouse, monoclonal	1:1000	Alexa Fluor 488 goat anti mouse IgG 1:500
human integrin α 3	Chemicon	ASC-1	mouse, monoclonal	1:1000	Alexa Fluor 488 goat anti mouse IgG 1:500
human integrin β 1	Prof. Hemler, Dana-Farber Cancer Institute, Harvard Medical School	12G10	mouse, monoclonal	1:1000	Alexa Fluor 488 goat anti mouse IgG 1:500
unspecific	BD Biosciences	/	purified mouse IgG1	1:1000	Alexa Fluor 488 goat anti mouse IgG 1:500

2.2.2 Protein analysis

2.2.2.1 Preparation of cell lysates

“Crude” membrane preparation:

For crude membrane preparations, subconfluent cell monolayers were washed with PBS, collected by scraping and washed twice with PBS for 5min at 200g at 4°C. The cell pellet was suspended in 1ml Ca-free PBS supplemented with protease inhibitors (Sigma Aldrich, München, Germany) and subjected to three cycles of freezing/thawing using a dry ice/EtOH bath and a 37°C water bath. Lysates were further homogenized by shearing 20 times through a 20G needle and centrifuged for 5 min at 400g at 4°C. Collected supernatants were centrifuged at 1500g at 4°C for 30min to pellet cell membranes, which were resuspended in PBS containing protease inhibitors.

Preparation of whole cell lysates:

Subconfluent cell monolayers were directly lysed in RIPA buffer containing general protease inhibitors (Sigma Aldrich, München, Germany). To study phosphorylated proteins, the RIPA buffer was supplemented additionally with 1mM sodium vanadate, to inhibit phosphatase activity. Lysates were incubated over night under rotation at 4°C followed by centrifugation in a precooled centrifuge (5min, 1500g) and the supernatants transferred to new tubes.

The protein concentration was determined using a commercial protein assay (BCA™ Protein assay, Pierce, Bonn, Germany) according to the manufacturer's instructions. A freshly prepared gradient of BSA served as standard curve. Lysates were stored at -20°C until use.

2.2.2.2 SDS-PAGE and immunoblotting

Proteins were electrophoretically separated on 10 or 12% polyacrylamide gels containing SDS (SDS-PAGE) and transferred onto a Hybond-C Super™ nitrocellulose membrane (Amersham, Freiburg, Germany) by semi-dry-blotting system (Sigma-Aldrich, München, Germany). Ponceau Red staining of the membranes was used to assess transfer efficiency. Blocking was performed in 5% milk PBS-Tween (0.5% Tween) at RT for 1h. To analyze phosphorylated proteins the blocking buffer also contained 5mM sodium fluoride, to inhibit phosphatase activity. Incubation with the primary antibodies (for information see Table 5) was conducted in blocking buffer over night at 4°C. The next day, after extensive washes, blots were incubated in HRP-coupled secondary antibodies (1:2000 in 5% milk powder in PBS-Tween; Dako, Glostrup, Denmark) at RT for 1h, followed by detection with the ECL system (ECL®, Amersham, Freiburg, Germany) and membranes exposed to X-ray films (Thermo Fisher, Karlsruhe, Germany). Specific signals were quantified using the Image J program.

Table 5: Primary and secondary antibodies used for immunoblot analysis.

Antigen	Source	Host, Type	Dilution	Secondary antibody
human ADAM-9 ectodomain	R&D Systems	goat, polyclonal	1:500	polyclonal HRP-coupled anti goat IgG 1:2000
mouse ADAM-9 ectodomain	R&D Systems	goat, polyclonal	1:500	polyclonal HRP-coupled anti goat IgG 1:2000
human β -actin	Sigma Aldrich	rabbit, polyclonal	1:2000	polyclonal HRP-coupled anti rabbit IgG 1:2000
human ERK1/2	Santa Cruz	rabbit, polyclonal	1:500	polyclonal HRP-coupled anti rabbit IgG 1:2000
human JNK1/2/3	Santa Cruz	rabbit, polyclonal	1:500	polyclonal HRP-coupled anti rabbit IgG 1:2000
human laminin β 3 chain	Prof. M. Koch, Cologne	rabbit, polyclonal	1:200	polyclonal HRP-coupled anti rabbit IgG 1:2000
human pERK	Santa Cruz	mouse, polyclonal	1:500	polyclonal HRP-coupled anti mouse IgG 1:2000
human pJNK	Santa Cruz	mouse, monoclonal	1:500	polyclonal HRP-coupled anti mouse IgG 1:2000

2.2.2.3 Immunohistochemistry

Immunohistochemical stainings were performed on cryo or paraffin sections (7 μ m). Cryosections were fixed with ice-cold acetone for 10min at RT and allowed to air-dry or, alternatively, fixed using Roti®-Histofix 4% (Roth, Karlsruhe, Germany) for 10min at RT.

Paraffin sections were deparaffinized in xylene (20 min) followed by a graded alcohol series (1min each): 100 % 2-Propanol, 96% EtOH, 75% EtOH, aqua bidest.

To detect collagen type IV, deparaffinized sections were pre-treated for 5min at 37°C with pepsin (DCS, Hamburg, Germany), for antigen retrieval. Prior to incubation with primary antibodies, unspecific binding sites were blocked by incubation with 10% normal goat serum for 1h. After washing, sections were incubated at 4°C over night with the first antibodies in PBS. For anti-CD31, anti-LVYE-1 and anti laminin α 3-chain staining, antibodies were diluted in PBS containing 1% BSA. Bound first antibodies were visualized by incubation with corresponding fluorescently labelled secondary antibodies (1:800; Invitrogen, Darmstadt, Germany). Cell nuclei were visualized with fluorescent dye DAPI (4,6-diamidino-2-phenylindol; Sigma Aldrich, München, Germany) or with propidiumiodid (Sigma Aldrich, München, Germany). In Table 6 the used primary antibodies and the corresponding secondary antibodies are shown. Negative controls were performed by omission of the primary antibodies. Images were captured with a Nikon Eclipse E800 microscope and a Nikon Digital Camera DXM 1200 connected to a computer equipped with an imaging program (NIS-Elements AR 2.30, NIS-Elements, Melville, NY, USA).

Table 6: Information about antibodies used for immunohistochemistry.

Antigen	Source	Host, Type	Dilution	Secondary antibody
mouse ADAM-9 ectodomain	R&D Systems	rat, monoclonal	1:50	Alexa Fluor 488 goat anti rat IgG 1:800
mouse CD3 ϵ	Acris	rabbit, polyclonal	1:200	Alexa Fluor 488 goat anti rabbit IgG 1:800
mouse CD4	Abcam	rat, monoclonal	1:200	Alexa Fluor 488 goat anti rat IgG 1:800
mouse CD8	Abcam	rat, monoclonal	1:200	Alexa Fluor 488 goat anti rat IgG 1:800
mouse CD31 (platelet endothelial cell adhesion molecule-1)	BD Biosciences	rat, monoclonal	1:1000	Alexa Fluor 488 goat anti rat IgG 1:800
mouse CD45	Serotec	rat, monoclonal	1:200	Alexa Fluor 488 goat anti rat IgG 1:800
mouse CD68	Serotec	rat, monoclonal	1:60	Alexa Fluor 488 goat anti rat IgG 1:800
mouse cleaved caspase-3	Cell Signalling	rabbit, polyclonal	1:200	Alexa Fluor 594 goat anti rabbit IgG 1:800
human collagen IV	Biogenex	mouse, monoclonal	ready to use	Alexa Fluor 488 goat anti mouse IgG 1:800
human collagen IV	Progen	rabbit, polyclonal	1:100	Alexa Fluor 488 goat anti rabbit IgG 1:800
mouse CXCR4	R&D Systems	rat, monoclonal	1:50	Alexa Fluor 488 goat anti rat IgG 1:800
mouse cytokeratin 14	Covance	rabbit, polyclonal	1:1000	Alexa Fluor 594 goat anti rabbit IgG 1:800
mouse Ki67	Dako	rat, monoclonal	1:100	Alexa Fluor 488 goat anti rat IgG 1:800
human laminin α 3-chain	Prof. M. Aumailley, Cologne	mouse, monoclonal	1:10	Alexa Fluor 488 goat anti mouse IgG 1:800
human laminin β 3-chain	Prof. M. Koch, Cologne	rabbit, polyclonal	1:200	Alexa Fluor 488 goat anti rabbit IgG 1:800

mouse loricrin	Covance	rabbit, polyclonal	1:2000	Alexa Fluor 594 goat anti rabbit IgG 1:800
mouse Ly6B.2 alloantigen (neutrophils)	Serotec	rat, monoclonal	1:100	Alexa Fluor 488 goat anti rat IgG 1:800
mouse LYVE-1 (lymphatic vessel endothelial hyaluronan receptor-1)	Abcam	rabbit, polyclonal	1:800	Alexa Fluor 594 goat anti rabbit IgG 1:800
mouse TRP-1 (tyrosinase related protein-1)	Prof. V. Hearing, NIH, Bethesda	rabbit, polyclonal	1:100	Alexa Fluor 488 goat anti rabbit IgG 1:800

2.2.2.4 Immunocytochemistry

For cellular staining of aquaporin-3, α -tubulin and integrin receptor subunits cells were fixed with 4% PFA for 5min and permeabilized by incubation with 0.1% Tween in PBS. Unspecific binding sites were blocked with 10% BSA in PBS (for aquaporin-3 and α -tubulin) or with 10% normal goat serum diluted in 0.05% PBST (for anti integrin antibodies) for 1h at RT. Incubation with primary antibodies diluted in PBS (for aquaporin-3 and α -tubulin) or 0.05% PBST (for anti-integrin antibodies) was carried out over night at 4°C. Bound primary antibodies were detected by incubation with fluorescently labelled secondary antibodies (1:800; Invitrogen, Darmstadt, Germany). Information about the primary and secondary antibodies used are supplied in Table 7. For staining of the actin cytoskeleton cells were incubated with fluorescently labelled phalloidin (1:200 in PBS; Sigma Aldrich) for 30min at RT. Cell nuclei were visualized with DAPI (Sigma Aldrich, München, Germany). Images were captured with a Nikon Eclipse E800 microscope and a Nikon Digital Camera DXM 1200 connected to a computer equipped with an imaging program (NIS-Elements AR 2.30, NIS-Elements, Melville, NY, USA).

Table 7: Information about antibodies used for immunocytochemistry.

Antigen	Company	Host, Type	Dilution	Secondary antibody
human aquaporin-3	Santa Cruz	goat, polyclonal	1:100	Alexa Fluor 594 donkey anti goat IgG 1:800
human integrin α 1	Chemicon	rabbit, polyclonal	1:500	Alexa Fluor 488 goat anti rabbit IgG 1:800
human integrin α 2	Chemicon	rabbit, polyclonal	1:500	Alexa Fluor 488 goat anti rabbit IgG 1:800
human integrin α 3	Chemicon	rabbit, polyclonal	1:500	Alexa Fluor 488 goat anti rabbit IgG 1:800
human integrin β 1	Prof. Hemler, Dana-Farber Cancer Institute, Harvard Medical School	mouse, monoclonal	1:500	Alexa Fluor 488 goat anti mouse IgG 1:800
human α -tubulin	Oncogene	mouse, monoclonal	1:100	Alexa Fluor 488 goat anti mouse IgG 1:800

2.2.2.5 Histological analysis

For histological analysis of mouse and human tissues, specimens were either directly embedded in Tissue-Tek® or fixed for 12h in Roti®-Histofix 4% (Roth, Karlsruhe, Germany) at 4°C and embedded in paraffin. Paraffin sections (7µm) of mouse skin from different parts of the body (head, back, belly, tail) were stained with H&E (Thermo Fischer Scientific, Schwerte, Germany). To analyze collagen organization and distribution Sirius Red staining (Junqueira *et al.*, 1979) was used.

Haematoxylin and eosin staining (H&E-staining):

Deparaffinized skin sections (chapter 2.2.2.3) were first stained with hematoxylin for 3 to 5min and rinsed with lukewarm tap water. Slides were shortly (2sec) destained by dipping in acid alcohol (1% HCl in 70% EtOH) and stained with Eosin for 5-8sec.

Sirius Red staining:

After deparaffinizing (chapter 2.2.2.3), sections were stained for 5min with Weigert's iron haematoxylin (Waldeck GmbH, Münster, Germany) followed by several rinsing steps in lukewarm tap water. After destaining cell cytoplasm in 1% HCl (in 96% EtOH), rinsed sections were incubated in 0.5% Sirius Red in watery picric acid for 1h at RT and rinsed twice with 0.5% acetic acid.

All rinsed sections were dehydrated using ascending alcohol series, mounted with GLC™ Mounting Medium (Sakura, Zoeterwoude, Netherlands) and covered with a cover slip.

2.2.2.6 Processing of basement membrane proteins by ADAM-9

Enzymatic assay with BM proteins were performed using 0.5µg of recombinant human recombinant ADAM-9 and 0.5µg of proteins in a total volume of 20µl substrate buffer overnight. The following human proteins were used: recombinant fibronectin, collagen IV and laminin 511, or purified laminin 332.

For the enzymatic processing of recombinant human laminin β3-chain, 1µg of the recombinant human laminin β3-chain (N-terminal fragment; amino acids 4-575; kindly provided by Prof. M. Koch) and 1µg of human recombinant ADAM-9 were used. Protein preparations without recombinant ADAM-9 or with ADAM-9 and 10mM EDTA used as inhibitor of enzyme activity, were used as controls. Processing was carried out overnight at 37°C and proteins were subsequently separated on 1mm NuPAGE® 4-12% Bis-Tris-Gels (Invitrogen, Karlsruhe, Germany) under reducing conditions. Protein bands were visualized by silver staining using the SilverQuest™ Silver staining kit (Invitrogen, Karlsruhe, Germany) according to the manufacturer's instructions or by immunoblotting (chapter 2.2.2.2).

For peptide mass fingerprinting, protein bands were cut out from the silver stained gel and processed by LC-MS/MS (liquid-chromatographie mass-spectroscopy/mass-spectroscopy) after pre-digestion with trypsin. The obtained fragment spectra were used for protein identification using Mascot searches in fragmentation libraries. The LC-MS/MS sequencing

including trypsin pre-digestion and protein identification was performed in the Central Bioanalytic Core of the Center for Molecular Medicine Cologne.

2.2.2.7 Cytokine antibody array

Cytokine antibody array was performed using serum from animals (see 2.2.4.3). Raybio[®] Mouse Cytokine Antibody Array-3 (HölzelDiagnostika, Cologne, Germany) was used according to the manufacturer's manual. Briefly, membranes were blocked for 30min at RT with blocking buffer, then incubated overnight at 4°C with 500µl blocking buffer containing 60µl of serum pooled from three animals (20µl from each animal). After five washes, the membranes were incubated with biotin-conjugated anti-cytokine antibodies diluted 1:200 with blocking buffer overnight at 4°C. Bound antibodies were detected with HRP-conjugated streptavidin secondary antibodies and proteins visualized by chemiluminescence detection system. Specific signals were quantified using the ImageJ program. The blank was subtracted from all values, which were normalized to the internal positive control and expressed as relative expression of genetically modified versus control animals. Only proteins, which were more than 2-fold regulated, were considered.

2.2.3 Analysis of nucleic acids

2.2.3.1 RNA isolation

Total RNA was isolated from subconfluent cells. After one wash in PBS, cells were directly lysed into RNAzol (WAK Chemie, Steinbach, Germany) for 5min at RT and collected by scraping. For isolation of RNA from blood, 125µl blood was taken from heart puncture and mixed with 875µl RNAzol. DNA was sheared by 20 passages through a 27G needle, RNA extracted using 1/3 volume of chloroform and precipitated by adding 1 volume of isopropanol for 30min on dry ice. After centrifugation for 15min at 1500g, RNA pellet was washed using 75% EtOH, air dried for 10min and resuspended in DEPC-treated H₂O. Integrity of RNA was analyzed by electrophoresis on a 1% agarose-TBE gel and concentration determined by measuring the optical density at 260nm ($OD_{260} \times 40\mu\text{g/ml RNA}$).

2.2.3.2 Reverse transcription and polymerase chain reaction (RT-PCR)

1 µg of total RNA protected by adding RNase Inhibitors (20U/µl) was reverse transcribed into cDNA by using Oligo d(T)₁₆ primers (50µM), MuLV reverse transcriptase (50U/µl) and 10µM of dNTPs. Reverse transcription was performed using the following conditions: 21°C 10min; 42°C 20min; 99°C 5min.

After reverse transcription, PCR fragments were generated from cDNA using REDtaq[™]ReadyMix[™] PCR Reaction Mix (Sigma Aldrich, München, Germany) and 10µM of each forward and reverse specific primers whose sequences are shown in Table 8. PCR amplification was performed with initial denaturation step at 94°C for 5min, followed by cycles

of 1min at 94°C, 1min at annealing temperature, 1min elongation at 72°C. The cycle number used was within the linear amplification range. To detect transcripts of Pmel17/gp100 used as markers for melanoma cells (Kobayashi *et al.*, 1994; Singh *et al.*, 2008) a nested PCR was used. The cDNA was first amplified using external Pmel17 primers and the fragment reamplified using nested primers and 2µl of the first PCR reaction (Tsukamoto *et al.*, 2000). Figure 6 shows a schematic overview about the performance of the nested PCR. Size of PCR products was analyzed on agarose gels in TBE. Densitometry was performed using the ImageJ software.

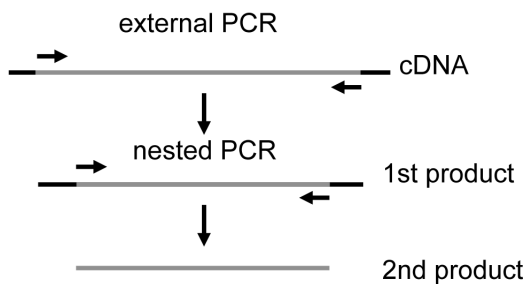


Figure 6: Schematic overview about the nested PCR.

Table 8: Information about primers used in RT-PCR reactions.

Human gene	Primer sequences 5'-3'	Annealing temperature [°C]	Cycle number	Product size [bp]
ADAM-9	CCTCGGGGACCCTTCGTGT	52	30	424
	ATCCCATAACTCGCATTCTCTAAA			
ADAM-10	ACACCAGCGTGCCAAAAGAG	58	30	440
	CCTCTACACCAGTCATCTGG			
ADAM-12	TGCAGGCAGAGGCTTCTGAGG	58	30	514
	GTTTGGCTTTGGAGGAAGCACAG			
ADAM-15	GGCTGGCAGTGTCGTCCTACCA	65	30	421
	GTGCACCCAGCTGCAGTTCAGC			
ADAM-17	TTTCAAGTTCGTGGTGGTGG	52	30	451
	TTCCCTCTGCCCATGTATC			
ADAM-19	GAACATCCGGATTGCTCTCG	52	30	456
	TGGGTCATGCCAAAGTTGTG			
ADAM-21	CCCTCCCAGCATTTCACTTC	57	30	299
	AAGCCCCAAAACAAGCAC			
Aquaporin-3	GAAAGTTCCAGGAGGGTGTGTAT	52	30	334
	CGGATCCCTAAGACTGTAAC			
IL-1α	CCAAGATGAAGACCAACCAG	54	33	261
	TGAGATTTTTAGAGTAACAGG			
MMP-2	AAGATTCCAGAGAGTGGCTC	58	35	470
	TGCACTGTCAGTGACTTCA			
MMP-9	CAGGCTCCGGTGGACGATGCC	60	30	243
	GCCCTCAGAGAATCGCCAGTA			
MMP-13	CTGGCTGCCTTCCTCTTCTT	58	35	608
	ATGTCAGCAATGCCATCGTG			
MMP-14	ATGTTCGAAGGAAGCGCTAC	55	35	948
	TCCAGAAGAGAGCAGCATCA			
S26	CCGTGCCTCCAAGATGACAA	52	30	375
	AGAACTCAGCTCCTTACA			

Mouse gene	Primer sequences 5'-3'	Annealing temperature [°C]	Cycle number	Product size [bp]
ADAM-9	TTGCCTCTCTGCGACTAAG	48	40	130
	GTAAGAGATCTGCTGTGAACTG			
β1 integrin	GCAGAGCATAAAGAATGTGT	60	30	335
	CAAGGCAAGGCCAATAAGAA			
β3 integrin	TTACCCCGTGGACATCTACTA	50	30	456
	AGTCTTCCATCCAGGGCAATA			
ICAM-1	GTGTCTCCTTCTTTGACACT	48	30	237
	ATGACATGCTTGAGCCAGG			
Pmel17 (external)	CGGATGGTCAGGTTATCTGG	58	30	334
	ATGGTGAAGGTTGAACTGGC			
Pmel17 (nested)	ACAGCCAGTGTATCCACAGG	58	30	202
	ACTTCCATTGTGTGTGTGCC			
S26	AATGTGCAGCCCATTTCGATG	56	30	324
	CTTCCGTCCTTACAAAACGG			
VCAM	GAGAACCCAGATAGACAGCC	50	30	238
	CAAACACTTGAGCGTGACC			
VE-cadherin	ACGGACAAGATCAGCTCCTC	57	30	200
	TCTCTTCATCGATGTGCATT			

2.2.3.3 Quantitative real-time PCR

For quantitative real-time PCR analysis 1 µg of RNA was reverse transcribed according to the protocol described in chapter 2.2.3.2. Each PCR reaction was carried out in triplicate in a total volume of 20 µl, containing 10 µl of Power SYBR®Green PCR Master Mix (Applied Biosciences, Foster City, CA, USA), 0.2 µl of each, 10 µM forward and reverse primers, 8.6 µl water and 1 µl cDNA. Forward and reverse primer sequences, annealing temperature, cycle number and product size for every primer pair used, are summarized in Table 9. The thermal cycling conditions were set to 95°C for 2min, followed by 40 cycles of amplification at 95°C for 10sec and 60°C for 2min for each cycle. The specificity of the PCR products was confirmed by melting curve analysis.

The relative expression levels were determined by normalizing to the house keeping gene to S26 signals used as control and calculating the expression by the comparative $\Delta\Delta C_t$ method.

Table 9: Information about primers used in real-time PCR reactions.

Human gene	Primer sequences 5'-3'	Annealing temperature [°C]	Cycle number	Product size [bp]
ADAM-9	CCTCGGGGACCCTTCGTGT	60	40	424
	ATCCCATAACTCGCATTCTCTAAA			
S26	CCGTGCCTCCAAGATGACAA	60	40	375
	AGAACTCAGCTCCTTACA			
Mouse gene	Primer sequences 5'-3'	Annealing temperature [°C]	Cycle number	Product size [bp]
ADAM-9	TGACCATCCCAACGTACAGA	60	40	131
	TTCCAAAACCTGGCATTCTCC			
S26	GTGCCATCCATAGCAAGGTT	60	40	105
	GTGGAGGTCGAGGTGCAG			

2.2.3.4 Analysis of genomic DNA

Approximately 0.5cm of the tail of three week old mice were cut and incubated in 750µl tail lysis buffer supplemented with 50U/ml proteinase K (Fermentas, St. Leon-Rot, Germany) over night under shaking conditions (~80g) at 55°C. The next day 250µl of 6M NaCl were added and the solution was mixed at 100g for additional 5min at 55°C. Subsequently the solution was centrifuged for 10min at 1500g at RT. The supernatant was mixed with 1 volume of isopropanol to precipitate genomic DNA and centrifuged for 10min at 1500g at RT. The DNA pellet was washed with 70% EtOH, air dried and suspended in H₂O by incubation at 50°C for 1h. The genomic DNA was stored at 4°C until genotyping.

PCR fragments were generated from genomic DNA using REDtaq™ReadyMix™ PCR Reaction Mix (Sigma Aldrich, München, Germany) and 10µM of each forward and reverse specific primers. Forward and reverse primer sequences, annealing temperature, cycle number and product sizes for every primer pair used, are summarized in Table 10. PCR amplification for ADAM-9 was initiated by incubation at 94°C for 5min and followed by cycles of amplification of 1min at 94°C, 45sec at annealing temperature, 1min at 72°C. For CDK4 PCR amplification was initiated by incubation at 94°C for 5min and followed by cycles of 30sec at 94°C, 40sec at annealing temperature, 1min at 72°C. Size of PCR products was analyzed on agarose gels in TBE.

Table 10: Primers and amplification products for genotyping PCR

Mouse gene	Primer sequences 5'-3'	Annealing temperature [°C]	Cycle number	Product sizes [bp]
ADAM-9	ACTTGGAACAGACTGTCCA	54	30	121 wt 1000 ko
	CGTTCATAGTTCTCAGAAG			
CDK4	ACTGTGTGATCCTCTTTGTG	54	40	640 wt 740 mut
	ATCCATCAGCCTGAGAAG			

2.2.4 In vivo experiments

2.2.4.1 Animal housing

All animals were kept in the animal facility of the Institute of Pathology or Pharmacology of the University of Cologne, in cages covered with air filters under specific pathogen-free conditions with 12h light-dark cycle and free access to water and food. All animal experiments were performed in compliance with the German Law for Welfare of Laboratory Animals and approved by the Regierungspräsidium Köln, Germany. Reference for official approval: 50.203.2-K 37a, 20/05 and 87-51.04.2010 A356.

2.2.4.2 Generation of Adam-9^{-/-}/Hgf/Cdk4^{R24C/R24C} animals

Hgf/Cdk4^{R24C/R24C} C57/Bl6 mice (Tormo, *et al.*, 2006) were crossbred with Adam-9^{-/-} Sv129/Bl6 mice (Weskamp *et al.*, 2002). A summary of the crossbreeding scheme for the generation of the animals is depicted in Table 11.

Table 11: Overview about the generation of Adam-9^{+/-}//Hgf/Cdk4^{R24C/R24C} and Adam-9^{-/-}//Hgf/Cdk4^{R24C/R24C} animals.

Gener-ation	Genotype		Offspring used for following generation
	female	male	
	Adam-9 ^{-/-}	Hgf/Cdk4 ^{R24C/R24C}	♀ Adam-9 ^{+/-} //Cdk4 ^{R24C/wt} ♂ Adam-9 ^{+/-} //Hgf/Cdk4 ^{R24C/wt}
F1	Adam-9 ^{+/-} //Cdk4 ^{R24C/wt}	Adam-9 ^{+/-} //Hgf/Cdk4 ^{R24C/wt}	♀ Adam-9 ^{-/-} //Cdk4 ^{R24C/wt} ♀ Adam-9 ^{+/-} //Cdk4 ^{R24C/R24C} ♂ Adam-9 ^{-/-} //Hgf/Cdk4 ^{R24C/wt} ♂ Adam-9 ^{+/-} //Hgf/Cdk4 ^{R24C/R24C}
F2	Adam-9 ^{+/-} //Cdk4 ^{R24C/R24C} or Adam-9 ^{-/-} //Cdk4 ^{R24C/wt}	Adam-9 ^{+/-} //Hgf/Cdk4 ^{R24C/R24C} or Adam-9 ^{-/-} //Hgf/Cdk4 ^{R24C/wt}	♀ Adam-9 ^{-/-} //Cdk4 ^{R24C/R24C} ♀ Adam-9 ^{+/-} //Cdk4 ^{R24C/R24C} ♂ Adam-9 ^{-/-} //Hgf/Cdk4 ^{R24C/R24C} ♂ Adam-9 ^{+/-} //Hgf/Cdk4 ^{R24C/R24C}
F3	Adam-9 ^{-/-} //Cdk4 ^{R24C/R24C} and Adam-9 ^{+/-} //Cdk4 ^{R24C/R24C}	Adam-9 ^{-/-} //Hgf/Cdk4 ^{R24C/R24C} and Adam-9 ^{+/-} //Hgf/Cdk4 ^{R24C/R24C}	♀ Adam-9 ^{-/-} //Cdk4 ^{R24C/R24C} ♀ Adam-9 ^{+/-} //Cdk4 ^{R24C/R24C} ♂ Adam-9 ^{-/-} //Hgf/Cdk4 ^{R24C/R24C} ♂ Adam-9 ^{+/-} //Hgf/Cdk4 ^{R24C/R24C}

Briefly, male Hgf/Cdk4^{R24C/R24C} mice, which were heterozygous for Hgf were paired with Adam-9^{-/-} female mice. The offspring was composed of approximately one-third Adam-9^{+/-}//Hgf/Cdk4^{R24C/wt} animals. Animals, which were positive for Hgf, could be phenotypically distinguished from their Hgf negative littermates, because overexpression of Hgf leads to a dark skin phenotype, which was most prominent at the ears and the bottom side of the paws. Heterozygous Adam-9^{+/-}//Hgf/Cdk4^{R24C/wt} male mice were paired with Adam-9^{+/-}//Cdk4^{R24C/wt} female mice. Pairing of heterozygous male Adam-9^{+/-}//Hgf/Cdk4^{R24C/wt} directly with female Adam-9^{+/-}//Hgf/Cdk4^{R24C/wt} mice was not possible as female mice carrying the Hgf transgene are not fertile, due to presently unknown reasons. The animals used for the experiments were obtained from the F3 progeny and were Adam-9^{-/-}//Hgf/Cdk4^{R24C/R24C} mice and Adam-9^{+/-}//Hgf/Cdk4^{R24C/R24C} littermates. In all following chapters the Adam-9^{+/-}//Hgf/Cdk4^{R24C/R24C} mice will be termed control and the Adam-9^{-/-}//Hgf/Cdk4^{R24C/R24C} mice Adam-9^{mutated/ko}.

2.2.4.3 Induction and analysis of melanoma formation

At postnatal day three the back of male and female Adam-9^{mutated/ko} and littermate control animals was painted with 40µg DMBA (Sigma Aldrich, München, Germany) dissolved in a final volume of 10µl acetone (16nmol/µl). The number of developing tumors was carefully recorded on a weekly basis from week four after DMBA treatment onwards. When the animals were killed the volume (mm³) of all developed tumors was calculated after measurement of the tumor size in three bisecting diameters using a digital caliper. Additionally tumor growth was recorded by digital photography. Most of the animals were killed when largest tumors exceeded a size of at least 200 mm³ at ~week 13 after DMBA treatment. Occasionally animals were also killed at earlier time points due to signs of illness.

Animals were killed by CO₂ inhalation and lung, liver, spleen, kidneys, heart, brain and the intestinal tract were carefully inspected for macroscopically visible metastases. The number of black nodules on the organ surface was counted as indicator of metastatic spread of the primary cutaneous tumors. To determine the metastatic spread to the lymph nodes, the size (mm³) of axillary and groin lymph nodes was determined by measurement of lymph node size in three bisecting diameters. The largest tumors were excised with the surrounding stroma and all tissues were either processed for paraffin embedding or directly embedded in Tissue-Tek[®] (chapter 2.2.2.5).

At the time when the animals were killed, also blood was collected for further analysis. To obtain serum, 400-700µl blood were taken by heart puncture using a 2ml syringe and a 22G needle. The blood was allowed to clot for ~2h on ice and the serum was separated from the cellular components by centrifugation at 4°C for 30min at 110g. The cleared serum was stored at -20°C until using for further analysis. For isolation of RNA from the blood see chapter 2.2.3.1.

2.2.4.4 Tail vein injection of B16-F1 melanoma cells

For tail vein injection of B16-F1 cells (chapter 2.2.1.5) six to ten weeks old female and male Adam-9^{+/+} Sv129/Bl6 mice were used. To dilate and better visualize the blood vessels, the tail of the mice was illuminated using a heat lamp for 1min. Afterwards the mice were transferred to a holding device and 100,000 B16-F1 cells in a final volume of 100µl PBS were injected into the tail vein. The animals were sacrificed three weeks after injection and the inner organs including lung, liver, kidney, heart, stomach, intestine, spleen, lymph nodes and brain were carefully prepared and inspected for visible metastases. The number of black nodules on the organ surface was counted as indicator of metastasis. Additionally formed metastases were recorded by digital photography.

2.2.5 Statistical analysis

Statistically significant differences were calculated employing the Graph Pad Prism 4.03 software using two-tailed unpaired or paired Student's t-test, depending if independent or matched samples were analyzed with p<0.05 considered to be statistically significant.

3. Results

3.1 Analysis of ADAM expression in melanoma cells

3.1.1 ADAM expression in human melanoma cells lines

Expression of several ADAM proteases was shown in melanoma. ADAM-9 expression was detected in both, tumor cells and peritumoral stromal cells (Zigrino *et al.*, 2005) whereas others, e.g. ADAM-15, were primarily detected in melanoma cells of primary tumors (Ungerer *et al.*, 2010). To analyze which other known ADAMs are expressed by melanoma cells, RT-PCR analysis for ADAM-9, -10, -15 and -17 was performed on RNA isolated from cell monolayers of cell lines with various invasive capacities. The melanoma cell lines investigated were characterized as: low invasive cell lines: Skmel23, Skmel28, WM164/4, IF6; high invasive cell lines: BLM, MeWo, VMM5; and WM75/6 cells whose invasive capacity is not known. This analysis revealed transcript expression of ADAM-9, -10, -15 and 17 in all assayed cell lines. The expression level of ADAM-10, -15 and 17 varied between the cell lines, the expression of ADAM-9 was comparable. No correlation of the expression level and the invasive capacity was found for any of the analyzed ADAM (Figure 7).

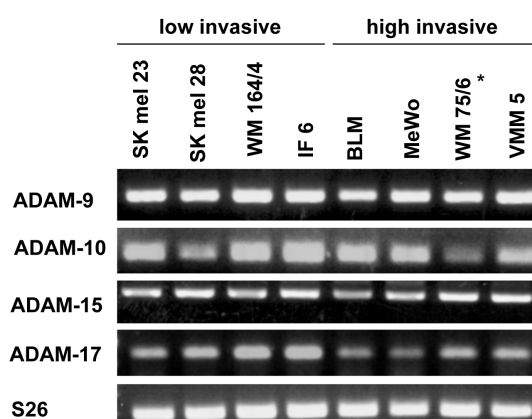


Figure 7: RT-PCR analysis of the expression of ADAMs in human melanoma cell lines. The expression of several ADAMs was analyzed in RNA isolated from human melanoma cell lines after growing to subconfluency in tissue culture plates. The invasive capacities of the used melanoma cell lines are indicated apart from the WM75/6 (*), which has not been tested. Amplification of S26 transcripts was used as loading control. The figure shows a representative of two independent experiments.

3.1.2 ADAM-9 transcript and protein expression

The most ubiquitous expression detected was for ADAM-9 and -15, with a stronger intensity for ADAM-9. However, *in vitro* no correlation between ADAM-9 expression and invasive capacity of the cells was observed.

To further investigate the ADAM-9 expression in melanoma cells, the transcript analysis was extended to three additional cell lines, A375 known to be high invasive (Kozłowski *et al.*, 1984) and the two cell lines Ma-Mel-119 and Ma-Mel-85, which were isolated from a melanoma metastasis, but have not been tested again for invasive potential.

However also for these lines, quite comparable levels of ADAM-9 transcripts were detected. As ADAM-9 is a proteolytic enzyme, protein synthesis was analyzed in an attempt to correlate the presence of the active form of ADAM-9 with cell invasiveness. Immunoblot analysis revealed the presence of the pro- and active form of ADAM-9 in all analyzed cell lines, except from the cell line Ma-Mel-119, which showed no detectable ADAM-9 protein. The low invasive cells lines Skmel23 and Skmel28 and the high invasive lines VMM5 and A375 displayed generally lower protein expression as compared to all other cells. Despite the differences in pro-form detection, e.g. higher in Ma-Mel-86a and WM 75/6, all cells exhibited active ADAM-9 on the cell surface (Figure 8). Thus in steady-state conditions of human melanoma cells, ADAM-9 protein amounts were variable, although expression was comparable on transcript level. However, both analyses failed to indicate any correlation with the invasive capacity of the cells.

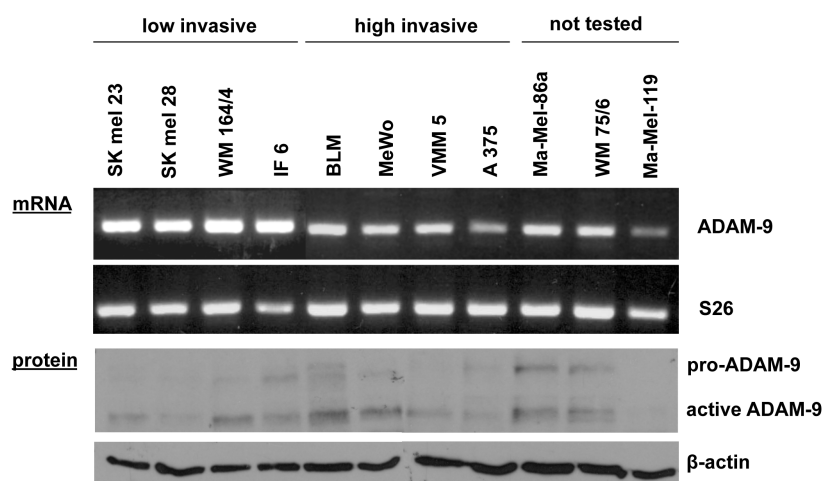


Figure 8: ADAM-9 expression in different melanoma cell lines.

ADAM-9 transcript and protein expression was analyzed in melanoma cell lines of different invasive capacities (chapter 2.2.1.1) by RT-PCR and immunoblot. ADAM-9 expression was variable in all cell lines on mRNA as well as on protein level (pro- and active form). No correlation with the invasive behaviour was observed. S26 or β -actin were used as loading control. The figure shows a representative of two independent experiments.

3.2 *In vitro* analysis of ADAM-9 function in melanoma cells

3.2.1 Stable down-regulation of ADAM-9

The results obtained so far showed that despite the fact that no correlation of ADAM-9 with the invasive characteristics of human melanoma cell lines exists, the active form of ADAM-9 is expressed in the majority of all analyzed melanoma cell lines. To explore the importance of ADAM-9 for tumor growth and invasion, ADAM-9 was stably down-regulated in BLM melanoma cells using shRNA. As control, cells were transfected with shRNA carrying a scrambled sequence not matching with any known sequence. The BLM cells were chosen, because these cells exhibited the highest active ADAM-9 expression among the analyzed cell lines and are characterized by their high invasive and metastatic phenotype. After

transfection, stable cell clones were isolated after selection pressure was applied (chapter 2.2.1.5). ADAM-9 expression in two selected control and ADAM-9 down-regulated clones was determined on transcriptional and protein level. A significant down-regulation of transcripts of about 90% was observed after quantitative real-time PCR analysis using S26 as internal control (shAdam-9 clone 1: 91% inhibition, $p = 0.002$; shAdam-9 clone 2: 88% inhibition, $p = 0.008$). The control clones were set as 100%. A similar result was also visible by RT-PCR analysis of ADAM-9 transcripts in those cells (Figure 9 A). Immunoblot analysis of cell lysates detected a reduction of ADAM-9 pro- and active form in both shADAM-9 clones, 1 and 2 (Figure 9 B). Densitometric analysis of ADAM-9 protein in shADAM-9 clones as compared to control cells, which were set as 100%, revealed a ~90% inhibition of ADAM-9 synthesis after normalization to actin, used as loading control (Figure 9 B). These results indicate that silencing of ADAM-9 in melanoma cells by shRNA resulted in an efficient protein down-regulation. Thus, stable cell clones of BLM melanoma cells with silencing of ADAM-9 have been generated, which can be used in further experiments.

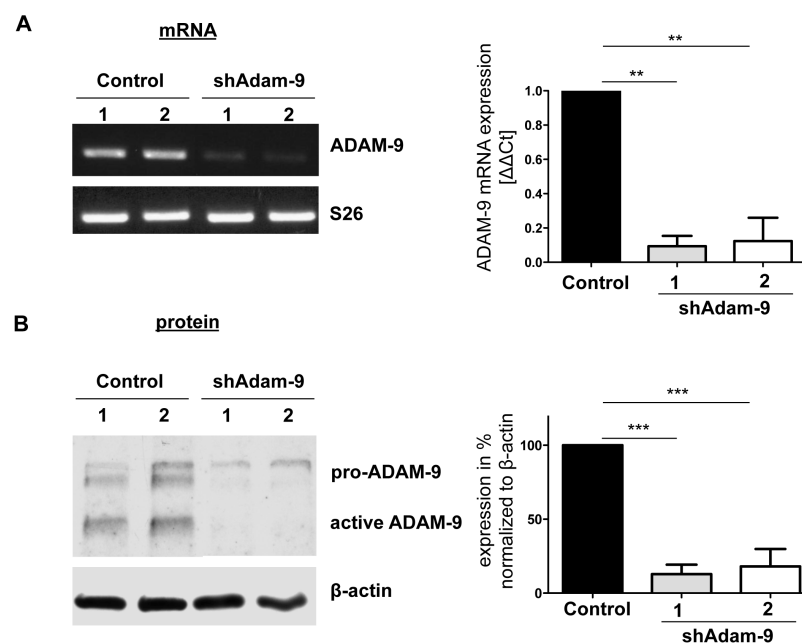


Figure 9: Stable down-regulation of ADAM-9 in high invasive BLM melanoma cells. High invasive BLM melanoma cells were stably transfected with shRNA targeted to ADAM-9. ADAM-9 transcript (A) and pro- and active protein (B) levels from two separately isolated clones for control and ADAM-9 down-regulated cells were determined. ADAM-9 expression levels were determined by quantitative real-time PCR and densitometric analysis of western blot signals normalized to respective loading control. Bars represent the average \pm SD of at least three independent experiments. Control cells were transfected with a scrambled shRNA sequence and considered to show 100% expression. The bars for the control cells represent the average of both control clones. **: $p < 0.01$; ***: $p < 0.001$.

To analyze whether depletion of ADAM-9 in BLM cells results in compensation by other ADAM proteases known to exert a similar function, expression of ADAM-10, -12, -15, -17, -19 and -21 was investigated by RT-PCR. Specific signals for indicated ADAMs were quantified by densitometry, normalized to S26 signals and expressed as percentage of the

control cells set as 100% expression. No significant change in the expression of other ADAMs was observed (Figure 10 A). Additional proteolytic enzymes, which are important in the context of melanoma and are implicated in the efficient processing of the ADAM-9 substrates gelatin, collagen and fibronectin (Schwettmann *et al.*, 2001), are the collagenolysins, MMP-13 and -14 and the gelatinases, MMP-2 and -9 (Hofmann *et al.*, 2005). Transcriptional analysis of MMP-2, -9, -13 and -14 did not reveal any significant altered expression profile upon ADAM-9 down-regulation (Figure 10 B).

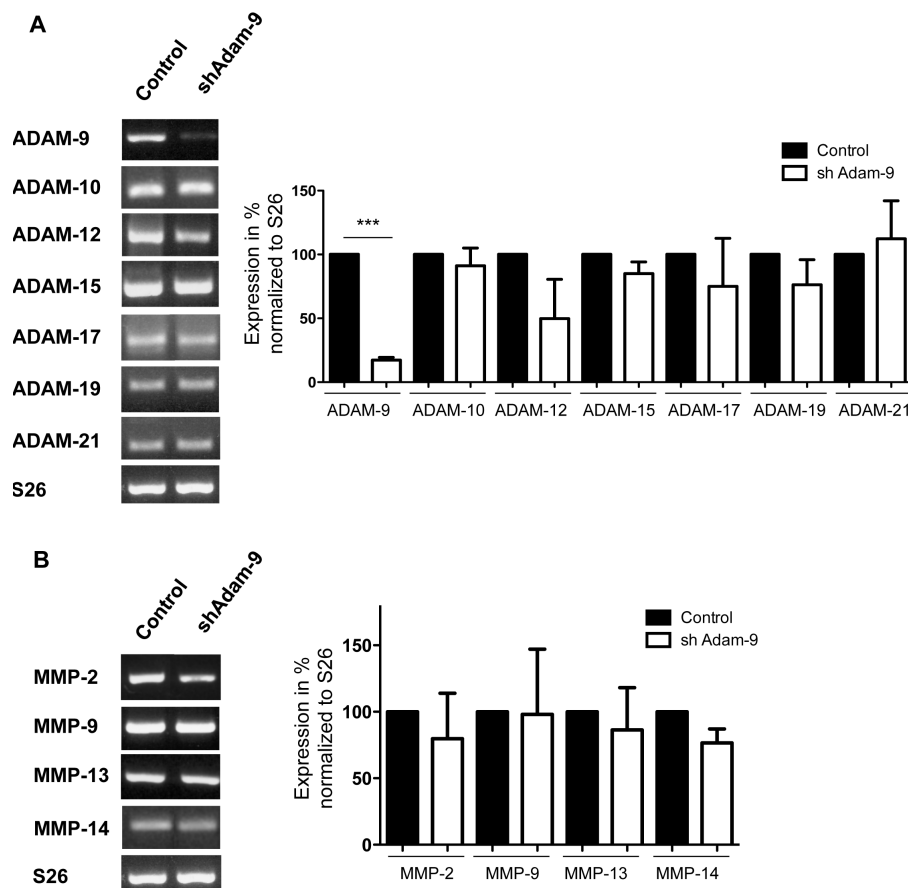


Figure 10: ADAM and MMP transcript expression in ADAM-9 down-regulated cells (shAdam-9). **(A)** ADAM-9 down-regulation did not alter expression of other ADAM as well as **(B)** MMP enzymes as determined by RT-PCR. Specific signals were measured and normalized to S26 control. Average expression \pm SD of two different control or ADAM-9 down-regulated clones of three independent experiments are shown. ***: $p < 0.001$.

3.2.1.1 Regulation of cell size by ADAM-9

Upon culture on plastic surfaces, the ADAM-9 down-regulated BLM cells appeared smaller in size than control clones (Figure 11 A). To quantify cell size, the cells were grown for 24h on plastic surface and cell area of 50 single grown cells for each clone was measured using the ImageJ program. This analysis revealed that ADAM-9 down-regulated cells showed a 2-fold smaller cell area in comparison to control cells (Control 1: $1531 \pm 697 \mu\text{m}^2$; Control 2: $1553 \pm 472 \mu\text{m}^2$; shAdam-9 clone: $841 \pm 303 \mu\text{m}^2$; shAdam-9 clone 2: $798 \pm 405 \mu\text{m}^2$; $p < 0.0001$) (Figure 11 B). Reduced cell area may result either from reduced ability of the cells to spread

or from reduced cellular volume. To address if cell volume was altered upon ADAM-9 silencing, the volume of suspended cells was estimated in an automated system, which is able to determine contemporarily the cell number as well as the cellular volume (CASY[®] device model TT). In these experiments ADAM-9 down-regulated cells exhibited a significant decrease ($p = 0.034$) of about a 2-fold in cell volume (mean of control 1 and 2: $4336 \pm 828\text{fl}$; mean of shAdam-9 clone 1 and 2: $3193 \pm 474\text{fl}$) (Figure 11 C).

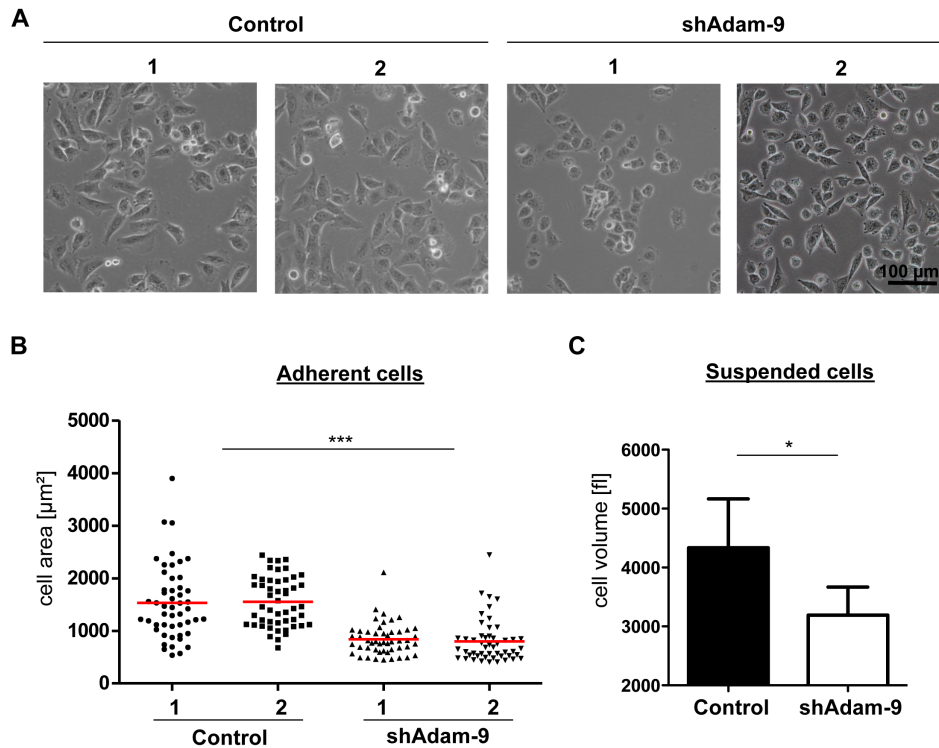


Figure 11: Analysis of cell area and volume in control and ADAM-9 down-regulated cells. **(A)** Representative phase contrast pictures of ADAM-9 down-regulated (shAdam-9) and control cells grown on plastic surface. ADAM-9 down-regulated cells appeared smaller than the control cells. **(B)** Cell area of single cells was measured in 50 different control and Adam-9 down-regulated cells by image analysis. The graphic shows a representative of two independent experiments. **(C)** Cell volume of suspended cells was determined in an automated cell counter revealing a significant decrease in cellular volume after ADAM-9 down-regulation. Bars represent the average \pm SD of two control or ADAM-9 down-regulated clones from four independent experiments. *: $p < 0.05$; ***: $p < 0.001$.

To investigate whether an altered cellular spreading, which is accompanied with cytoskeleton rearrangements, could also contribute to the reduced cell area, actin filaments were stained using phalloidin (Wulf *et al.*, 1979) and tubulin by immunocytochemistry. For these experiments the cells were grown for 24h on plastic surfaces in the presence of serum prior to the staining procedure. As observed in Figure 12 no obvious alterations in the organization of the actin filaments were visible in shAdam-9 down-regulated clones as compared to control cells, even though a more intense phalloidin signal was detected in the control. The tubulin cytoskeleton remained unaltered upon ADAM-9 down-regulation.

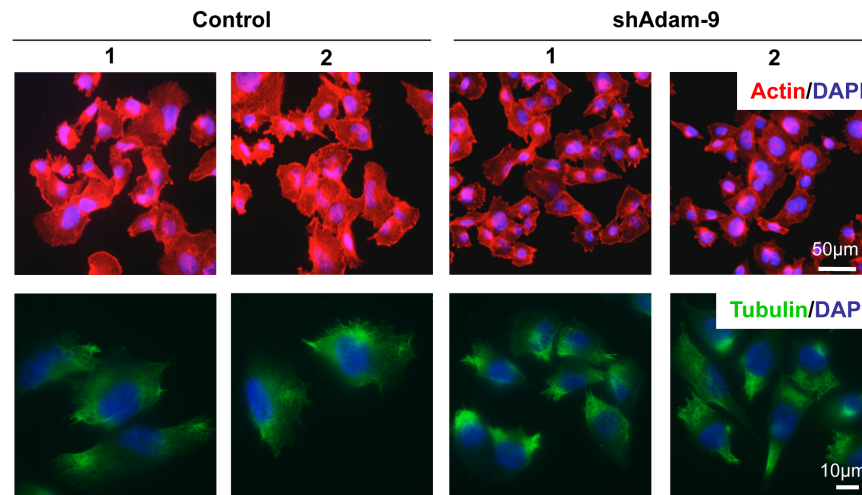


Figure 12: Cytoskeletal arrangement in control and ADAM-9 down-regulated cells. ADAM-9 down-regulated (shAdam-9) and control cells were plated on cover slips and grown for 24h. After fixing, actin was detected using fluorescently labelled phalloidin (red) and tubulin by immunocytochemistry using a specific antibody. Cell nuclei were visualized with the fluorescent dye DAPI.

Thus differences in cell size upon ADAM-9 down-regulation are most likely the result of altered cell volume, but not of altered cell spreading. The regulation of cell volume may occur through the expression and activity of aquaporin water channels, which transport fluids over the cell membrane (Verkman, 2005). In atopic eczema, cell shrinkage and water loss was shown as result of up-regulation of water channels such as aquaporin-3 (Hara-Chikuma and Verkman, 2008; Verkman, 2005). Alteration in this channel may also account for the altered cell volume upon ADAM-9 depletion. To find out whether melanoma cells express aquaporin-3 and if alterations in the expression of this molecule occur in ADAM-9 silenced BLM cells, aquaporin-3 expression was analyzed in control and ADAM-9 down-regulated clones. Aquaporin-3 transcripts were not altered upon ADAM-9 down-regulation, however by immunolocalization in cells, the protein expression levels seemed increased in the ADAM-9 silenced compared to the control cells (Figure 13 A). To investigate whether increased expression of aquaporin-3 also leads to altered channel function and thereby altered cell size in ADAM-9 down-regulated cells, channel activity was inhibited by mercuric chloride (HgCl_2), which is a general aquaporin inhibitor (Ismail *et al.*, 2009). For this experiment, control and ADAM-9 silenced cells, were suspended, treated with 0.15mM HgCl_2 for 1h and cell volume was determined subsequently. As already shown in Figure 11 C cell volume of ADAM-9 down-regulated cells was decreased, when no inhibitor was applied ($p < 0.0001$). After application of the inhibitor the volume of the ADAM-9 down-regulated cells (3842 ± 924 fl) was comparable to that of the untreated control cells (3898 ± 70 fl). However, upon treatment also the volume of the control cells increased (1,4-fold). Thus upon treatment of both, the control and the ADAM-9 silenced cells, the ADAM-9 down-regulated cells still exhibited a

decreased cell volume ($p = 0.0001$), indicating that differential activity of water channels is not the reason for decreased cell volume (Figure 13 B).

Taken together these data indicate that silencing of ADAM-9 in melanoma cells results in altered cell volume, which is not resulting from functional water channel alterations.

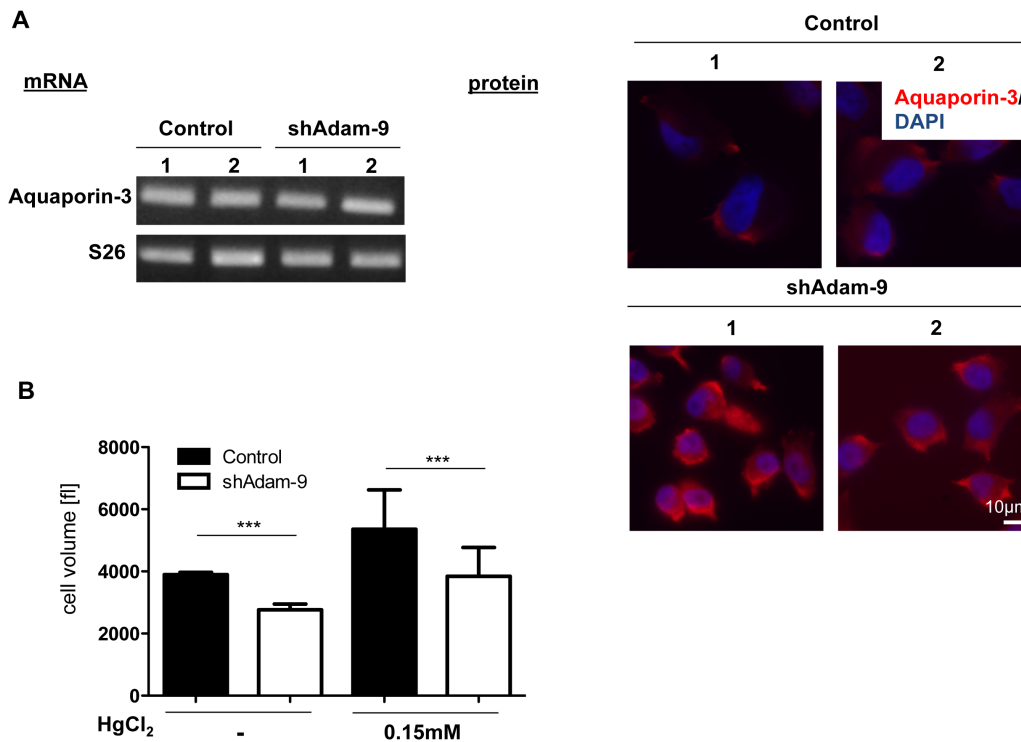


Figure 13: Expression of aquaporin-3 in control and ADAM-9 down cells.

(A) Expression of aquaporin-3 mRNA was determined by RT-PCR. Immunocytochemistry on PFA-fixed cells revealed stronger staining for aquaporin-3 in ADAM-9 down-regulated BLM cells (shAdam-9) compared to control cells. Cell nuclei were visualized with the fluorescent dye DAPI. **(B)** For inhibition of aquaporin activity, cells were treated with the general aquaporin inhibitor HgCl₂. Control and ADAM-9 down-regulated cells were grown for 24h and afterwards treated in suspension with 0.15mM HgCl₂ for 1h. Bars represent the mean \pm SD of two independent experiments performed in triplicate. ***: $p < 0.001$.

3.2.1.2 Analysis of proliferation

A remarkably altered cytoskeleton arrangement as well as changed aquaporin-3 activity turned out not to be the reason for the altered cell size upon ADAM-9 down-regulation. Another possible explanation for the altered cell size might be an increased proliferation rate of the ADAM-9 down-regulated cells, because if the cells divide faster compared to the control cells, the time to spread and regulate cell volume to the same extent as in the control cells, is reduced. It was shown that stimulation of B16 melanoma cells with TPA, which induces ADAM-9 mediated ectodomain shedding, decreased proliferation resulting in an increased cell size (Izumi *et al.*, 1998; La Porta *et al.*, 1998). To analyze if silencing of ADAM-9 effects cellular proliferation, the proliferative potential was determined by BrdU incorporation of cells grown in monolayer culture. After BrdU labelling the proliferation of

ADAM-9 down-regulated cells was increased (shAdam-9 clone 1: $p = 0.04$, shAdam-9 clone 2: $p = 0.17$) after 48 hours, but not after 24h (Figure 14). However the difference was only significant for clone 1.

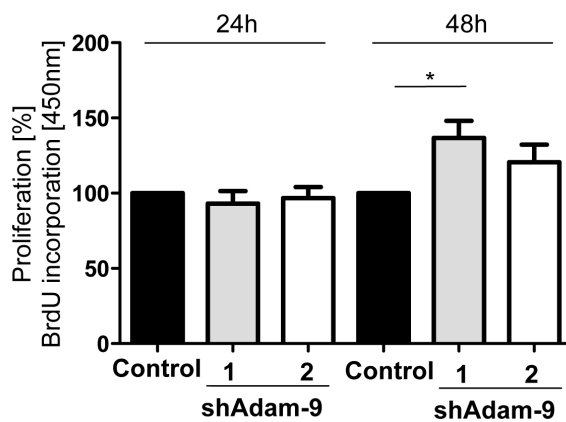


Figure 14: Analysis of anchorage dependent proliferation upon ADAM-9 down-regulation (shAdam-9). Proliferation was analyzed by BrdU incorporation after 24 and 48h. The graph shows percent proliferation and the mean of triplicate measurements of four independent experiments. The values for the control cells were set to 100% and the bars represent the average \pm SD of the two different control clones. *: $p < 0.05$.

As melanoma cells do also have the capability to grow in suspension, which would not be detected by the BrdU incorporation assay, cell proliferation was tested in a soft agar colony formation assay over a period of 21 days. This analysis revealed that ADAM-9 silenced cells formed significantly (control: 37 ± 16 ; shAdam-9 clone 1: 60 ± 20 , $p = 0.012$; shAdam-9 clone 2: 63 ± 20 , $p = 0.012$) more colonies as compared to control cells (Figure 15).

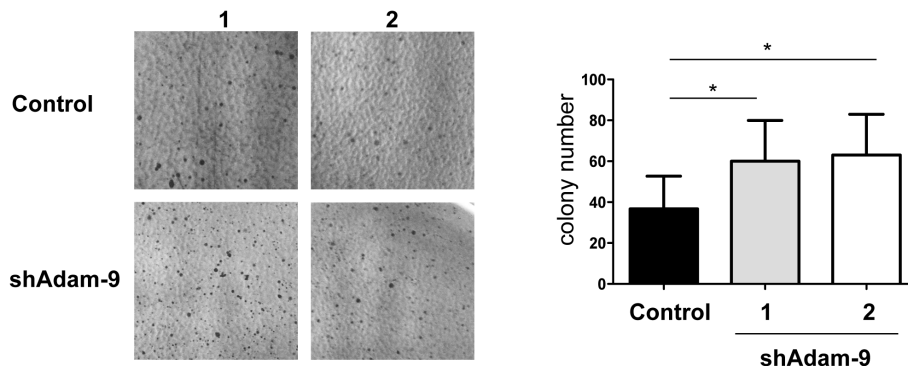


Figure 15: Analysis of anchorage independent proliferation upon ADAM-9 down-regulation. ADAM-9 down-regulated (shAdam-9) and control cells were grown for three weeks in 0.2% soft agar and the number of formed colonies was counted. For every clone the experiment was performed in triplicate and for each culture dish the number of formed colonies was counted in 8 randomly chosen microscopic fields (100 x magnification). Bars represent the average \pm SD of counted colonies of three independent experiments (control: average of the two control clones). *: $p < 0.05$.

3.2.1.3 *In vitro* cell invasion

ADAM-9 exhibits proteolytic as well as adhesive functions (Peduto, 2009), indicating that ADAM-9 may participate in cell invasion. The previous experiments also detected its ability to modulate melanoma cell proliferation. To analyze how down-regulation of ADAM-9 and thereby reduced proliferation and cellular volume influences the invasive capacity of BLM cells, these cells were seeded on dermal equivalents (dead de-epidemized skin) and their

capacity to penetrate the tissue was measured over time. The de-epidermized, devitalized dermal equivalent was chosen as invasion assay as it represents closely the *in vivo* situation (Dennhöfer *et al.*, 2003). In this assay cells are tested for both, their ability to invade the dermal compartment or to penetrate the BM before invasion of the dermis. The migrated distance within the tissue is then a direct measure of their invasive capacity.

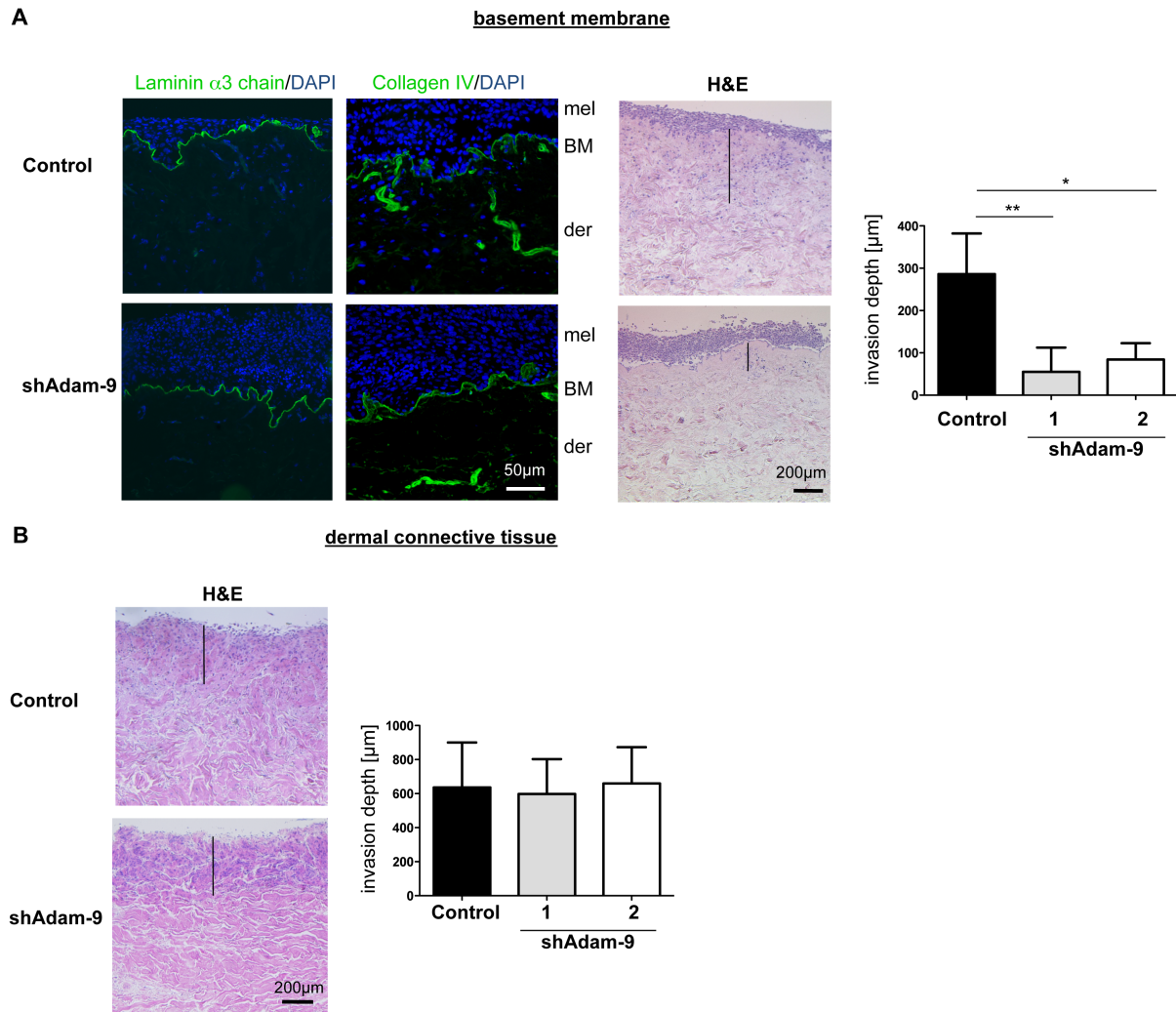


Figure 16: Invasion in DDS upon ADAM-9 down-regulation.

BLM cells were seeded either on top of the basement membrane (BM) (**A**) or directly on the dermal side (**B**) of skin composites (chapter 2.2.1.9) and cultured for three weeks at the air-liquid interface.

(**A**) Representative H&E stained sections of cultures using ADAM-9 down regulated (shAdam-9) and control cells seeded on the BM side. The presence of the BM was confirmed by staining for laminin α 3-chain and collagen IV, in green. Cell nuclei were stained in blue with DAPI. (**B**) H&E stained sections of cultures using control and shAdam-9 cells grown on the dermal connective tissue side. Graphs in (**A**) and (**B**) show the quantification of the invasion depth through the BM and the dermal connective tissue. The bars represent the mean \pm SD of three independent experiments performed in triplicate. Control cells, two different clones, are here averaged. *: $p < 0.05$; **: $p < 0.01$.

When cells were seeded on the BM side, control cells penetrated into the dermal connective tissue. In contrast down-regulation of ADAM-9 clearly resulted in reduced invasion as seen in H&E stained tissue sections. The presence of the BM in cultures was tested by detection of the BM proteins collagen IV and laminin α 3-chain. Quantification of the invasion depth

revealed a significantly reduced invasion through the BM from shAdam-9 clones as compared to controls (control: $316\mu\text{m} \pm 22\mu\text{m}$; shAdam-9 clone 1: $55\mu\text{m} \pm 26\mu\text{m}$; $p = 0.011$; shAdam-9 clone 2: $84\mu\text{m} \pm 27\mu\text{m}$; $p = 0.006$) (Figure 16 A). Quantification of the distance migrated within the dermal compartment by either ADAM-9 down-regulated or control cells, when seeded on the dermal side showed a similar invasion depth in both (control: $636\mu\text{m} \pm 264\mu\text{m}$; shAdam-9 clone 1: $597\mu\text{m} \pm 205\mu\text{m}$; shAdam-9 clone 2: $659\mu\text{m} \pm 213\mu\text{m}$) (Figure 16 B). Thus, whereas ADAM-9 depletion in melanoma cells does not affect their migratory ability through the dermal compartment, it interestingly impairs penetration of the basement membrane and thereby invasion.

3.2.1.4 Adhesion to basement membrane proteins

Invasion through the BM follows a step-wise process, which involves firstly substrate recognition followed by adhesion and degradation thus allowing cell penetration (Haass *et al.*, 2005; Bacac and Stamenkovic, 2008).

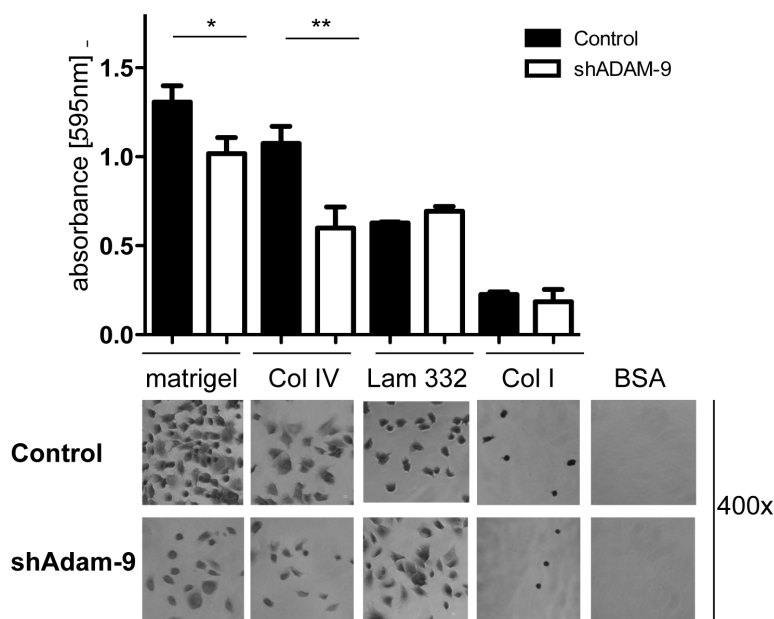


Figure 17: Adhesion of ADAM-9 silenced (shAdam-9) and control cells to BM components. Tissue culture plates were coated over night with matrigel, collagen IV ($10\mu\text{g/ml}$), laminin 332 ($5\mu\text{g/ml}$), collagen I ($10\mu\text{g/ml}$). Cells were allowed to adhere for 1h, stained with crystal violet and the extent of adhesion measured at 595nm. The bars represent the mean \pm SD of quadruplicate measurements and it is representative of four independent experiments shown. *: $p < 0.05$; **: $p < 0.01$.

The photographs below show pictures of crystal violet stained cells, adhering to the different substrates. Col IV: collagen IV; Lam 332: laminin 332; Col I; collagen I.

To test whether altered recognition and adhesion to BM components occurs when ADAM-9 is down-regulated, adhesion of ADAM-9 silenced and control cells to matrigel, which is a protein mixture resembling a complex extracellular environment containing BM proteins extracted from EHS tumors (Benton *et al.*, 2010; Hughes *et al.*, 2010), collagen IV ($10\mu\text{g/ml}$) and laminin 332 ($5\mu\text{g/ml}$), was tested. Additionally adhesion to collagen I ($10\mu\text{g/ml}$) was

tested, as this is the main component of the dermal connective tissue. Analyzing adhesion towards BSA (1%) served as a control. The melanoma cells were allowed to adhere for 1h at 37°C to the respective substrates. Significantly decreased adhesion of ADAM-9 silenced compared to control cells to matrigel ($p = 0.043$) and collagen IV ($p = 0.007$) was observed. In contrast adhesion to laminin 332 and to collagen I was not affected. However the adherence of the cells to collagen I in general was low. No adhesion to BSA was observed (Figure 17).

3.2.1.5 Analysis of integrin expression

Integrins are molecules mediating adhesion of cells towards extracellular matrix proteins (Hynes, 2002). In the adhesion assays the ADAM-9 down-regulated cells exhibited a significantly reduced adhesion towards collagen IV, which is the main component of the BM (Kalluri, 2003). Cellular receptors for collagen type IV belong to the integrin family and among those are the integrins $\alpha1\beta1$, $\alpha2\beta1$ and $\alpha3\beta1$ (Khoshnoodi *et al.*, 2008). To test whether altered adhesion of shAdam-9 clones derives from disturbed receptor expression, cells were either plated on plastic (steady-state expression level) or on collagen type IV coated dishes (induced receptor expression) and integrin expression was assayed by FACS analysis using antibodies directed against the extracellular domain of the integrins. This analysis revealed an unchanged expression of $\alpha1$, $\alpha3$ and antibodies directed against the extracellular domain of the $\alpha2$ integrin was significantly increased upon ADAM-9 down-regulation, when cells were grown on plastic ($p = 0.036$). When cultured on top of collagen IV expression of $\alpha1$ integrin was significantly lower in the ADAM-9 down-regulated cells compared to the control cells ($p = 0.009$). In parallel the $\alpha2$ integrin chain was up-regulated in the ADAM-9 down-regulated cells upon culture on collagen IV ($p = 0.017$). Compared to the steady-state conditions on plastic the induction of the $\alpha2$ integrin was higher on collagen IV. The expression of $\alpha3$ integrin was also induced upon culture on collagen IV compared to culture upon plastic, but the induction was comparable in the ADAM-9 down-regulated and control cells. The $\beta1$ integrin chain was slightly lower expressed in the ADAM-9 down-regulated cells on collagen IV, resulting from a lower induction of the protein compared to the control cells. However this difference was not significant. Unspecific IgG antibodies, which were used as isotype control, showed no staining (Figure 18).

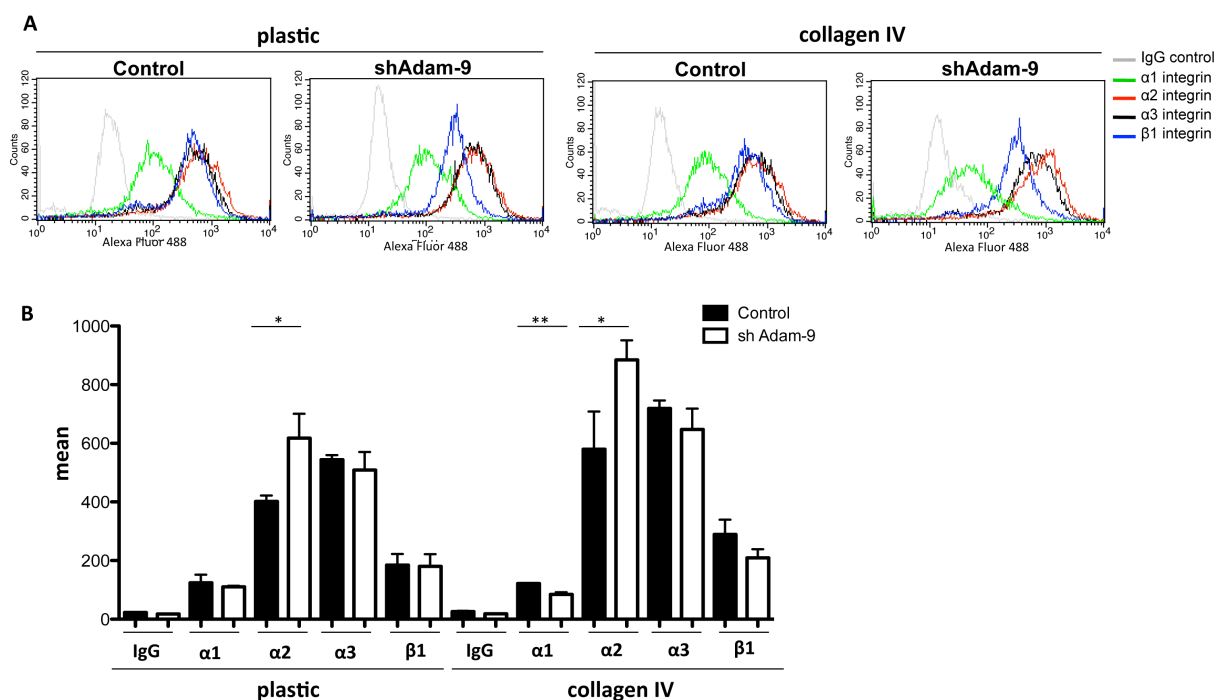


Figure 18: FACS analysis of integrin expression.

(A) ADAM-9 down-regulated (shAdam-9) and control cells were plated for 2h on plastic or collagen IV (10 μ g/ml) coated culture dishes. After trypsinization the expression profile of $\alpha 1$, $\alpha 2$, $\alpha 3$ and $\beta 1$ integrins was analyzed by FACS. **(B)** The graph shows the average expression \pm SD of triplicate stainings. Unspecific IgG were used as negative control. *: $p < 0.05$; **: $p < 0.01$.

At points of contacts between cells and the substrate integrins form clusters, which facilitate intracellular signalling and adhesion. To analyze if ADAM-9 down-regulation not only leads to an altered integrin expression level on the cell surface, but also to an altered integrin clustering, the cells were plated for 2h on collagen IV (10 μ g/ml) and immunohistochemically stained using antibodies directed against $\alpha 1$, $\alpha 2$, $\alpha 3$ and $\beta 1$ integrin. These experiments showed that the integrins $\alpha 1$, $\alpha 2$ and $\alpha 3$ were arranged in clusters and located at the cell membrane, in cellular protrusions, which contact the substrate (indicated by the arrows in Figure 19). A difference in the clustering of those integrins could not be observed. The $\beta 1$ integrin was also present in clusters on the cell surface in the control as well as in the ADAM-9 down-regulated cells, but a lower expression of this integrin chain together with reduced number of clusters was observed in the ADAM-9 down-regulated cells (Figure 19). The data from the FACS analysis together with the immunohistochemical stainings indicate that upon ADAM-9 silencing the $\alpha 1$ integrin chain is significantly lower expressed, while the $\alpha 2$ integrin is up-regulated on the cell surface upon culture of the cells on collagen IV. The $\beta 1$ integrin chain is also tendentially lower expressed upon ADAM-9 down-regulation. Integrin clustering was not altered in both control and ADAM-9 silenced cells. In summary the adhesion experiments and the integrin analyses showed that reduced adhesion upon ADAM-9 down-regulation is reflected by an altered integrin expression pattern.

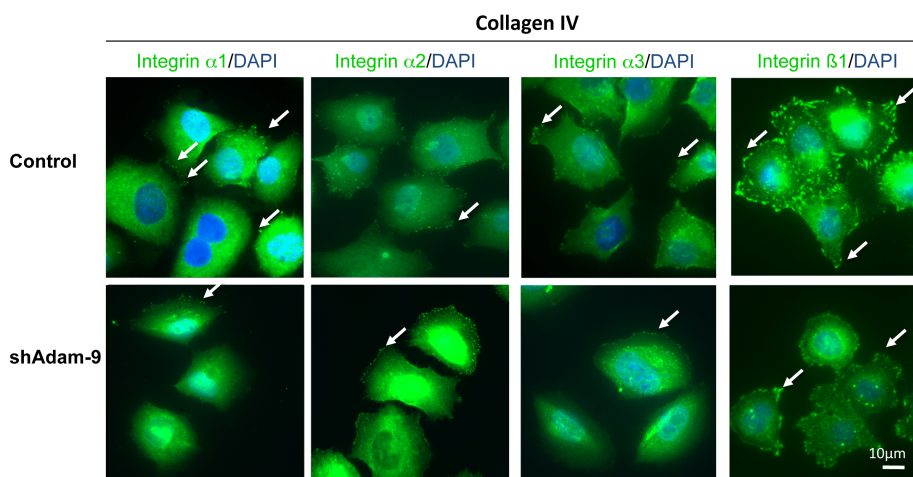


Figure 19: Immunohistochemical analysis of integrin expression of ADAM-9 down-regulated (shAdam-9) and control cells on collagen type IV. shAdam-9 and control cells were plated for 2h on collagen IV coated dishes, fixed and immunohistochemically stained using antibodies against the cytoplasmic domain of $\alpha 1$, $\alpha 2$, $\alpha 3$ and extracellular domain of $\beta 1$ integrins. Cell nuclei, in blue, were stained with DAPI. White arrowheads indicate clustered integrins at cell protrusions contacting the substrate.

3.2.1.6 Analysis of cell migration

Upon ADAM-9 down-regulation the adhesion of BLM melanoma cells towards collagen IV and matrigel was reduced, however not completely abolished, indicating that some cells are still able to adhere to the BM. Moreover in the DDS assay a clearly impaired invasion through the BM was observed. Since proteolytic activity of ADAM-9 can modulate cell migration (Fry *et al.*, 2010; Mauch *et al.*, 2010), which is a critical process for invasion through the extracellular matrix, it was next assayed if ADAM-9 down-regulation affects migration of these cells over BM components. For these experiments tissue culture plates were coated with matrigel, collagen IV (10 μ g/ml) or laminin 332 (5 μ g/ml). Fibronectin (10 μ g/ml) was also included in this analysis, because ADAM-9 can degrade fibronectin (Schwettmann *et al.*, 2001). On these matrices ADAM-9 down-regulated and control cells were seeded in cloning rings and their migration over the matrix was followed over a period of 24h. For all used substrates no significant difference in migration between control and ADAM-9 down-regulated cells was observed at any analyzed time point. However a tendency towards higher migration of the ADAM-9 down-regulated cells was detected at 18 and 24h of migration over collagen IV, fibronectin and laminin 332 (Figure 20). Taken together the migration experiments demonstrated that migration of BLM melanoma cells over BM components is not significantly altered upon down-regulation of ADAM-9.

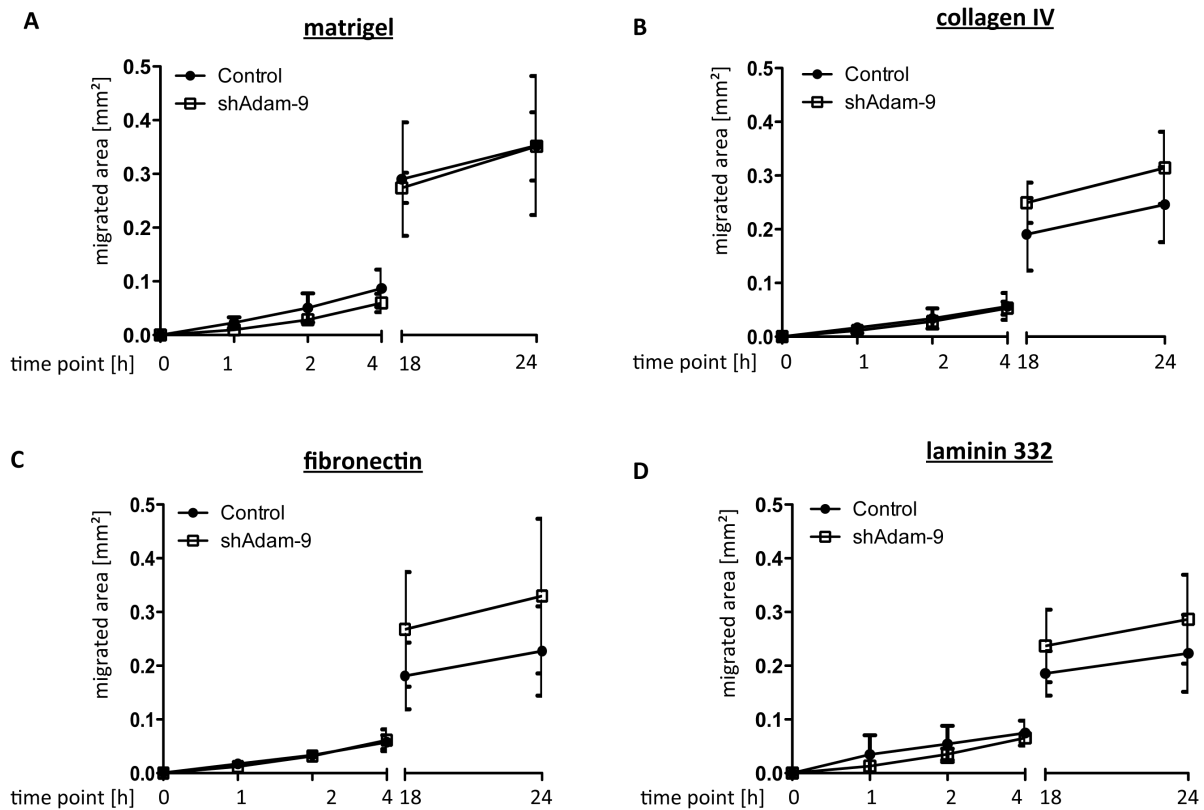


Figure 20: Migration of ADAM-9 down-regulated (shAdam-9) cells over BM components. shADAM-9 and control cells were seeded on culture plates coated with matrigel (A), 10µg/ml collagen IV (B), 10µg/ml fibronectin (C) or 5µg/ml laminin 332 (D). Cells were allowed to attach for 1h before starting to record cell migration over a period of 24h. The migrated area was measured at the indicated time points. Every line represents the average \pm SD of the two control or ADAM-9 down-regulated clones of three independent experiments performed in triplicates.

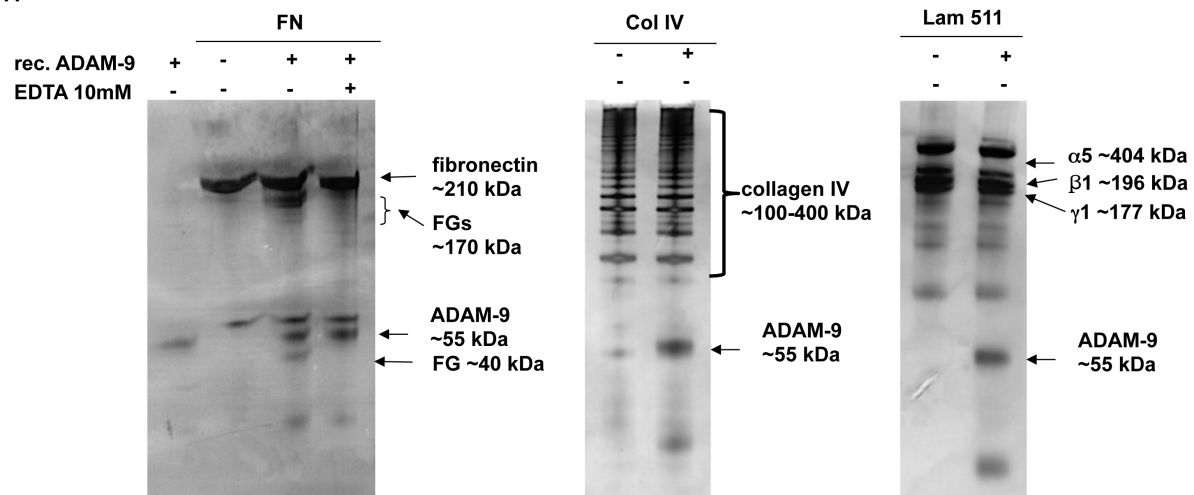
3.2.2 Processing of basement membrane proteins by ADAM-9

The DDS assay revealed a significantly reduced invasion of the ADAM-9 down-regulated BLM cells through the BM. Migration of melanoma cells through the BM involves enzymatic cleavage of the BM components to allow cells to invade the underlying dermis (Bacac and Stamenkovic, 2008). To investigate whether ADAM-9 contributes to BM breakdown, various human BM proteins (collagen IV, laminin 332, laminin 511; each 0.5µg) were incubated in the presence of proteolytically active human recombinant ADAM-9 (0.5µg). Fibronectin, which is a known substrate of ADAM-9 (Schwettmann *et al.*, 2001), was used as control for ADAM-9 activity. The 210kDa fibronectin protein was cleaved by active ADAM-9 (~55kDa), releasing two fragments of ~170kDa and ~40kDa (Figure 21 A). These bands were not visible in the presence of EDTA, which inhibits ADAM-9 metalloprotease activity by chelating Zn^{2+} ions required for enzyme activity. This indicates that these fragments resulted from enzymatic processing of fibronectin by ADAM-9. In contrast recombinant collagen IV was not cleaved by ADAM-9. SDS-PAGE under reducing conditions resulted in several bands ranging from ~100-400kDa. This protein laddering of collagen IV may be due to the fact that it is composed of three different α -chains, which are processed by many co- and

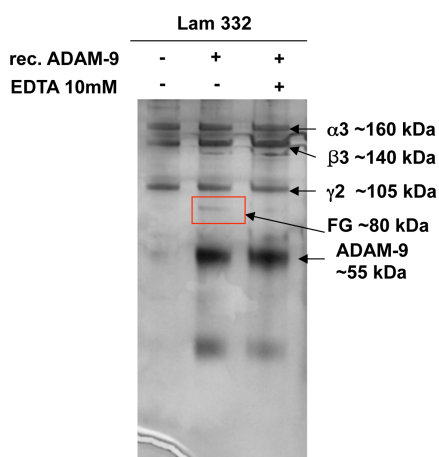
posttranslational modifications, thus appearing in several molecular weight forms (Khoshnoodi *et al.*, 2008). No difference in the band pattern was observed after incubation with ADAM-9, indicating that collagen type IV is not a substrate of ADAM-9.

Laminins are composed of three chains, namely the α -, β -, and γ -chain (Tzu and Marinkovich, 2008). The α -, β - and γ -chain of laminin 511 were observed at ~404, ~196 and ~177kDa. Some additional bands were also visible, but no differences were detected after incubation with ADAM-9 (Figure 15 A). Strikingly, laminin 332 was cleaved by ADAM-9 releasing a ~80kDa fragment. For laminin 332 the α -, β - and γ -chains of the protein were visible at ~160, ~140, and ~105kDa under reducing conditions. After incubation of human laminin 332 together with ADAM-9 an additional band appeared at ~80kDa. This fragment was not detected after addition of EDTA and identified laminin 332 as so far not described substrate of ADAM-9 (Figure 21 B).

A



B



To confirm that the obtained fragment is indeed a product of laminin 332 digestion, the fragment underwent peptide mass fingerprinting. This analysis revealed that the fragment originates from the laminin β 3-chain. Matching sequences were located in the C-terminal

region of the β 3-chain from amino acid 680 to 1153 (Figure 22, position 1). The molecular weight of the proteolytically released fragment was ~80kDa as observed by the silver stain. Thus it is expected that one fragment is generated and spans from about amino acid 420 to 1170 with the cleavage site expected to be located in the EGF-like domain III or IV of the laminin β 3-chain (Figure 22, position 2).

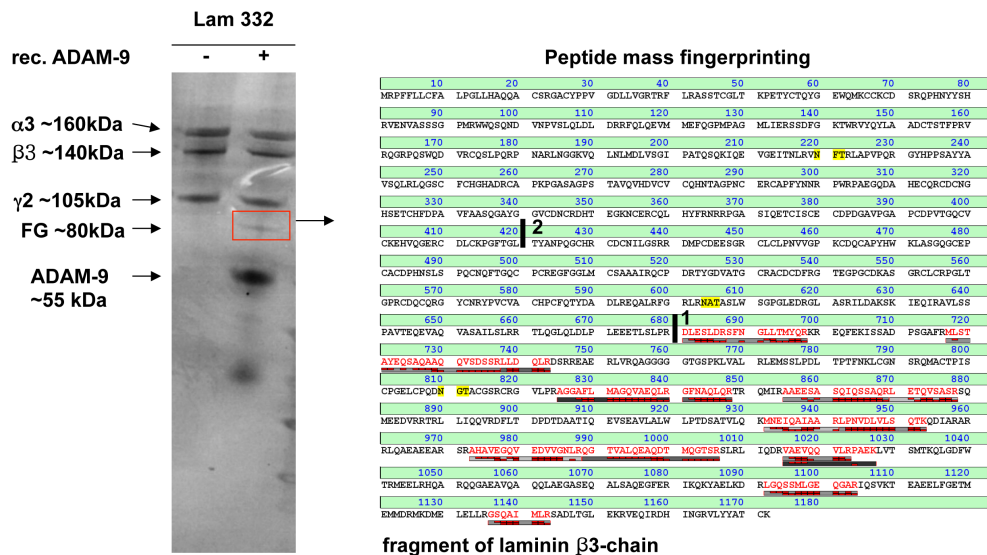


Figure 22: Identification of Laminin 332 proteolytically released fragment by peptide mass fingerprinting. Human laminin 332 (Lam 332; 0.5 μ g) was incubated with 0.5 μ g human recombinant ADAM-9 and processed proteins resolved under reducing conditions on 4-12% SDS gels followed by silver staining. The originated ~80kDa fragment was identified by peptide mass fingerprinting. The matching peptides covered the amino acid sequence from 1153 up to 680 in the coil-coiled region of the β 3-chain of laminin 332 (position 1). The fragment of ~80kDa which was visible on gel was predicted to cover this molecule up to amino acid 420 in the EGF-like domain III or IV (position 2). FG; proteolytic fragment.

To further confirm that the laminin β 3-chain is a substrate for ADAM-9 and to localize the cutting site of ADAM-9 in the laminin β 3-chain, the enzymatic assay was conducted using a recombinant protein corresponding to amino acids 4-575 of the human laminin β 3-chain, indicated by the black line in Figure 23 A. Proteins were separated by gel electrophoresis, immunoblotted and the membrane was incubated with a polyclonal antibody raised against the human laminin β 3-chain.

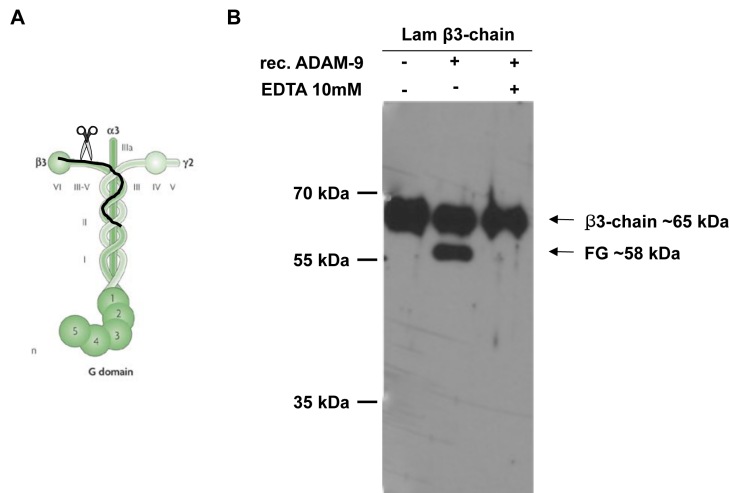


Figure 23: Digestion of recombinant laminin β 3-chain.

(A) Recombinant laminin (Lam) β 3-chain (N-terminal fragment; amino acid 4-575; 1 μ g) was incubated with 1 μ g human recombinant ADAM-9 with or w/o 10mM EDTA. **(B)** Proteins were separated under reducing conditions and visualized by immunoblotting using an antibody to the human laminin β 3-chain. FG: proteolytic fragment. The drawing was adapted from Marinkovich, Nat. Rev. Cancer, 2007.

The recombinant laminin β 3-chain was detected as a band of ~65 kDa (Figure 23 B). After incubation with active ADAM-9, an additional band of ~58kDa was observed. Incubation in the presence of EDTA completely blocked the processing and this band was no longer visible by immunoblotting (Figure 23 B). As the released fragment has now a reduction of ~13kDa, corresponding to ~120 amino acids, it is possible that, as expected, the cleavage site would be located around amino acid 420.

This result confirmed the previous finding that human laminin β 3-chain is cleaved by ADAM-9 in the N-terminal region.

3.3 Regulation of ADAM-9 expression

3.3.1 Analysis of ADAM-9 regulation by IL-1 α

3.3.1.1 Regulation of ADAM-9 by exogenous IL-1 α

The tumor microenvironment is enriched by cytokines including IL-1 α produced at high levels by tumor cells, activated fibroblasts and inflammatory cells generating a highly pro-inflammatory peritumoral environment (Apte *et al.*, 2006). *In vitro* it was demonstrated that one function of IL-1 α is to down-regulate ADAM-9 transcripts in melanoma cells (Zigrino *et al.*, 2005). However, *in vivo*, expression of ADAM-9 is detected in tumor cells of primary melanoma, but not of metastases (Zigrino *et al.*, 2005). Thus it is possible that there is a concentration-dependent effect of IL-1 α on the regulation of ADAM-9 *in vivo*. To analyze if IL-1 α expression correlates with the expression of ADAM-9 in high invasive melanoma cells, four human melanoma cell lines grown as monolayer cultures were studied for mRNA expression of these molecules. This analysis showed transcript expression of IL-1 α in all high invasive melanoma cell lines, with the highest expression in BLM cells. No correlation between the expression of IL-1 α and that of ADAM-9 could be detected (Figure 24).

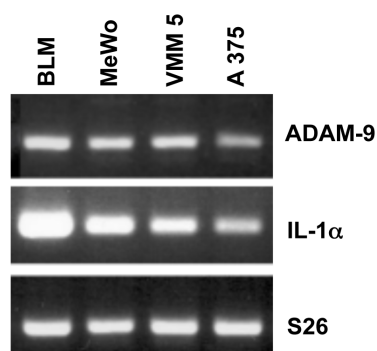


Figure 24: Expression of ADAM-9 and IL-1 α in high invasive melanoma cell lines. Four cell lines with high invasive capacity were analyzed by RT-PCR, using primers for IL-1 α and ADAM-9. S26 was used loading control. The figure shows a representative experiment out of two independent experiments.

To mimic the *in vivo* situation, where increased extracellular IL-1 α is available within the microenvironment, and to analyze how this effects the expression and activation of ADAM-9 in invasive BLM melanoma cells, these cells were grown as monolayers and stimulated with 10U/ml recombinant human IL-1 α for 24h. In agreement with previous data (Zigrino *et al.*, 2005), this stimulation resulted in a significant ($p = 0.012$) down-regulation of ADAM-9 transcript level to $56 \pm 17\%$ as compared to unstimulated control cells (Figure 25 A). In parallel, immunoblotting analysis of ADAM-9 in crude membrane fractions from IL-1 α stimulated cells showed a significant ($p = 0.046$) reduction of $50 \pm 19\%$ in the synthesis of ADAM-9, as detected after densitometry and normalization to proteins stained with Coomassie blue, used as control (Figure 25 B).

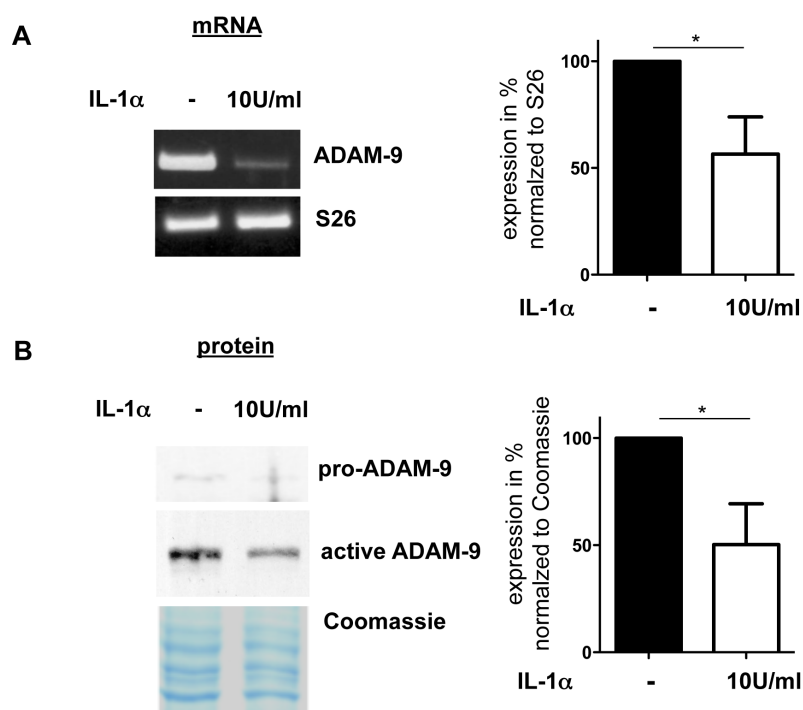


Figure 25: Stimulation of high invasive BLM melanoma cells with IL-1 α .

BLM melanoma cells grown as monolayer were stimulated with 10U/ml human recombinant IL-1 α for 24h. ADAM-9 transcripts (**A**) and protein levels, in crude membrane fractions (**B**) were quantified by densitometry and normalized to S26 or Coomassie as loading control from at least three independent experiments. The graphs on the right side show the mean \pm SD of these quantifications. The values of unstimulated cells were set as 100%. *: $p < 0.05$.

The molecular mechanisms leading to ADAM-9 down-regulation by IL-1 α are undiscovered. It is known that the IL-1 receptor signals through the NF κ B pathway, but can also activate MAP kinases like p38 and JNK (O'Neill *et al.*, 1998). Therefore a pharmacological approach was used blocking either nuclear translocation of activated NF κ B using the inhibitor SN50 (18 μ M) or phosphorylation of c-Jun by the inhibitor SP600125 (10 μ M). BLM melanoma cells were incubated for 24h with 10U/ml IL-1 α alone or in combination with one of the inhibitors, or with 0.0002% DMSO the solvent for SP600125, used as control. ADAM-9 expression was down-regulated in BLM cells when IL-1 α was applied alone, together with DMSO or in combination with the NF κ B inhibitor SN50. However, when IL-1 α was applied together with the JNK inhibitor SP600125, IL-1 α -induced ADAM-9 down-regulation was abolished (Figure 26). These results indicate that exogenously supplied IL-1 α regulates expression of ADAM-9 in BLM melanoma cells through the JNK pathway.

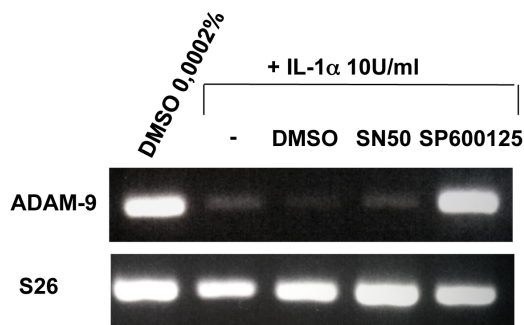


Figure 26: Pharmacological inhibition of signalling pathways upon IL-1 α stimulation. BLM melanoma cells were stimulated for 24h with 10U/ml IL-1 α in presence of the inhibitors of NF κ B SN50 (10 μ M) or JNK SP600125 (18 μ M). DMSO (0.0002%), the solvent for the inhibitors, was used as control. ADAM-9 expression was determined by RT-PCR. S26 was used as loading control. The figure shows a representative of two independent experiments.

3.3.1.2 Analysis of melanoma cell derived IL-1 α on ADAM-9 expression in high invasive melanoma cells

IL-1 α is very little secreted and the majority of this cytokine is stored intracellularly. However, also intracellular IL-1 α appears to be functionally active (Apte *et al.*, 2006). To investigate whether alterations in intracellular retained IL-1 α may impact ADAM-9 expression in melanoma cells, IL-1 α endogenous expression was stably down-regulated in BLM melanoma cells. These cells showed highest IL-1 α transcript expression among all the analyzed high invasive melanoma cell lines (see 3.3.1.1). Clones with stable IL-1 α down-regulation, were generated within the diploma work of Birgit Seyfarth and were used for further experiments. These cells showed IL-1 α down-regulation of ~85% on mRNA and ~47% on protein level, as observed by RT-PCR and immunoblot analysis of cellular lysates (Figure 27). Secreted IL-1 α was reduced by ~29% in cellular supernatants of IL-1 α silenced compared to scrambled transfected control cells, as assessed by ELISA measurements (Diploma thesis Birgit Seyfarth).

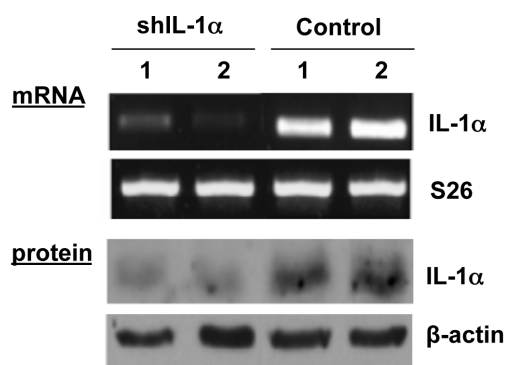


Figure 27: Stable down-regulation of IL-1α in BLM melanoma cells.

Two clones, either transfected with a scrambled control shRNA sequence (Control 1 and 2) or sequences targeted to IL-1α (shIL-1α) were assayed for IL-1α expression on mRNA and protein level. S26 or β-actin, respectively, served as loading control (adopted from the Diploma thesis of Birgit Seyfarth).

Expression of ADAM-9 was determined at transcript and protein level in BLM shIL-1α and control cells after growing for 24h in monolayer culture. Analysis of ADAM-9 expression showed that upon stable silencing of IL-1α, increased expression of ADAM-9 transcripts was detected. After densitometric analysis of ADAM-9 signals and their normalization to S26, the ADAM-9 expression for the two analyzed clones was increased to 154% as compared to controls cells set as 100%. The increased expression of ADAM-9 was significant in clone 2 ($p=0.011$). Analysis of ADAM-9 protein content in crude membrane preparations revealed an up-regulation, with a detected maximal 2-fold in clone 1, of both, the pro- and active protein forms (Clone 1: $214 \pm 76\%$; Clone 2: $147 \pm 86\%$), as observed after densitometric quantification of the ADAM-9 signals and normalization to Coomassie (Figure 28).

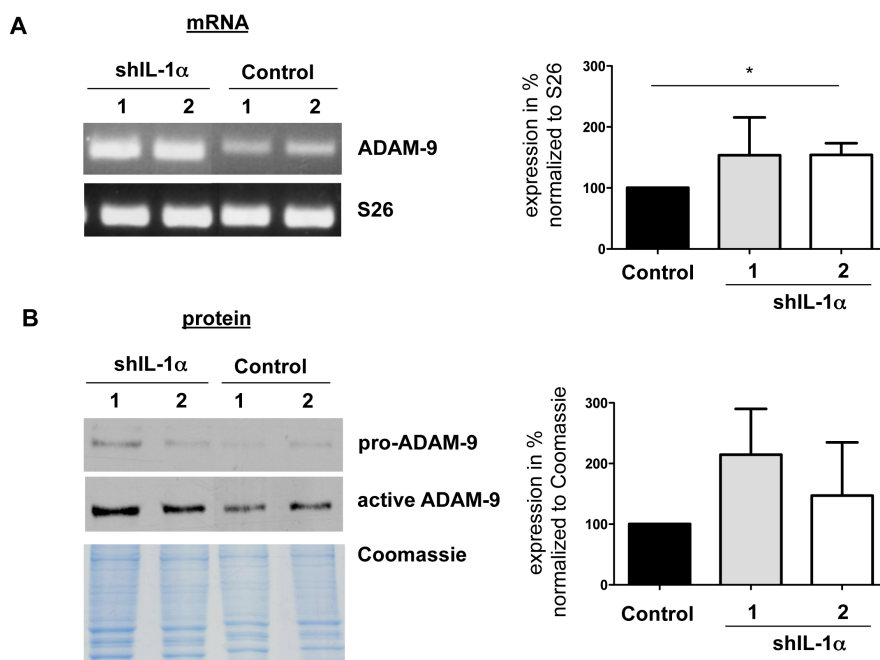


Figure 28: Analysis of ADAM-9 in IL-1α down-regulated BLM cells.

BLM shIL-1α and control cells were grown for 24h as monolayers and RNA or proteins were extracted. ADAM-9 transcript (**A**) and protein (**B**) levels in IL-1α down-regulated and control cells were analyzed by RT-PCR and immunoblot analysis using crude membrane fractions. The graphs on the right side show the densitometric quantification of ADAM-9 mRNA and protein levels after normalization to S26 or Coomassie as loading controls of three independent experiments. Bars represent the average \pm SD. The control represents the average of two control clones set as 100%. *: $p < 0.05$.

To investigate whether stable silencing of IL-1 α activates JNK or ERK mediated intracellular signalling pathways regulating ADAM-9 expression levels in cell steady-state conditions, the phosphorylated forms of these mediators were measured by immunoblot analysis. The signals for phosphorylated ERK and JNK were quantified by densitometry and normalized to the expression of total unphosphorylated ERK or JNK, respectively. This analysis revealed a significantly reduced phosphorylation of ERK upon IL-1 α down-regulation compared to control cells (Clone 1: 46 \pm 21%, p = 0.048; Clone 2: 36 \pm 23%, p = 0.039), whereas phosphorylation levels of JNK were not remarkably altered (Clone 1: 66 \pm 32%; Clone 2: 77 \pm 55%) (Figure 29). Thus, endogenous IL-1 α controls constitutive expression of ADAM-9 through the activity of ERK.

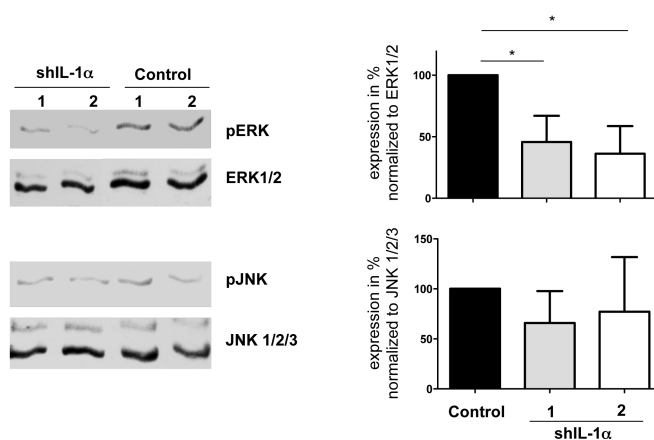


Figure 29: ERK and JNK phosphorylation upon IL-1 α down-regulation.

Immunoblot analysis of phosphorylated ERK and JNK levels was performed on lysates from control and IL-1 α silenced cells. The graphs show the densitometric quantification of pERK or pJNK protein levels after normalization to ERK 1/2 or JNK 1/2/3 as loading control of three independent experiments. Bars represent the average \pm SD. The control represents the average of two control clones set as 100%. *: p <0.05.

3.3.1.3 Invasion through the basement membrane upon IL-1 α down-regulation

In order to determine the functional relevance of IL-1 α down-regulation, leading to increased ADAM-9 synthesis, for invasion of melanoma cells, both, IL-1 α down-regulated and control cells, were analyzed in DDS invasion assay (described in chapter 3.2.1.3). When cells were seeded on the BM side the IL-1 α down-regulated cells invaded slightly more the underlying tissue as compared to control cells (Figure 30 A). Presence of the BM was confirmed by staining for laminin α 3-chain (Figure 30 A). Quantification of the invasion depth of the cells into the dermal compartment revealed that at least for clone 1, this increased invasiveness of BLM cells is significantly higher than for control clones (invaded depth of control cells: 106 μ m \pm 37 μ m; shIL-1 α clone 1: 192 μ m \pm 76 μ m; p = 0.009). The other IL-1 α down-regulated clone (number 2) showed only a tendency to higher invasion, but due to the higher variability detected, no significant difference could be measured (shIL-1 α clone 2: 133 μ m \pm 93 μ m; p = 0.399).

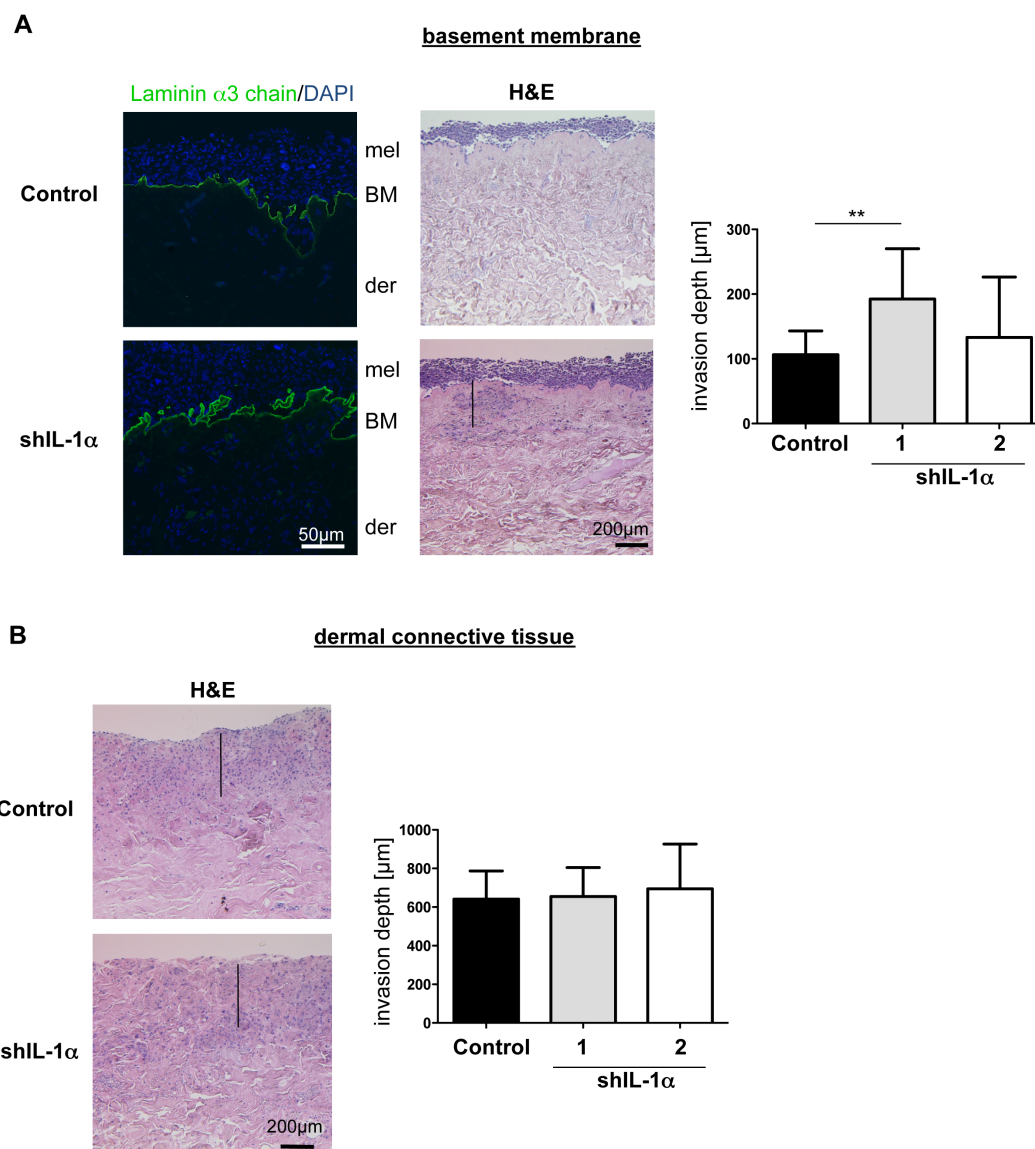


Figure 30: Invasion of DDS composites by IL-1 α down-regulated BLM cells.

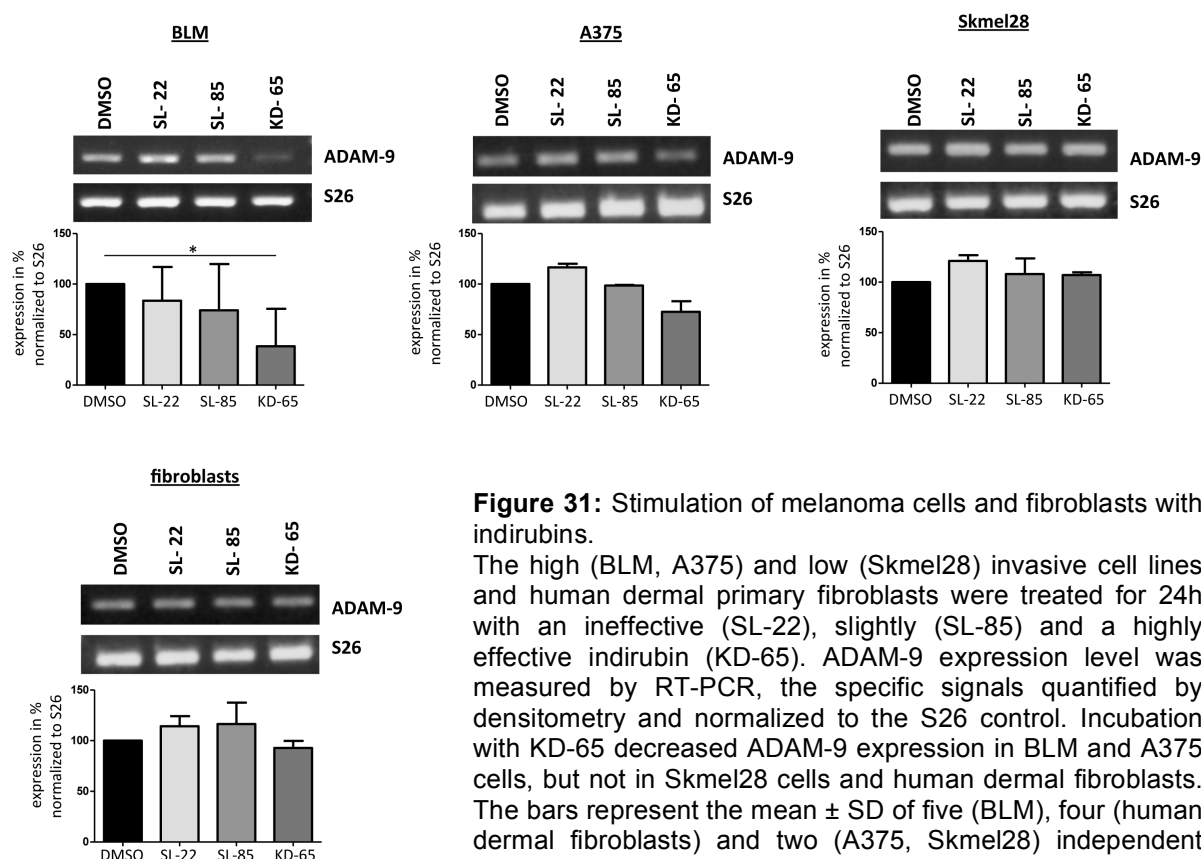
Invasion of DDS composites by shIL-1 α and control cells was tested either through the BM (basement membrane) or the dermal connective tissue. **(A)** Representative sections of H&E stained cultures with control or shIL-1 α cells seeded on the BM side. The presence of a BM was visualized by staining for laminin $\alpha 3$ -chain (green). Cell nuclei were stained in blue by DAPI. **(B)** Representative sections of H&E stained cultures of cells on the dermal side. Graphs in **(A)** and **(B)** show the quantification of the migrated distance in the tissues depth. Shown is the mean \pm SD of three independent experiments performed in triplicate. The average of two different control clones is shown. **: $p < 0.01$.

When the cells were seeded on the dermal side, IL-1 α down-regulated as well as control cells invaded into the tissue and no difference in the invasion depth was measured (control: $641\mu\text{m} \pm 146\mu\text{m}$; shIL-1 α clone 1: $654\mu\text{m} \pm 150\mu\text{m}$; shIL-1 α clone 2: $692\mu\text{m} \pm 232\mu\text{m}$) (Figure 30 B).

These results indicate that endogenous IL-1 α regulates ADAM-9 steady-state levels of expression in BLM melanoma cells. Furthermore, up-regulation of ADAM-9 leads to increased invasion through the BM, which further confirms a direct role for ADAM-9 in mediating BM penetration as seen in 3.2.1.3 together with the data shown in 3.2.2.

3.3.2 Modulation of ADAM-9 expression by indirubins

Indirubins were initially characterized as the active ingredient of a traditional Chinese medicine preparation, consisting of eleven herbal components (Eisenbrand *et al.*, 2004). These molecules have already been used for anticancer treatment and they were shown to reduce cancer cell proliferation by inhibiting cyclin dependent kinase activity (Eisenbrand *et al.*, 2004). By a cooperative project within the Melanoma Research Network we had access to indirubin derivatives (chapter 2.2.1), which have been generated to specifically interfere with pathways activated in melanoma cells. In order to find potential inhibitors of tumor cell invasion, the effect of indirubins on ADAM-9 synthesis was analyzed. To test indirubin activity, the low invasive melanoma cell line Skmel28, the high invasive cell lines BLM and A375 and primary human dermal fibroblast monolayers were treated for 24h with 10 μ M of either an “ineffective” indirubin (SL-22), an indirubin causing a slight antiproliferative effect (SL-85) or a highly effective indirubin (KD-65). The efficacy of the indirubins to affect melanoma cell proliferation was tested in the lab of Prof. M. Kunz (University of Rostock). The solvent 0.001% DMSO served as control. Intensity of ADAM-9 transcript fragments amplified by RT-PCR was quantified by densitometry, normalized to S26 signals and expressed as percentage of the expression of DMSO treated cells, which were set as 100%.



Whereas the application of SL-22 and SL-85 did not alter ADAM-9 transcript levels in any of the analyzed cells, application of the effective indirubin KD-65 led to significantly decreased

ADAM-9 transcript expression in the high invasive line BLM ($p = 0.02$) as compared to DMSO treatment control (Figure 31). The decrease of ADAM-9 transcripts caused by KD-65 was lower in A375 cells, and no effect was detected in the low invasive Skmel28 cells and in fibroblasts (Figure 31).

This data showed that the efficient indirubin, KD-65, can selectively reduce ADAM-9 expression in the high invasive melanoma cells, but does not alter ADAM-9 expression in Skmel28 cells and fibroblasts.

To test if indirubins also influence ADAM-9 protein synthesis, BLM melanoma cells, which showed the highest response to KD-65 and primary human dermal fibroblasts were treated with indirubins for 24h followed by crude membrane preparation. Immunoblot analysis of ADAM-9 on SDS-PAGE resolved lysates from treated cells, showed that the highly effective indirubin KD-65 decreased ADAM-9 production by melanoma cells, but not by fibroblasts (Figure 32).

Taken together indirubins are molecules controlling ADAM-9 expression, specifically in high invasive, but not low invasive melanoma cells and stromal fibroblasts.

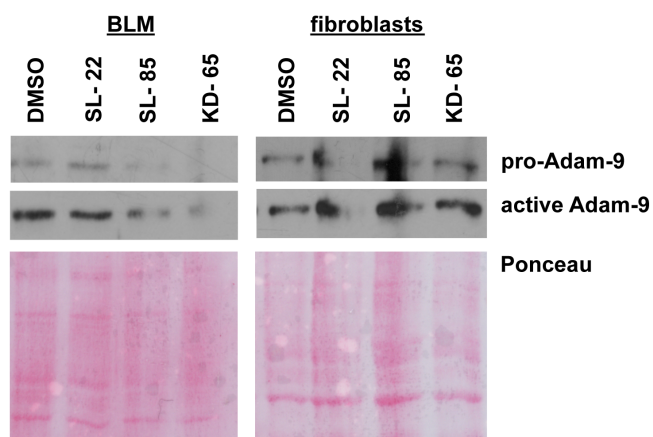


Figure 32: Stimulation of melanoma cells and fibroblasts with indirubins. The indirubins SL-22, SL-85 and KD-65 were applied for 24h to cells prior to analyze ADAM-9 protein content in crude membrane preparations. The effective indirubin KD-65 decreased ADAM-9 production in BLM cells, but not in fibroblasts.

3.4 *In vivo* analysis of ADAM-9 function in a mouse model for spontaneous melanoma development

The so far obtained *in vitro* data have shown that ADAM-9, produced by melanoma cells, is important for tumor cell invasion through the BM. Thus one can hypothesize that ADAM-9 also in the *in vivo* situation is involved in melanoma invasion and metastases formation, as BM penetration is one key event in those processes. In order to investigate the contribution of melanoma-derived ADAM-9 for tumor development, growth and metastases formation *in vivo*, Adam-9^{-/-} animals (Weskamp *et al.*, 2002) were crossed with Hgf/Cdk4^{R24C/R24C} animals (Tormo *et al.*, 2006), which develop tumors spontaneously. DMBA treatment in perinatal stages has been also shown to accelerate tumor formation in these animals (Tormo, *et al.*, 2006).

3.4.1 Generation of Adam-9^{-/-}//Hgf/Cdk4^{R24C/R24C} animals

After four generations of crossing, Adam-9^{+/+}//Hgf/Cdk4^{R24C/R24C} (control) and Adam-9^{-/-}//Hgf/Cdk4^{R24C/R24C} animals named Adam-9^{mutated/ko} in the following chapters were obtained. The crossing schema is shown in 2.2.4.2. The deletion of the Adam-9 gene was confirmed by PCR on genomic DNA isolated from tails of three-week old animals. This analysis revealed a 121bp fragment in the control animals corresponding to amplification of the wild-type gene and a 1000bp fragment in the Adam-9^{mutated/ko} animals, which contains the neomycin cassette inserted within the gene leading to an interruption of the ADAM-9 sequence. Loss of Adam-9 gene transcription was further confirmed by RT-PCR on cDNA from RNA isolated from tails of three weeks old animals (Figure 33 A). The fragment containing the mutation of the Cdk4 gene was amplified by PCR on genomic DNA and revealed for all animals a 740bp fragment, resembling the mutated Cdk4 gene. The not mutated gene should create a fragment of 640bp, which was not detected (Figure 33 A). Animals, which were positive for the Hgf transgene could be phenotypically distinguished from their Hgf-negative littermates, because of their black skin phenotype. This was most obvious on the bottom side of the paws (Figure 33 B). All animals were viable after birth and developed normally. They had no obvious, macroscopically visible, phenotype. In Figure 33 B representative photos of three weeks old control and Adam-9^{mutated/ko} mice are shown.

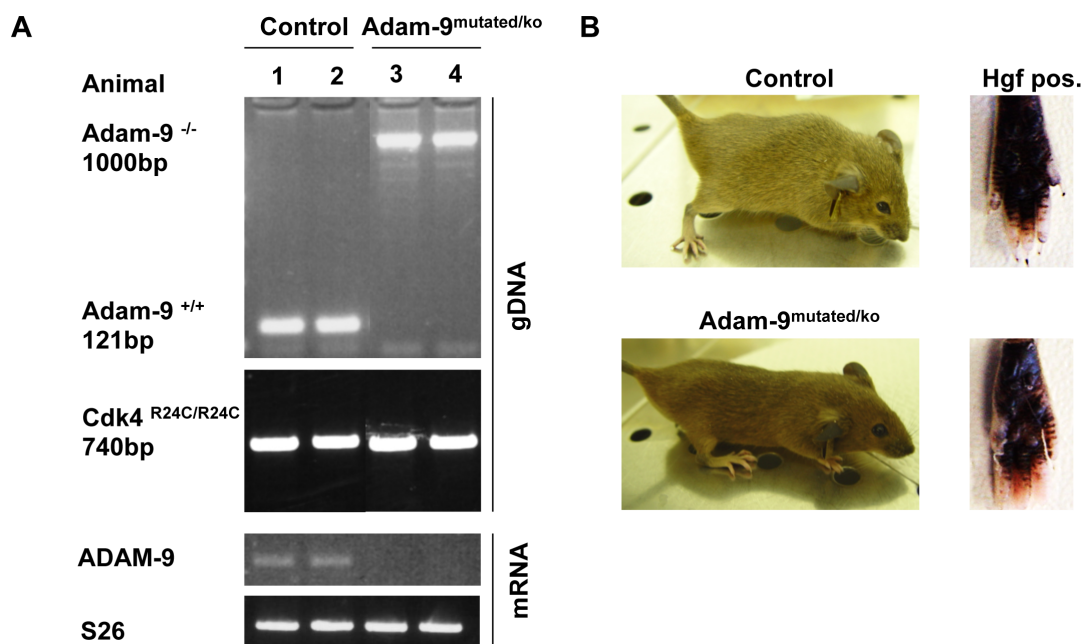


Figure 33: Generation of control and Adam-9^{mutated/ko} animals.

To generate animals, which spontaneously develop tumors in the absence of ADAM-9 expression, Adam-9^{-/-} animals were crossed with Hgf/Cdk4^{R24C/R24C} animals. **(A)** PCR amplification of the wild type or mutated Adam-9 allele on genomic DNA detects ablation of the Adam-9 (1000bp fragment) or the presence the Adam-9 wildtype gene (121bp fragment). The homozygous insertion of the mutated Cdk4 gene (Cdk4^{R24C/R24C}) was proven by PCR on genomic DNA generating a fragment of 740bp in all animals. RT-PCR using cDNA from RNA of tails of control and Adam-9^{mutated/ko} animals further confirmed Adam-9 transcript deletion. **(B)** Representative photographs of three weeks old control and Adam-9^{mutated/ko} animals. The transgenic overexpression of Hgf (Hgf pos.) could be phenotypically observed by the black skin phenotype most prominent at the bottom side of the paws.

3.4.1.1 Analysis of skin architecture and differentiation

To test if ablation of ADAM-9 in addition to transgene expression of Hgf/Cdk4^{R24C/R24C} influenced skin homeostasis, skin samples from different parts of the body (head, back, belly, tail) were collected from control and Adam-9^{mutated/ko} animals at postnatal day 1 (P1; new born skin) and postnatal day 21 (P21; adult skin). Skin histology in these animals was analyzed by common established histological staining procedures, such as H&E and Sirius red staining, this last allowing visualization of fibrillar collagens by polarized light. At P1 (Figure 34) as well as at P21 (Figure 35) no differences in skin histology between control and Adam-9^{mutated/ko} were detected. In all studied parts of the body, the epidermis and dermis, including hair follicles, collagen and fat content was comparable among control and Adam-9^{mutated/ko} mice. Visualization of Sirius red stained sections with polarized light also indicated that collagen fibril bundles, visible with this light, are comparable in thickness and density in both animal genotypes at both analyzed time points (Figures 34 and 35).

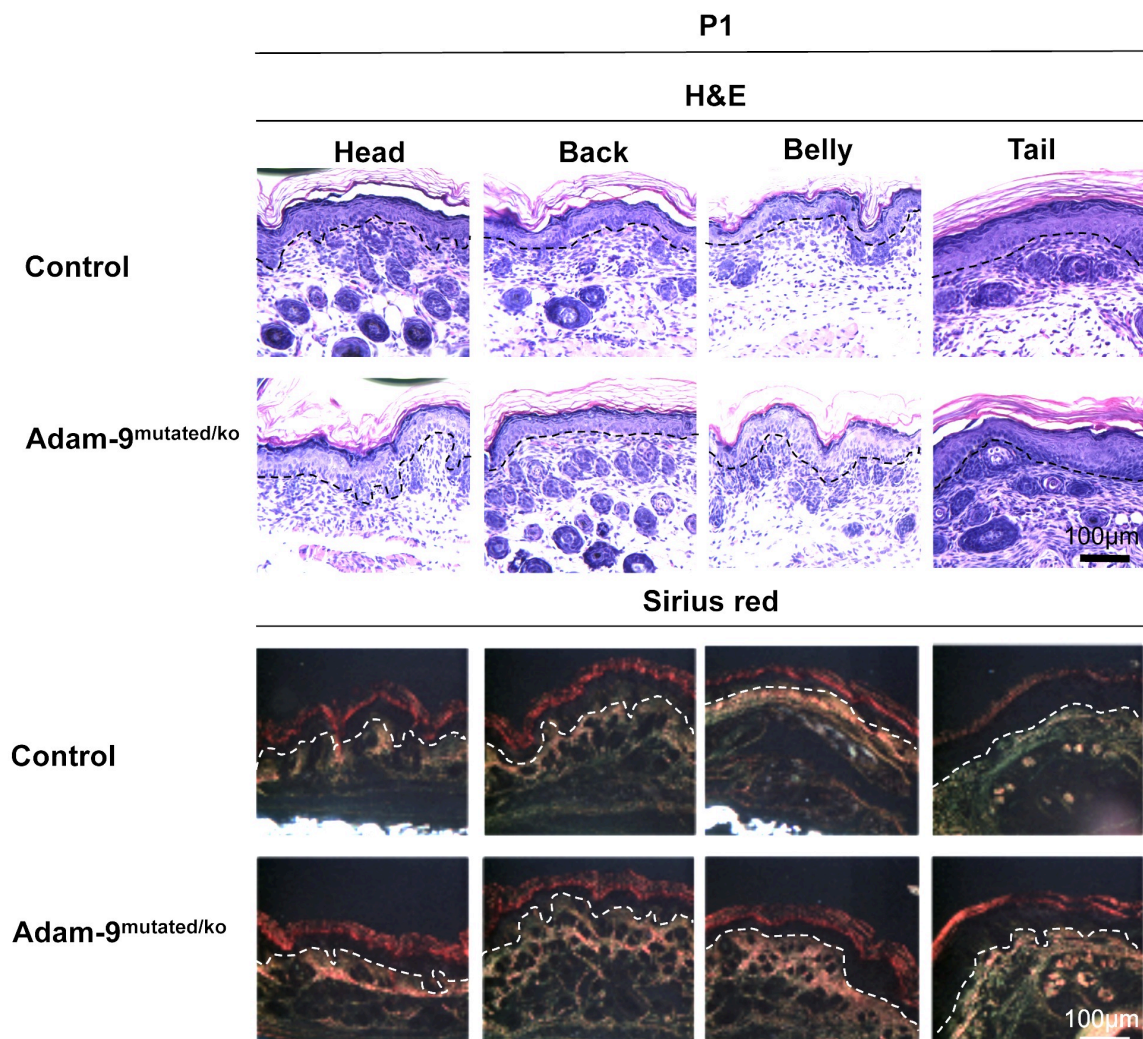


Figure 34: Skin histology at postnatal day 1 (P1) in control and Adam-9^{mutated/ko} animals. Skin sections obtained from head, back, belly and tail of one day old mice were stained with H&E and Sirius red. The Sirius Red stained sections were visualized with polarized light. No differences between control and Adam-9^{mutated/ko} animals were observed in any staining or body region. The dotted line indicates the epidermal-dermal border.

In H&E stained tissue sections of P21 animals of both genotypes many heavily pigmented cells, which most likely represent melanocytes, could be found in the dermis and particularly at the epidermal-dermal junction (Figure 35). In tail sections these cells were additionally found accumulated around the hair follicles and in the dermis between the hair follicles, whereas in head and back skin these cells were more evenly distributed. The belly turned out to be the only region with less pigmented cells than the other analyzed body parts. Some pigmented cells were also found in the epidermis in all inspected body regions (Figure 35).

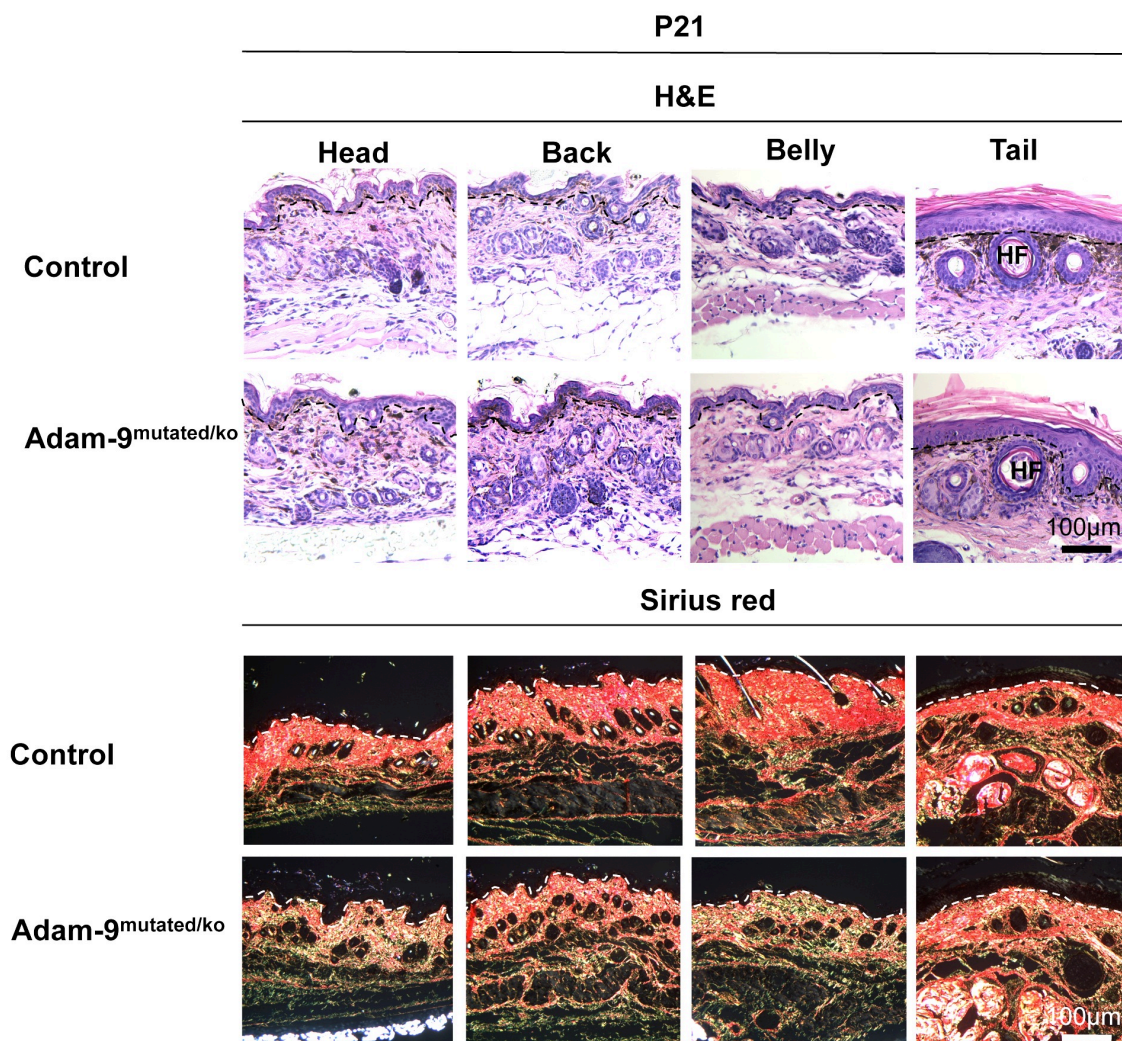


Figure 35: Skin histology at postnatal day 21 (P21) in control and Adam-9^{mutated/ko} animals. Skin sections from head, back, belly and tail of 21 days old mice were stained with H&E and Sirius red (visualized by polarized light). No alterations were detected in any staining or body region in both animal genotypes. In H&E stained sections of the head, back and tail many pigmented cells could be found in the dermis particularly located at the epidermal-dermal junction and in the tail also around the hair follicles (HF). The dotted line indicates the epidermal-dermal border.

To investigate whether these heavily pigmented cells do actually represent melanocytes, skin sections obtained from back and tail at P1 and P21 were immunohistochemically stained against the melanocyte specific antigen tyrosinase related protein-1 (TRP-1). In back skin from P1 animals TRP-1 positive cells were located in the basal layer of the epidermis and in

the hair follicles (Figure 36 A, B). Some single positive cells could be found inside the dermis (arrowheads Figure 36 A, B). In tail skin from P1 animals TRP-1 positive cells were also present in the basal layer of the epidermis as well as in the hair follicles (Figure 36 E, F). However staining in the hair follicles in tail skin was not as strong as in the hair follicles in the back skin. In the tail some positive cells were also located inside the dermis (arrowheads Figure 36 E, F). In back and tail skin from P21 animals a similar staining pattern compared to one day old mice could be observed with positive cells in the basal layer of the epidermis and the hair follicles (Figure 36 C, D, G, H) and single positive cells inside the dermis (arrowheads Figure 36 C, D, G, H). At both analyzed time points and body regions no obvious differences in the distribution and number of melanocytes between control and Adam-9^{mutated/ko} animals were detectable.

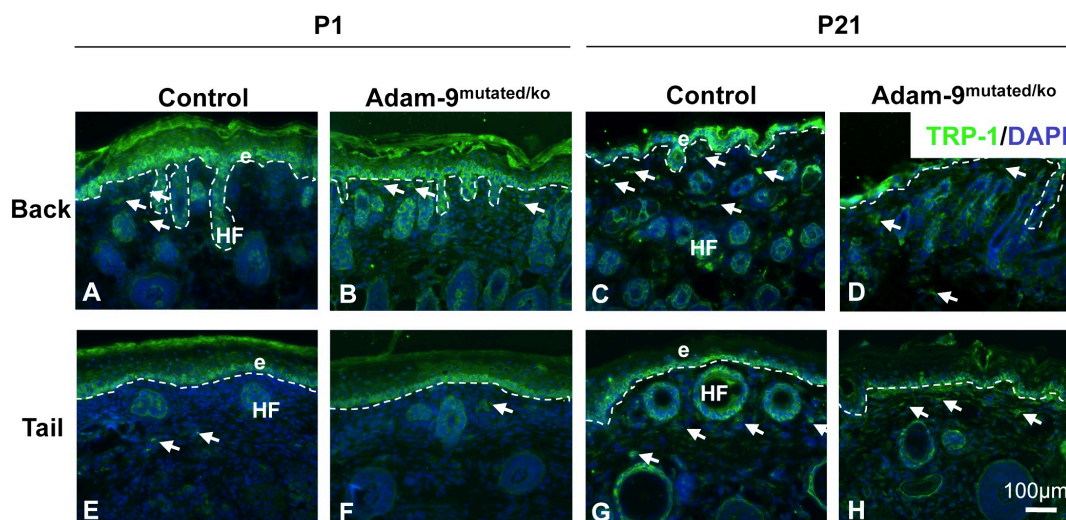


Figure 36: Localization of melanocytes at postnatal day 1 (P1) and 21 (P21) in control and Adam-9^{mutated/ko} animals. Melanocytes were detected using antibodies for the melanocyte specific protein TRP-1 (green). Cell nuclei, in blue, were visualized with DAPI. In skin collected at P1 (A, B, E, F) as well as at P21 (C, D, G, H) TRP-1 positive cells were located in the basal layer of the epidermis (e) and in the hair follicles (HF). Some positive cells were also detected inside the dermis (arrows). The dotted line indicates the epidermal-dermal border. TRP-1: tyrosinase related protein- 1.

Skin differentiation was investigated in Adam-9^{mutated/ko} animals in skin sections from P1 and P21 animals using antibodies directed against cytokeratin 14, a marker for undifferentiated keratinocytes, and the late differentiation marker loricrin. The studied skin sections were taken from back skin and the tail, as the latter one is the only part of the mouse body with a multilayered epidermis in adulthood. Neither at P1 nor at P21 any difference in the expression of the used differentiation markers was observed (Figure 37). In back and tail skin of control and Adam-9^{mutated/ko} animals, cytokeratin 14 positive cells were found in the basal layer of the epidermis and the outer layer of the hair follicles at P1 and P21 (Figure 37 left panel). In tail skin of one day old mice, some positive cells were also detected in suprabasal layers. Positive staining for loricrin was exclusively found at both analyzed time points and

body regions in the upper layers of the epidermis, located in the *stratum granulosum* (g, Figure 37 right panel).

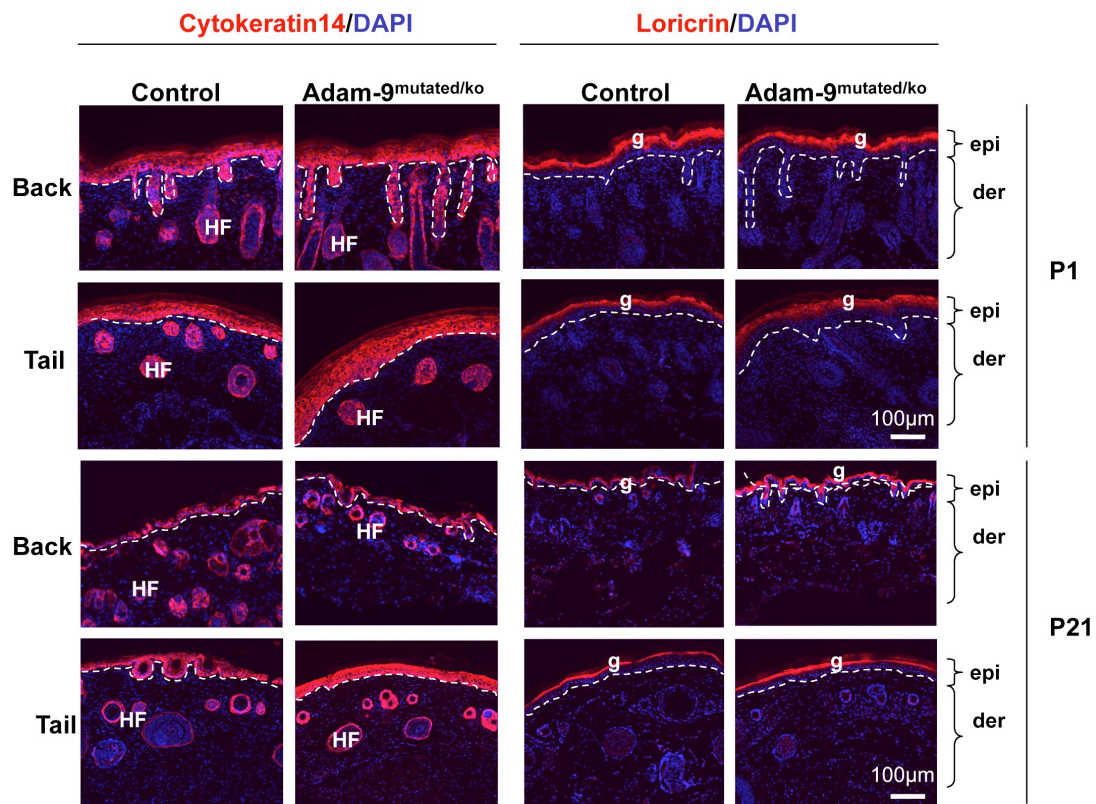


Figure 37: Skin differentiation at postnatal day 1 (P1) and 21 (P21) in control and Adam-9^{mutated/ko} animals. Skin sections of back and tail of one and 21 day old mice were stained for cytokeratin 14 (red; undifferentiated keratinocytes) and the late differentiation marker loricrin (red). Cell nuclei were visualized in blue by DAPI. Cytokeratin 14 positive staining was localized in the basal layer of the epidermis (epi) and in hair follicles (HF) at both time points in back and tail skin (left). Loricrin was detected in the *stratum granulosum* (g) at both time points and both analyzed body regions (right). No difference in the expression of both markers was detected in both animal genotypes. The dotted line marks the epidermal-dermal border. der: dermis.

3.4.2 ADAM-9 expression in melanomas developed in control mice

It was shown that the Hgf/Cdk4^{R24C/R24C} animals develop spontaneous melanomas and that treatment with DMBA or UV light induces these tumors also at earlier time points (Tormo *et al.*, 2006; Landsberg *et al.*, 2010; Gaffal *et al.*, 2011).

A first investigation was aimed to determine whether also in the mice used here expression of ADAM-9 is induced and localized at the tumor-stroma border in stromal cells as well as in the tumor cells as our group has shown before in human specimens and in melanomas developed in C57/Bl6 mice upon dermal injection of murine B16-F1 cells (Zigrino *et al.*, 2005; Abety *et al.*, 2012). Analysis of ADAM-9 transcript expression was performed by RT-PCR using RNA isolated from DMBA induced tumors (n=4) 13 weeks after DMBA treatment and from normal skin from 13 weeks old untreated animals (n=3). This analysis showed that ADAM-9 transcripts are induced in the tumors (Figure 38 A).

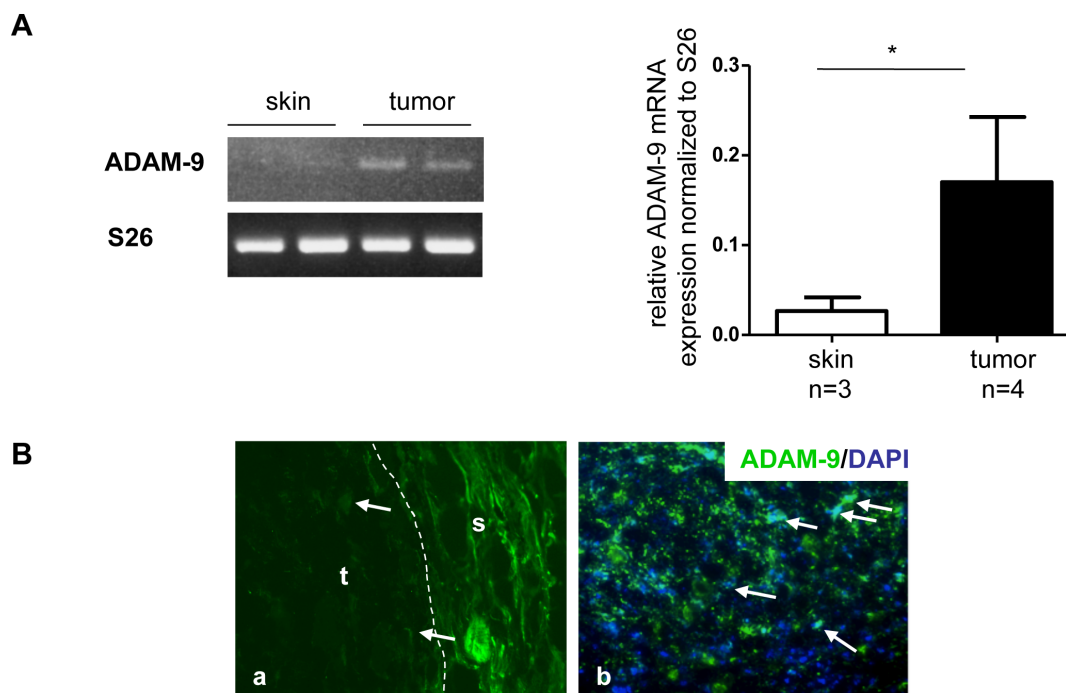


Figure 38: Expression and localization of ADAM-9 in DMBA induced tumors in control animals. **(A)** ADAM-9 transcript expression was measured in normal skin from 13 week old untreated animals (n=3) and DMBA induced tumors (n=4) harvested 13 weeks after DMBA treatment. The graph shows the average \pm SD of signal intensities after normalization to S26, used as control. *: p<0.05. **(B)** ADAM-9 immunodetection in tumors shows the protein localized at the tumor-stroma-border (a), marked by the dashed line, in the stroma and in some tumor cells, indicated by the arrow. Higher magnification of the tumor mass (b) revealed ADAM-9 positivity in tumor cells (arrows). The fluorescent dye DAPI was used to visualize cell nuclei. s: stroma; t: tumor.

To localize ADAM-9 protein in these tumors, sections obtained from control animals were immunohistochemically stained with an antibody directed against the ectodomain of ADAM-9. ADAM-9 staining appeared to be localized at the tumor-stroma border in stromal cells and in some tumor cells at the periphery indicated by the arrow (Figure 34 B, a). Inside the tumor stained cells were also found at larger magnification (Figure 34 B, b).

3.4.3 Analysis of DMBA-induced tumor growth and development

Next, we induced tumor growth in control and Adam-9^{mutated/ko} animals. For this back skin of mice was painted once with DMBA at day three after birth. The number of developing tumors was counted on a weekly basis over time. In both genotypes the first visible tumors were observed four weeks after DMBA treatment. The tumors appeared as dots, smaller than 1mm³, on the back of the animals and tumor number was recorded from week four after DMBA treatment until the animals were sacrificed, around week 13. In Figure 39 A, representative photographs of the back of control and Adam-9^{mutated/ko} animals at week four and 13 after DMBA treatment are shown. The tumors appeared primarily on the back of the animals, but occasionally tumors were also observed at the head, paws and the tail in both genotypes, likely due to scratching and mutual touching of the animals, which led to spreading of the DMBA to other body regions than the back.

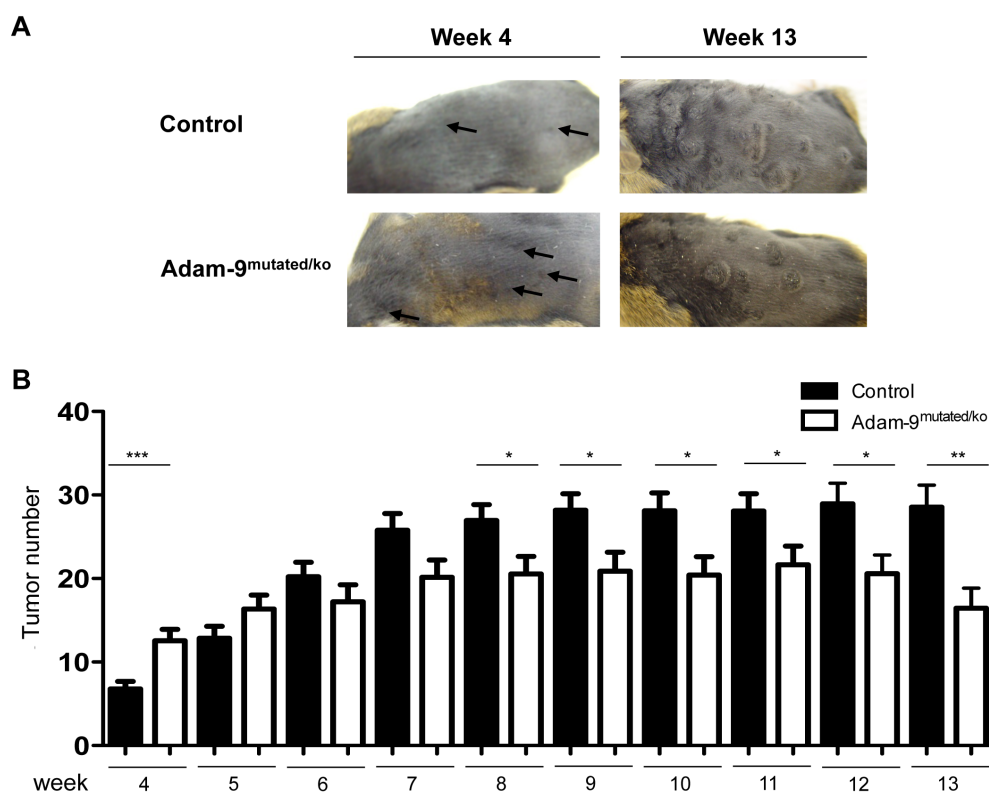


Figure 39: Tumor development in control and Adam-9^{mutated/ko} animals. Tumors were induced by treatment of mice back skin with DMBA at postnatal day three. **(A)** Macroscopic pictures of the back of control and Adam-9^{mutated/ko} mice bearing melanomas at week four (arrows indicate the tumors) and 13 after DMBA application. **(B)** The number of tumors developed in control or Adam-9^{mutated/ko} mice, counted weekly from week four to 13 after DMBA treatment. The graph shows the mean \pm SEM. *: $p < 0.05$; **: $p < 0.01$; ***: $p < 0.001$.

When the tumor number was counted at week four after DMBA treatment a significantly increased tumor number was observed in Adam-9^{mutated/ko} mice compared to the control animals ($p = 0.0009$). Interestingly, from week six onwards the Adam-9^{mutated/ko} mice exhibited a reduced number of tumors as compared to control animals. This reduced tumor number in the absence of ADAM-9 was observed in all the following analyzed time points and was significant from week eight till week 13 (Figure 39 B).

To find out if ADAM-9 depletion influenced not only the generation, but also the growth of the tumors, in one cohort of control ($n=10$) and Adam-9^{mutated/ko} ($n=8$) animals, the size of all developed tumors was measured after the animals were sacrificed at week 13. The tumors were divided into groups according to the tumor size and the proportion of the different tumor groups of the total tumor number was calculated in percent (Figure 40). This analysis revealed that in the control animals 1,6-fold higher number of tumors of 0-10mm³ volume developed compared to the Adam-9^{mutated/ko} mice. However the proportion of tumors with larger size was higher in the Adam-9^{mutated/ko} animals (10-50mm³: 1,4-fold; 50-200mm³: 1,7-fold; >200mm³: 1,9-fold). This indicates that the Adam-9^{mutated/ko} mice developed more tumors with a larger size compared to the control animals.

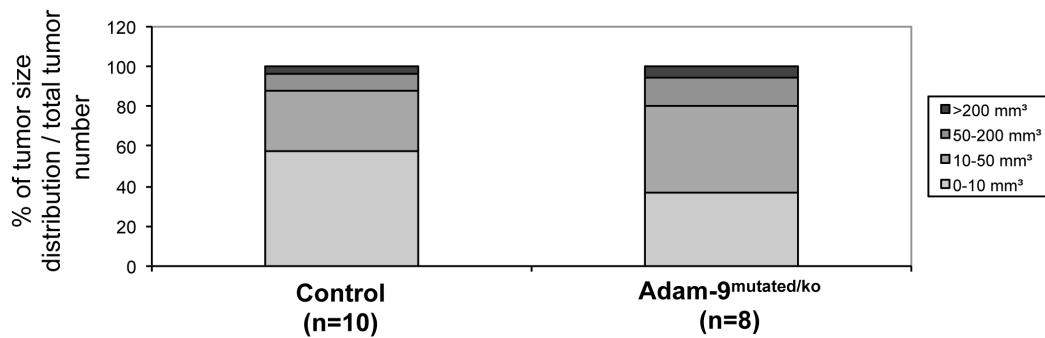


Figure 40: Tumor growth in control and Adam-9^{mutated/ko} animals. Tumor formation was induced by treatment with DMBA on the back skin at postnatal day three. Mice were sacrificed at week 13 and the number of developed tumors counted. The volume of each tumor was determined by measurement of the three tumor diameters using a caliper. The tumors were divided into different groups according to their size and expressed as percent of total number.

3.4.3.1 Histology of DMBA-induced tumors

To analyze the histomorphology of grown tumors, the largest tumors were isolated and stained with H&E. In Figure 41 photographs of H&E stained sections from tumors isolated at week four and week 13 (control (A, E); Adam-9^{mutated/ko} (B, C, F, G)) are shown. The tumors consisted of a mixed population of many heavily pigmented, epitheloid shaped cells, arranged among lightly pigmented cells, which were all identified as melanocytes by the TRP-1 immunostaining (Figure 42 D, H). After analysis of several tumor sections (n=6) no obvious difference neither in the density of these differentially pigmented cells nor in the structural appearance of the tumors could be detected in Adam-9^{mutated/ko} as compared to control mice.

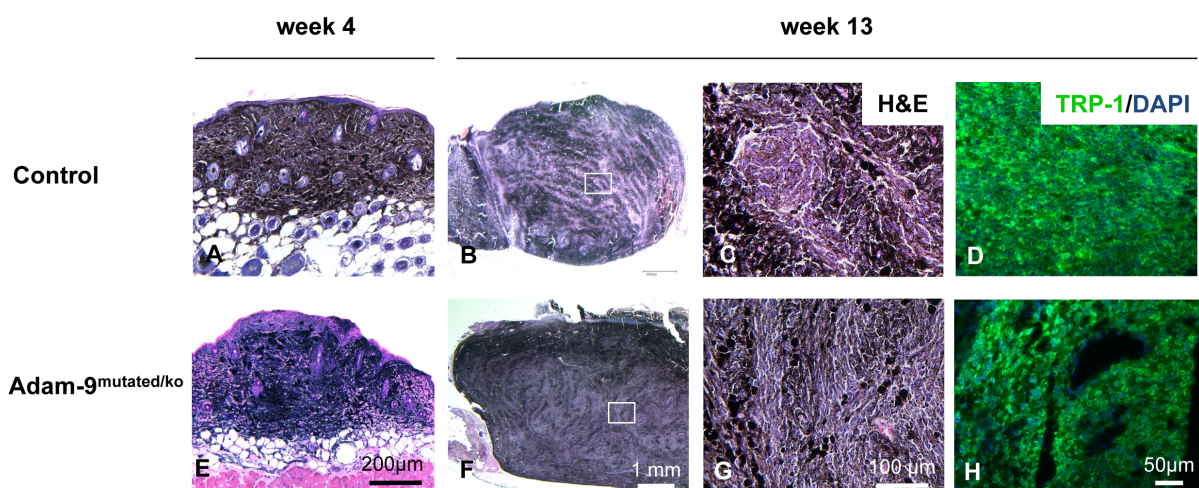


Figure 41: Histomorphology of DMBA-induced tumors grown in control and Adam-9^{mutated/ko} animals four and 13 weeks after DMBA application. Animals were sacrificed at the indicated time points and the largest tumors were fixed, sectioned and stained using H&E. Representative pictures of tumors are shown. In C, G higher magnification of the internal parts of tumors at week 13 is shown (magnifications of squares in B, F). Immunohistochemical detection of the melanocyte specific protein TRP-1 (D, H) in tumor sections. Cell nuclei were visualized with the fluorescent dye DAPI, blue. TRP-1: tyrosinase related protein- 1.

3.4.3.2 Analysis of vascularization and proliferation of DMBA-induced tumors

The DMBA treatment experiments revealed an initial increase (week 4) in tumor development in the absence of ADAM-9, whereas at later time-points (weeks 6-13) the tumor number in the Adam-9^{mutated/ko} animals was decreased compared to the control mice. A different vascularization of the tumors might provide, among others, an explanation for the difference in the tumor growth between control and Adam-9^{mutated/ko} animals.

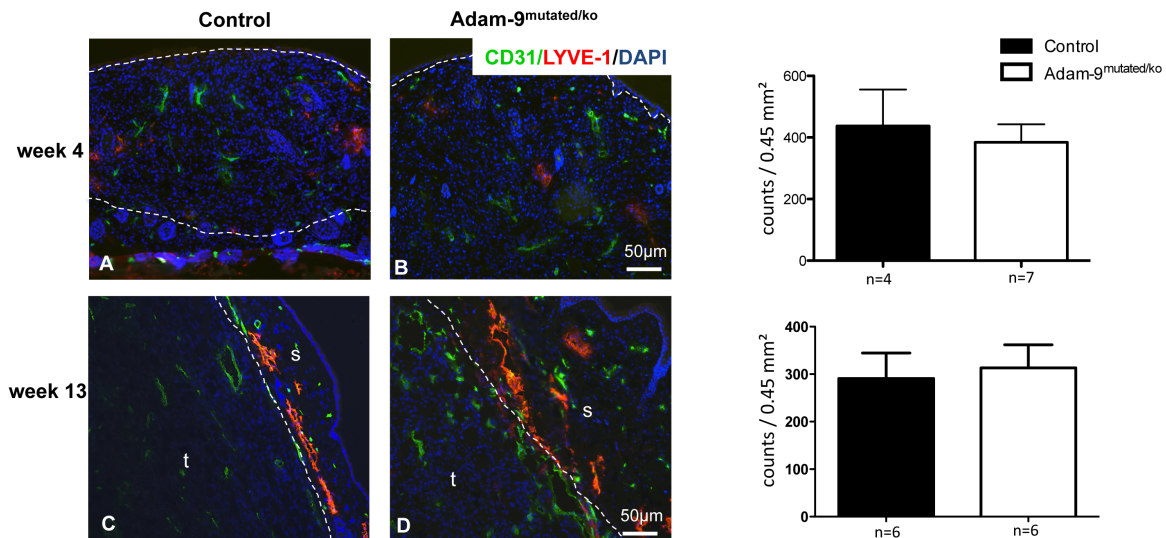


Figure 42: Vascularization of tumors grown in control and Adam-9^{mutated/ko} animals. Frozen tumor sections were double stained for the blood vessel endothelial cell specific marker CD31 (green) and the lymphatic endothelial cell specific marker LYVE-1 (red). Cell nuclei were visualized with the fluorescent dye DAPI (blue). Photographs show a representative picture of stained tumors from four and 13 weeks after DMBA application. The tumor (t)-stroma (s) border is indicated by the dashed line. The graphs in the right panel show quantification of the CD31 staining. Different parts of the tumors from the indicated number of animals (n) were analyzed and the average expressed \pm SEM.

Indeed, ADAM-9 was previously shown to be expressed by endothelial cells and moreover being functionally involved in pathological neovascularization of the retina (Guaiquil *et al.*, 2009). To determine if ablation of ADAM-9 caused an altered vascularization in the DMBA induced tumors, tissue sections, obtained from tumors isolated four and 13 weeks after the DMBA application, were double-stained against CD31 (also known as PECAM and expressed by vascular endothelial cells) and LYVE-1 (expressed by lymphatic endothelial cells). Representative pictures of these stainings are shown in Figure 42. In tumors from control and Adam-9^{mutated/ko} animals vessels positive for CD31 are found in the tumor-stroma as well as within the tumor mass at week four as well as at week 13, whereas lymphatic vessels are preliminary located at the tumor-stroma border. Quantification of the CD31 staining using the ImageJ program revealed no differences in vascularization.

Another reason, which may account for the difference in tumor development, might be an altered proliferation or apoptosis of the tumor cells. In Figure 43 representative photographs of Ki67 (proliferating cells) and cleaved caspase-3 (apoptotic cells) double-stained tumor sections from week four and 13 are shown. In all tumors many proliferating cells could be

found within the tumor mass, whereas apoptotic cells were only barely detected, indicated by the white arrowheads.

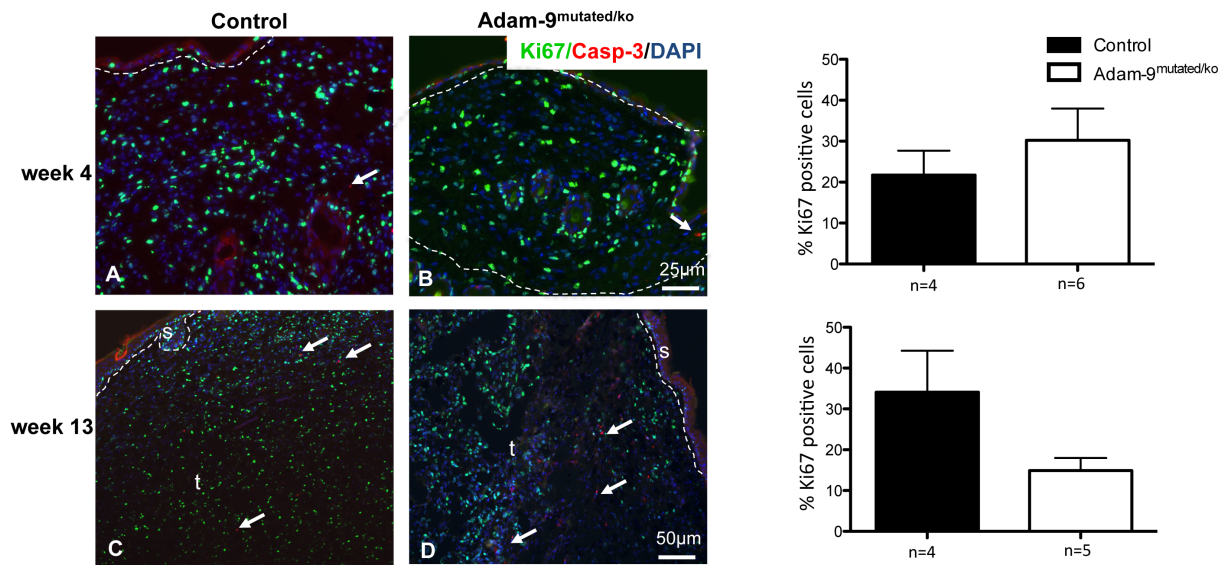


Figure 43: Proliferation and apoptosis of tumors grown in control and Adam-9^{mutated/ko} animals. Frozen tumor sections were double stained for Ki67 (green) and cleaved caspase-3 (red). Cell nuclei were visualized with the fluorescent dye DAPI (blue). The photographs show representative pictures of the proliferation and apoptosis in tumors obtained from control (A, C) and Adam-9^{mutated/ko} (B, D) animals four and 13 weeks after DMBA application. The white arrowheads point to cleaved caspase-3 positive cells. The tumor (t)-stroma (s) border is indicated by the dashed line. In the graph, the number of Ki67 positive cells were counted in different parts of the tumors and expressed as percent of all counted cells. The bars represent the mean of different animals \pm SEM.

Apart from some single cells in the basal layer of the epidermis no proliferating cells were found in the tumor-stroma at any time-point, whereas inside the tumors many proliferating cells were found in control as well as in Adam-9^{mutated/ko} animals at week four and week 13. To quantify the amount of proliferating cells in the tumors, the Ki67 positive cells were counted in different parts of the tumors and expressed as percent of the total number of counted cells. This analysis showed that at week four slightly more proliferating cells were found in the tumors of Adam-9^{mutated/ko} animals, whereas at week 13 proliferation was reduced in the absence of ADAM-9.

3.4.3.3 Inflammatory infiltration of DMBA-induced tumors

The tumor microenvironment is enriched by inflammatory cells, which are a critical component of tumor progression by influencing proliferation, survival and migration of cancer cells (Coussens and Werb, 2002). The expression of ADAM-9 in inflammatory cells was shown for peripheral blood monocytes and macrophages, where the protein is involved in the formation of multinuclear giant cells (Namba *et al.*, 2001; Mackiewicz *et al.*, 2005; Ma *et al.*, 2006). To analyze if ADAM-9 depletion altered the inflammatory infiltration of DMBA induced tumors, tissue sections from tumors obtained at week 13 were immunohistochemically stained with antibodies directed against lymphocytes (CD45), macrophages (CD68) and

neutrophils. CD45 positive cells were mainly found in the tumor-stroma (Figure 44 A, B) and some cells also infiltrated the tumor tissue (arrowheads Figure 44 C, D). Macrophages were also located in the tumor stroma and no CD68 positive cells were detected inside the tumor (Figure 44 E-H). Neutrophil infiltration was not detected in the tumors. No obvious difference in the recruitment of macrophages or lymphocytes to the tumor of control and Adam-9^{mutated/ko} animals was found.

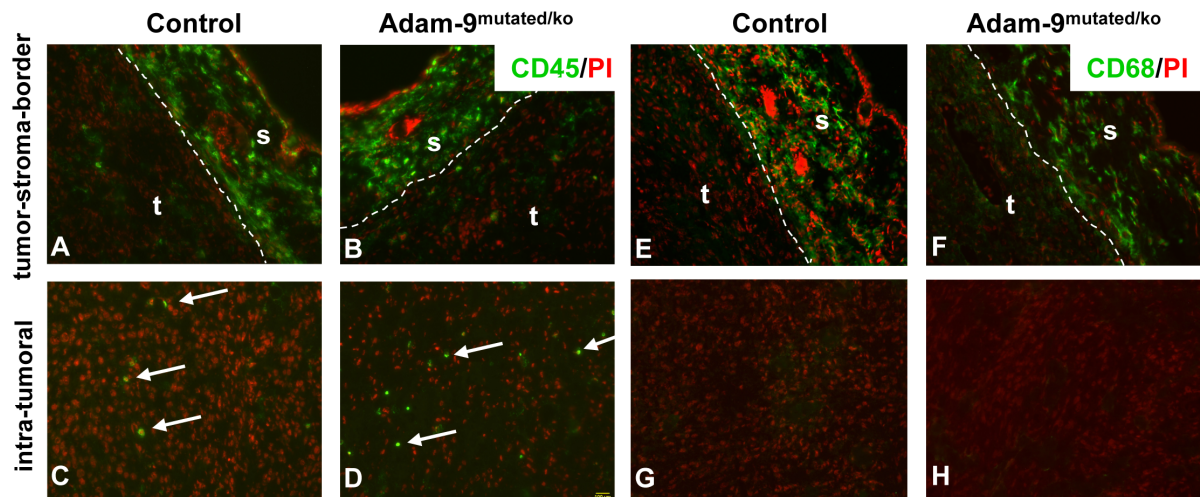


Figure 44: Inflammation of tumors grown in control and Adam-9^{mutated/ko} animals. Frozen tumor sections were obtained from animals 13 weeks after DMBA application, fixed in acetone and immunohistochemically stained using specific antibodies against CD45 (lymphocytes) and CD68 (macrophages). The fluorescent dye propidium iodide (PI) was used to visualize the cell nuclei (red). The dotted line indicates the border between tumor (t) and stroma (s) tissue. Arrows indicate CD45 positive cells. CD68 positive cells were found in the peritumoral stroma (E, F), but not inside the tumor (G, H).

3.4.4 Metastatic spread in control and Adam-9^{mutated/ko} animals

Once melanoma has invaded the tissue cells spread through lymphatic and blood vessels to distant organs of which, apart from skin, lung, liver, kidneys, heart and brain include the most frequently metastasized organs by melanomas (Leiter *et al.*, 2004). To study metastases formation to the different organs, lung, liver, kidneys, heart, brain and the intestinal tract of control and Adam-9^{mutated/ko} animals were inspected for visible metastases after tumor bearing animals were killed. Metastases were found predominantly in the lungs. Only in two control animals metastases were also detected in the liver and the kidney. In none of the other analyzed organs macroscopically visible metastases were observed. The axillary and groin lymph nodes were prepared and size was measured in three bisecting diameters using a precision caliper. The mean size of the right and the left lymph node was calculated and the average depicted in Figure 45. The average size of the axillary and groin lymph nodes measured in DMBA treated control animals (n=28) and in Adam-9^{mutated/ko} animals (n=29) was comparable (Figure 45).

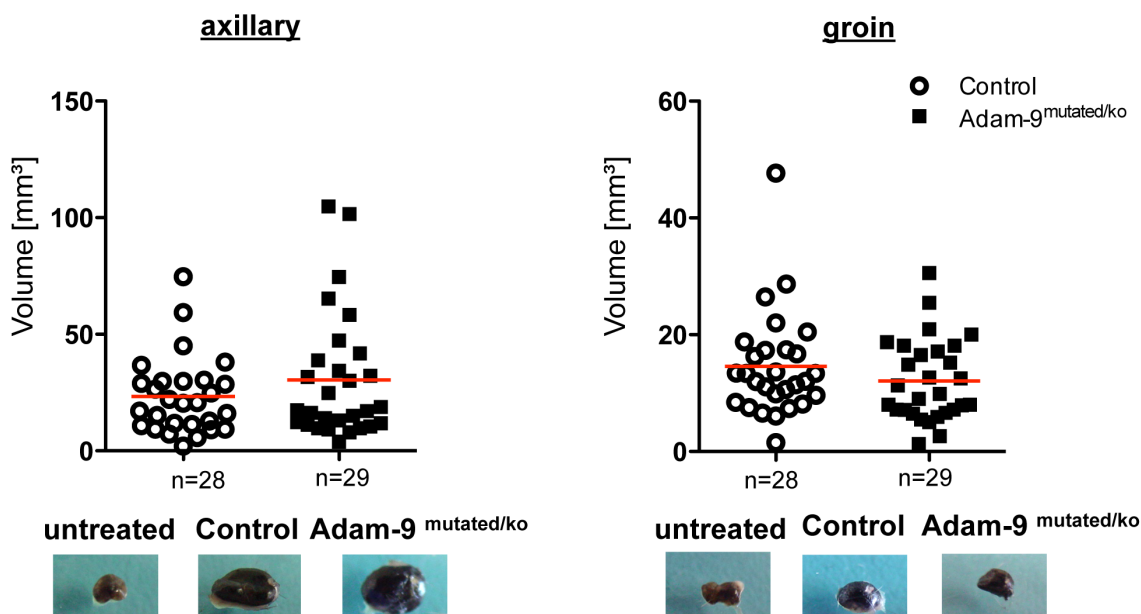


Figure 45: Metastases in lymph nodes of DMBA treated control and Adam-9^{mutated/ko} animals. 13 weeks post DMBA tumor induction animals were killed. Axillary and groin lymph nodes were prepared and their volume was measured. Each dot represents the mean volume of the right and the left lymph node of a single animal. The red line indicates the mean value of all animals. No significant difference in lymph node volume between control (n=28) and Adam-9^{mutated/ko} (n=29) animals was detected. Photographs show representative pictures of the macroscopic appearance of the lymph nodes of both genotypes.

Macroscopically all lymph nodes obtained from DMBA-treated animals, from both genotypes, were much darker in color compared to lymph nodes from untreated animals indicating melanoma cell colonization (Figure 45). Representative photographs of axillary and groin lymph nodes of DMBA treated and untreated control and Adam-9^{mutated/ko} animals are shown in the lower panel of Figure 45.

Lymph node morphology was further explored in tissue sections stained by H&E. In sections of axillary lymph nodes from control as well as from Adam-9^{mutated/ko} animals infiltrates of dark pigmented cells could be detected in the periphery and the inner parts of the lymph nodes (Figure 46 A, D). Higher magnifications of areas containing these pigmented cells show a mixed population of these cells and the normal lymphatic tissue (Figure 46 B, E). This was also visible by staining with TRP-1 and CD45, a lymphocyte specific marker (Figure 46 C, F). In lymph nodes from untreated animals no pigmented and TRP-1 positive cells were detected (Figure 46 G, H, I). Also when the groin lymph nodes were analyzed the same result was obtained.

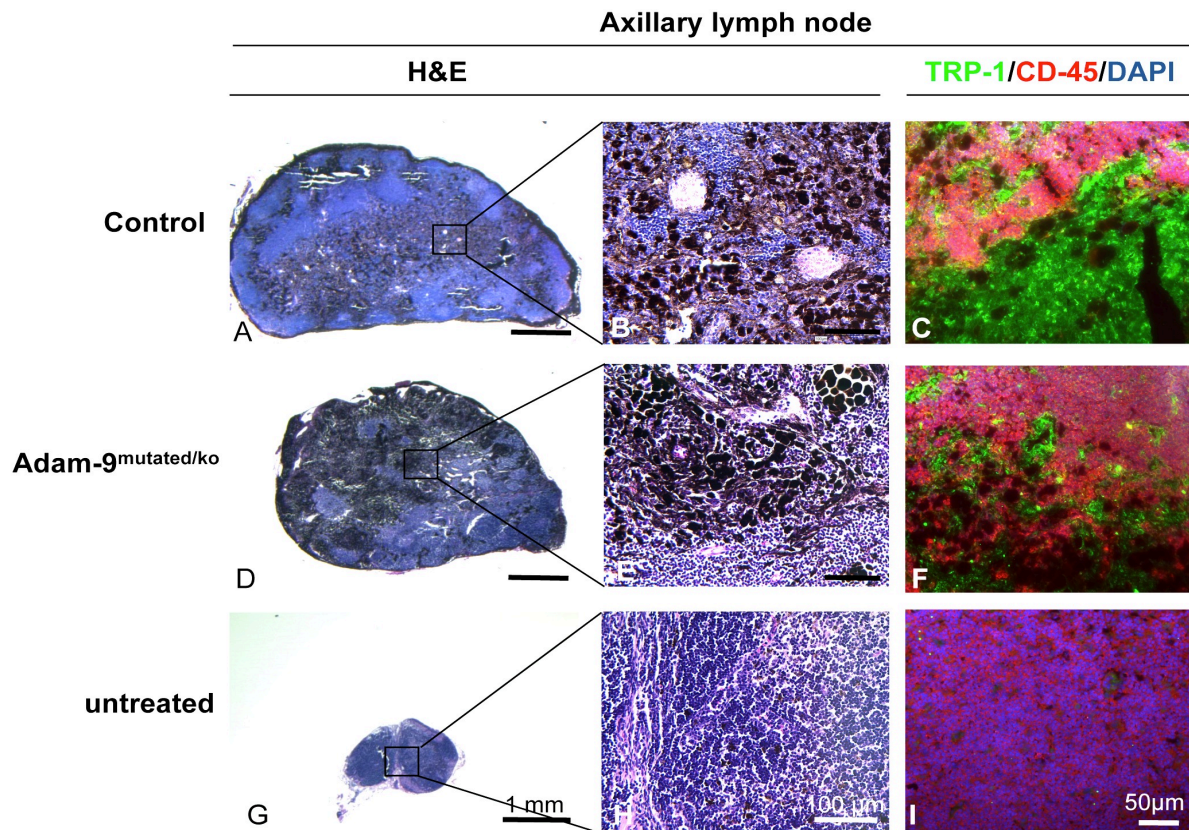


Figure 46: Histological appearance of lymph nodes of DMBA treated control and Adam-9^{mutated/ko} animals. Sections of axillary nodes stained with H&E. In addition lymph nodes of an untreated animal were included into the analysis. In the left column overview photographs of axillary (A, D) lymph nodes are shown. High magnifications (B, E) show pigmented cells within the tissue. In untreated lymph nodes no pigmented cells were detected (G, H). Staining of lymph node tissue with the melanoma cell specific marker TRP-1 and the lymphocyte marker CD45 detected infiltrated melanoma cells (green) within axillary lymph nodes of DMBA treated animals. These cells were surrounded by normal lymph node tissue, which was positive for CD45 (red). In untreated animals only CD45 positive, but no TRP-1 positive cells were observed. The fluorescent dye DAPI was used to visualize the cell nuclei (blue). TRP-1: tyrosinase related protein- 1.

The metastatic spread to the lungs, was quantified by counting the number of visible metastases on the surface of the lungs. This analysis revealed a significantly reduced ($p=0.03$) number of metastases to the lungs in Adam-9^{mutated/ko} (3 ± 1 metastases; $n=29$) compared to control (7 ± 1 ; $n=30$) animals at ~week 13 post DMBA treatment (Figure 47). Representative pictures of lungs, with metastatic nodules (indicated by the arrows) obtained from Adam-9^{mutated/ko} and control animals are shown in Figure 47. In H&E stained lung sections from control animals, metastases could be clearly detected as pigmented nodules in these sections (arrows in Figure 48 A), whereas metastases in lungs of Adam-9^{mutated/ko} animals were hardly detectable (Figure 48 B).

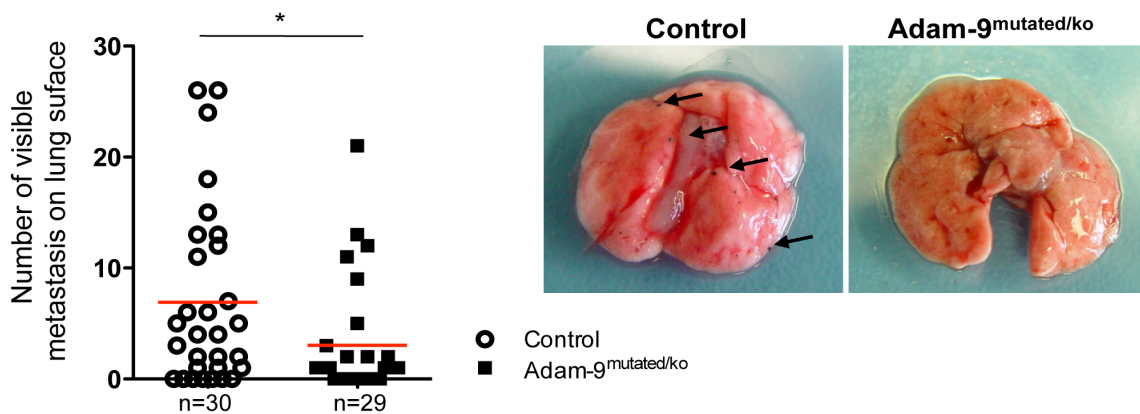


Figure 47: Metastases formation in lungs of DMBA treated control and Adam-9^{mutated/ko} animals. The back of control and Adam-9^{mutated/ko} animals was painted once with DMBA on postnatal day three and at ~week 13 the animals were killed. The number of black nodules visible on the surface of the lungs was counted. Every dot represents the average number of visible metastases counted in a single animal. The red line indicates the mean value. A significantly reduced number of metastatic nodules on the lungs of Adam-9^{mutated/ko} (n=30) compared to control (n=29) animals was found. *: p<0.05. The photographs on the right show pictures of lungs from representative animals. The arrows indicate visible metastases on the lung surface.

Further immunohistological staining using the TRP-1 marker, confirmed the presence of TRP-1 positive nodules in the lungs of control animals (Figure 48 C). In lungs of Adam-9^{mutated/ko} animals TRP-1 reactivity could not be detected in nodules as seen in the control animals (Figure 48 D).

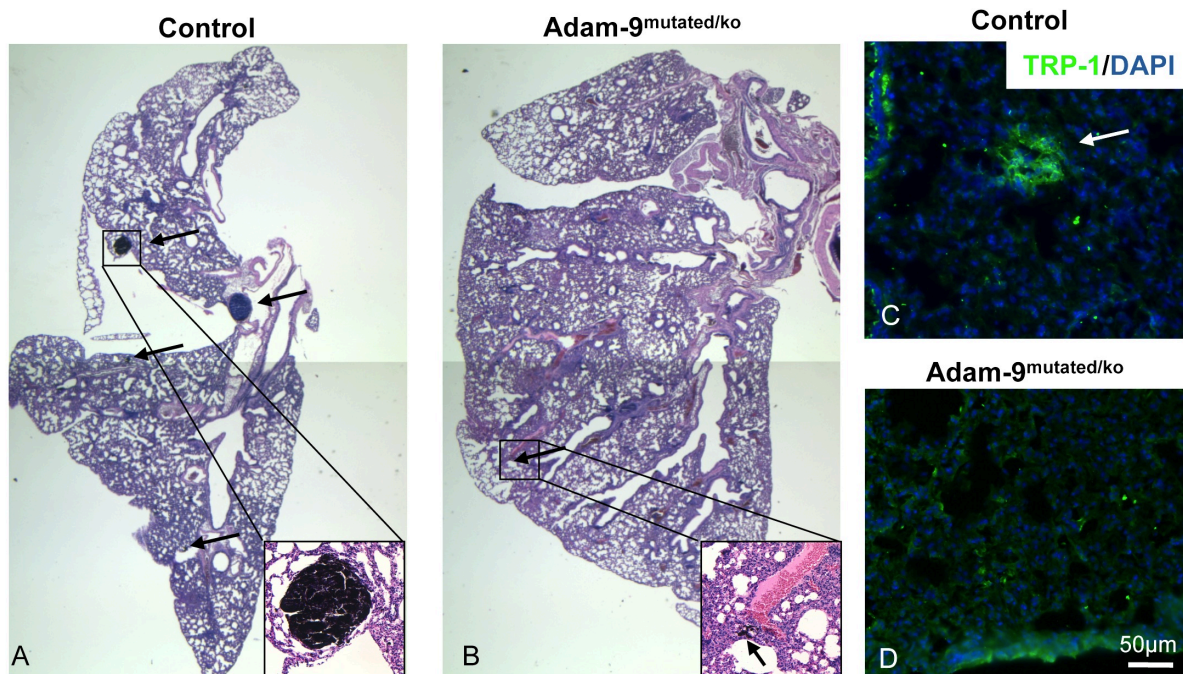


Figure 48: Histological appearance of lungs of DMBA treated control and Adam-9^{mutated/ko} animals. H&E stained sections of the lungs obtained from DMBA treated control and Adam-9^{mutated/ko} animals, revealed the presence of metastatic nodules (arrows) in the lungs of control mice, whereas in Adam-9^{mutated/ko} animals metastases were only hardly detected (A, B). The metastatic nodules in control were positive for the melanoma cell specific marker TRP-1 (white arrow) (C, D). The fluorescent dye DAPI was used to visualize the cell nuclei. TRP-1: tyrosinase related protein- 1.

According to theories on metastatic spreading, it is still matter of discussion in the scientific society how metastases formation occurs. From the one side it is believed that metastatic spread parallels tumor growth, with larger tumors having higher probability to metastasize (Klein, 2009). A second more recent and likely realistic theory, indicates that the two processes are independent from each other and thus, when tumor is not yet diagnosed it may have already spread to distant organs (Klein, 2009). To investigate whether in our animal model, the reduced number of metastases is the result of reduced tumor growth, thus agreeing with the older theory of metastasis, we compared control and Adam-9^{mutated/ko} animals bearing tumors larger than 200 mm³ or having more than 20 tumors.

In every group the number of lung metastases was significantly reduced in Adam-9^{mutated/ko} animals independently of the size of primary tumor, which was comparable in both animals and of number of tumors. This would indicate that metastatic spread in these animals is not dependent on the tumor size and number. In Table 12 the size of the tumors, age of mice, tumor and metastases number and the statistical significance for the different groups is summarized.

Table 12: DMBA treated animals were subdivided into different groups, matching the animals either for the tumor size, the number or the age. Values show the mean \pm SEM, except for the age where the SD is shown. Significance was tested with Student's t-test, with $p < 0.05$ considered to be statistically significant.

Group	Genotype	Number of animals	Animal age [days]	Volume of largest tumor [mm ³]	Tumor number	Number of metastases	p-value
>200 mm ³	control	20	98 \pm 19	560 \pm 78	35 \pm 13	8 \pm 2	0.04
	Adam-9 ^{mutated/ko}	17	95 \pm 16	599 \pm 106	23 \pm 10	3 \pm 1	
>20 tumors	control	24	97 \pm 17	390 \pm 77	37 \pm 10	8 \pm 2	0.04
	Adam-9 ^{mutated/ko}	19	91 \pm 17	454 \pm 110	34 \pm 10	3 \pm 1	

Taken together these analyses interestingly indicated that in the absence of ADAM-9 metastatic spreading of melanoma cells to the lung indeed is reduced.

3.4.5 Characterization of mechanisms responsible for reduced lung metastases formation in Adam-9^{mutated/ko} animals

3.4.5.1 Melanoma cell chemoattraction

Melanoma cells were shown to be attracted to organs of metastases by the activity of chemokines and cytokines (Kakinuma and Hwang, 2006). Thus, reduced lung colonization in Adam-9^{mutated/ko} animals may result from altered release of chemotactic factors. To investigate whether ADAM-9 depletion leads to alterations in the amount of circulating cytokines released in tumor bearing animals, the amount of different cytokines present in the

serum of DMBA treated control and Adam-9^{mutated/ko} mice was determined using RayBio[®] mouse cytokine array (Figure 49). These membranes, which allow simultaneous analysis of 62 different factors, were incubated with serum pooled from three different animals per genotype, obtained at week 13 after DMBA treatment. The expression of the cytokines was quantified by densitometry. Only those proteins, which were more than 2-fold regulated, were considered as valid. Among the 62 cytokines increased amounts of 12 proteins were detected in the serum of Adam-9^{mutated/ko} compared to control animals (Table in Figure 49). The highest difference was detected for interleukin-17 (IL-17) and Lymphotactin with 3,93- or 3,97-fold, higher amounts in the serum of Adam-9^{mutated/ko} as compared to control animals. Surprisingly, none of the analyzed proteins was found to be reduced more than 2-fold in the Adam-9^{mutated/ko} serum compared to control animals. Interestingly SDF-1 α also known as CXCL12 was up-regulated 3,17-fold in the serum from Adam-9^{mutated/ko} compared to control animals. This cytokine has previously been reported to be important for recruiting melanoma cells to the lung. CXCL12 is released in lung tissue and reacts with the receptor CXCR4 expressed on melanoma cells, thereby attracting them to the lung (Kakinuma and Hwang, 2006).

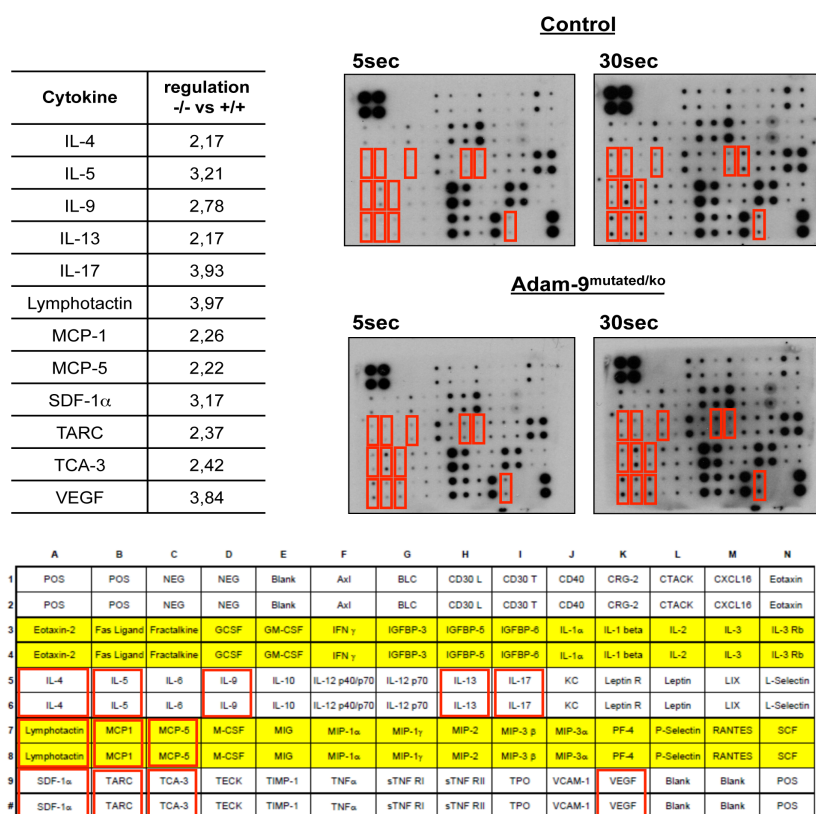


Figure 49: RayBio[®] mouse cytokine antibody array. RayBio[®] mouse cytokine antibody array detecting 62 different murine cytokines was used to analyze serum from control and Adam-9^{mutated/ko} animals 13 weeks after treatment with DMBA. Membranes were incubated with serum pooled from three different animals for each genotype. Specific signals were quantified by densitometry, normalized to the positive control and expressed as ratio of Adam-9^{mutated/ko} versus control. The table summarizes factors, which were at least 2-fold regulated after 5sec exposure time. To detect all proteins present in the serum of the animals, even if in reduced amounts, films were also exposed for a longer time, which is not in the linear amplification range (30 sec).

This increased amount of CXCL12 would not agree with reduced attraction of the melanoma cells to the lung in the absence of ADAM-9. As CXCL12 needs to interact with the relative receptor on melanoma cells, CXCR4, it is yet possible that despite the increased levels, melanoma cells do not express the receptor.

To analyze expression of the CXCR4 receptor, sections of tumors from control and Adam-9^{mutated/ko} animals obtained 13 weeks after DMBA application were immunostained using an antibody directed against CXCR4. Despite the positive staining seen in the spleen, which served as control (Figure 50 C), in the tumor very low and diffuse staining was observed (Figure 50 A, B), suggesting that those tumors do not express high amounts of CXCR4.

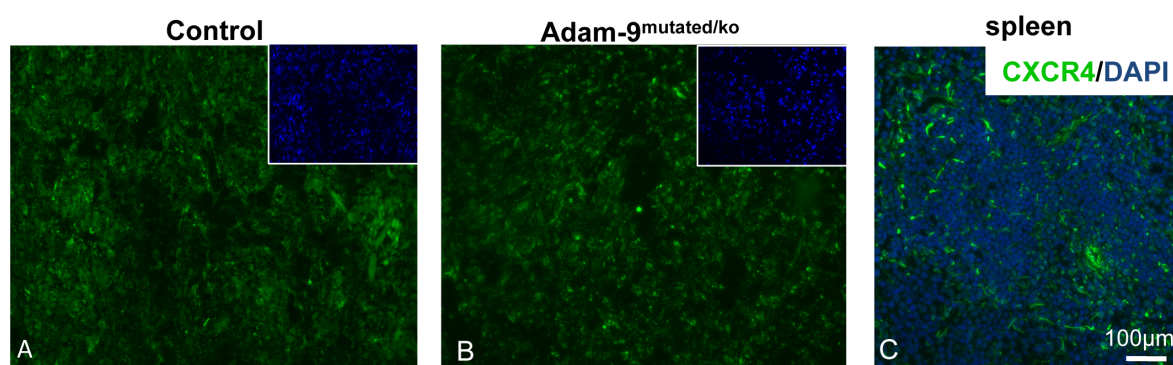


Figure 50: CXCR4 expression in DMBA induced tumors from control and Adam-9^{mutated/ko} animals. Tumor sections from animals at 13 weeks after DMBA application were immunohistochemically stained using an antibody against CXCR4 (green). DAPI was used to visualize the cell nuclei, in blue. Only very faint staining was present in the tumor cells (A, B). Spleen sections from control animals were used as positive control (C).

Once the metastatic cell seeds into the organ, it needs to generate a favorable microenvironment and to counteract the host-immunity, which is activated (Bacac and Stamenkovic, 2008). Thus higher infiltration of the lung by inflammatory cells may counteract metastases formation in lungs of Adam-9^{mutated/ko} animals. However, inflammatory reaction around the lung metastases in control and Adam-9^{mutated/ko} animals as analyzed by immunodetection of the lymphocytes markers CD45, CD3, CD3 and CD8 was not altered (data not shown). These data indicate that host-immunity does not play a role in the observed reduced metastatic load to the lung in Adam-9^{mutated/ko} animals.

3.4.5.2 Basement membranes in DMBA-induced tumors

One characteristic of malignant tumors is the presence of a discontinuous BM. Degradation of this barrier by the tumor cells enables them to invade the surrounding connective tissue (Baluk *et al.*, 2005; Bacac and Stamenkovic, 2008). The *in vitro* studies using ADAM-9 down-regulated cells in the DDS invasion system revealed a reduced invasion through the BM upon ADAM-9 silencing (chapter 3.2.1.3). Moreover the BM protein laminin β 3-chain could be identified as a substrate for ADAM-9 (chapter 3.2.2). To analyze if the absence of ADAM-

9 in DMBA induced tumors results in reduced BM degradation in the tumors, immunostainings for laminin β 3-chain were performed on tumor tissues.

Tissue sections of tumors obtained from control and Adam-9^{mutated/ko} animals four and 13 weeks after DMBA application were immunohistochemically stained with an antibody against the laminin β 3-chain, which is a subunit of laminin 332, present in the BMs of the skin (Tzu and Marinkovich, 2008).

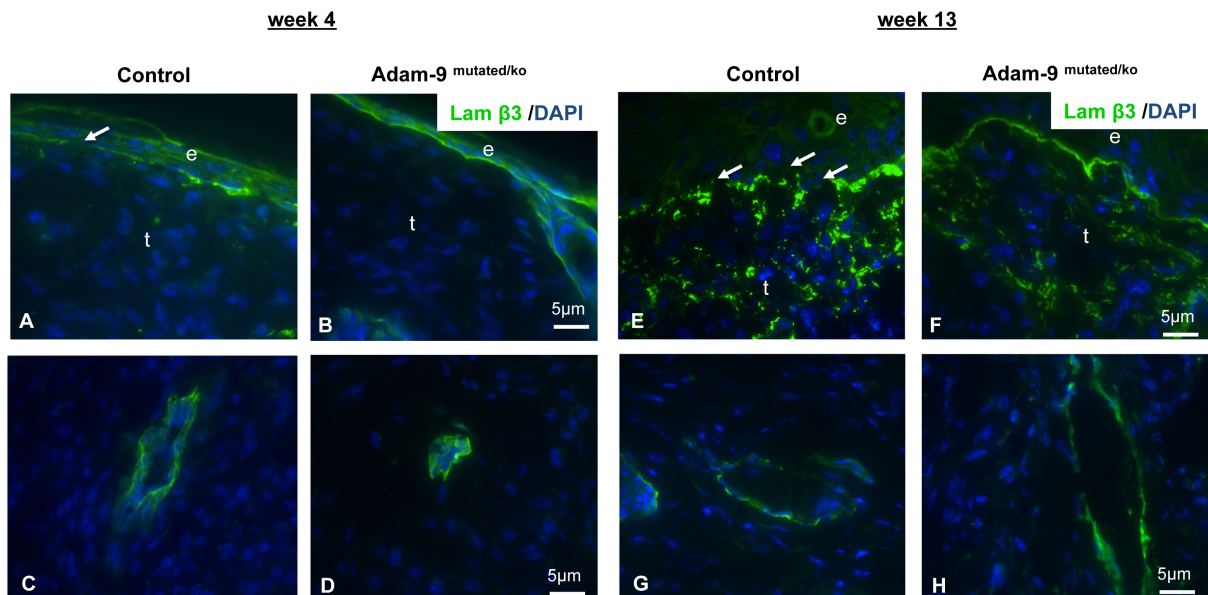


Figure 51: BMs in tumors grown in control and Adam-9^{mutated/ko} animals. To visualize BMs, acetone-fixed frozen tumor sections were immunohistochemically stained with an antibody directed against the laminin β 3-chain. The fluorescent DAPI was used to visualize the cell nuclei. The appearance of the BM between the epidermis (e) and the tumor (t) at week four (A, B) and week 13 (E, F) after DMBA treatment is shown. Additionally high power magnifications of BMs surrounding tumoral vessels at week four (C, D) and week 13 (G, H) are depicted.

At week four and 13 after DMBA treatment the BM separating the epidermis and tumor was clearly destructed and appeared discontinuous with clear interruptions in the BM zone indicated by the white arrows in Figure 51 in control animals (Figure 51 A, E). Additionally at week 13 laminin β 3-positive areas were also found in these animals below the BM (Figure 51 E). In contrast in tumors of Adam-9^{mutated/ko} animals a mostly regular and continuous staining pattern was observed with only little interruptions (Figure 51 B, F). The BM around the tumor blood vessels did not show destruction in both genotypes at week four (Figure 51 C, D). At week 13 the BM surrounding tumor blood vessels was also discontinuous and partially destructed in control animals, whereas in tumors obtained from Adam-9^{mutated/ko} mice the BM appeared more continuous, however also destructed parts were observed (Figure 51 G, H). These data indicated that also in the *in vivo* situation cleavage of the laminin β 3-chain occurs leading to destruction of the BM, which is reduced in the Adam-9^{mutated/ko} animals.

3.4.5.3 Intra- and extravasation of melanoma cells

The data of previous chapter showed that in absence of ADAM-9 the destruction of the BM around tumor vessels is reduced, which leads to the hypothesis that in the Adam-9^{mutated/ko} animals the intravasation of melanoma cells might be decreased. If melanoma cells are able to intravasate in the absence of ADAM-9, they should be detectable as circulating cells in the blood. To address this question we have collected blood from 13 weeks old tumor bearing animals and used the prepared RNA/cDNA for amplification of the melanoma marker Pmel17 also known in human as gp100 (Kobayashi *et al.*, 1994; Singh *et al.*, 2008). For improved amplification a nested PCR was employed (chapter 2.2.3.2). Pmel17 transcripts could be amplified in control as well as in Adam-9^{mutated/ko} animals, indicating that in both genotypes melanoma cells are present in circulation suggesting that melanoma cells are able to cross the vessel wall and intravasate independent of the presence of ADAM-9. As a control, PCR was also performed using blood from a control animal, which was not treated with DMBA and therefore showed not tumor formation. No signal for Pmel17 was detected, thus excluding the presence of any circulating melanocytes (Figure 52).

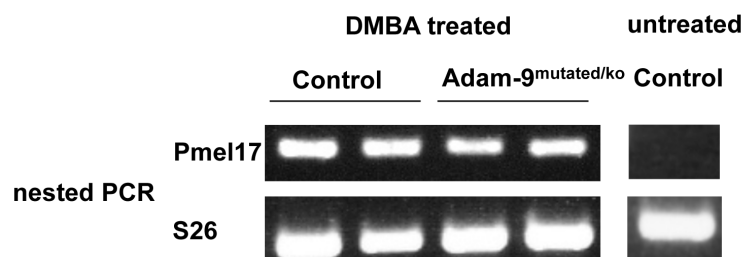


Figure 52: Analysis of circulating melanoma cells.

Circulating tumor cells were detected by nested PCR on RNA isolated from the blood of control and Adam-9^{mutated/ko} tumor bearing animals at week 13 post DMBA application. Isolated RNA was reverse transcribed into cDNA and subsequently used to amplify Pmel17, a melanocyte specific glycoprotein (chapter 2.2.3.2). Pmel17 transcripts were detected in the control as well as Adam-9^{mutated/ko} animals. No fragment was generated from blood of untreated control animals, which did not develop melanoma. S26 served as loading control.

A prerequisite of metastases formation is that melanoma cells are able to leave the circulation. Melanoma cells require first attaching to endothelial cells and thereafter penetrating the vessel wall to enter the tissue of a distinct organ. A role for ADAM-9 in mediating these cell-cell interactions has been demonstrated for adhesion of human lung cancer cells to endothelial cells (Monagret *et al.*, 2010). As culture of melanoma cells isolated from the control and in Adam-9^{mutated/ko} animals was not successful in our hands, we used B16-F1 melanoma cells, in which ADAM-9 was stably down-regulated via shRNA to study if silencing of ADAM-9 reduces adhesion of melanoma cells to endothelial cells. ADAM-9 silencing in B16-F1 cells resulted in a ~80% inhibition of transcripts expression ($p = 0.02$) as compared to scrambled transfected control cells shown by quantitative real-time PCR (Figure 53 A). Immunoblotting confirmed efficient down-regulation of ADAM-9 pro- and active form (Figure 53 A right). To mimic the adhesion of melanoma cells to an activated

endothelium, as it occurs *in vivo*, endothelial cell monolayers were treated with TNF- α before melanoma cells were added to measure adhesion.

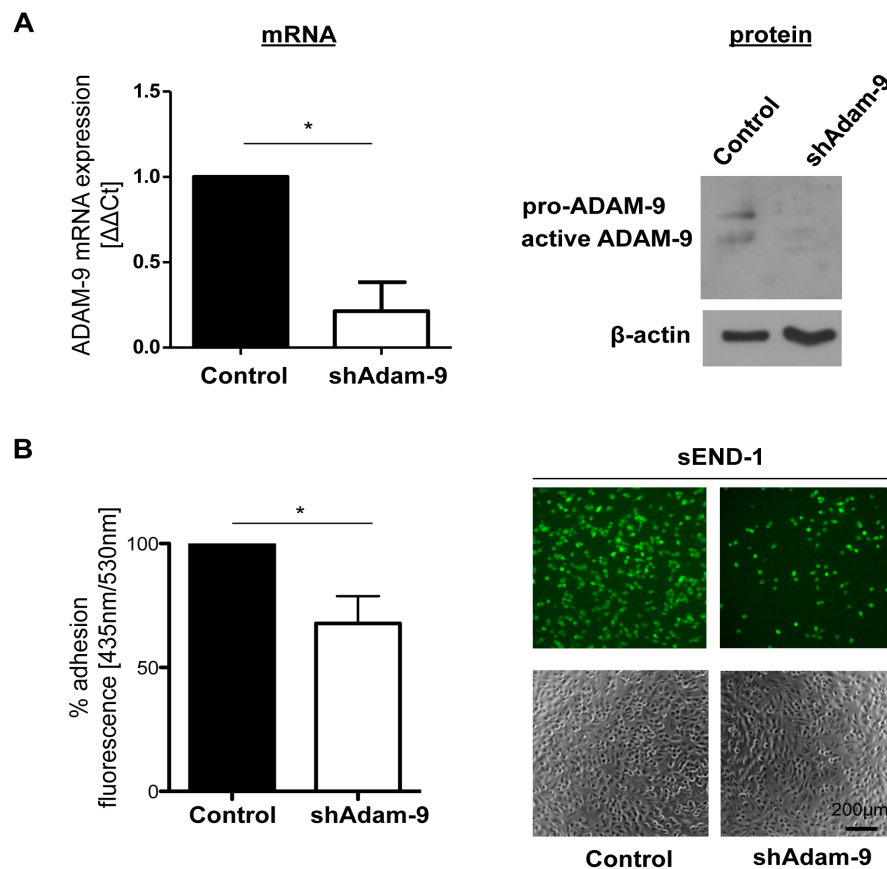


Figure 53: Analysis of adhesion of melanoma cells to endothelial cells.

(A) B16-F1 mouse melanoma cells were stably transfected with shRNA targeted to ADAM-9 or a scrambled control sequence. ADAM-9 expression was measured by quantitative real-time PCR and shown in the graph as mean \pm SD of three independent experiments. ADAM-9 expression was also analyzed by immunoblotting using antibodies against ADAM-9. β -actin was used as control. **(B)** Control or shAdam-9 B16-F1 melanoma cells, were seeded for 1h on top of TNF- α activated sEND-1 mouse endothelial cell monolayers. Adhesion was measured by quantifying the B16-F1-fluorescence and expressed as mean \pm SD of control, set as 100%. The data represent the mean of four independent experiments performed in sextuplicate. *: $p < 0.05$. The pictures on the right show representative photographs of fixed melanoma cells (green) adhering to the endothelial cell monolayer visualized by phase contrast (lower panel).

B16-F1 melanoma cells with stable down-regulation of ADAM-9 or carrying unspecific shRNA sequences, used as controls, were labeled with a fluorescent substance, which is retained from the cells upon entry, were seeded on TNF- α activated endothelial cell monolayers and allowed to adhere for 1h. In this assay the ADAM-9 down-regulated melanoma cells exhibited a significantly reduced ($p = 0.01$) adhesion towards the endothelial cells as compared to scrambled transfected control cells (Figure 53 B). This finding for the first time indicates that ADAM-9 expressed by melanoma cells is important for melanoma cell adhesion to endothelial cells.

Activation of endothelial cells with TNF- α up-regulates several adhesion molecules, which are involved in the interaction of melanoma cells with endothelial cells (Sikorski *et al.*, 1993;

McAteer *et al.*, 2008). In an attempt to identify a ligand for ADAM-9 on the surface of TNF- α activated endothelial cells, after 18h stimulation of sEND-1 endothelial cells, the expression of adhesion molecules, such as β 1 and β 3 integrin, ICAM-1, VCAM and VE-cadherin, was investigated by RT-PCR. Transcripts of all assayed molecules were up-regulated by TNF- α stimulation. The highest induction was observed for β 1 integrin and VCAM. ICAM-1, β 3 integrin and VE-cadherin were also clearly induced, but to lower extent (Figure 54). These data indicate that these analyzed adhesion molecules can provide potential binding candidates for ADAM-9, which need to be further investigated in future studies.

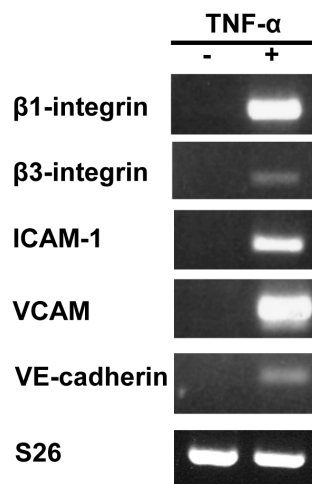


Figure 54: Analysis of adhesion molecule regulation after TNF- α stimulation of endothelial cells.

Monolayer cultures of sEND-1 mouse endothelial cells were stimulated with 50ng/ml recombinant TNF- α for 18h in serum-free medium and the expression of different adhesion molecules was determined by RT-PCR. S26 was used as control.

To analyze the direct contribution of melanoma cell-derived ADAM-9 to tumor cell extravasation *in vivo*, B16-F1 control and B16-F1 ADAM-9 down-regulated cells were injected into the tail vein of wild-type mice. The mice were killed three weeks after cell injection and the inner organs were prepared and carefully inspected for macroscopically visible metastases. Injection of B16-F1 control cells resulted in metastases formation in various organs in 100% of the injected animals (n=5/5), whereas only in 43% (n=3/7) of the animals, which were injected with ADAM-9 silenced cells, metastases were observed (Figure 55). Metastases were found in the lungs (Figure 55 A, E), the liver (Figure 55 B, F) and the heart (Figure 55 C, G). Control cells also metastasized into the kidney in one animal (Figure 55 D), whereas ADAM-9 silenced did not (Figure 55 H). In summary this experiment revealed that ADAM-9 down-regulation in B16-F1 cells, present in the circulation, reduced the general metastatic potential of the cells. No organ could be identified, which was preferentially affected, however a larger number of animals in future studies is necessary to identify organ specificity.

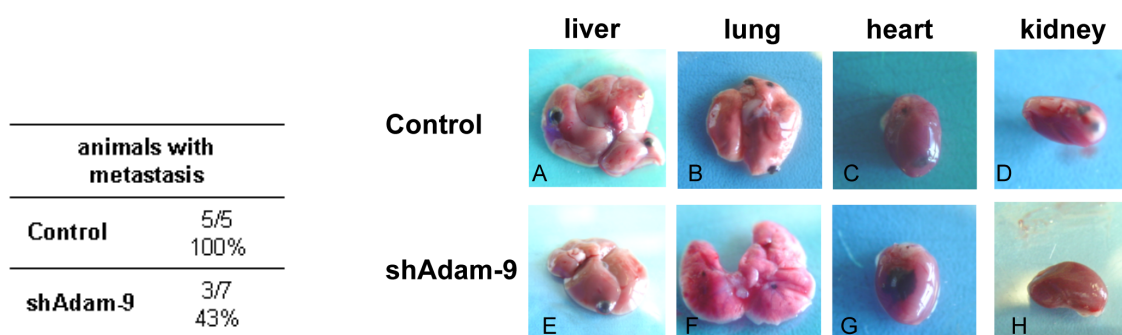


Figure 55: Tail vein injection of ADAM-9 silenced B16-F1 melanoma cells
100,000 B16-F1 control or B16-F1 shAdam-9 cells were injected in the tail vein of six-to-ten week old male and female Adam-9^{+/+} mice. The animals were killed three weeks after injection and the inner organs were inspected for macroscopically visible metastases. In the table the number and percentage of metastases bearing mice is summarized for control and shAdam-9 silenced cells. The photographs show pictures of metastatic nodules in the liver (A, E), the lung (B, F), the heart (C, G) and the kidney (D, H).

3.5 Role of ADAM-15 in growth and invasion of melanoma

Another member of the ADAM family, which is implicated in tumor growth and invasion, is ADAM-15 (Chen *et al.*, 2008; Najy *et al.*, 2008; Ungerer *et al.*, 2010). ADAM-15 is highly expressed by endothelial cells and, as well as in ADAM-9^{-/-} animals, in ADAM-15^{-/-} mice pathological neovascularization of the retina and growth of B16-F0 melanomas is reduced (Horiuchi *et al.*, 2003; Guaiquil *et al.*, 2009). These data suggest that ADAM-9 and ADAM-15 might exhibit overlapping functions in vascularization and melanoma growth.

One further aim of the laboratory was the investigation of the expression of ADAM-15 in skin and its role in skin repair and melanoma development.

In particular I have investigated the functional role for ADAM-15 in melanoma development and performed *in vivo* experiments using grafts of B16-F1 melanoma cells in the skin of control and Adam-15^{-/-} mice. I have further proceeded into the microscopical analysis of vascularization, inflammatory infiltration around the tumors and metastatic spread in those animals. These data have been recently published and the publication can be found at the end of this thesis (Schönefuß *et al.*, 2012). The published data will be summarized in the following.

Expression of ADAM-15 in skin was detected in epidermal keratinocytes and by dermal vascular structures as well as by fibroblast-like cells. Analysis of ADAM-15 transcripts by RT-PCR performed on dissociated epidermis and dermis, as well as on entire human skin detected ADAM-15 in comparable levels in both skin compartments. In cultured primary human skin cells, ADAM-15 transcripts were detected in keratinocytes, endothelial cells, fibroblasts and melanocytes. A similar expression pattern was detected in murine cells. Despite this broad expression pattern in skin, ablation of ADAM-15 did not affect skin homeostasis and morphology. Intradermal injection of B16-F1 melanoma cells in ADAM-15^{+/+}

and ADAM-15^{-/-} animals resulted in comparable melanoma growth kinetics in both mice, but, in agreement with previously published data (Horiuchi *et al.*, 2003) at day 21 post injection, tumors grown in the in Adam-15^{-/-} animals were smaller as compared to control. Analysis of vascularization in tumor specimens from day 12 and 21 post injection, by staining for CD31 (blood vessel endothelial cells) and LYVE-1 (lymphatic vessel endothelial cells), failed to detect any significant alterations in blood vessel density in peritumoral or intratumoral areas in Adam-15^{-/-} as compared to ADAM-15^{+/+} animals at both analyzed time points. Similarly, no significant alterations in the infiltration of tumors by neutrophils, macrophages (F4/80), cytotoxic T-cells (CD8) and lymphocytes (CD45) were detected.

Finally, analysis of the metastatic dissemination of the injected B16-F1 cells to the lungs and the lymph nodes revealed that lung metastases formation 16 days post B16-F1 injection was consistently reduced. The number of lungs positive for melanoma cells in Adam-15^{-/-} was only 13% of the total as compared to 54% detected in ADAM-15^{+/+} animals. A similar, though less prominent difference was detected in lymph nodes, where 13% of examined organs were positive in Adam-15^{-/-} as compared to 23% in ADAM-15^{+/+} animals.

In conclusion, while stromal expression of ADAM-15 is not important for melanoma growth *in vivo*, this study highlights ADAM-15 as a pro-metastatic molecule.

4. Discussion

Proteases, like MMPs and ADAMs, are implicated in the biology of melanoma. Expression of these enzymes is localized in stromal cells including fibroblasts and inflammatory cells, but also in tumor cells. In both compartments these enzymes exhibit distinct functions, e.g. shedding of surface molecules and degradation of the extracellular matrix, which support or counteract tumor growth, depending on the particular proteases and their expression sites. For example expression of MMP-2 in melanoma cells facilitates tumor invasion, and stromal expression of ADAM-15 contributes to melanoma metastases formation (Hofmann *et al.*, 2005; Schönefuß *et al.*, 2012). On the contrary stromal expression of ADAM-8 decreased melanoma growth (Guaiquil *et al.*, 2010). Interestingly a similar effect was shown to be associated with stromal expression of ADAM-9 (Abety *et al.*, 2012). However, in another study stromal expression of ADAM-9 was supporting growth of other melanoma cells (Guaiquil *et al.*, 2009). Despite these discrepancies, the function of ADAM-9 expression in the melanoma cells, where the protease is up-regulated during tumor development (Zigrino *et al.*, 2005), is unknown. The present work was intended to unravel the cell-specific function of ADAM-9 produced by tumor cells for development, growth and metastases formation of melanoma *in vivo* and *in vitro*. An additional aim of this work was to investigate the molecular mechanisms by which ADAM-9 expression is regulated in melanoma cells by IL-1 α as well as by anti-cancer drugs, the indirubins, and their potential use as therapeutic.

4.1 Expression of ADAM-9 in melanoma cells

Several proteases have been implicated in the invasive process of cancer cells and these include also the ADAMs. The versatile functions of ADAMs and the documented evidence of their over-expression in a variety of tumors suggest that these proteins are potential targets for tumor therapy. Although several ADAMs e.g. ADAM-10 and -12 have been detected in melanoma cells we identified ADAM-9 as being induced in melanoma cells at the periphery of the tumor and by adjacent peritumoral stromal cells. This observation suggests that ADAM-9 plays a role in mediating tumor-stroma communication (Zigrino *et al.*, 2005; Zigrino *et al.*, 2011). In a high-throughput analysis of human melanomas Alonso *et al.* demonstrated a correlation of ADAM-9 expression and tumor progression (Alonso *et al.*, 2007). In mouse models for prostate, breast and intestinal cancer high ADAM-9 expression correlated with poor differentiation of the tumors (Peduto *et al.*, 2005). Furthermore, in human renal cell cancer ADAM-9 protein expression was associated with higher tumor grade (Fitzsche *et al.*, 2008) and in human hepatocellular carcinoma ADAM-9 positive tumors were less differentiated compared to negative tissues (Tao *et al.*, 2010). Although we described induction of ADAM-9 protein in melanoma cells and in stromal cells at the invasive part of the tumors (Zigrino *et al.*, 2005), *in vitro* analysis of ADAM-9 transcripts in melanoma cell lines

did not show any correlation between ADAM-9 expression and the invasive potential of the tumor cells (Zigrino *et al.*, 2005). In line with these data is the study showing that ADAM-9 gene amplifications in human breast cancer tissues, were not related to tumor grade (Moelans *et al.*, 2010).

The studies presented herein confirm the findings relative to melanoma cells not only at the transcriptional level but also at the protein level, showing that expression of active protease on the cell surface of melanoma cells does not correlate to their invasive potential. On one side one can consider that the used monolayer cultures are simplified *in vitro* systems, thus the complexity of the *in vivo* system may be important to address the functional relevance for expression data. Several studies detected reactive oxygen species as modulators of ADAM-9 expression in different cancer cell lines (Fischer *et al.*, 2004; Sung *et al.*, 2006; Monagret *et al.*, 2010). It might be possible that different levels of oxidative stress at the periphery of the tumor and the inner tumor mass result in distinct induction of ADAM-9 in different parts of the tumor *in vivo*, which is not mimicked by the *in vitro* situation. On the other hand it is also possible that additional molecular events contribute to define protease functional relevance in this pathological condition. For instance, ADAM-9 proteolytic activity is not inhibited by TIMPs (Amour *et al.*, 2002), but it is possible that additional factors may be necessary to modulate its function. Thus, ADAM-9 expression and “co-factor” levels may be important to define its function in melanoma. A similar concept was described for MMP-14, whose expression was comparable in melanoma cells of high and low invasive potential, but levels of the TIMP-2, higher in the low invasive cells, which was necessary not only for enzyme inhibition but also activity, determined the net activity of the enzyme (Kurschat *et al.*, 1999).

4.2 Role of ADAM-9 for melanoma growth and invasion *in vitro*

4.2.1 Involvement of ADAM-9 in melanoma cell proliferation

To investigate the function of ADAM-9 for melanoma growth and invasion *in vitro*, we decided to stably down-regulate the expression of ADAM-9 using shRNA. A stable approach was necessary, as functional assessment of melanoma cell invasion *in vitro* and *in vivo* requires long-term experiments. BLM melanoma cells were chosen because they exhibited very high ADAM-9 transcript and protein expression levels as compared to other analyzed melanoma cell lines. The down-regulation was efficient at both, transcriptional and protein levels and despite the known redundancy in protease activities, no additional ADAM members were found up-regulated.

Interestingly, ADAM-9 down-regulation in BLM melanoma cells led to increased growth in presence and absence of anchorage. Even though no direct link between ADAM-9 and melanoma cell proliferation has been published, lines of evidence suggest a direct or indirect connection between ADAM-9 and cell proliferation or cycle control. A distinct protein, which

may provide a possible link between ADAM-9 and cell proliferation, is the mitotic arrest deficient 2 β (MAD2 β) molecule. Nelson *et al.* (1999) have shown that the intracellular tail of ADAM-9 interacts with MAD2 β . MAD2 β is a variant of MAD2, which is involved in the control of spindle assembly during mitosis, however the function of this further variant is largely unknown. It has been suggested that also MAD2 β may exert similar functions, but this hypothesis has not been proven yet. As described above, this protein binds the cytoplasmic tail of ADAM-9, thus one could speculate that ablation of ADAM-9 leads to an altered localization of MAD2 β , which in turn induces cellular events leading to increased cell proliferation. It was shown that the proline rich domain of the ADAM-9 intracellular tail binds to endophilin and paxin 3, which are involved in receptor recycling (Howard *et al.*, 1999), but it also binds PKC- δ , which leads upon phosphorylation of the intracellular domain to modulation of HB-EGF shedding (Izumi *et al.*, 1998). HB-EGF as many other EGF-like molecules have a potent effect in modulating cellular proliferation (Hashimoto, 2000), thus altered proteolysis of growth factors can also result from reduced ADAM-9 expression and lead to modification of proliferation. However it is possible that other mechanisms are responsible for increased cell proliferation upon ADAM-9 down-regulation mediated by other proteolytic enzymes, which compensate the lack or reduced expression. Other ADAMs like ADAM-10 or ADAM-17 were shown to contribute to proliferation of various tumor cell types by shedding and activating growth factors or receptors (Mochizuki and Okada, 2007; Rocks *et al.*, 2008). Indeed an up-regulation of ADAM-10 and -17 was observed in lysates obtained from wounds created in ADAM-9^{-/-} animals (Mauch *et al.*, 2010) or in fibroblasts from ADAM-9^{-/-} mice (Abety *et al.*, 2012). However within this work no significant alteration of these proteins was found in ADAM-9 silenced melanoma cells.

In contrast to the increased proliferation upon ADAM-9 down-regulation in BLM cells are the data obtained using indirubins. These substances are known to inhibit with different efficiency several CDKs, which are important molecules in cell cycle control and lead to inhibition of cell proliferation (Eisenbrand *et al.*, 2004). Treatment of BLM cells, most prominently down-regulates expression of ADAM-9. However, as silencing of ADAM-9 in the same cells leads to increased proliferation, it is possible that the effect detected on ADAM-9 expression by indirubins is indirect, mediated by a yet unknown molecule. One candidate could be c-jun, because it was shown that application of indirubin derivatives to melanoma cells caused beside CDK inhibition also inhibition of c-jun (Kunz *et al.*, 2010). Furthermore c-jun responsive elements have been identified in the ADAM-9 promoter (Cong and Jia, 2009). However, contrasting results were also shown using other tumor cell species, thus application of siRNA targeted to ADAM-9 led to reduced cell proliferation in adenoid cystic carcinoma cells (Xu *et al.*, 2010). An additional study conducted using gastric cancer cell lines revealed that treatment of cells with anti-ADAM-9 antibodies led to decreased cell

proliferation of one cell line, but not of all tested cell lines (Carl McGrath *et al.*, 2005). When breast or gastric cancer cells were treated with anti-ADAM-15 or anti ADAM-17 antibodies proliferation was also reduced, but when anti ADAM-12 antibodies were applied cell growth of some cell lines was stimulated (Lendeckel *et al.*, 2005). Altogether, these data may indicate that specific ADAM proteases may exert different effects on cancer cell proliferation depending on the cell type expressing them.

4.2.2 Regulation of cell size by ADAM-9

Besides increasing the proliferation rate, down-regulation of ADAM-9 showed a major impact on the cellular shape of melanoma cells. Analysis of actin distribution in these cells revealed reduced polymerization of intracellular actin. It is unclear whether this is a direct effect of ADAM-9 silencing or an indirect effect due to reduced cellular volume followed by adjustment of cell cytoskeleton. This aspect is important for tumor cell invasion as changes in cell volume and the actin cytoskeleton may indeed alter tumor cell ability to cross three-dimensional structural molecules in a protease independent fashion (Wyckoff *et al.*, 2006). A recent study using prostate cancer cells treated with siRNA targeted to ADAM-9 also detected phenotypical changes in these cells after several passages, changing from an epithelial into a cobblestone morphology, accompanied with increased E-cadherin and altered integrin expression (Josson *et al.*, 2011). The cellular volume might be regulated from activity of water channels like aquaporins and among the different members aquaporin-3 is expressed in human and murine skin (Verkman, 2005). We also found expression of aquaporin-3 in melanoma cells and we could detect increased aquaporin-3 protein synthesis in ADAM-9 silenced cells by immunolocalization.

Interestingly, aquaporin-3 overexpression has been shown in human squamous cell carcinomas and aquaporin-3 knockout mice were resistant to the development of skin tumors after carcinogen treatment (Hara-Chikuma and Verkman, 2008). Aquaporin-3 was found to facilitate glycerol transport, suggesting that up-regulation of this protein could result in increased proliferation by providing a substrate for increased ATP generation (Hara-Chikuma and Verkman, 2008). However when we inhibited aquaporins function with mercuric chloride (Ismail *et al.*, 2009) we could not rescue the cell volume phenotype upon ADAM-9 silencing, although a higher protein expression level of aquaporin-3 was observed. This might be due to the performance of this experiment as inhibition of aquaporins was only conducted for one hour prior to cell volume determination to avoid toxicity. This time might not be long enough for synthesis of new membrane or cytoskeletal proteins leading to restoration of the cell volume. In TGF- β stimulated breast cancer cells it was shown that actin transcripts peaked not until 4-8h after TGF- β addition (Leof *et al.*, 1896) and in mitogen activated bovine lymphocytes actin mRNA synthesis increased within 3h (Degen *et al.*, 1983). On the other

side, as mercuric chloride is a general aquaporin inhibitor (Ismail *et al.*, 2009), other substances like copper ions might be necessary to more specifically inhibit aquaporin-3 activity (Zelenina *et al.*, 2004). Another putative explanation for the observed effect is that the reduced cell size upon ADAM-9 silencing might also result from increased proliferation of these cells. Due to the higher proliferation rate the time to synthesize new proteins and gain cell volume in the G1-phase of the cell cycle might be reduced, leading to a decreased cell size. Interestingly stimulation of B16 melanoma cells with TPA, which was shown to activate ADAM-9, caused a block in the G1 phase of the cell cycle resulting in an increased cell size (Izumi *et al.*, 1998; La Porta *et al.*, 1998). Thus one could envision that active ADAM-9 in control cells might delay cell cycle progression, giving the cells enough time to restore cell volume after mitosis, whereas in the ADAM-9 down-regulated cells, cell cycle progression is enhanced resulting in a decreased cell size.

4.2.3 Basement membrane penetration mediated by ADAM-9

Upon silencing of ADAM-9 in BLM melanoma cells, these cells displayed a significant reduced penetration of the basement membrane (BM) in an *in vivo* like system, while invasion of the dermal compartment was not altered. The finding that ADAM-9 up-regulation upon IL-1 α silencing led to a modest increase in BM penetration partly supports the suggested pro-invasive role of ADAM-9 in melanoma cells. The reduced effectiveness is likely due to the fact that down-regulation of IL-1 α is not sufficient to up-regulate ADAM-9 to an extent, which is high enough to lead to increased invasion. Furthermore while application of shRNA targeted to ADAM-9 is specific to down-regulate ADAM-9, down-regulation of IL-1 α via shRNA also might lead to regulation of other proteins apart from ADAM-9, which are involved in melanoma cell invasion.

Involvement of ADAM-9 in BM invasion was also provided by the studies from Xu *et al.* (2010). These authors used siRNA against ADAM-9 in adenoid cystic carcinoma cells, which led to reduced cell invasion through matrigel. In addition, treatment of lung carcinoma cells with H₂O₂, which induces ADAM-9 expression increased invasion through matrigel, whereas shRNA targeted to ADAM-9 reduced H₂O₂-induced invasion (Monagret *et al.*, 2010). In prostate cancer cells ADAM-9 down-regulation led to decreased invasion in transwell assays (Josson *et al.*, 2011). However all these *in vitro* invasion systems employed matrigel, which is a mixture of several BM components produced by EHS tumor cells (Benton *et al.*, 2010; Hughes *et al.*, 2010) and only represent an “equivalent” *in vitro* system for the BM. Although the epidermal cell layers have been removed in the DDS skin equivalent system used in the studies here, this system likely resembles more closely a normal BM containing all proteins present in the *in vivo* situation in a ratio and distribution comparable to human skin. This was the case for laminin α 3-chain and collagen IV, which appeared to localize normally within the BM in the composites. As in the DDS system the epidermis was stripped off and the

fibroblasts killed before seeding the melanoma cells on top of the BM, with this system an evaluation of the invasive capacity of melanoma cells, which might also depend on interactions with keratinocytes or factors produced by either epidermal cells or fibroblasts is not possible. For this purpose additional experiments using organotypic culture systems (Stark *et al.*, 1999; Meier *et al.*, 2007) may help to address whether ADAM-9 silencing in melanoma cells results in altered melanoma-stroma cross talk and also results in reduced invasion.

Altered invasion through the BM may be due to an altered recognition of and adhesion to BM components or degradation products to allow penetration. Analysis of the adhesive abilities of ADAM-9 down-regulated cells, indicated reduced adhesion to matrigel and collagen IV, the latter being the most abundant BM protein (Kalluri, 2003). This provides an explanation for the observed effect. Decreased adhesion towards BM proteins would point to an altered expression of integrin receptors upon ADAM-9 silencing. Integrins are the main cellular receptors mediating cell-matrix interactions (Hynes, 2002). Several studies showed a parallel regulation of ADAM-9 and integrins. Thus transfection of lung cancer cells with ADAM-9 resulted in increased expression of $\alpha 3 \beta 1$ integrin resulting in increased adhesion to brain tissue (Shintani *et al.*, 2004). In smooth muscle cells stimulated by PDGF, increased ADAM-9 expression was paralleled by expression of integrins $\alpha v \beta 5$ and $\alpha 5 \beta 1$ (Al-Fakhri *et al.*, 2003). In prostate cancer cells ADAM-9 silencing resulted in increased expression of $\alpha 1$, $\alpha 2$, $\alpha 5$, and $\beta 1$ integrin and decreased expression of αv integrin (Josson *et al.*, 2011). In BLM melanoma cells plated on collagen type IV-coated surfaces, down-regulation of ADAM-9 led to significantly decreased expression of $\alpha 1$ integrin chain and an up-regulation of the $\alpha 2$ integrin compared to control cells, as detected by FACS analysis. The $\alpha 3$ integrin remained unchanged. The fact that $\alpha 1$ integrin was down-regulated, whereas the expression of the $\alpha 2$ integrin was increased indicated that loss of $\alpha 1$ integrin might be compensated by an up-regulation of the $\alpha 2$ integrin. The integrins $\alpha 1 \beta 1$ and $\alpha 2 \beta 1$ were shown to interact with collagen IV with different affinities. The affinity of $\alpha 1 \beta 1$ integrin for collagen IV is very high, whereas the $\alpha 2 \beta 1$ exhibits a lower affinity towards this collagen (Khoshnoodi *et al.*, 2008). Therefore down-regulation of the $\alpha 1$ integrin may be responsible for decreased adhesion towards collagen IV, although the $\alpha 2$ integrin was up-regulated. As matrigel is a protein mixture of several proteins secreted by EHS tumor cells, which contains collagen IV (Benton *et al.*, 2010; Hughes *et al.*, 2010), the reduced adhesion towards this matrix can also be explained with decreased integrin expression. Despite the fact that adhesion to collagen type IV was reduced, few cells still retained their ability to penetrate the BM and migrate in the tissue underneath. One explanation for this event may be the reduced cell size of BLM cells with ADAM-9 down-regulation. These cell size alterations may facilitate the tumor cells to cross the three-dimensional structure.

Besides the role in cell adhesion, we could also demonstrate that ADAM-9 exhibits proteolytic activity towards the β 3-chain of laminin 332 *in vitro*. ADAM-9 has already been reported to cleave different extracellular matrix proteins, among them fibronectin, gelatin or laminin 111 (Schlöndorff and Blobel, 1999; Mazzocca *et al.*, 2005). However no BM protein was identified as ADAM-9 substrate so far. Laminin 332 is a component of the dermal-epidermal BM and is located in the hemidesmosome complex, connecting the basal keratinocytes to the BM via interaction of the C-terminal part of the α 3-chain with α 6 β 4 and α 3 β 1 integrins (Aumailley *et al.*, 2003). Furthermore the N-terminal regions of the laminin α 3, β 3- and the γ 2-chains interact with collagen VII, establishing a connection of the BM to the underlying dermis (Aumailley *et al.*, 2003). For the laminin β 3-chain additional binding to laminin 321 and laminin 311 was shown. Hence laminin 332 promotes mechanical stability of the BM, which is underlined by the fact that mutations in any of the three chains lead to blistering diseases (Tzu and Marinkovich, 2008). Thus proteolytic cleavage of laminin β 3-chain by ADAM-9, expressed on melanoma cells, might destabilize the laminin 332 structure and in turn disturb BM integrity and consequently facilitate invasion. Processing of the laminin 332 molecule is a physiological process and truncations are common in the α 3-chain as well as in the γ 2-chain (Aumailley *et al.*, 2003; Tzu and Marinkovich, 2008), which are present only in their processed forms in the epidermal-dermal BM (Tunggal *et al.*, 2002). Data on the physiological processing of the β 3-chain are rare and only one study identified proteolytic cleavage of the N-terminal region of the β 3-chain by endogenous proteases in keratinocytes (Nakashima *et al.*, 2005). In prostate and colon carcinoma cells processing of the laminin β 3-chain via the activity of MMP-14 or MMP-7, respectively was shown (Udayakumar *et al.*, 2003; Remy *et al.*, 2006). Both proteases created a C-terminal fragment of the laminin β 3-chain of around 80-90kDa, similar to the fragment we have detected by the cleavage of laminin β 3-chain by ADAM-9, indicating that this region of the laminin β 3 molecule is prone to proteolytic cleavage. The exact cleavage site was only identified for MMP-7 and located between Ala⁵¹⁵ and Ile⁵¹⁶ (Remy *et al.*, 2006). Processing by ADAM-9 occurs upstream of this site as proteolysis of the recombinant N-terminal fragment of laminin- β 3 around aspartic acid⁴²⁰ generated a proteolytic fragment localizing the cleavage site ~100 amino acids upstream of the Ala⁵¹⁵ and Ile⁵¹⁶ sequence. The exact ADAM-9 cleavage site within this molecule remains to be determined. Interestingly both fragments generated by MMP-14 and MMP-7, exhibited pro-migratory activity towards cancer cells *in vitro* (Udayakumar *et al.*, 2003; Remy *et al.*, 2006). Thus one can speculate that processing of laminin β 3-chain by ADAM-9 can destabilize the laminin structure and release a fragment that promotes cell migration through the BM. However, when migration assays were performed, no differences in migration between control and ADAM-9 silenced cells were detected when cells were seeded on laminin 332-coated plates. We cannot exclude that the

small amount of ADAM-9 still expressed in silenced cells is sufficient to generate the fragment or that the pro-migratory effect might only be visible in a more complex system, e.g. on collagen gels or DDS. If the cleavage of the laminin β 3-chain by ADAM-9 results in a pro-migratory signal for melanoma cells, this should at least partially rescue the observed reduced invasion through the BM upon ADAM-9 down-regulation.

Taken together the obtained *in vitro* data strongly suggest a role of melanoma-derived ADAM-9 for tumor cell proliferation and invasion. The effects observed upon ADAM-9 down-regulation are summarized in the working model for the reduced BM invasion in Figure 56.

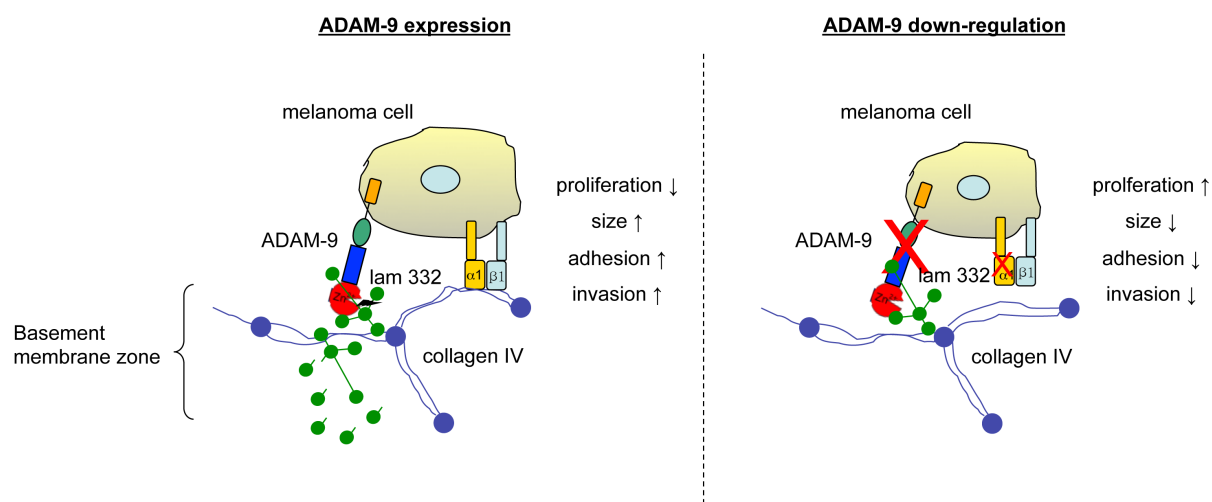


Figure 56: Effects of ADAM-9 down-regulation and working model for reduced BM penetration. Upon ADAM-9 silencing BLM melanoma cells exhibited higher proliferation and reduced cell size as well as decreased invasion through the BM and reduced adhesion towards BM proteins, which might be attributed to a reduced expression of integrins. The reduced penetration through the BM might also result from a decreased cleavage of laminin 332 (lam 332) in the β 3-chain by ADAM-9 and subsequent hindered migration through the BM zone.

4.3 Regulation of ADAM-9 expression in melanoma cells by IL-1 α

In vivo host-derived IL-1 α was shown to be required for melanoma invasiveness and angiogenesis (Voronov *et al.*, 2003) and systemic treatment with IL-1 receptor antagonist inhibited melanoma xenograft growth of IL-1-producing tumor cells (Elaraj *et al.*, 2006). However, the clear molecular mechanism by which IL-1 α modulates melanoma growth is not fully understood. It was previously shown that this cytokine may be responsible for induction of MMP-1 in stromal fibroblasts, which degrades the collagenous extracellular environment favouring tumor progression (Löffek *et al.*, 2005). It was also shown that ADAM-9 is an additional target for IL-1 α in melanoma cells (Zigrino *et al.*, 2005). The data presented herein confirmed and extended these data indicating not only down-regulation at the transcriptional, but also on the protein level. Two intracellular signalling molecules were identified, namely JNK and ERK, being involved in ADAM-9 regulation by IL-1 α in melanoma cells. Although NF κ B is the main mediator conveying signals of the IL-1 receptor, also ERK and JNK have

been shown to be downstream targets in the IL-1 signalling pathway (O'Neill *et al.*, 1998). A recent study has identified transcription factor binding sites in the promoter of ADAM-9 and those include that for AP-1 (Cong and Jia, 2009), which is a transcription factor composed either of a c-jun-c-fos heterodimer or of a c-jun-c-jun monomer (Ashida *et al.*, 2005). Thus regulation of the expression of ADAM-9 by exogenously supplied IL-1 α , which was shown to depend on the phosphorylation of c-jun is likely to occur via binding of the AP-1 factor to the ADAM-9 promoter. However, we have also shown that ERK may represent an additional molecular regulator of ADAM-9 endogenous expression. This kinase was also shown to influence the activation of the AP-1 complex (Whitmarsch and Davis, 1996; Ashida *et al.*, 2005), thus the final molecular target that regulates ADAM-9 at the transcriptional level may be the same, even though two signalling molecules can be envisioned. Taken together these data for the first time provide evidence for involvement of JNK and ERK in the intracellular signalling pathways leading to transcriptional regulation of ADAM-9 by IL-1 α .

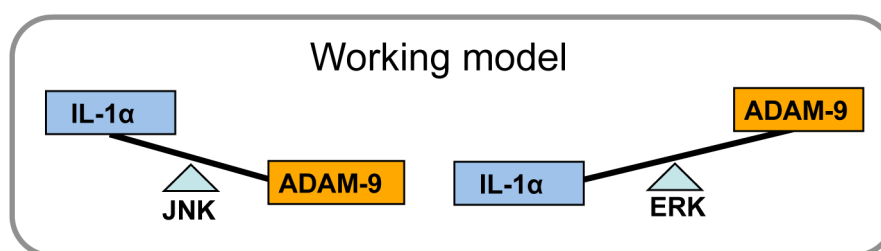


Figure 57: Working model for regulation of ADAM-9 by IL-1 α in BLM melanoma cells. High extracellular IL-1 α concentrations lead to decreased ADAM-9 expression via a JNK mediated mechanism. Down-regulation of IL-1 α production in BLM melanoma cells induces up-regulation of ADAM-9 by decreasing ERK phosphorylation.

4.4 Role of ADAM-9 for melanoma growth and invasion *in vivo*

4.4.1 Role of ADAM-9 for melanoma development and growth

To investigate the role of ADAM-9 for melanomagenesis *in vivo* the Hgf/Cdk4^{R24C/R24C} mice were crossed with Adam-9^{-/-} mice (Weskamp *et al.*, 2002). In the Hgf/Cdk4^{R24C/R24C} mice melanomas arise spontaneously because of the HGF overexpression and the mutation in the cyclin (CDK4), a situation that resembles human melanomas (Sotillo *et al.*, 2001; Tormo *et al.*, 2006), mice. The generated control (Adam-9^{+/+}//Hgf/Cdk4^{R24C/R24C}) and Adam-9^{mutated/ko} (Adam-9^{-/-}//Hgf/Cdk4^{R24C/R24C}) mice developed normally and exhibited no differences in skin architecture and differentiation. Thus no developmental or skin phenotype was visible in these animals by combining three genetic alterations (ADAM-9 knock out, CDK4 mutation, HGF overexpression). In all Hgf positive animals, melanocytes were located at the epidermal-dermal junction in the dermis as well as in the epidermis, independent if the animals were control or Adam-9^{mutated/ko}. Upon treatment with DMBA control as well as Adam-9^{mutated/ko} animals developed tumors at about four weeks after the carcinogen application. This in agreement with the data published for the Hgf/Cdk4^{R24C/R24C} mice, although in this

study the classical two-step carcinogen model, including initial treatment with DMBA and subsequent consecutive application of TPA, was used (Tormo *et al.*, 2006). In the present study DMBA applied once at postnatal day three, evoked melanoma development similar to that observed in the DMBA/TPA treated animals, indicating that mutations generated by the DMBA alone are sufficient to induce melanoma formation.

Upon tumor formation starting at week four post DMBA treatment, surprisingly an increased tumor number was found in Adam-9^{mutated/ko} animals compared to control animals. This situation was inverted at later stages (weeks 6-13) where reduced numbers of tumors were detected in Adam-9^{mutated/ko} animals. Comparison of the tumor numbers in the same animal over time, did not show any decrease in tumor number, thus implicating that no regression, e.g. by immunological defense, is ongoing in Adam-9^{mutated/ko} animals. This was further supported by the observation, that comparable numbers of infiltrated inflammatory cells, including T-lymphocytes, were detected in tumors from both animal genotypes. The Adam-9^{mutated/ko} animals at week four exhibited a higher tumor number compared to control animals. At later stages (after week six) the number of developed tumors in ADAM-9 deficient mice was reduced and remained steady as compared to control for the remaining time. At the endpoint the total number of tumors developed in the absence of ADAM-9 is lower than in control mice. As the Adam-9^{mutated/ko} animals carry a full ADAM-9 deletion in all tissues, thus not only in the melanoma cells, at early stages (week four and five) the influence of ablation of ADAM-9 expression in stromal cells might be important for determining tumor development. Interestingly, in support of this hypothesis are the recent data of Abety *et al.* (2012) showing that as early as day six from murine melanoma cell grafting in ADAM-9^{-/-} animals, a significant increase in tumor growth was detected as compared to wild type littermates and proceeded exponentially over time. This increased tumor growth resulted from decreased apoptosis and higher proliferation rate of melanoma cells. The molecules mediating these effects were shown to be TIMP-1 and soluble TNFR1, increasingly released by stromal fibroblasts (Abety *et al.*, 2012). In agreement with these data, in the present study we also found increased tumor cell proliferation at week four in the absence of ADAM-9. The initially increased proliferation of the tumor cells in the absence of ADAM-9 might provide an explanation for the appearance of a higher proportion of tumors with a larger tumor volume in the Adam-9^{mutated/ko} animals. In later time points this effect is not observed owing to either compensation by additional proteases or by a more important function of tumor-derived ADAM-9 in tumor progression. Several biological processes, beside proliferation, like apoptosis and vascularization, are key events in cancer progression (Hanahan and Weinberg, 2011) and might also account for the difference in tumor number observed overtime in control and Adam-9^{mutated/ko} animals. However, no differences in apoptosis and vascularization were detected between control and Adam-9^{mutated/ko} animals. Vascularization

was unaffected, confirming data from Guaiquil *et al.*, 2009, who did not detect an altered size or number of blood vessels in ADAM-9^{-/-} compared to Adam-9^{+/+} mice in tumors arising from injected B16-F0 cells (Guaiquil *et al.*, 2009). *In vitro* ADAM-9 mediates shedding of molecules, like Tie-2, VCAM, Flk-1 or FGFR2iib, which are implicated in influencing the angiogenic response (Peduto *et al.*, 2005; Guaiquil *et al.*, 2009), however none of these substrates have been shown to be relevant for the *in vivo* situation.

As only week four and week 13 were investigated so far, the analysis of an additional time-point between week five and six might provide more insight the mechanism responsible for differential tumor development in control and Adam-9^{mutated/ko} mice.

4.4.2 Role of ADAM-9 for metastases formation

The most striking *in vivo* finding was the reduced lung metastases formation in Adam-9^{mutated/ko} animals, which was independent of tumor size as well as of the tumor number. This indicates that the reduced metastases formation is indeed attributed to the ablation of ADAM-9. To further prove that reduced expression of ADAM-9 in the melanoma cells has an effect on metastases formation *in vivo*, ADAM-9 silenced B16-F1 melanoma cells were injected intravenously into the tail vein of Adam-9^{+/+} animals. Three weeks after injection a generally reduced formation of metastases was observed. Together these data strongly suggest that ADAM-9 produced by melanoma cells is a pro-metastatic protein *in vivo*. Similar findings were obtained when ADAM-9 down-regulated adenoid cystic carcinoma cells were injected into the tail vein of nude mice resulting in reduced metastases formation in the lung (Xu *et al.*, 2010). Furthermore, intravenous injection of ADAM-9 overexpressing lung cancer cells resulted in metastases in the brain and lung whereas mock-transfected cells only colonized the lungs (Shintani *et al.*, 2004). Several studies on different human cancer types also suggested a connection between ADAM-9 expression, metastases formation and patient survival. Thus patients with ADAM-9 positive hepatocellular carcinoma had poorer outcome and more frequently intrahepatic metastases (Tao *et al.*, 2010). In renal cell cancer ADAM-9 protein expression was associated with distant metastases and shortened patient survival (Fritzsche *et al.*, 2008). In pancreatic carcinoma ADAM-9 mRNA expression was related to lymph node metastases and prognosis (Yamada *et al.*, 2007).

The molecular mechanisms leading to reduced metastases in the lung in the absence of ADAM-9 may be various. The data from the *in vitro* studies performed within this work using the ADAM-9 down-regulated BLM cells indicate that ADAM-9 is important for BM penetration and apart from cleaving the laminin β 3-chain, ADAM-9 also modulates integrin expression. One could envision that *in vivo* all these events may play a distinct role in the metastatic process. Immunohistochemical stainings of the tumors with an antibody directed against the laminin β 3-chain showed that in the control animals the BMs at the epidermal-dermal junction

above the tumor as well as around the intratumoral vessels is clearly destructed and discontinuous, whereas in the Adam-9^{mutated/ko} animals these BMs appeared more intact. Thus in the control animals melanoma cell invasion through the destructed BM might be facilitated whereas in the absence of ADAM-9 crossing of the BM is impaired and melanoma cell intravasation might be reduced. This would also explain why reduced metastases formation only occurred in the lungs, but not in the lymph nodes, because in contrast to blood vessels a discontinuous BM containing intraendothelial gaps frequently surrounds the lymphatic vessels, which facilitates cancer cell invasion (Karkkainen *et al.*, 2002). However the nested PCR for Pmel17 performed on blood from tumor bearing control and Adam-9^{mutated/ko} animals showed that melanoma cells are present in the circulation of the both animal genotypes. Being this type of PCR not quantitative, we cannot prove that in the absence of ADAM-9 reduced number of cells can enter the circulation from the primary tumor.

The cell-cell adhesion assays performed with TNF- α activated endothelial cells and ADAM-9 regulated B16-F1 melanoma cells showed that upon ADAM-9 silencing in melanoma cells adhesion to endothelial cells is reduced. This indicates that in melanoma cells, ADAM-9 can mediate adhesion of melanoma cells to endothelial cells. These results imply that ADAM-9 is involved in the initial cell-cell adhesion step leading to extravasation of melanoma cells into an organ *in vivo*. It was shown that ADAM-9 present on the surface of melanoma cells can interact with β 1 integrin receptors. Application of β 1 integrin blocking antibodies reduced ADAM-9 mediated adhesion of human lung cancer cells towards human umbilical vein endothelial cells (Monagret *et al.*, 2010; Zigrino *et al.*, 2011). Considering that TNF- α stimulation of endothelial cells up-regulated β 1 integrin transcripts, it is possible that also adhesion of melanoma cells to endothelial cells is mediated via ADAM-9 β 1 integrin interactions. This would explain the reduced melanoma cell adhesion to endothelial cell monolayers, when ADAM-9 is down-regulated. As both endothelial cells and melanoma cells express ADAM-9, it is possible that this interaction occurs in both directions. ADAM-9 present on melanoma cell surface may interact with β 1 integrin and the other way around is true when it is expressed on endothelial cells. This assumption could be proven by the application of β 1 integrin blocking antibodies in further experiments.

Reduced, but not abolished adhesion to endothelial cells can partly explain the lung metastatic phenotype in the absence of ADAM-9. For those cells that are still able to penetrate, once reached the organ, they have to counteract the immunological activity of the organs to be able to survive and to form metastases. It is known that T-cells can mediate anti-tumor immunity against melanoma cells, leading to growth restriction or tumor regression (Nagorsen *et al.*, 2003; Ramirez-Montagut *et al.*, 2003). Furthermore it was shown that ADAM-9 mediates shedding of MICA molecules from the surface of tumor cells

(Kogha *et al.*, 2010a; Kogha *et al.*, 2010b). These proteins are ligands for NKG2D receptors, which are expressed on natural killer cells and mediate recognition of tumor cells by natural killer cells. Thus it might be possible that in the absence of ADAM-9 shedding of MICA from the surface of metastatic tumor cells is reduced, leading to elevated recognition of tumor cells by natural killer cells and subsequent increased antitumor immunity. By staining lung sections with antibodies against the T-cell markers CD3, CD4, CD8 and CD45 no altered inflammatory reaction around the lung metastases in control and Adam-9^{mutated/ko} animals was observed, indicating that an inflammatory reaction targeting the metastatic cells is not responsible for the reduced metastases formation in the lungs of Adam-9^{mutated/ko} animals.

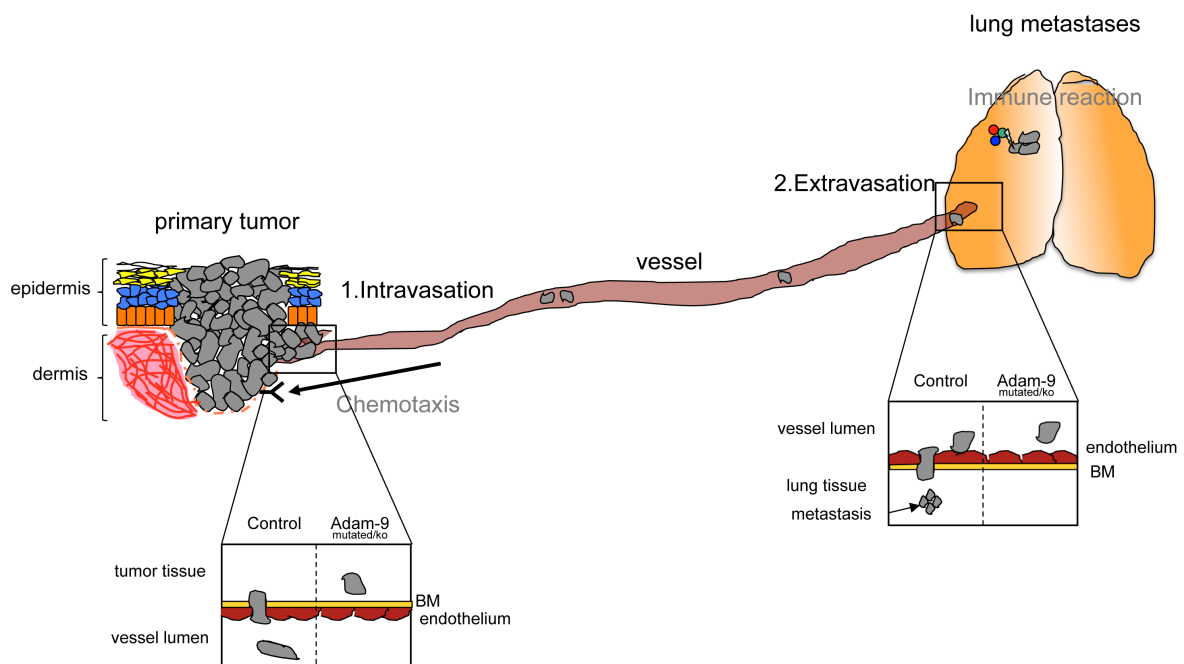


Figure 58: Mechanisms responsible for reduced lung metastases formation in Adam-9^{mutated/ko} animals. First, at the site of the primary tumor ADAM-9 expressing melanoma cells are able to adhere to and invade through the basement membrane (BM) in order to intravasate. In contrast adhesion and invasion of ADAM-9 deficient melanoma cells might be impaired. Second, after the cells have been transported to the lung via the circulation ADAM-9 expressing cells can adhere to the vascular endothelium, subsequently extravasate and form lung metastases, whereas adhesion of ADAM-9 deficient cells to the endothelial cells is reduced. Other possible mechanisms like altered chemotaxis of the melanoma cells to the lung or an increased immune reaction in the lung counteracting metastases formation were not detected.

Taken together the obtained data indicated that in the presence of ADAM-9, melanoma cell derived ADAM-9 promotes lung metastases formation by two main molecular pathways. First, intravasation of melanoma cells at the site of the primary tumor might be driven by ADAM-9, which mediates adhesion to the BM and leads to destruction of it via initial cleavage of the laminin β 3-chain. This last also generates pro-migratory signals for melanoma cells. Second, ADAM-9 mediates adhesion of melanoma cells to endothelial cells, possibly through the interaction with β 1 integrins, and leads to extravasation, which involves passage through endothelial cells and degradation of the underlying BM.

In the absence of ADAM-9, the additive effects of both, impaired intravasation and reduced extravasation, finally lead to reduced metastases formation. This model is shown in Figure 58.

4.5 Outlook

The *in vitro* experiments using ADAM-9 down-regulated melanoma cells showed that ADAM-9 participates in penetration of the epidermal-dermal BM. The studies using animals with spontaneous melanoma formation indicate that also *in vivo* ADAM-9 might contribute to this process. Additionally ADAM-9 is involved in the interaction of melanoma cells with endothelial cells. By these two processes, facilitating BM penetration and melanoma-endothelial cell interaction, ADAM-9 contributes to lung metastases formation.

Importantly, in this study we identified the laminin β 3-chain as the first BM substrate for ADAM-9. Further investigations addressing the exact cleavage site in the molecule and the functional role for the cleavage and the generation of the laminin β 3 fragment will help to better understand the importance of this event for melanoma function.

In further studies it will be of importance to create strategies to cell-specifically inhibit ADAM-9 expression in melanoma cells *in vivo*. Cell-specificity will be necessary as ablation of ADAM-9 in stromal cells leads to increased melanoma growth in animal experiments (Abety *et al.*, 2012). The results with the indirubins presented in this work indicate that these molecules can be used to specifically inhibit ADAM-9 expression in high invasive melanoma cells, but not in dermal fibroblasts. Meanwhile, within the melanoma consortium, modified indirubins with putatively higher efficiency have been developed and could be further tested for their ADAM-9 “silencing” activity in melanoma cells but also in fibroblasts, keratinocytes or endothelial cells. These experiments might reveal potent inhibitory molecules for therapeutical applications.

A completely different approach to target ADAM-9 expression in melanoma cells would comprise the application of siRNA to the melanoma cells. To target the siRNA specifically to melanoma cells, the siRNA can be packed in viral envelopes, which carry short peptides containing RGD sequences. These peptides are recognized by RGD dependent integrins highly expressed on the melanoma cells (Nahde *et al.*, 2001).

Finally such molecules could be tested in the *in vivo* situation for their ability to reduce melanoma metastases formation and thereby prolonging patient outcome.

5. References

- Abety,A., Fox,J.W., Schönefuß,A., Zamek,J., Landsberg,J., Krieg,T., Blobel,C., Mauch,C., and Zigrino,P. (2012) Stromal fibroblast-specific expression of ADAM-9 modulates proliferation and apoptosis in melanoma cells in vitro and in vivo. *J.Invest Dermatol.* in press
- Al Fakhri,N., Wilhelm,J., Hahn,M., Heidt,M., Hehrlein,F.W., Endisch,A.M., Hupp,T., Cherian,S.M., Bobryshev,Y.V., Lord,R.S., and Katz,N. (2003) Increased expression of disintegrin-metalloproteinases ADAM-15 and ADAM-9 following upregulation of integrins alpha5beta1 and alphavbeta3 in atherosclerosis. *J.Cell Biochem.*2003.Jul.1;89.(4):808.-23.
- Alonso,S.R., Tracey,L., Ortiz,P., Perez-Gomez,B., Palacios,J., Pollan,M., Linares,J., Serrano,S., Saez-Castillo,A.I., Sanchez,L., Pajares,R., Sanchez-Aguilera,A., Artiga,M.J., Piris,M.A., and Rodriguez-Peralto,J.L. (2007) A high-throughput study in melanoma identifies epithelial-mesenchymal transition as a major determinant of metastasis. *Cancer Res.* 67:3450-3460.
- Amour,A., Slocombe,P.M., Webster,A., Butler,M., Knight,C.G., Smith,B.J., Stephens,P.E., Shelley,C., Hutton,M., Knauper,V., Docherty,A.J., and Murphy,G. (1998) TNF-alpha converting enzyme (TACE) is inhibited by TIMP-3. *FEBS Lett.* 435:39-44.
- Amour,A., Knight,C.G., Webster,A., Slocombe,P.M., Stephens,P.E., Knauper,V., Docherty,A.J., and Murphy,G. (2000) The in vitro activity of ADAM-10 is inhibited by TIMP-1 and TIMP-3. *FEBS Lett.* 473:275-279.
- Amour,A., Knight,C.G., English,W.R., Webster,A., Slocombe,P.M., Knauper,V., Docherty,A.J., Becherer,J.D., Blobel,C.P., and Murphy,G. (2002) The enzymatic activity of ADAM8 and ADAM9 is not regulated by TIMPs. *FEBS Lett.*2002.Jul.31:524:154-158.
- Apte,R.N., Dotan,S., Elkabets,M., White,M.R., Reich,E., Carmi,Y., Song,X., Dvozkin,T., Krelin,Y., and Voronov,E. (2006) The involvement of IL-1 in tumorigenesis, tumor invasiveness, metastasis and tumor-host interactions. *Cancer Metastasis Rev.*2006.Sep.:25:387-408.
- Ashida,R., Tominaga,K., Sasaki,E., Watanabe,T., Fujiwara,Y., Oshitani,N., Higuchi,K., Mitsuyama,S., Iwao,H., and Arakawa,T. (2005) AP-1 and colorectal cancer. *Inflammopharmacology.* 13:113-125.
- Aumailley,M., El Khal,A., Knoss,N., and Tunggal,L. (2003) Laminin 5 processing and its integration into the ECM. *Matrix Biol.* 22:49-54.
- Bacac,M. and Stamenkovic,I. (2008) Metastatic cancer cell. *Annu.Rev.Pathol.* 3:221-247.
- Baluk,P., Hashizume,H., and McDonald,D.M. (2005) Cellular abnormalities of blood vessels as targets in cancer. *Curr.Opin.Genet.Dev.* 15:102-111.
- Becker,J.C., Houben,R., Schrama,D., Voigt,H., Ugurel,S., and Reisfeld,R.A. (2010) Mouse models for melanoma: a personal perspective. *Exp.Dermatol.* 19:157-164.
- Benbow,U., Tower,G.B., Wyatt,C.A., Buttice,G., and Brinckerhoff,C.E. (2002) High levels of MMP-1 expression in the absence of the 2G single nucleotide polymorphism is mediated by p38 and ERK1/2 mitogen-activated protein kinases in VMM5 melanoma cells. *J.Cell Biochem.* 86:307-319.
- Benjamin,C.L., Melnikova,V.O., and Ananthaswamy,H.N. (2007) Models and mechanisms in malignant melanoma. *Mol.Carcinog.* 46:671-678.
- Benton,G., Kleinman,H.K., George,J., and Arnaoutova,I. (2010) Multiple uses of basement membrane-like matrix (BME/Matrigel) in vitro and in vivo with cancer cells. *Int.J.Cancer.*
- Black,R.A., Rauch,C.T., Kozlosky,C.J., Peschon,J.J., Slack,J.L., Wolfson,M.F., Castner,B.J., Stocking,K.L., Reddy,P., Srinivasan,S., Nelson,N., Boiani,N., Schooley,K.A., Gerhart,M., Davis,R., Fitzner,J.N., Johnson,R.S., Paxton,R.J., March,C.J., and Cerretti,D.P. (1997) A metalloproteinase disintegrin that releases tumour-necrosis factor-alpha from cells. *Nature* 385:729-733.
- Bray,S.J. (2006) Notch signalling: a simple pathway becomes complex. *Nat.Rev.Mol.Cell Biol.* 7:678-689.
- Brooks,P.C., Stromblad,S., Sanders,L.C., von Schalscha,T.L., Aimes,R.T., Stetler-Stevenson,W.G., Quigley,J.P., and Cheresh,D.A. (1996) Localization of matrix metalloproteinase MMP-2 to the surface of invasive cells by interaction with integrin alpha v beta 3. *Cell* 85:683-693.
- Carey,T.E., Takahashi,T., Resnick,L.A., Oettgen,H.F., and Old,L.J. (1976) Cell surface antigens of human malignant melanoma: mixed hemadsorption assays for humoral immunity to cultured autologous melanoma cells. *Proc.Natl.Acad.Sci.U.S.A* 73:3278-3282.
- Carl-McGrath,S., Lendeckel,U., Ebert,M., Roessner,A., and Rocken,C. (2005) The disintegrin-metalloproteinases ADAM9, ADAM12, and ADAM15 are upregulated in gastric cancer. *Int.J.Oncol.* 26:17-24.
- Chambers,A.F., Groom,A.C., and MacDonald,I.C. (2002) Dissemination and growth of cancer cells in metastatic sites. *Nat.Rev.Cancer* 2:563-572.
- Chen,Q., Meng,L.H., Zhu,C.H., Lin,L.P., Lu,H., and Ding,J. (2008) ADAM15 suppresses cell motility by driving integrin alpha5beta1 cell surface expression via Erk inactivation. *Int.J.Biochem.Cell Biol.* 40:2164-2173.
- Chudnovsky,Y., Khavari,P.A., and Adams,A.E. (2005) Melanoma genetics and the development of rational therapeutics. *J.Clin.Invest* 115:813-824.
- Cong,L. and Jia,J. (2009) Promoter polymorphisms which regulate ADAM9 transcription are protective against sporadic Alzheimer's disease. *Neurobiol.Aging.*

- Coussens, L.M. and Werb, Z. (2002) Inflammation and cancer. *Nature*. 2002. Dec. 420:860-867.
- Cruz, J., Reis-Filho, J.S., Silva, P., and Lopes, J.M. (2003) Expression of c-met tyrosine kinase receptor is biologically and prognostically relevant for primary cutaneous malignant melanomas. *Oncology* 65:72-82.
- Curtin, J.A., Fridlyand, J., Kageshita, T., Patel, H.N., Busam, K.J., Kutzner, H., Cho, K.H., Aiba, S., Brocker, E.B., LeBoit, P.E., Pinkel, D., and Bastian, B.C. (2005) Distinct sets of genetic alterations in melanoma. *N.Engl.J.Med.* 353:2135-2147.
- Davies, H., Bignell, G.R., Cox, C., Stephens, P., Edkins, S., Clegg, S., Teague, J., Woffendin, H., Garnett, M.J., Bottomley, W., Davis, N., Dicks, E., Ewing, R., Floyd, Y., Gray, K., Hall, S., Hawes, R., Hughes, J., Kosmidou, V., Menzies, A., Mould, C., Parker, A., Stevens, C., Watt, S., Hooper, S., Wilson, R., Jayatilake, H., Gusterson, B.A., Cooper, C., Shipley, J., Hargrave, D., Pritchard-Jones, K., Maitland, N., Chenevix-Trench, G., Riggins, G.J., Bigner, D.D., Palmieri, G., Cossu, A., Flanagan, A., Nicholson, A., Ho, J.W., Leung, S.Y., Yuen, S.T., Weber, B.L., Seigler, H.F., Darrow, T.L., Paterson, H., Marais, R., Marshall, C.J., Wooster, R., Stratton, M.R., and Futreal, P.A. (2002) Mutations of the BRAF gene in human cancer. *Nature* 417:949-954.
- De Fabo, E.C., Noonan, F.P., Fears, T., and Merlino, G. (2004) Ultraviolet B but not ultraviolet A radiation initiates melanoma. *Cancer Res.* 64:6372-6376.
- de Vries, E, Tyczynski, J, and Parkin, M. Cutaneous malignant melanoma in Europe. European network of cancer registries. 1-11-2003.
Ref Type: In Press
- Degen, J.L., Neubauer, M.G., Degen, S.J., Seyfried, C.E., and Morris, D.R. (1983) Regulation of protein synthesis in mitogen-activated bovine lymphocytes. Analysis of actin-specific and total mRNA accumulation and utilization. *J.Biol.Chem.* 258:12153-12162.
- Dennhofer, R., Kurschat, P., Zigrino, P., Klose, A., Bosserhoff, A., van Muijen, G., Krieg, T., Mauch, C., and Hunzelmann, N. (2003) Invasion of melanoma cells into dermal connective tissue in vitro: evidence for an important role of cysteine proteases. *Int.J.Cancer* 106:316-323.
- Durko, M., Navab, R., Shibata, H.R., and Brodt, P. (1997) Suppression of basement membrane type IV collagen degradation and cell invasion in human melanoma cells expressing an antisense RNA for MMP-1. *Biochim.Biophys.Acta* 1356:271-280.
- Eberle, J., Spangler, B., Becker, J.C., Heinemann, S.H., Klein, C.A., Kunz, M., Kuphal, S., Langer, P., Mauch, C., Meierjohann, S., Paschen, A., Schadendorf, D., Scharlt, M., Schitteck, B., Schonherr, R., Tuting, T., Zigrino, P., and Bosserhoff, A.K. (2010) Multicentre study on standardisation of melanoma cell culture--an initiative of the German Melanoma Research Network. *Pigment Cell Melanoma Res.* 23:296-298.
- Edwards, D.R., Handsley, M.M., and Pennington, C.J. (2008) The ADAM metalloproteinases. *Mol.Aspects Med.* 29:258-289.
- Eisenbrand, G., Hippe, F., Jakobs, S., and Muehlbeyer, S. (2004) Molecular mechanisms of indirubin and its derivatives: novel anticancer molecules with their origin in traditional Chinese phytochemistry. *J.Cancer Res.Clin.Oncol.* 130:627-635.
- Elaraj, D.M., Weinreich, D.M., Varghese, S., Puhlmann, M., Hewitt, S.M., Carroll, N.M., Feldman, E.D., Turner, E.M., and Alexander, H.R. (2006) The role of interleukin 1 in growth and metastasis of human cancer xenografts. *Clin.Cancer Res.* 2006 12:1088-1096.
- Fidler, I.J. and Nicolson, G.L. (1976) Organ selectivity for implantation survival and growth of B16 melanoma variant tumor lines. *J.Natl.Cancer Inst.* 57:1199-1202.
- Fischer, O.M., Hart, S., Gschwind, A., Prenzel, N., and Ullrich, A. (2004) Oxidative and osmotic stress signaling in tumor cells is mediated by ADAM proteases and heparin-binding epidermal growth factor. *Mol.Cell Biol.* 2004. Jun.; 24(12):24:5172-5183.
- Flaherty, K.T., Puzanov, I., Kim, K.B., Ribas, A., McArthur, G.A., Sosman, J.A., O'Dwyer, P.J., Lee, R.J., Grippo, J.F., Nolop, K., and Chapman, P.B. (2010) Inhibition of mutated, activated BRAF in metastatic melanoma. *N.Engl.J.Med.* 363:809-819.
- Fritzsche, F.R., Wassermann, K., Jung, M., Tolle, A., Kristiansen, I., Lein, M., Johannsen, M., Dietel, M., Jung, K., and Kristiansen, G. (2008) ADAM9 is highly expressed in renal cell cancer and is associated with tumour progression. *BMC.Cancer.* 2008. Jun. 26. 8:179.
- Fritzsche, F.R., Jung, M., Tolle, A., Wild, P., Hartmann, A., Wassermann, K., Rabien, A., Lein, M., Dietel, M., Pilarsky, C., Calvano, D., Grutzmann, R., Jung, K., and Kristiansen, G. (2008) ADAM9 expression is a significant and independent prognostic marker of PSA relapse in prostate cancer. *Eur.Urol.* 54:1097-1106.
- Fry, J.L. and Toker, A. (2010) Secreted and membrane-bound isoforms of protease ADAM9 have opposing effects on breast cancer cell migration. *Cancer Res.* 70:8187-8198.
- Fu, P.P., Cheng, S.H., Coop, L., Xia, Q., Culp, S.J., Tolleson, W.H., Wamer, W.G., and Howard, P.C. (2003) Photoreaction, phototoxicity, and photocarcinogenicity of retinoids. *J.Environ.Sci.Health C.Environ.Carcinog.Ecotoxicol.Rev.* 21:165-197.
- Gaffal, E., Landsberg, J., Bald, T., Sporleder, A., Kohlmeyer, J., and Tuting, T. (2011) Neonatal UVB exposure accelerates melanoma growth and enhances distant metastases in Hgf-Cdk4(R24C) C57BL/6 mice. *Int.J.Cancer.*

- Gaggioli, C. and Sahai, E. (2007) Melanoma invasion - current knowledge and future directions. *Pigment Cell Res.* 2007.Jun. 20:161-172.
- Giard, D.J., Aaronson, S.A., Todaro, G.J., Arnstein, P., Kersey, J.H., Dosik, H., and Parks, W.P. (1973) In vitro cultivation of human tumors: establishment of cell lines derived from a series of solid tumors. *J.Natl.Cancer Inst.* 51:1417-1423.
- Guaiquil, V., Swendeman, S., Yoshida, T., Chavala, S., Campochiaro, P., and Blobel, C.P. (2009) ADAM9 is involved in pathological retinal neovascularization. *Mol.Cell Biol.* 2009.Mar.9.
- Guaiquil, V.H., Swendeman, S., Zhou, W., Guaiquil, P., Weskamp, G., Bartsch, J.W., and Blobel, C.P. (2010) ADAM8 is a negative regulator of retinal neovascularization and of the growth of heterotopically injected tumor cells in mice. *J.Mol.Med.* 88:497-505.
- Haass, N.K. and Herlyn, M. (2005) Normal human melanocyte homeostasis as a paradigm for understanding melanoma. *J.Investig.Dermatol.Symp.Proc.* 10:153-163.
- Haass, N.K., Smalley, K.S., Li, L., Herlyn, M. (2005) Adhesion, migration and communication in melanocytes and melanoma. *Pigment Cell Res.* 18(3):150-9.
- Hamada, S., Satoh, K., Fujibuchi, W., Hirota, M., Kanno, A., Unno, J., Masamune, A., Kikuta, K., Kume, K., and Shimosegawa, T. (2011) MiR-126 Acts as a Tumor Suppressor in Pancreatic Cancer Cells via the Regulation of ADAM9. *Mol.Cancer Res.*
- Hanahan, D. and Weinberg, R.A. (2011) Hallmarks of cancer: the next generation. *Cell* 144:646-674.
- Hara-Chikuma, M. and Verkman, A.S. (2005) Aquaporin-3 functions as a glycerol transporter in mammalian skin. *Biol.Cell.* 2005.Jul.: 97:479-486.
- Hara-Chikuma, M. and Verkman, A.S. (2008) Prevention of skin tumorigenesis and impairment of epidermal cell proliferation by targeted aquaporin-3 gene disruption. *Mol.Cell Biol.* 28:326-332.
- Hashimoto, K. (2000) Regulation of keratinocyte function by growth factors. *J.Dermatol.Sci.* 24 Suppl 1:S46-S50.
- Herlyn, M., Berking, C., Li, G., and Satyamoorthy, K. (2000) Lessons from melanocyte development for understanding the biological events in naevus and melanoma formation. *Melanoma Res.* 10:303-312.
- Hirobe, T., Osawa, M., and Nishikawa, S. (2004) Hepatocyte growth factor controls the proliferation of cultured epidermal melanoblasts and melanocytes from newborn mice. *Pigment Cell Res.* 17:51-61.
- Hocker, T.L., Singh, M.K., and Tsao, H. (2008) Melanoma genetics and therapeutic approaches in the 21st century: moving from the benchside to the bedside. *J.Invest Dermatol.* 2008.Nov.: 128:2575-2595.
- Hofmann, U.B., Houben, R., Brocker, E.B., and Becker, J.C. (2005) Role of matrix metalloproteinases in melanoma cell invasion. *Biochimie* 87:307-314.
- Holmes, C., Foley, P., Freeman, M., and Chong, A.H. (2007) Solar keratosis: epidemiology, pathogenesis, presentation and treatment. *Australas.J.Dermatol.* 48:67-74.
- Hotary, K., Li, X.Y., Allen, E., Stevens, S.L., and Weiss, S.J. (2006) A cancer cell metalloprotease triad regulates the basement membrane transmigration program. *Genes Dev.* 20:2673-2686.
- Hotoda, N., Koike, H., Sasagawa, N., and Ishiura, S. (2002) A secreted form of human ADAM9 has an alpha-secretase activity for APP. *Biochem.Biophys.Res.Commun.* 2002.May. 293:800-805.
- Howard, L., Nelson, K.K., Maciewicz, R.A., and Blobel, C.P. (1999) Interaction of the metalloprotease disintegrins MDC9 and MDC15 with two SH3 domain-containing proteins, endophilin I and SH3PX1. *J.Biol.Chem.* 274:31693-31699.
- Hughes, C.S., Postovit, L.M., and Lajoie, G.A. (2010) Matrigel: a complex protein mixture required for optimal growth of cell culture. *Proteomics.* 10:1886-1890.
- Hynes, R.O. (2002) Integrins: bidirectional, allosteric signaling machines. *Cell* 110:673-687.
- Iba, K., Albrechtsen, R., Gilpin, B.J., Loebel, F., and Wewer, U.M. (1999) Cysteine-rich domain of human ADAM 12 (meltrin alpha) supports tumor cell adhesion. *Am.J.Pathol.* 154:1489-1501.
- Iida, J., Wilhelmson, K.L., Price, M.A., Wilson, C.M., Pei, D., Furcht, L.T., and McCarthy, J.B. (2004) Membrane type-1 matrix metalloproteinase promotes human melanoma invasion and growth. *J.Invest Dermatol.* 122:167-176.
- Ishikawa, M., Fernandez, B., and Kerbel, R.S. (1988) Highly pigmented human melanoma variant which metastasizes widely in nude mice, including to skin and brain. *Cancer Res.* 48:4897-4903.
- Ishikawa, M., Dennis, J.W., Man, S., and Kerbel, R.S. (1988) Isolation and characterization of spontaneous wheat germ agglutinin-resistant human melanoma mutants displaying remarkably different metastatic profiles in nude mice. *Cancer Res.* 48:665-670.
- Ismail, M., Bokae, S., Morgan, R., Davies, J., Harrington, K.J., and Pandha, H. (2009) Inhibition of the aquaporin 3 water channel increases the sensitivity of prostate cancer cells to cryotherapy. *Br.J.Cancer.* 2009.Jun.16.; 100:1889-1895.
- Itoh, T., Tanioka, M., Matsuda, H., Nishimoto, H., Yoshioka, T., Suzuki, R., and Uehira, M. (1999) Experimental metastasis is suppressed in MMP-9-deficient mice. *Clin.Exp.Metastasis* 17:177-181.
- Izumi, Y., Hirata, M., Hasuwa, H., Iwamoto, R., Umata, T., Miyado, K., Tamai, Y., Kurisaki, T., Sehara-Fujisawa, A., Ohno, S., and Mekada, E. (1998) A metalloprotease-disintegrin, MDC9/meltrin-gamma/ADAM9 and PKCdelta are involved in TPA-induced ectodomain shedding of membrane-anchored heparin-binding EGF-like growth factor. *EMBO J.* 17:7260-7272.

- Josson, S., Anderson, C.S., Sung, S.Y., Johnstone, P.A., Kubo, H., Hsieh, C.L., Arnold, R., Gururajan, M., Yates, C., and Chung, L.W. (2011) Inhibition of ADAM9 expression induces epithelial phenotypic alterations and sensitizes human prostate cancer cells to radiation and chemotherapy. *Prostate* 71:232-240.
- Junqueira, L.C., Bignolas, G., and Brentani, R.R. (1979) Picrosirius staining plus polarization microscopy, a specific method for collagen detection in tissue sections. *Histochem.J.* 11:447-455.
- Kakinuma, T. and Hwang, S.T. (2006) Chemokines, chemokine receptors, and cancer metastasis. *J.Leukoc.Biol.* 79:639-651.
- Kalluri, R. (2003) Basement membranes: structure, assembly and role in tumour angiogenesis. *Nat.Rev.Cancer* 3:422-433.
- Karkkainen, M.J., Makinen, T., and Alitalo, K. (2002) Lymphatic endothelium: a new frontier of metastasis research. *Nat.Cell Biol.* 4:E2-E5.
- Khoshnoodi, J., Pedchenko, V., and Hudson, B.G. (2008) Mammalian collagen IV. *Microsc.Res.Tech.* 71:357-370.
- Kim, D., Song, J., Kim, S., Kang, S.S., and Jin, E.J. (2011) MicroRNA-142-3p regulates TGF-beta3-mediated region-dependent chondrogenesis by regulating ADAM9. *Biochem.Biophys.Res.Commun.* 414:653-659.
- Klein, C.A. (2009) Parallel progression of primary tumours and metastases. *Nat.Rev.Cancer* 9:302-312.
- Klose, A., Wilbrand-Hennes, A., Zigrino, P., Weber, E., Krieg, T., Mauch, C., and Hunzelmann, N. (2006) Contact of high-invasive, but not low-invasive, melanoma cells to native collagen I induces the release of mature cathepsin B. *Int.J.Cancer* 118:2735-2743.
- Klose, A., Zigrino, P., Dennhofer, R., Mauch, C., and Hunzelmann, N. (2006) Identification and discrimination of extracellularly active cathepsins B and L in high-invasive melanoma cells. *Anal.Biochem.* 353:57-62.
- Kobayashi, T., Urabe, K., Orlow, S.J., Higashi, K., Imokawa, G., Kwon, B.S., Potterf, B., and Hearing, V.J. (1994) The Pmel 17/silver locus protein. Characterization and investigation of its melanogenic function. *J.Biol.Chem.* 269:29198-29205.
- Kohga, K., Takehara, T., Tatsumi, T., Ishida, H., Miyagi, T., Hosui, A., and Hayashi, N. (2009) Sorafenib inhibits the shedding of major histocompatibility complex class I-related chain A on hepatocellular carcinoma cells by down-regulating a disintegrin and metalloproteinase 9. *Hepatology.*
- Kohga, K., Tatsumi, T., Takehara, T., Tsunematsu, H., Shimizu, S., Yamamoto, M., Sasakawa, A., Miyagi, T., and Hayashi, N. (2010) Expression of CD133 confers malignant potential by regulating metalloproteinases in human hepatocellular carcinoma. *J.Hepatol.*
- Kozlowski, J.M., Fidler, I.J., Campbell, D., Xu, Z.L., Kaighn, M.E., and Hart, I.R. (1984) Metastatic behavior of human tumor cell lines grown in the nude mouse. *Cancer Res.* 44:3522-3529.
- Kumar, P., Wu, H., McBride, J.L., Jung, K.E., Kim, M.H., Davidson, B.L., Lee, S.K., Shankar, P., and Manjunath, N. (2007) Transvascular delivery of small interfering RNA to the central nervous system. *Nature.* 2007.Jul.5;448.(7149.):39-43. Epub.2007.Jun.17. 448:39-43.
- Kunz, M., Driller, K.M., Hein, M., Libnow, S., Hohensee, I., Ramer, R., Hinz, B., Berger, A., Eberle, J., and Langer, P. (2010) Synthesis of thia-analogous indirubin N-Glycosides and their influence on melanoma cell growth and apoptosis. *ChemMedChem.* 5:534-539.
- Kuphal, S. and Bosserhoff, A.K. (2011) E-cadherin cell-cell communication in melanogenesis and during development of malignant melanoma. *Arch.Biochem.Biophys.*
- Kurschat, P., Zigrino, P., Nischt, R., Breitkopf, K., Steurer, P., Klein, C.E., Krieg, T., and Mauch, C. (1999) Tissue inhibitor of matrix metalloproteinase-2 regulates matrix metalloproteinase-2 activation by modulation of membrane-type 1 matrix metalloproteinase activity in high and low invasive melanoma cell lines. *J.Biol.Chem.* 274:21056-21062.
- La Porta, C.A., Porro, D., and Comolli, R. (1998) Opposite effects of TPA on G1/S transition and on cell size in the low metastatic B16F1 with respect to high metastatic BL6 murine melanoma cells. *Cancer Lett.* 132:159-164.
- Landsberg, J., Gaffal, E., Cron, M., Kohlmeyer, J., Renn, M., and Tuting, T. (2010) Autochthonous primary and metastatic melanomas in Hgf-Cdk4 R24C mice evade T-cell-mediated immune surveillance. *Pigment Cell Melanoma Res.* 23:649-660.
- Larue, L. and Beermann, F. (2007) Cutaneous melanoma in genetically modified animals. *Pigment Cell Res.* 20:485-497.
- Lee, D.C., Sunnarborg, S.W., Hinkle, C.L., Myers, T.J., Stevenson, M.Y., Russell, W.E., Castner, B.J., Gerhart, M.J., Paxton, R.J., Black, R.A., Chang, A., and Jackson, L.F. (2003) TACE/ADAM17 processing of EGFR ligands indicates a role as a physiological convertase. *Ann.N.Y.Acad.Sci.* 995:22-38.
- Leiter, U., Meier, F., Schitteck, B., and Garbe, C. (2004) The natural course of cutaneous melanoma. *J.Surg.Oncol.* 2004.Jul.1: 86:172-178.
- Lendeckel, U., Kohl, J., Arndt, M., Carl-McGrath, S., Donat, H., and Rocken, C. (2005) Increased expression of ADAM family members in human breast cancer and breast cancer cell lines. *J.Cancer Res.Clin.Oncol.* 2005.Jan.;131.(1):41-8. Epub.2004.Sep.30. 131:41-48.
- Leof, E.B., Proper, J.A., Getz, M.J., and Moses, H.L. (1986) Transforming growth factor type beta regulation of actin mRNA. *J.Cell Physiol* 127:83-88.

- Li, G., Schaidler, H., Satyamoorthy, K., Hanakawa, Y., Hashimoto, K., and Herlyn, M. (2001) Downregulation of E-cadherin and Desmoglein 1 by autocrine hepatocyte growth factor during melanoma development. *Oncogene* 20:8125-8135.
- Liu, H., Chen, S.E., Jin, B., Carson, J.A., Niu, A., Durham, W., Lai, J.Y., and Li, Y.P. (2010) TIMP3: a physiological regulator of adult myogenesis. *J. Cell Sci.* 123:2914-2921.
- Lockshin, A., Giovanella, B.C., De Ipolyi, P.D., Williams, L.J., Jr., Mendoza, J.T., Yim, S.O., and Stehlin, J.S., Jr. (1985) Exceptional lethality for nude mice of cells derived from a primary human melanoma. *Cancer Res.* 45:345-350.
- Loffek, S., Zigrino, P., Angel, P., Anwald, B., Krieg, T., and Mauch, C. (2005) High invasive melanoma cells induce matrix metalloproteinase-1 synthesis in fibroblasts by interleukin-1alpha and basic fibroblast growth factor-mediated mechanisms. *J. Invest Dermatol.* 2005.Mar.;124.(3):124:638-643.
- Lowe, S.W. and Sherr, C.J. (2003) Tumor suppression by Ink4a-Arf: progress and puzzles. *Curr. Opin. Genet. Dev.* 13:77-83.
- Luca, M., Xie, S., Gutman, M., Huang, S., and Bar-Eli, M. (1995) Abnormalities in the CDKN2 (p16INK4/MTS-1) gene in human melanoma cells: relevance to tumor growth and metastasis. *Oncogene* 11:1399-1402.
- Ma, G.F., Liljestrom, M., Ainola, M., Chen, T., Tiainen, V.M., Lappalainen, R., Konttinen, Y.T., and Salo, J. (2006) Expression of ADAM9 (meltrin-gamma) around aseptically loosened total hip replacement implants. *Rheumatology (Oxford)* 45:808-814.
- Mackiewicz, Z., Rimkevicius, A., Petersen, J., Andersen, C.B., Dudek, E., Vytrasova, M., and Konttinen, Y.T. (2005) Macrophages overloaded with tissue debris in Wegener's granulomatosis. *Ann. Rheum. Dis.* 64:1229-1232.
- Maretzky, T., Yang, G., Ouerfelli, O., Overall, C.M., Worpenberg, S., Hassiepen, U., Eder, J., and Blobel, C.P. (2009) Characterization of the catalytic activity of the membrane-anchored metalloproteinase ADAM15 in cell-based assays. *Biochem. J.* 420:105-113.
- Marinkovich, M.P. (2007) Tumour microenvironment: laminin 332 in squamous-cell carcinoma. *Nat. Rev. Cancer* 7:370-380.
- Mauch, C., Zamek, J., Abety, A.N., Grimberg, G., Fox, J.W., and Zigrino, P. (2010) Accelerated wound repair in ADAM-9 knockout animals. *J. Invest Dermatol.* 130:2120-2130.
- Mazzocca, A., Coppari, R., De Franco, R., Cho, J.Y., Libermann, T.A., Pinzani, M., and Toker, A. (2005) A secreted form of ADAM9 promotes carcinoma invasion through tumor-stromal interactions. *Cancer Res.* 2005.Jun.1;65.(11): 65:4728-4738.
- McAteer, M.A., Schneider, J.E., Ali, Z.A., Warrick, N., Bursill, C.A., von zur, M.C., Greaves, D.R., Neubauer, S., Channon, K.M., and Choudhury, R.P. (2008) Magnetic resonance imaging of endothelial adhesion molecules in mouse atherosclerosis using dual-targeted microparticles of iron oxide. *Arterioscler. Thromb. Vasc. Biol.* 28:77-83.
- McGary, E.C., Lev, D.C., Bar-Eli, M. (2002) Cellular adhesion pathways and metastatic potential of human melanoma. *Cancer Biol Ther.* 1(5):459-65.
- Meier, F., Busch, S., Lasithiotakis, K., Kulms, D., Garbe, C., Maczey, E., Herlyn, M., and Schitteck, B. (2007) Combined targeting of MAPK and AKT signalling pathways is a promising strategy for melanoma treatment. *Br. J. Dermatol.* 156:1204-1213.
- Moelans, C.B., de Weger, R.A., Monsuur, H.N., Vijzelaar, R., and van Diest, P.J. (2010) Molecular profiling of invasive breast cancer by multiplex ligation-dependent probe amplification-based copy number analysis of tumor suppressor and oncogenes. *Mod. Pathol.*
- Mongaret, C., Alexandre, J., Thomas-Schoemann, A., Bermudez, E., Chereau, C., Nicco, C., Goldwasser, F., Weill, B., Batteux, F., and Lemare, F. (2010) Tumor invasion induced by oxidative stress is dependent on membrane ADAM 9 protein and its secreted form. *Int. J. Cancer.*
- Murphy, G. (2008) The ADAMs: signalling scissors in the tumour microenvironment. *Nat. Rev. Cancer.* 2008.Dec.; 8:929-941.
- Nahde, T., Muller, K., Fahr, A., Muller, R., and Brusselbach, S. (2001) Combined transductional and transcriptional targeting of melanoma cells by artificial virus-like particles. *J. Gene Med.* 3:353-361.
- Najy, A.J., Day, K.C., and Day, M.L. (2008) ADAM15 supports prostate cancer metastasis by modulating tumor cell-endothelial cell interaction. *Cancer Res.* 2008.Feb.15.; 68:1092-1099.
- Nakahara, H., Howard, L., Thompson, E.W., Sato, H., Seiki, M., Yeh, Y., and Chen, W.T. (1997) Transmembrane/cytoplasmic domain-mediated membrane type 1-matrix metalloprotease docking to invadopodia is required for cell invasion. *Proc. Natl. Acad. Sci. U.S.A.* 94:7959-7964.
- Nakashima, Y., Kariya, Y., Yasuda, C., and Miyazaki, K. (2005) Regulation of cell adhesion and type VII collagen binding by the beta3 chain short arm of laminin-5: effect of its proteolytic cleavage. *J. Biochem.* 138:539-552.
- Namba, K., Nishio, M., Mori, K., Miyamoto, N., Tsurudome, M., Ito, M., Kawano, M., Uchida, A., and Ito, Y. (2001) Involvement of ADAM9 in multinucleated giant cell formation of blood monocytes. *Cell Immunol.* 213:104-113.
- Nelson, K.K., Schlondorff, J., and Blobel, C.P. (1999) Evidence for an interaction of the metalloprotease-disintegrin tumour necrosis factor alpha convertase (TACE) with mitotic arrest deficient 2 (MAD2), and of the metalloprotease-disintegrin MDC9 with a novel MAD2-related protein, MAD2beta. *Biochem. J.* 343 Pt 3:673-680.

- O'Neill, L.A. and Greene, C. (1998) Signal transduction pathways activated by the IL-1 receptor family: ancient signaling machinery in mammals, insects, and plants. *J. Leukoc. Biol.* 63:650-657.
- Parry, D.A., Toomes, C., Bida, L., Danciger, M., Towns, K.V., McKibbin, M., Jacobson, S.G., Logan, C.V., Ali, M., Bond, J., Chance, R., Swendeman, S., Daniele, L.L., Springell, K., Adams, M., Johnson, C.A., Booth, A.P., Jafri, H., Rashid, Y., Banin, E., Strom, T.M., Farber, D.B., Sharon, D., Blobel, C.P., Pugh, E.N., Jr., Pierce, E.A., and Inglehearn, C.F. (2009) Loss of the metalloprotease ADAM9 leads to cone-rod dystrophy in humans and retinal degeneration in mice. *Am. J. Hum. Genet.* 2009. May.; 84.(5):683.-91. Epub. 2009. Apr 30. 84:683-691.
- Peduto, L., Reuter, V.E., Shaffer, D.R., Scher, H.I., and Blobel, C.P. (2005) Critical function for ADAM9 in mouse prostate cancer. *Cancer Res.* 2005. Oct. 15.: 65:9312-9319.
- Peduto, L. (2009) ADAM9 as a potential target molecule in cancer. *Curr. Pharm. Des.* 2009.; 15.(20.):15:2282-2287.
- Quintanilla-Dieck, M.J., Codriansky, K., Keady, M., Bhawan, J., and Runger, T.M. (2008) Cathepsin K in melanoma invasion. *J. Invest Dermatol.* 128:2281-2288.
- Ramirez-Montagut, T., Turk, M.J., Wolchok, J.D., Guevara-Patino, J.A., and Houghton, A.N. (2003) Immunity to melanoma: unraveling the relation of tumor immunity and autoimmunity. *Oncogene* 22:3180-3187.
- Remy, L., Trespeuch, C., Bachy, S., Scoazec, J.Y., and Rousselle, P. (2006) Matrilysin 1 influences colon carcinoma cell migration by cleavage of the laminin-5 beta3 chain. *Cancer Res.* 66:11228-11237.
- Rocks, N., Paulissen, G., El Hour, M., Quesada, F., Crahay, C., Gueders, M., Foidart, J.M., Noel, A., and Cataldo, D. (2008) Emerging roles of ADAM and ADAMTS metalloproteinases in cancer. *Biochimie.* 2008. Feb.; 90.(2):369.-79. Epub. 2007. Sep. 2. 90:369-379.
- Roghani, M., Becherer, J.D., Moss, M.L., Atherton, R.E., Erdjument-Bromage, H., Arribas, J., Blackburn, R.K., Weskamp, G., Tempst, P., and Blobel, C.P. (1999) Metalloprotease-disintegrin MDC9: intracellular maturation and catalytic activity. *J. Biol. Chem.* 274:3531-3540.
- Schlomann, U., Rathke-Hartlieb, S., Yamamoto, S., Jockusch, H., and Bartsch, J.W. (2000) Tumor necrosis factor alpha induces a metalloprotease-disintegrin, ADAM8 (CD 156): implications for neuron-glia interactions during neurodegeneration. *J. Neurosci.* 20:7964-7971.
- Schönefuß A., Abety, A., Zamek, J., Mauch, C., and Zigrino, P. (2012) Role of ADAM-15 in wound healing and melanoma development. *Exp. Dermatol.* in press
- Schwettmann, L. and Tschesche, H. (2001) Cloning and expression in *Pichia pastoris* of metalloprotease domain of ADAM 9 catalytically active against fibronectin. *Protein Expr. Purif.* 2001. Feb.: 21:65-70.
- Schwinn, N., Vokhminova, D., Sucker, A., Textor, S., Striegel, S., Moll, I., Nausch, N., Tuettenberg, J., Steinle, A., Cerwenka, A., Schadendorf, D., and Paschen, A. (2009) Interferon-gamma down-regulates NKG2D ligand expression and impairs the NKG2D-mediated cytotoxicity of MHC class I-deficient melanoma by natural killer cells. *Int. J. Cancer* 124:1594-1604.
- Shintani, Y., Higashiyama, S., Ohta, M., Hirabayashi, H., Yamamoto, S., Yoshimasu, T., Matsuda, H., and Matsuura, N. (2004) Overexpression of ADAM9 in non-small cell lung cancer correlates with brain metastasis. *Cancer Res.* 2004. Jun. 15.; 64:4190-4196.
- Sikorski, E.E., Hallmann, R., Berg, E.L., and Butcher, E.C. (1993) The Peyer's patch high endothelial receptor for lymphocytes, the mucosal vascular addressin, is induced on a murine endothelial cell line by tumor necrosis factor-alpha and IL-1. *J. Immunol.* 151:5239-5250.
- Singh, S.K., Nizard, C., Kurfurst, R., Bonte, F., Schnebert, S., and Tobin, D.J. (2008) The silver locus product (Silv/gp100/Pmel17) as a new tool for the analysis of melanosome transfer in human melanocyte-keratinocyte co-culture. *Exp. Dermatol.* 17:418-426.
- Solomon, E., Li, H., Muggy, S.D., Syta, E., and Zolkiewska, A. (2010) The role of SnoN in transforming growth factor beta1-induced expression of metalloprotease-disintegrin ADAM12. *J. Biol. Chem.* 285:21969-21977.
- Soond, S.M., Everson, B., Riches, D.W., and Murphy, G. (2005) ERK-mediated phosphorylation of Thr735 in TNFalpha-converting enzyme and its potential role in TACE protein trafficking. *J. Cell Sci.* 118 :2371-2380.
- Sosman, J.A., Kim, K.B., Schuchter, L., Gonzalez, R., Pavlick, A.C., Weber, J.S., McArthur, G.A., Hutson, T.E., Moschos, S.J., Flaherty, K.T., Hersey, P., Kefford, R., Lawrence, D., Puzanov, I., Lewis, K.D., Amaravadi, R.K., Chmielowski, B., Lawrence, H.J., Shyr, Y., Ye, F., Li, J., Nolop, K.B., Lee, R.J., Joe, A.K., and Ribas, A. (2012) Survival in BRAF V600-mutant advanced melanoma treated with vemurafenib. *N. Engl. J. Med.* 366:707-714.
- Sotillo, R., Garcia, J.F., Ortega, S., Martin, J., Dubus, P., Barbacid, M., and Malumbres, M. (2001) Invasive melanoma in Cdk4-targeted mice. *Proc. Natl. Acad. Sci. U.S.A.* 2001. Nov. 6. 98:13312-13317.
- Stark, H.J., Baur, M., Breitkreutz, D., Mirancea, N., and Fusenig, N.E. (1999) Organotypic keratinocyte cocultures in defined medium with regular epidermal morphogenesis and differentiation. *J. Invest Dermatol.* 112:681-691.
- Stark, M. and Hayward, N. (2007) Genome-wide loss of heterozygosity and copy number analysis in melanoma using high-density single-nucleotide polymorphism arrays. *Cancer Res.* 67:2632-2642.
- Sung, S.Y., Kubo, H., Shigemura, K., Arnold, R.S., Logani, S., Wang, R., Konaka, H., Nakagawa, M., Mousses, S., Amin, M., Anderson, C., Johnstone, P., Petros, J.A., Marshall, F.F., Zhou, H.E., and Chung, L.W. (2006) Oxidative stress induces ADAM9 protein expression in human prostate cancer cells. *Cancer Res.* 2006. Oct. 1; 66:9519-9526.
- Szalad, A., Katakowski, M., Zheng, X., Jiang, F., and Chopp, M. (2009) Transcription factor Sp1 induces ADAM17 and contributes to tumor cell invasiveness under hypoxia. *J. Exp. Clin. Cancer Res.* 28:129.

- Tang,A., Eller,M.S., Hara,M., Yaar,M., Hirohashi,S., and Gilchrest,B.A. (1994) E-cadherin is the major mediator of human melanocyte adhesion to keratinocytes in vitro. *J.Cell Sci.* 107 (Pt 4):983-992.
- Tao,K., Qian,N., Tang,Y., Ti,Z., Song,W., Cao,D., and Dou,K. (2010) Increased expression of a disintegrin and metalloprotease-9 in hepatocellular carcinoma: implications for tumor progression and prognosis. *Jpn.J.Clin.Oncol.* 40:645-651.
- Tormo,D., Ferrer,A., Gaffal,E., Wenzel,J., Basner-Tschakarjan,E., Steitz,J., Heukamp,L.C., Gutgemann,I., Buettner,R., Malumbres,M., Barbacid,M., Merlino,G., and Tuting,T. (2006) Rapid growth of invasive metastatic melanoma in carcinogen-treated hepatocyte growth factor/scatter factor-transgenic mice carrying an oncogenic CDK4 mutation. *Am.J.Pathol.*2006.Aug.;169:665-672.
- Tsai,K.Y. and Tsao,H. (2004) The genetics of skin cancer. *Am.J.Med Genet.C.Semin.Med Genet.*2004.Nov.15.: 131C:82-92.
- Tsukamoto,K., Hirata,S., Osada,A., Kitamura,R., and Shimada,S. (2000) Detection of circulating melanoma cells by RT-PCR amplification of three different melanocyte-specific mRNAs in a mouse model. *Pigment Cell Res.* 13:185-189.
- Tucker,M.A. and Goldstein,A.M. (2003) Melanoma etiology: where are we? *Oncogene* 22:3042-3052.
- Tunggal,L., Ravoux,J., Pesch,M., Smola,H., Krieg,T., Gaill,F., Sasaki,T., Timpl,R., Mauch,C., and Aumailley,M. (2002) Defective laminin 5 processing in cylindroma cells. *Am.J.Pathol.* 160:459-468.
- Tzu,J. and Marinkovich,M.P. (2008) Bridging structure with function: structural, regulatory, and developmental role of laminins. *Int.J.Biochem.Cell Biol.* 40:199-214.
- Udayakumar,T.S., Chen,M.L., Bair,E.L., Von Bredow,D.C., Cress,A.E., Nagle,R.B., and Bowden,G.T. (2003) Membrane type-1-matrix metalloproteinase expressed by prostate carcinoma cells cleaves human laminin-5 beta3 chain and induces cell migration. *Cancer Res.* 63:2292-2299.
- Ugurel,S., Thirumaran,R.K., Bloethner,S., Gast,A., Sucker,A., Mueller-Berghaus,J., Rittgen,W., Hemminki,K., Becker,J.C., Kumar,R., and Schadendorf,D. (2007) B-RAF and N-RAS mutations are preserved during short time in vitro propagation and differentially impact prognosis. *PLoS.One.* 2:e236.
- Ungerer,C., Doberstein,K., Burger,C., Hardt,K., Boehncke,W.H., Bohm,B., Pfeilschifter,J., Dummer,R., Mihic-Probst,D., and Gutwein,P. (2010) ADAM15 expression is downregulated in melanoma metastasis compared to primary melanoma. *Biochem.Biophys.Res.Commun.*
- Uong,A. and Zon,L.I. (2010) Melanocytes in development and cancer. *J.Cell Physiol* 222:38-41.
- van Muijen,G.N., Cornelissen,L.M., Jansen,C.F., Figdor,C.G., Johnson,J.P., Brocker,E.B., and Ruiter,D.J. (1991) Antigen expression of metastasizing and non-metastasizing human melanoma cells xenografted into nude mice. *Clin.Exp.Metastasis* 9:259-272.
- Verkman,A.S. (2005) More than just water channels: unexpected cellular roles of aquaporins. *J.Cell Sci.*2005.Aug.1.: 118:3225-3232.
- Voronov,E., Shouval,D.S., Krelin,Y., Cagnano,E., Benharroch,D., Iwakura,Y., Dinarello,C.A., and Apte,R.N. (2003) IL-1 is required for tumor invasiveness and angiogenesis. *Proc.Natl.Acad.Sci.U.S.A.*2003.Mar.4;100:2645-2650.
- Waldhauer,I., Goehlsdorf,D., Gieseke,F., Weinschenk,T., Wittenbrink,M., Ludwig,A., Stevanovic,S., Rammensee,H.G., and Steinle,A. (2008) Tumor-associated MICA is shed by ADAM proteases. *Cancer Res.* 68:6368-6376.
- Walker,G.J. and Hayward,N.K. (2002) Pathways to melanoma development: lessons from the mouse. *J.Invest Dermatol.*2002.Oct.: 119:783-792.
- Welch,D.R., Bisi,J.E., Miller,B.E., Conaway,D., Seftor,E.A., Yohem,K.H., Gilmore,L.B., Seftor,R.E., Nakajima,M., and Hendrix,M.J. (1991) Characterization of a highly invasive and spontaneously metastatic human malignant melanoma cell line. *Int.J.Cancer* 47:227-237.
- Weskamp,G., Kratzschmar,J., Reid,M.S., and Blobel,C.P. (1996) MDC9, a widely expressed cellular disintegrin containing cytoplasmic SH3 ligand domains. *J.Cell Biol.* 132:717-726.
- Weskamp,G., Cai,H., Brodie,T.A., Higashiyama,S., Manova,K., Ludwig,T., and Blobel,C.P. (2002) Mice lacking the metalloprotease-disintegrin MDC9 (ADAM9) have no evident major abnormalities during development or adult life. *Mol.Cell Biol.*2002.Mar.;22.(5):1537.-44. 22:1537-1544.
- Whitmarsh,A.J. and Davis,R.J. (1996) Transcription factor AP-1 regulation by mitogen-activated protein kinase signal transduction pathways. *J.Mol.Med.* 74:589-607.
- Williams,R.L., Courtneidge,S.A., and Wagner,E.F. (1988) Embryonic lethalties and endothelial tumors in chimeric mice expressing polyoma virus middle T oncogene. *Cell* 52:121-131.
- Wolfsberg,T.G., Primakoff,P., Myles,D.G., and White,J.M. (1995) ADAM, a novel family of membrane proteins containing A Disintegrin And Metalloprotease domain: multipotential functions in cell-cell and cell-matrix interactions. *J.Cell Biol.* 131:275-278.
- Wulf,E., Deboben,A., Bautz,F.A., Faulstich,H., and Wieland,T. (1979) Fluorescent phallotoxin, a tool for the visualization of cellular actin. *Proc.Natl.Acad.Sci.U.S.A* 76:4498-4502.
- Wyckoff,J.B., Pinner,S.E., Gschmeissner,S., Condeelis,J.S., and Sahai,E. (2006) *Curr.Biol.* 16:1515-1523.

- Xu,Q., Liu,X., Cai,Y., Yu,Y., and Chen,W. (2010) RNAi-mediated ADAM9 gene silencing inhibits metastasis of adenoid cystic carcinoma cells. *Tumour.Biol.*
- Yamada,D., Ohuchida,K., Mizumoto,K., Ohhashi,S., Yu,J., Egami,T., Fujita,H., Nagai,E., and Tanaka,M. (2007) Increased expression of ADAM 9 and ADAM 15 mRNA in pancreatic cancer. *Anticancer Res.* 27:793-799.
- Zelenina,M., Tritto,S., Bondar,A.A., Zelenin,S., and Aperia,A. (2004) Copper inhibits the water and glycerol permeability of aquaporin-3. *J.Biol.Chem.* 279:51939-51943.
- Zhou,C., Liu,J., Li,Y., Liu,L., Zhang,X., Ma,C.Y., Hua,S.C., Yang,M., and Yuan,Q. (2011) microRNA-1274a, a modulator of sorafenib induced a disintegrin and metalloproteinase 9 (ADAM9) down-regulation in hepatocellular carcinoma. *FEBS Lett.* 585:1828-1834.
- Zigrino,P., Mauch,C., Fox,J.W., and Nischt,R. (2005) Adam-9 expression and regulation in human skin melanoma and melanoma cell lines. *Int.J.Cancer.*2005.Oct.10:116:853-859.
- Zigrino,P., Loffek,S., and Mauch,C. (2005) Tumor-stroma interactions: their role in the control of tumor cell invasion. *Biochimie* 87:321-328.
- Zigrino,P., Steiger,J., Fox,J.W., Loffek,S., Schild,A., Nischt,R., and Mauch,C. (2007) Role of ADAM-9 disintegrin-cysteine-rich domains in human keratinocyte migration. *J.Biol.Chem.*2007.Oct. 282 :30785-30793.
- Zigrino,P., Kuhn,I., Bauerle,T., Zamek,J., Fox,J.W., Neumann,S., Licht,A., Schorpp-Kistner,M., Angel,P., and Mauch,C. (2009) Stromal expression of MMP-13 is required for melanoma invasion and metastasis. *J.Invest Dermatol.* 129:2686-2693.
- Zigrino,P., Nischt,R., and Mauch,C. (2011) The Disintegrin-like and Cysteine-rich domains of ADAM-9 Mediate Interactions between Melanoma Cells and Fibroblasts. *J.Biol.Chem.* 286:6801-6807.
- Zuo,L., Weger,J., Yang,Q., Goldstein,A.M., Tucker,M.A., Walker,G.J., Hayward,N., and Dracopoli,N.C. (1996) Germline mutations in the p16INK4a binding domain of CDK4 in familial melanoma. *Nat.Genet.* 12:97-99.

6. Abbreviations

µg	microgram
µl	microliter
µm	micrometer
µM	micromolar
7-AAD	7-Amino-Actinomycin
ADAM	A Disintegrin And Metalloprotease
Adam-9 ^{mutated/ko}	Adam-9 ^{-/-} //Hgf/Cdk4 ^{R24C/R24C}
AKT	protein kinase B
AP-1	activator protein-1
APP	amyloid-precursor-protein
ATP	adenosine triphosphate
BCA	bicinchoninic acid
BM	basement membrane
BODIPY	8-chromomethyl-4-difluoro-1,3,5,7-tetramethyl-4-bora-3a,4a-diaza-s-indacene
bp	basepair
BRAF	v-rat fibrosarcoma murine sarcoma viral oncogene homolog B1
BrdU	5-bromo-2-deoxyuridine
BSA	bovine serum albumine
Casp-3	caspase-3
CCL	C-C chemokine ligand
CCR	C-C chemokine receptor
CDK	cyclin dependent kinase
CDKN2A	cyclin dependent kinase inhibitor 2A
cm	centimeter
Col I	collagen type I
Col IV	collagen type IV
CXCL	chemokine (C-X-C motif) ligand
CXCR	C-X-C chemokine receptor
Cy3	cyanid 3
DAPI	4, 6-diamidino-2-phenylindol
DDS	dead deepidermized skin
DEPC	diethylpyrocarbonate
DMBA	7,12-Dimethylbenzanthracene
DMEM	Dulbecco's Modified Eagle Medium
DMSO	dimethyl sulfoxide
DNA	deoxyribonucleic acid
dNTP	desoxy nucleoside triphosphate
EDTA	ethylendiamintetraacetat
EGF	epidermal growth factor

EGFR	epidermal growth factor receptor
EHS	Engelbreth-Holm-Swarm
ELISA	enzyme linked immunoabsorbent assay
EphB4	ephrin type-B receptor
ERK	extracellular related kinase
EtOH	ethanol
FACS	fluorescence activated cell sorting
FCS	fetal calf serum
FGFR2	fibroblast growth factor receptor 2
Fik-1	fetal liver kinase-1
FN	fibronectin
gDNA	genomic deoxyribonucleic acid
GPCR	G-protein-coupled-receptor
HB-EGF	heparin binding-epidermal growth factor
HGF	hepatocyte growth factor
HGF/SF	hepatocyte growth factor/scatter factor
HRAS	transforming protein p21
HRP	horseradish peroxidase
ICAM-1	intercellular adhesion molecule-1
IgG	immunoglobulin G
IL-1 α	interleukin-1 alpha
IL-1 β	interleukin-1 beta
ITS	insulin-transferrin-sodium selenite
JNK	c-Jun N-terminal kinase
kDa	kilodalton
Lam 332	laminin 332
Lam 511	laminin 511
LYVE-1	lymphatic vessel endothelial hyaluronan receptor-1
MAD2 β	mitotic arrest deficient 2 beta
MAPK	mitogen-activated protein kinase kinase
MCAM	melanoma cell adhesion molecule
MCP-1	monocyte chemoattractant protein-1 (=CCL2)
MCP-5	monocyte chemoattractant protein-5 (=CCL12)
MDM2	murine double minute oncogene 2
mg	milligram
MHC	major Histocompatibility Complex
MICA/B	major histocompatibility complex related chain 1 A/B
MITF	microphthalmia transcription factor
ml	milliliter
mm	millimetre
mM	millimolar

MMP	matrix metalloprotease
mRNA	messenger ribonucleic acid
MuLV	moloney murine leukemia virus
NF κ B	nuclear factor kappa B
ng	nanogram
NGS	normal goat serum
NKG2D	activating natural killer cell receptor
nm	nanometer
NRAS	neuroblastoma Ras viral oncogene homolog
OD	optical density
PAGE	polyacrylamid gel electrophoresis
PBS	phosphate buffered saline
PCR	polymerase chain reaction
PDGF	platelet derived growth factor
PECAM	platelet endothelial cell adhesion molecule
pERK	phosphorylated extracellular related kinase
PFA	para formaldehyde
PI	propidium iodide
PI3K	phosphatidylinositol 3-kinase
pJNK	phosphorylated c-Jun N-terminal kinase
PKC- δ	protein kinase C delta
Pmel17	melanocyte lineage-specific antigen GP100
PTEN	phosphatase and tensin homolog
RAS	rat sarcoma proto-oncogene
RIP	regulated intramembrane proteolysis
RIPA	radioimmunoprecipitation assay
RGP	radial growth phase
RNA	ribonucleic acid
RPMI	Roswell Park Memorial Institute
RT-PCR	reverse transcription polymerase chain reaction
SD	standard deviation
SDF-1 α	stromal derived factor -1 α (=CXCL12)
SDS	sodiumdodecylsulfate
SEM	standard error of the mean
SH-3	sarcoma-homolgy-3
shRNA	small hairpin ribonucleic acid
SnoN	ski-related novel protein N
Sp1	specificity protein 1
TARC	thymus and activation-regulated chemokine (=CCL17)
TBE	Tris/borate/EDTA
TCA-3	T-cell activation-3 (=CCL1)

TGF- β	transforming growth factor beta
Tie-2	tyrosine kinase with immunoglobulin-like and EGF-like domains 2
TIMP	tissue inhibitor of metalloproteases
TNF- α	tumor necrosis factor alpha
TNFR1	tumor necrosis factor receptor 1
TPA	12-O-tetradecanoylphorbol-13-acetate
TRP-1	tyrosinase related protein-1
U	unit
UV	ultraviolet
VCAM	vascular cell adhesion molecule
VE-cadherin	vascular endothelial cadherin
VEGF	vascular endothelial growth factor
VGP	vertical growth phase
(v/v)	volume/volume
(w/v)	weight/volume

Acknowledgement

In particular I want to thank Dr. Paola Zigrino and Prof. Dr. Dr. Cornelia Mauch for the supervision of the project, their permanent availability and enthusiasm for scientific discussions and helpful ideas. They helped me to critically look at the results and bring the project forward.

In addition I would like to thank Prof. Dr. Dr. Thomas Krieg for providing me the possibility to prepare my PhD thesis at the Department of Dermatology and Venerology at the University of Cologne.

Furthermore I want to thank PD Dr. Roswitha Nischt for taking over the position of the first supervisor from the site of the Mathematical-Natural Science Faculty of the University of Cologne and for the fruitful discussions during the preparation of this thesis. I want to thank Prof. Dr. Matthias Hammerschmidt to accept being the second referee.

For providing the Hgf/Cdk^{R24C/R24C} animals and their disposition for discussion and always straight forward answers to many questions I would like to thank Prof. Dr. Thomas Tüting and Dr. Jenny Landsberg from the University of Bonn. Prof. Manuel Koch and Prof. Monique Aumailley from the University of Cologne I want to thank for providing antibodies as well as recombinant laminin β 3-chain proteins.

In particular I thank all present and former members of the Tumorbiology working group of the Department of Dermatology, Anna Abety, Angelika Arora, Ouissam Ayachi, Jan Grützner, Dr. Anke Klose, Claudia Ochsmann, Birgit Seyfarth, Julia Steiger and Jan Zamek (in alphabetical order) as well as the other members of the Dermatology Department for creating a great working atmosphere, their help with experiments and for many scientific and non-scientific discussions.

Last but not least I specially thank my partner Catherine and my family for their absolute support and many encouraging words, which helped me not to give up also in difficult situations and to always to believe in the successful completion of this project.

Role of ADAM-15 in wound healing and melanoma development

Alexander Schönefuß, Anna N. Abety, Jan Zamek, Cornelia Mauch and Paola Zigrino

Departments of Dermatology and Venerology, University of Cologne, Cologne, Germany

Correspondence: Paola Zigrino, PhD, Department of Dermatology, University Hospital of Cologne, Kerpener Strasse 62, 50937 Cologne, Germany, Tel.: +49 221 478 97443, Fax: +49 221 478 5949, e-mail: paola.zigrino@uni-koeln.de

Abstract: Proteins of the A disintegrin and metalloprotease (ADAM) family are transmembrane proteins involved in ectodomain shedding and in cellular interactions. In skin, ADAM-15 is detected in the epidermis and dermal vascular structures by immunolocalization. Expression is also detected in isolated fibroblast, keratinocytes and endothelial cells in culture. Despite high expression of ADAM-15 throughout the wound repair process, wound healing experiments *in vivo* revealed a dispensable role of ADAM-15 for the healing process. No alterations in wound closure, re-epithelialization, contraction, scar formation and angiogenesis were detected in animals carrying Adam-15^{-/-} deletion. When analysing melanoma development by grafting melanoma cells into the flank of Adam-15^{-/-}, no significant alteration in tumor growth was detected. However, at later stages,

melanomas in the Adam-15^{-/-} animals were smaller than those grown in WT animals. At all time points, no significant differences in vascularization of the peritumoral stroma and tumors were detected. Interestingly, we could detect a reduced number of metastasized lungs and lymph nodes in Adam-15^{-/-} animals as compared to control littermate mice. In conclusion, our study indicated that ADAM-15 is dispensable for cutaneous wound healing and B16F1 melanoma growth, but significantly contributes to metastasis formation.

Key words: A disintegrin and metalloprotease – melanoma – metastasis – proteases – wound healing

Accepted for publication 20 March 2012

Introduction

A disintegrin and metalloprotease-15 belongs to the ADAM family and exhibits the general conserved protein structure of the members of this family, containing a pro- and metalloprotease domain, disintegrin-like domain and cysteine-rich domain followed by an EGF-like, transmembrane domain and short cytoplasmic tail (1). ADAM-15 is produced as glycosylated proform and is converted to the mature protease by the activity of furin-like proteases (2). Complete deletion of ADAM-15 in mice is compatible with life, and apart from development of osteoarthritic lesions 1 year after birth, no additional developmental phenotype has been described (3,4).

A structural feature of human ADAM-15 is the presence of an RGD-motif in the disintegrin domain that mediates cell–cell and cell–matrix interactions (5) with integrin receptors as shown with the integrin $\alpha v \beta 3$ (6) and the $\alpha 5 \beta 1$ integrin (7). ADAM-15 is expressed in immune cells and mediates cellular interactions crucial for homing and recruitment of inflammatory cells (5), whereas its expression in endothelial cells (3,8–10) is believed to regulate endothelial cell permeability and transepithelial migration of neutrophils (10).

Although ADAM-15 is highly expressed in mouse endothelium, animals lacking ADAM-15 do not show defects with respect to developmental vascularization, but reduced neo-vascularization in induced retinopathies model (3). In co-cultures of melanoma and endothelial cells, VEGF-A produced by melanoma cells mediated expression of ADAM-15 in endothelial cells and led to tube formation *in vitro* (11).

A disintegrin and metalloprotease-15 expression in prostate cancer cells promotes tumor growth *in vitro* (12). In this study, loss of ADAM-15 in the tumor cells inhibits their transmigration through endothelial cell monolayers and their metastatic potential

in an animal model *in vivo* (12). In contrast with these data, ADAM-15 has been postulated to have a protective function in tumor development of murine melanoma as ADAM-15 overexpression in B16F10 cells leads to reduced lung metastasis (13). Similarly, overexpression of ADAM-15 in human melanoma cells also reduced cell proliferation, migration and invasion (14), thus suggesting a controversial role of ADAM-15 in cancer.

In physiological conditions as in tissue repair processes, up-regulation of ADAM-15 was described in wounded human lens (15). Furthermore, overexpression of ADAM-15 was also detected in human intestinal cells upon wounding and was associated with reduced repair *in vitro* (8,16). Surprisingly, very little is known about the role of ADAM-15 in repair processes of the skin.

To shed more light into the role of ADAM-15 in physiological and pathological conditions, we used mice carrying the complete ADAM-15 deletion. We investigated the role of ADAM-15 in neoangiogenesis and inflammation occurring during both skin excisional wound repair and melanoma invasion *in vivo*.

Methods

Cells and tissues

Epidermal–dermal split of human skin was performed as previously described (17). Keratinocytes and fibroblasts were isolated from skin specimens and cultured for 1–4 passages before use as described earlier (18,19). Melanocytes and microvascular endothelial cells were cultured according to the provided protocol (Promocell, Heidelberg, Germany). Total RNA was extracted from cells and separated skin compartments using RNAzol (WAK Chemie, Steinbach, Germany). See Data S1 for further information.

Wound healing experiments

A disintegrin and metalloprotease-15 knockout (Adam-15^{-/-}) and their wild-type littermates (WT) mice were kindly provided

by Prof C. Blobel (Hospital for Special Surgery, New York, NY, USA) and described elsewhere (3). Adam-15^{-/-} and WT littermates (8- to 10-week-old male and female; see Data S1) control mice were anaesthetized with a single intraperitoneal injection of ketamine/xylazine. After removal of back hairs by shaving, two full-thickness excisional wounds (4 mm diameter) were generated on each animal by excising skin and *panniculus carnosus* as described earlier (20). All animal experiments, including those described later, were performed in compliance with the German Law for Welfare of Laboratory Animals and were approved by the local veterinary authority (NRW authorization 50.203.2-K 37a, 20/05).

Tumor growth and metastasis

Tumor growth assay *in vivo* was performed by intradermal injection of 0.5×10^6 B16F1-GFP cells (21) in 100 μ l PBS into the flank of 6- to 8-week-old female Adam-15^{-/-} and WT littermate mice. Tumor size was measured as a function of time using a precision calliper, and tumor volume was calculated by multiplying length, width and depth and expressed as average \pm SEM.

To analyse metastasis formation, 16 days postintralesional injection of 1×10^6 B16F1-GFP cells, lungs and groin lymph nodes were isolated and total RNA was extracted. Briefly, organs were finely minced, placed in RNazol (WAK Chemie) and homogenized using the mixer mill device at 40 Hz for 5 min. After 10-min centrifugation at 4°C, RNA was extracted from cleared supernatants as described above. After reverse transcription, 2 μ l of the cDNA was used to amplify specific GFP transcripts by PCR (21). Amplification products were analysed on 2% agarose gels in TBE.

Immunohistochemistry

For immunohistochemical analysis, cryo-sections (7 μ m) were fixed with ice-cold acetone for 10 min at RT and allowed to air-dry. Blocking of unspecific binding sites was performed using 10% normal goat serum in PBS for 1 h at room temperature in a humidified chamber. Subsequently, sections were incubated with the first antibodies overnight at 4°C in humidified chamber. All used antibodies are indicated in the Data S1.

Bound primary antibodies were detected using Alexa-fluorochrome-conjugated secondary antibodies (1:800; Invitrogen, Darmstadt, Germany) for 1 h at RT and nuclei counterstained with DAPI (Roche, Mannheim, Germany). Negative controls were analysed using non-specific IgG as primary antibodies.

To detect ADAM-15, bound primary antibodies were detected with AP-labelled anti-rabbit polymer/Dako REAL™ detection system (Dako). The nuclei were stained with haematoxylin (Thermo Scientific, Asbach, Germany).

Images were captured with a Nikon Eclipse E800 microscope and a Nikon Digital Camera DXM 1200 connected to a computer equipped with an imaging program (NIS-Elements AR 2.30; NIS-Elements, Melville, NY, USA).

CD31, LYVE-1 and CD45 immunostained sections from five different specimens were analysed with the Image J software (http://rsb.info.nih.gov/ij). Different fields (2–11 depending on the tissue, wounds or tumor) in each section were examined, and the average number of counts was calculated.

Statistics

Two-tailed Student's *t*-test was used for data analysis, with $P < 0.05$ considered to be statistically significant.

Results

A disintegrin and metalloprotease-15 is expressed in skin resident cells

In human healthy skin, expression of ADAM-15 is localized in epidermal keratinocytes as shown by the immunohistochemical staining of human skin sections using two different antibodies (Fig. 1a). In this specimen, ADAM-15 was also associated with dermal vascular structures and with fibroblast-like cells (arrowheads). To further corroborate this expression pattern, we analysed the expression of ADAM-15 transcripts in thermolysin-dissociated epidermis and dermis, as well as in entire human skin (Fig. 1b). ADAM-15 transcripts were detected at similar intensities in both skin compartments, epidermis and dermis.

In cultured primary human skin cells, specific ADAM-15 transcripts were detected in cultured keratinocytes, endothelial cells and fibroblasts with the highest expression in keratinocytes and the lowest in melanocytes (Fig. 1b). In murine skin, expression of ADAM-15 was detected in total skin extracts, in keratinocytes and endothelial cells, but the highest expression was found in mouse fibroblasts (Fig. 1c). To test whether ADAM-15 is regulated during wound healing, we have generated full-thickness excisional wounds on the back of C57/Bl6 control animals. At the indicated time points, mice were killed and wounds processed for RNA

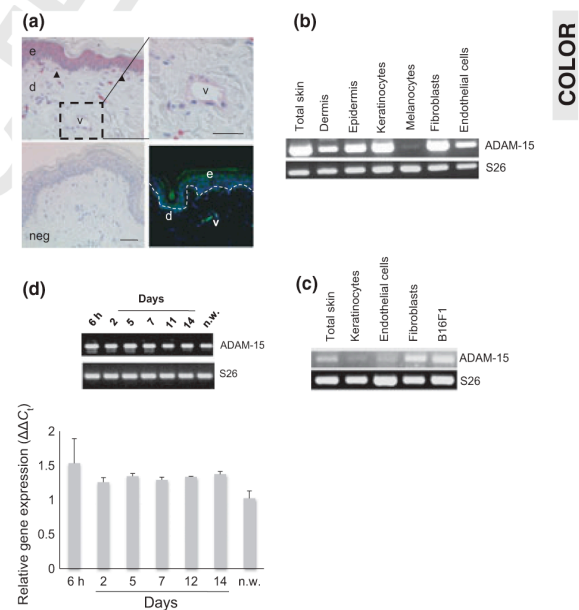


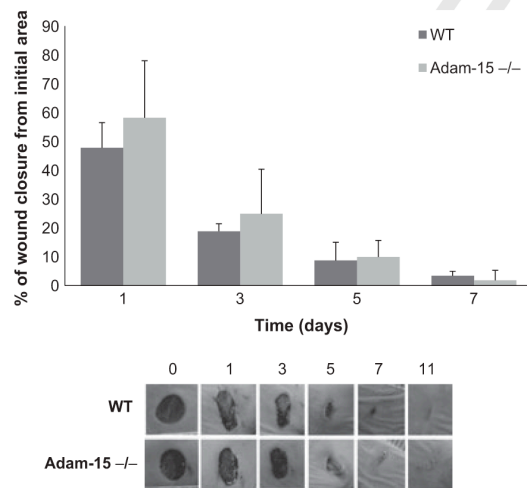
Figure 1. A disintegrin and metalloprotease-15 expression in skin. (a) Sections from human skin were stained by immunohistochemistry using antibodies to ADAM-15. Cell nuclei are shown in light blue. Epidermis (e), fibroblast-like cells (arrowheads), dermis (d) and vascular structures (v). The immunofluorescence shows in green ADAM-15 positivity using an additional antibody. The negative control is shown below (neg). Scale bar 50 μ m. (b) RT-PCR amplification of human ADAM-15 in dissociated epidermis and dermis as compared to total skin from the same specimen, and cultured human skin cells. (c) Amplification of ADAM-15 transcripts from cultured murine cells or (d) from wounds of mice at different time points as compared to unwounded skin (n.w.). Transcripts in wounds were quantified by Q-PCR and here shown as average $\Delta\Delta C_t$ values \pm SD ($n = 2$). Amplification of S26 was used as control.

1 extraction. High ADAM-15 transcript levels were detected
 2 throughout the time course of repair and were almost comparable
 3 to those detected in not wounded skin (n.w.), slightly lower, by
 4 both semi (microphotographs)- and quantitative (lower graph)
 5 RT-PCR analysis (Fig. 1d).

6 **Wound repair in Adam-15^{-/-} animals**

7 Using animals with complete inactivation of ADAM-15 (Adam-
 8 15^{-/-}) and their littermate controls (WT), we have first analysed
 9 whether ablation of this protein affects morphology and epidermal
 10 differentiation in murine adult skin. H&E staining of paraffin sections
 11 from those animals showed an overall comparable skin
 12 structure in WT and Adam-15^{-/-} animals. Furthermore, expres-
 13 sion analysis of keratin 14 (K14), present in the basal keratinocyte
 14 layer of the skin and loricrin, *stratum granulosum*, and keratin 6
 15 (K6) in hair follicles, displays a similar expression pattern as in
 16 WT control animals, thus indicating a normal keratinocyte differ-
 17 entiation in Adam-15^{-/-} mice (Figure S1a).

18 In addition, RT-PCR transcript analysis of RNA isolated from
 19 skin of WT or ADAM-15^{-/-} mice failed to show any prominent
 20 alteration in ADAM-9, 10 and 17 upon ablation of ADAM-15
 21 (Figure S1b). To analyse the role of ADAM-15 expression in skin
 22 during wound healing, we have used 8-week-old female Adam-
 23 15^{-/-} and WT animals. Full-thickness excisional wounds were
 24 generated on the back of the animals, and wound closure kinetics
 25 were assessed by measuring the wound area in time as com-
 26 pared to the initial area. No significant differences in wound
 27 closure were detected in Adam-15^{-/-} ($n = 8$) as compared to
 28 WT ($n = 10$) animals at different time points after wounding, as
 29 shown in Fig. 2. This was further corroborated by analysis of the
 30 length between the epithelial edges on sections (Figure S1c).



31
32
33
34
35
36
37
38
39
40
41
42
43
44
45
46
47
48
49
50 **Figure 2.** Wound healing in wild-type (WT) and A disintegrin and
 51 metalloprotease-15^{-/-} animals. Excisional wounds were generated on the back
 52 skin of Adam-15 WT and^{-/-} mice, and wound closure was followed over time
 53 ($n = 10$ Adam-15 WT; $n = 8$ Adam-15^{-/-}). Wound area at days 1, 3, 5 and 7 is
 expressed as per cent of the initial area of the same wound. Averages \pm SEM are
 shown. The lower panel shows a representative wound from Adam-15^{-/-} and
 WT mice over time. (Significance: day 3, $P < 0.8$; day 5, $P < 0.6$; day 7, $P < 0.4$).

Histological and morphometric analysis of wound re-epithelial-
 ization was performed by measuring the length of the migrated
 keratinocytes tip (marked by the black dashed line) of the wound
 at days 3 and 5 postwounding. This analysis indicated a compar-
 able tip length, thus similar keratinocytes migration for re-epi-
 thelialization in Adam-15^{-/-} and WT animals (Figure S2a,b).
 The distance of the ends of the *panniculus carnosus* in Adam-
 15^{-/-} and WT animals was comparable in both animal geno-
 types (Figure S2e).

Angiogenesis is a key process for normal wound repair (22).
 We therefore have stained tissue sections at day 5 postwounding
 with the vascular endothelial cell marker CD31/PECAM-1 and
 lymphatic vessel cell marker LYVE-1. At this analysed time point
 as well as at day 3 postwounding (data not shown), the number
 and density of lymph and blood vascular structures invading the
 wounds was comparable in WT and Adam-15^{-/-} animals (Figure
 S2c). Furthermore, at day 7, a qualitatively similar density of
 alpha-smooth muscle positive cells (α SMA) populated the granu-
 lation tissue beneath the wound and covered the resident vascula-
 ture (arrows, Figure S2c). Wound closure at day 15 was complete,
 and late granulation tissue formation was similar in both animals,
 as shown by trichrome staining (showing in green the collagen
 accumulation in the newly formed skin). Furthermore, lymph and
 blood vascularization was present, suggestive of the late remodel-
 ling processes still ongoing (Figure S2d). In summary, ADAM-15
 expression is dispensable for skin morphogenesis, homeostasis
 and wound repair.

54 **Depletion of A disintegrin and metalloprotease-15 in the
 55 host does not affect tumor growth but alters lung metastasis
 56 formation**

Tissue remodelling, angiogenesis and cell-cell interactions play
 also an important role in cancer (23). To analyse the role of
 ADAM-15 in melanoma development, we have grafted the meta-
 static cell line B16F1 intradermally into the flank of Adam-15^{-/-}
 and WT animals and followed tumor growth as function of time
 (Fig. 3). Up to day 12, the size of tumors grown in Adam-15^{-/-}
 animals was comparable to those developed in WT animals
 (Fig. 3a, $n = 12$), whereas at later time points tumors grown in
 the Adam-15^{-/-} animals were smaller, even though not signifi-
 cant ($P > 0.05$), than those developed in WT animals (Fig. 3a).
 Furthermore, quantification of the number of proliferating cells in
 tumors developed at day 21 shows a reduced number of prolifera-
 ting melanoma cells in Adam-15 null animals as compared to
 WT, whereas no differences were detected in both animal geno-
 types at day 12 postinjection (Fig. 3d). Histological analysis of
 tumors at day 12 and day 21 by H&E staining revealed no
 remarkable differences in tumor architecture with a well-defined
 tumor mass and peritumoral stroma (Fig. 3b).

To analyse metastatic dissemination to lungs and the lymph
 nodes, we have amplified GFP transcripts, retained in B16F1 cells,
 from RNA isolated from entire organs. This analysis revealed that
 lung metastasis formation 16 days post-B16F1 injection was con-
 sistently reduced. The number of positive lungs in Adam-15^{-/-}
 was only 13% of the total ($n = 13$) as compared to 54% detected
 in WT ($n = 16$) animals. A similar, though less prominent differ-
 ence was detected in lymph nodes, where 13% of analysed organs
 were positive in Adam-15^{-/-} ($n = 13$) as compared to 23% in
 WT ($n = 16$) animals (Fig. 3c).

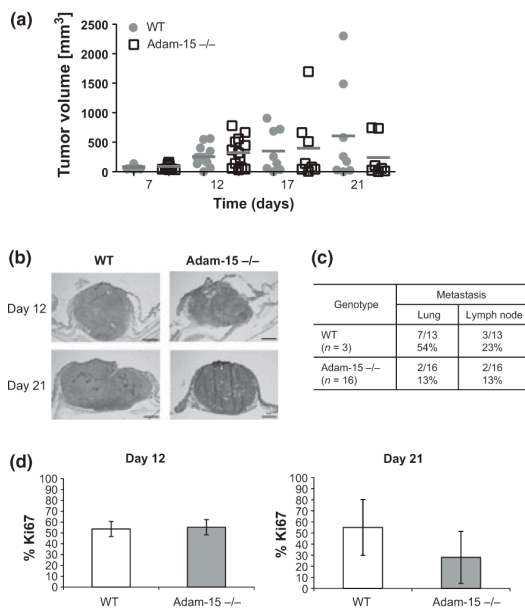


Figure 3. Melanoma growth and metastasis by murine melanoma cells was studied after intradermal injection of tumor cells in the flank of A disintegrin and metalloprotease-15^{-/-} and wild-type (WT) animals. (a) The volume of tumors was calculated at the indicated time points after injection. Every full dot WT or square (ADAM-15^{-/-}) indicates the volume of a single tumor. The grey line represents the mean size. (b) Representative histological images of tumor sections from day 12 and 21. Bar, 1 mm. (c) In a separate experiment, 16 days after melanoma cell injection, lungs and lymph nodes from Adam-15^{-/-} (n = 13) and WT (n = 16) animals were prepared and RNA analysed for expression of GFP transcripts of GFP-B16F1 cells. The number of positive organs is expressed as percentage of the total number per genotype. (d) Ratio of Ki67-positive cells to total number of nuclei was quantified by automated counting in three separate fields of four different tumors from Adam-15 WT and ^{-/-} mice at days 12 and 21 postinjection.

Angiogenesis and inflammatory infiltration are not altered in tumors upon A disintegrin and metalloprotease-15 depletion

Tumor angiogenesis is an important factor not only for tumor growth but also for tumor cell dissemination to distant organs. To investigate whether ablation of ADAM-15 results in altered tumor-induced angiogenesis and thus be responsible for altered melanoma cell colonization to lungs and lymph nodes, we have analysed qualitatively and quantitatively tumor vascularization as described above in tumor specimens from day 12 and 21 postinjection. This analysis revealed no significant alterations in blood vessel density in peritumoral as well as intratumoral areas in Adam-15^{-/-} as compared to WT animals at both analysed time points (Fig. 4a). We could confirm these data by quantification of the number of CD31 positive area in both animal genotypes (Fig. 4b). Neutrophil infiltration was similar around and within the tumors at days 12 and 21 postmelanoma cell injection (data not shown).

Interestingly, analysis of lymphocyte marker CD45 detected an increased, but not significant, number of lymphocytes in the peritumoral stroma and within the melanomas at days 12 and 21 in Adam-15^{-/-} as compared to control WT animals (Figure S3a,b),

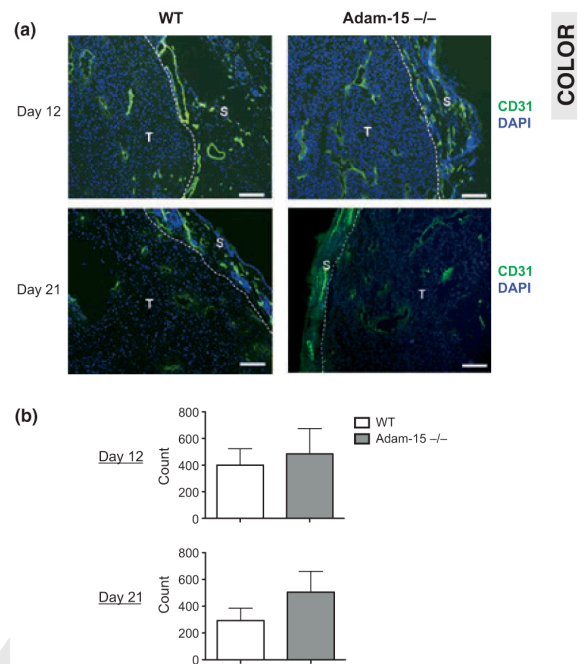


Figure 4. Tumor sections from days 12 and 21 tumors were stained for the endothelial cell marker CD31/PECAM-1 (green). Cell nuclei (blue) were visualized with fluorescent dye DAPI. The dotted line marks the border between the tumor (T) and the stroma (S). Bar, 100 μm.

but no alterations in either the CD8-positive T cells or macrophages (F4/80) were detected (Figure S4).

Discussion

A disintegrin and metalloprotease-15 is a multifunctional protein shown to function as adhesion molecule via interaction with integrins (7,24,25) and as protease towards extracellular matrix proteins (26). ADAM-15 is expressed in cells of the immune system and mediates cell–cell and cell–matrix interactions, which are crucial for homing and recruitment of immune cells to inflammatory sites (5). Apart from the presence in immune cells, ADAM-15 was found to be highly expressed in endothelial cells (3,9,10). However, the role of ADAM-15 in skin physiology has been elusive.

A disintegrin and metalloprotease-15 is expressed in skin in the epidermis and vascular structures within the dermis. In mice skin, we could detect transcripts in purified keratinocytes, fibroblasts and endothelial cells, thus indicating a similar expression profile as observed in human skin. Despite this abundant expression of ADAM-15, we show that complete ablation of ADAM-15 in mice did not lead to alterations in skin morphology and differentiation, indicating that ADAM-15 is dispensable for skin morphogenesis *in vivo*. During skin repair, ADAM-15 is expressed throughout all the phases, from inflammation, proliferation to remodelling, and its expression levels at all analysed time points were almost comparable to those detected in healthy not wounded skin. However, because of the lack of specific antibodies to detect the protein in murine skin, we cannot rule out whether, despite the constant expression throughout repair, altered localization in time occurs.

A disintegrin and metalloprotease-15 was detected high amounts in endothelial cells during development (3) and in inflammatory cells (5); thus, it is possible that expression of ADAM-15 during repair may be increased in the newly formed vessels and in infiltrating inflammatory cells but, at the same time, decreased in other compartments. To understand what is the role of ADAM-15 expression during wound healing, we have used an *in vivo* model for skin repair. We have analysed wound repair in animals carrying complete ADAM-15 depletion and in relative littermate controls. We observed no defect in wound closure kinetics upon depletion of ADAM-15, and in a microscopic analysis, we could not detect differences in wound re-epithelization, contraction and scar formation. In addition, we showed that vascularization or granulation tissue formation was not altered in the absence of ADAM-15. These data indicate that ADAM-15 is dispensable for skin repair processes. On the other hand, *in vitro* and *in vivo* studies have shown an important role for ADAM-15 in angiogenesis owing to the fact that this protease is highly expressed in endothelial cells. Several investigators proposed that ADAM-15 is involved in proteolytic processing of several factors, such as FGFR2iiiib (27,28), or in mediating cell–cell interactions in endothelial cells (6,29). Even though these data have implicated ADAM-15 in angiogenic processes, in our studies, ADAM-15 was dispensable for angiogenesis during physiological skin repair. In a model for *in vitro* intestinal tissue repair, ADAM-15 overexpression reduced healing of intestinal epithelial and fibroblast monolayers by decreasing the migration of these cells (16,30). Furthermore, in *ex vivo* experiments, ADAM-15 was up-regulated after wounding of human lens epithelium (15). It is therefore possible that ADAM-15 may have a tissue-specific function. In skin, however, we cannot exclude that high functional redundancy of proteases may compensate for ADAM-15 depletion. One additional limitation in ruling out the specific function of ADAM-15 is that most of the studies were performed *in vitro* using either full-length or isolated domains of ADAM-15. For instance, Lu et al. 2007 (25) showed that the recombinant ADAM-15 disintegrin domain reduced the migration and adhesion of airway smooth muscle cells through interaction with $\beta 1$ integrins. In agreement with these findings, *in vivo*, when ADAM-15 is depleted, we hypothesizes differences in α -smooth muscle actin (α -SMA)-positive cells populating the granulation tissue. However, at day 7 postwounding, SMA-positive cells populated the wounds, and transformation of the provisional extracellular matrix of the granulation tissue into scar tissue (31,32) occurred normally. This would suggest that ADAM-15 is not required for differentiation, migration and function of α SMA cells *in vivo*.

The situation may be different in pathological conditions as cancer development. However, upon grafting B16F1 murine melanoma cells intradermally into Adam-15^{-/-} and WT animals, tumor growth was not significantly different in both animal genotypes. Interestingly, at day 21, tumors in Adam-15^{-/-} were averagely smaller with reduced proliferation rate than in control animals.

Additionally, no alteration in vascularization of the tumors was detected. This finding was in agreement with the data published by Horiuchi et al. (3), who detected smaller B16F0 tumors in ADAM-15^{-/-} animals as compared to littermates and also failed to detect differences in vascularization of the tumors. Analysis of tumors at day 12 postinjection, an increased infiltration, even though not significant, of the tumors with CD45-positive lymphocytes was detected in ADAM-15^{-/-} animals. It is possible that the increased inflammatory reaction at early time points generated a host reaction that counteracted tumor progression, thus leading to reduced tumor size as observed at later time points.

Even though we did not detect a significant alteration in tumor growth, in ADAM-15^{-/-} mice, metastasis formation to lungs and lymph nodes was reduced as compared to wild-type controls. This difference was also observed when comparing animals bearing similar size tumors, indicating that this process was directly dependent on ADAM-15 ablation in the host rather than the result of different tumor burden. Indeed, ADAM-15, which is expressed in endothelial cells (3,9), may influence binding of tumor cells and in turn intra- or extravasation. Altered transendothelial migration has been shown in neutrophils by modulating ADAM-15 expression (10). We can envision that cell–cell interactions in homotypic or heterotypic fashion may contribute to this effect. Indeed, among the interacting partners of ADAM-15 are the cell surface receptors $\alpha v\beta 3$ and $\alpha 5\beta 1$ integrins (7) whose expression is detected not only in B16 melanoma cells (33,34), but also in neutrophils, monocytes and endothelial cells. The ability of ADAM-15 to ligate integrins on the surface of tumor cells has been shown with murine and human melanoma cells (14,35), but also human gastric cancer cells (36). Thus, the lack of expression of ADAM-15 might affect endothelial cell interaction with tumor cells and alter cell migration through the endothelium impairing their intravasation that ultimately leads to reduced metastasis formation.

In conclusion, while stromal expression of ADAM-15 is not important for skin repair and melanoma growth *in vivo*, our study highlights ADAM-15 as a pro-metastatic molecule. Further studies will be now aimed to investigate the molecular mechanism responsible for this effect.

Acknowledgements

We thank Prof. C. Blobel from the Hospital for Special Surgery, New York, for kindly providing the ADAM-15 animals and Mrs. A. Arora and Mrs J. Steiger for excellent technical assistance. This work was supported by the Melanoma Research Network of the Deutsche Krebshilfe (Melanoma Verbund to P.Z. and C.M.) and by the Deutsche Forschungsgemeinschaft through the SFB829 (to C.M.).

Authors Contribution

AS, AA, JZ and PZ performed the research; AS, JZ and PZ analysed the data; AS, CM and PZ wrote the paper; and CM and PZ designed the research study.

Conflict of Interest

The authors state no conflict of interest.

References

- Kratzschmar J, Lum L, Blobel C P. *J Biol Chem* 1996; **271**: 4593–4596.
- Lum L, Reid M S, Blobel C P. *J Biol Chem* 1998; **273**: 26236–26247.
- Horiuchi K, Weskamp G, Lum L et al. *Mol Cell Biol* 2003; **23**: 5614–5624.
- Bohm B B, Aigner T, Roy B et al. *Arthritis Rheum* 2005; **52**: 1100–1109.
- Charrier-Hisamuddin L, Laboisse C L, Merlin D. *FASEB J* 2008; **22**: 641–653.
- Zhang X P, Kamata T, Yokoyama K et al. *J Biol Chem* 1998; **273**: 7345–7350.

Schönefuß et al.

- 1 7 Nath D, Slocombe P M, Stephens P E *et al.* *J Cell*
2 *Sci* 1999; **112** (Pt 4): 579–587.
- 3 8 Charrier L, Yan Y, Nguyen H T *et al.* *J Biol Chem*
4 2007; **282**: 16948–16958. Epub 2007 Apr 6
5 2007; 282:16948–16958.
- 6 9 Mosnier J F, Jarry A, Bou-Hanna C *et al.* *Lab*
7 *Invest* 2006; **86**: 1064–1073.
- 8 10 Sun C, Wu M H, Guo M *et al.* *Cardiovasc Res*
9 2010; **?????:** ??????
- 10 11 Loffek S, Zigrino P, Steiger J *et al.* *Eur J Cell Biol*
11 2006; **85**: 1167–1177.
- 12 12 Najj A J, Day K C, Day M L. *Cancer Res* 2008;
13 **68**: 1092–1099.
- 14 13 Chen Q, Meng L H, Zhu C H *et al.* *Int J Biochem*
15 *Cell Biol* 2008; **40**: 2164–2173.
- 16 14 Ungerer C, Doberstein K, Burger C *et al.* *Biochem*
17 *Biophys Res Commun* 2010; **?????:** ??????
- 18 15 Hodgkinson L M, Wang L, Duncan G *et al.* *Mol*
19 *Vis* 2010; **16**: 2765–2776.
- 20 16 Charrier L, Yan Y, Driss A *et al.* *Am J Physiol*
21 *Gastrointest Liver Physiol* 2005; **288**: G346–
22 G353.
- 23 17 Zigrino P, Steiger J, Fox J W *et al.* *J Biol Chem*
24 2007; **282**: 30785–30793.
- 25 18 Mauch C, Zamek J, Abety A N *et al.* *J Invest Derma-*
26 *tol* 2010; **130**: 2120–2130.
- 27 19 Zigrino P, Nischt R, Mauch C. *J Biol Chem* 2011;
28 **286**: 6801–6807.
- 29 20 Werner S, Smola H, Liao X *et al.* *Science* 1994;
30 **266**: 819–822.
- 31 21 Zigrino P, Kuhn J, Bauerle T *et al.* *J Invest Derma-*
32 *tol* 2009; **129**: 2686–2693.
- 33 22 Li J, Zhang Y P, Kirsner R S. *Microsc Res Tech*
34 2003; **60**: 107–114.
- 35 23 Schäfer M, Werner S. *Nat Rev Mol Cell Biol*
36 2008; **9**: 628–638.
- 37 24 Eto K, Puzon-McLaughlin W, Sheppard D *et al.* *J*
38 *Biol Chem* 2000; **275**: 34922–34930.
- 39 25 Lu D, Xie S, Sukkar M B *et al.* *Am J Respir Cell*
40 *Mol Biol* 2007; **37**: 494–500.
- 41 26 Martin J, Eynstone L V, Davies M *et al.* *J Biol*
42 *Chem* 2002; **277**: 33683–33689.
- 43 27 Marezky T, Le Gall S M, Worpenberg-Pietruk S
44 *et al.* *Cancer Res* 2009; **69**: 4573–4576.
- 45 28 Marezky T, Yang G, Ouerfelli O *et al.* *Biochem J*
46 2009; **420**: 105–113.
- 47 29 Ham C, Levkau B, Raines E W *et al.* *Exp Cell Res*
48 2002; **279**: 239–247.
- 49 30 Herren B, Garton K J, Coats S *et al.* *Exp Cell Res*
50 2001; **271**: 152–160.
- 51 31 Nedelec B, Ghahary A, Scott P G *et al.* *Hand Clin*
52 2000; **16**: 289–302.
- 53 32 Darby I A, Hewitson T D. *Int Rev Cytol* 2007;
54 **257**: 143–179.
- 55 33 Daugimont L, Vandermeulen G, Defresne F *et al.*
56 *Eur J Pharm Biopharm* 2011; **?????:** ??????
- 57 34 Prakash M, Kale S, Ghosh I *et al.* *Cell Signal*
58 2011; **?????:** ??????
- 59 35 Wu J, Zhang L, Ma X *et al.* *Oncol Rep* 2008; **20**:
60 669–675.
- 61 36 Carl-McGrath S, Lendeckel U, Ebert M *et al.* *Int J*
62 *Oncol* 2005; **26**: 17–24.

Supporting Information

Additional Supporting Information may be found in the online version of this article:

Figure S1. (a) Analysis of epidermal tissue morphology and differentiation in Adam-15 WT and $-/-$ animals.

Figure S2. Analysis of wounds in Adam-15 WT and $-/-$ animals.

Figure S3. (a) quantification of the number of CD31 positive structures (counts) in both animal genotypes.

Figure S4. Infiltration of CD8 positive lymphocytes and macrophages (F4/80) was analyzed using antibodies to both markers (in green).

Data S1. Supplementary material and methods.

Please note: Wiley-Blackwell is not responsible for the content or functionality of any supporting materials supplied by the authors. Any queries (other than missing material) should be directed to the corresponding author for the article.

Erklärung

Ich versichere, dass ich die von mir vorgelegte Dissertation selbstständig angefertigt, die benutzten Quellen und Hilfsmittel vollständig angegeben und die Stellen der Arbeit - einschließlich Tabellen, Karten und Abbildungen -, die anderen Werken im Wortlaut oder dem Sinn nach entnommen sind, in jedem Einzelfall als Entlehnung kenntlich gemacht habe; dass diese Dissertation noch keiner anderen Fakultät oder Universität zur Prüfung vorgelegen hat; dass sie - abgesehen von den unten angegebenen Teilpublikationen - noch nicht veröffentlicht worden ist sowie, dass ich eine solche Veröffentlichung vor Abschluss des Promotionsverfahrens nicht vornehmen werde.

Die Bestimmungen der Promotionsordnung sind mir bekannt. Die von mir vorgelegte Dissertation ist von Frau Dr. Paola Zigrino und Frau Prof. Dr. Dr. Mauch betreut worden.

Ich versichere, dass ich alle Angaben wahrheitsgemäß nach bestem Wissen und Gewissen gemacht habe und verpflichte mich, jedmögliche, die obigen Angaben betreffenden Veränderungen, dem Dekanat unverzüglich mitzuteilen.

Teilpublikationen:

Schönefuß A, Abety A, Zamek J, Mauch C, Zigrino P (2012):

Role of ADAM-15 in wound healing and melanoma development.

Exp Dermatol. *in press* 2012.

Köln, den 11.07.2012

Alexander Schönefuß

Curriculum Vitae

Personal information

Name: Alexander Schönefuß
Date of birth: 25 September 1982
City of birth: Mülheim an der Ruhr
Nationality: German
Marital status: unmarried

Education

1993 - 2002: **Abitur:** Luisenschule (städt. Gymnasium an den Buchen)
2002 - 2003: **Civilian Service:** Johanniter Unfallhilfe
2003 - 2008: **Studies in Biology at Ruhr-University Bochum**
May 2006 - Aug. 2006: **Bachelor thesis**
“Gliotic alterations in rat models for neuropathic and inflammatory pain”; Department of Animal Physiology, Ruhr University Bochum
Sep. 2007 - Aug. 2008: **Master thesis**
“Cathepsins in normal and pathologically altered skin”; Department of Animal Physiology, Ruhr University Bochum
since Sep. 2008: **PhD thesis**
“Role of melanoma-derived ADAM-9 for invasion and metastasis of melanoma”; Department of Dermatology and Venerology, University of Cologne

Publications

Schönefuß A, Wendt W, Schattling B, Schulten R, Hoffmann K, Stuecker, M, Tigges C, Lübbert H, Stichel C (2010): *Upregulation of cathepsin S in psoriatic keratinocytes*. *Exp Dermatol.* 2010 Aug;19(8):e80-8.

Schönefuß A, Abety A, Zamek J, Mauch C, Zigrino P (2012): *Role of ADAM-15 in wound healing and melanoma development*. *Exp Dermatol. in press* 2012.

Abety A, Fox W, **Schönefuß A**, Zamek J, Landsberg J, Krieg T, Blobel C, Mauch M, Zigrino P (2012): *Stromal fibroblast-specific expression of ADAM-9 modulates proliferation and apoptosis in melanoma cells in vitro and in vivo*. *J Invest Dermatol. in press* 2012.

Abstracts/Posters

A. Schönefuß, B. Seyfarth, C. Mauch, P. Zigrino (2009): *Molecular events mediating ADAM-9 regulation in melanoma cells by interleukin -1 α* . *J Invest Dermatol* 129: S1-S103;
Poster: Annual Meeting of the European Society for Dermatological

Research, Budapest 2009

A. Schönefuß, B. Seyfarth, C. Mauch, P. Zigrino (2010):
Molecular regulation of ADAM-9 expression in melanoma cells.
European Journal of Cell Biology 89S1 Suppl. 60;
Poster: Annual Meeting of the German Society for Cell Biology,
Regensburg 2010

A. Schönefuß, C. Mauch, P. Zigrino (2011): *Down-regulation of melanoma-derived ADAM-9 impairs invasion of melanoma cells.*
Poster: Annual Meeting of the German Connective Tissue Society,
Cologne 2011